CHALLENGES IN THE DISCOVERY AND OPTIMIZATION OF MGLU$_{2/4}$ HETERODIMER POSITIVE ALLOSTERIC MODULATORS AND TOTAL SYNTHESIS OF EPI- AND PERICOANNOSIN A

By

Mark G. Fulton

Dissertation
Submitted to the Faculty of the
Graduate School of Vanderbilt University
in partial fulfillment of the requirements
for the degree of

DOCTOR of PHILOSOPHY

in

Chemistry

August 9th, 2019
Nashville, Tennessee

Approved:
Craig W. Lindsley, Ph.D.
Gary A. Sulikowski, Ph.D.
Brian O. Bachmann, Ph.D.
Colleen M. Niswender, Ph.D.

ACKNOWLEDGMENTS

The work presented here was generously financially supported by the Vanderbilt Institute for Chemical Biology, the Warren Foundation, and the National Institutes of Health.

I would first and foremost like to acknowledge my advisor, Dr. Craig Lindsley, for his help, guidance and support throughout my graduate career. His knowledge, both scientifically and towards my future career, have been invaluable in shaping me into the scientist that I have become at the end of this chapter of my journey. His tenacity in not giving up on me or my projects when things frequently looked grim has helped inspire me to learn to not take difficulties in lab personally, to be creative and to always try to think of new ideas and new work arounds when obstacles appear.

I would also like to acknowledge my committee members for challenging my general scientific knowledge and for helping me to think of my project in different ways. To Dr. Gary Sulikowski, for his vast knowledge in the realm of organic synthesis and for his unique ways of thinking about and understanding chemistry, biology, and pharmacology. To Dr. Brian Bachmann, for helping instruct me in the realms of NMR, chemical biology, and biosynthesis. To Dr. Colleen Niswender, for her help in better understanding the pharmacology of my project and for assistance in better describing and presenting my project throughout my graduate career.

I must also acknowledge the numerous people, both in the VCNDD and Vanderbilt University, without whom I would not have made it to where I am today.

First, I would like to thank my current lab members for both their scientific knowledge and their support and comraderie throughout the years. For current members, I'd like to thank Carson Reed, Jeanette Bertron, and Jacob Kalbfleisch. For past members, Dr. Dan Jeffries, Dr. Kayla Temple, Dr. Kevin McGowan, Mabel Seto, Dr. Kellie Nance, and Dr. Pedro Garcia-Barrantes were invaluable in sharing their knowledge and guidance during my years in the lab. I would also like to thank Dr. Hyekyung Plumley for being a source of support and optimism and helping me to see that this journey would be worth it in the end. Dr. Don Stec was extremely helpful in helping with the NMR facilities and interpretation. Finally, though there are too many people to name here, I would like to thank all of the people throughout the VCNDD who contributed to both my project and my knowledge base.

Outside of Vanderbilt, I must thank my family, for I would not be where I am today without their support. My parents specifically, who didn't understand my project or what this process was like, were unwaveringly supportive nonetheless. I must also thank my friends who made time to visit me, especially Jalen Chapman. And last, but most certainly not least, I must thank my wonderful partner through all of this, Claire Strothman, for her love and support through the highs and lows that were the past 4 years. Without her, I don't think I would have made it to this point. I'm excited for what the future has in store for us.

TABLE OF CONTENTS

Page

ACKNOWLEDGMENTS……………………………………………………………….ii

LIST OF TABLES………………………………………………………………...…..vi

LIST OF FIGURES……………………………………………………………………vii

LIST OF SCHEMES…………………………………………………………………..ix

LIST OF ABBREVIATIONS…………………………………………………………..xi

Chapter

1 Challenges In The Discovery And Optimization Of mGlu$_{2/4}$ Heterodimer Positive Allosteric Modulators

- Introduction..1
  - Metabotropic Glutamate Receptor Structure and Function……...…1
  - mGlus and Schizophrenia……………………………………….….....3
  - Orthosteric and Allosteric Ligands.......................……………….…5
  - Metabotropic Glutamate Receptor Heterodimers……….......….…8
  - Metabotropic Glutamate 2/4 Heterodimers *in Vitro*………………..…..9
  - Metabotropic Glutamate 2/4 Heterodimers *in Vivo*……….....……..10
  - mGlu$_{2/4}$ Heterodimer Ligand Selectivity…………………………....…11
  - Conclusion…………………………………………………………….12
- Materials and Methods…………………………………………………13
  - General Synthetic Methods and Instrumentation…………………13
  - mGlu Receptor Thallium Flux Assays……………………………...14
  - In-Vitro DMPK Methods-Intrinsic Clearance in Liver Microsomes.15
  - Plasma Protein Binding……………………………………………...16
  - Brain Homogenate Binding………………………………………….17
  - LC/MS/MS Analysis of Samples from *In Vitro* Assays……………18
  - *In-Vivo* PK Methods…………………………………………………19
  - Discrete Rat PK and Tissue Distribution Studies…………………19
  - Plasma and Brain Sample Preparation…………………………….20
  - LC/MS/MS Bioanalysis of Samples from *In Vivo* Assays………..20
- Challenges in the Development of a Selective mGlu$_{2/4}$ Heterodimer PAM…………………………………………………………21
  - Initial Screen of mGlu$_4$ PAMs……………………………………….21
  - SAR of VU041………………………………………………………...22
  - Screen of FDA Approved Drugs…………………………………….33
- High-Throughput Screening Campaign……………………………….37
  - VU6010417…………………………………………………………...37
  - VU6010427…………………………………………………………...46

VU0495443……………………………………………………………..49
VU6009122……………………………………………………………...53
Completion of HTS Screen……………………………………………….59
VU0503424……………………………………………………………...60
VU0507341……………………………………………………………...68
VU0544412………………………………………………………...….71
Conclusions…………………………………………………………...82
Tethering Strategy……………………………………………………….83
Background……………………………………………………………...83
mGlu$_{2/4}$ Tethered Ligand………………………………………….85
Tether Synthesis- BINA……………………………………………...89
Tether- VU374………………………………………………………..91
Tether- Synthesis……………………………………………………93
Tether-Pharmacology………………………………………………..95
Summary, Conclusions, and Future Directions…………………..100
Experimental Methods…………………………………………………..102
General Synthetic Methods And Instrumentation..………………..102

2 Total Synthesis of Epi- and Pericoannosin A

Introduction……………………………………………………………….138
Natural Products in Medicine……………………………………138
Natural Products from Periconia sp. F-31…………………...……140
Previous Total Synthesis of Pericoannosin A……………………142
First Retrosynthesis of Pericoannosin A…………………………146
First Generation Synthesis of Pericoannosin A…………………..147
Second Generation Route for the Formal Total Synthesis of Pericoannosin A……………………………….….155
Aldol Optimization and Attempted Completion of Synthesis……159
Summary and Future Directions…………………………………..164
Experimental Methods…………………………………………………..166
General Synthetic Methods and Instrumentation………………..166

Appendix…………………………………………………………………….187

A. Relevant Spectra for Chapter 1………………………………………..187
B. Relevant Spectra for Chapter 2………………………………………..244

References………………………………………………………….......…..270

LIST OF TABLES

Table Page

1.1. Structure and activities of aryl analogs of VU0155041……………………………..24

1.2. Structure and activities of carboxamide replacements for VU0155041…………..29

1.3. Structures and activities of core changes to the VU0155041 scaffold…………....31

1.4. Febuxostat analogs and their respective activities……………………………….36

1.5. Structures and activities for VU6010417 analogs………………………………… 41

1.6. Core changes to VU6010417 and their activities………………………………...45

1.7. Structures of varied 4-Aryl Substitutions and their activities of VU6010427……..48

1.8. Structure activity relationship surrounding the amide of pyridone VU0429553….50

1.9. Benzylamine analog SAR for analogs of VU6009122…………………………….55

1.10. Activities of two trifluoroethyl sulfonamide analogs of VU6009122……………...58

1.11. Sulfonamide analog SAR for VU0503424……………………………………….62

1.12. Varied aryl pyridazine substituents and their corresponding activities…………..64

1.13. Polyfluorinated sulfonamides for the improvement of potency of VU05034324..67

1.14. Structures of acylthiourea analogs and their activities for VU0507341…………70

1.15. Varied amide analogs of thiazepine VU0544412 and their activities……………73

1.16. Structures of 3,5-dihalogenated aryl analogs of VU0544412 and activities…….79

1.17. Activities of each linker length of the synthesized VU374/BINA tethers………..99

2.1. Wittig olefination optimization for synthesis of **2.44**……………………………….158

2.2. Comparison of diastereomeric synthetic ^{1}HNMR to the authentic sample……...183

2.3. Comparison of diastereomeric synthetic ^{13}CNMR to the authentic sample…….185

LIST OF FIGURES

Figure Page

1.1. Structural features of a generic mGlu receptor……………………………………2

1.2. Differences between orthosteric agonists and allosteric modulators………………6

1.3. FDA approved drugs that act through an allosteric mechanism of action…………7

1.4. Structures of $mGlu_{2/4}$/$mGlu_4$ PAM VU0155041 and $mGlu_4$ PAM PHCCC……..…10

1.5. Structures of VU0155041 and LU AF2193422……………………….............22

1.6. Structures, activities, and K_p for Febuxostat and VU6009638……………………..33

1.7. DMPK analysis for the most active analogs of VU6010417………………………..40

1.8. DMPK properties of 3 analogs of VU6009122……………………………………59

1.9. Structures of the 2 selective compounds from an HTS screen……………………59

1.10. Structure of the first HTS hit explored, VU0503424………………………………60

1.11. DMPK analysis of thiazepane VU6014297………………………………............81

1.12. CRC of an ideal dimeric antagonist/NAM exhibiting a biphasic curve…............85

1.13. Structures of VU0415374 and BINA for tether synthesis…………………………85

1.14. BINA analogs and activities for linker attachment…………………………………87

1.15. Structure of VU374 modified for linker attachment…………………….............87

1.16. Final design of linked molecules for the tethered ligand…………………………88

1.17. CRCs of tethered ligands exhibiting varied Hill slopes and potencies…............98

1.18. Tethered ligands activity in heterodimer selective cell lines………….............99

2.1. Structures of several natural products used in modern medicine………………..138

2.2. Periconiasin natural products derived from *Periconia* Sp. F-31…………………141

2.3. Proposed biosynthetic pathway for periconiasins and pericoannosins…………141

2.4. Structure of the natural product Pericoannosin A……………………………….142

2.5. ^{1}HNMR spectra of synthetic and authentic Pericoannosin A……………………..184

2.6. ^{13}CNMR spectra of synthetic and authentic Pericoannosin A……………………186

LIST OF SCHEMES

Scheme Page

1.1. Synthesis of VU0155041 analogs……………………………………………………22

1.2. Route for access of Febuxostat analogs……………………………………………..34

1.3. Three step synthesis of 1,2,4-oxadiazoles VU6010417……………………………38

1.4. Synthetic scheme for the synthesis of 1,3,4-oxadiazole VU6010427…………….47

1.5. Synthesis of aryl analogs of pyridone VU0495443………………………………….49

1.6. Route for synthesis of benzylamine analogs of $mGlu_2$ PAM CBiPES…………….54

1.7. Divergent routes for access to analogs of pyridazine VU0503424………………..61

1.8. One pot synthesis of acylthioureas VU0507341……………………………………69

1.9. Synthesis of thiazepane from methyl acrylate and L-cysteine…………………....72

1.10. Route for the synthesis of BINA analog **1.351** for tethering………………………90

1.11. Synthetic scheme for the synthesis of VU374 analog **1.362** for tethering………92

1.12. Final four steps for access to tethers of varied lengths…………………………...94

2.1. Synthesis of intermediate **2.16** from the first synthesis of Pericoannosin A…….143

2.2. Synthesis of lactam **2.19** for aldol with **2.16**………………………………………..144

2.3. Completion of the first synthesis of Pericoannosin A……………………………...145

2.4. First retrosynthetic analysis from our work on Pericoannosin A…………………146

2.5. Failed Weinreb ketone synthesis……………………………………………………148

2.6. Synthesis of **2.36** through an alternative ketone synthesis route………………..149

2.7. Route for the synthesis of enolate precursor **2.23**…………………………………152

2.8. Successful aldol condensation followed by failed lactam formation……………..153

2.9. Unsuccessful attempts of synthesizing Pericoannosin A using the initial route..154

2.10. Revised second retrosynthesis for key intermediate **2.16**……………………….156
.
2.11. Second generation route for the improved synthesis of **2.16**…………………...158

2.12. Aldol reaction for the second route toward Pericoannosin A…………………...161

2.13. End game synthesis of Epi- and Pericoannosin A……………………………….163

LIST OF ABBREVIATIONS

°C	Degrees Celsius
7TD	Seven-transmembrane domain
9-BBN	9-Borabicyclo(3.3.1)nonane
AC	Adenylyl Cyclase
AcOH	Acetic acid
AD	Alzheimer’s disease
ATP	Adenosine triphosphate
BACE1	Beta-secretase 1
BBB	Blood brain barrier
BINA	Biphenly-indanone A
BLQ	Below the limit of quantitation
Boc	*tert*-Butyloxycarbonyl
BRET	Bioluminescence Resonance Energy Transfer
Brsm	Based on recovered starting materials
cAMP	Cyclic Adenylyl Monophosphate
CBiPES	*N*-(4'-Cyano-[1,1'-biphenyl]-3-yl-*N*-(3-pyridinylmethyl)-ethanesulfonamide hydrochloride
CL_{hep}	Hepatic Clearance
CNS	Central Nervous System
CODA-RET	Complemented donor-acceptor resonance energy transfer
CRD	Cystein Rich Domain
CSA	Camphorsulfonic Acid

Da	Dalton
DCE	1,2-Dichloroethane
DCGIV	(2*S*,2'*R*,3'*R*)-2-(2',3'-Dicarboxycyclopropyl)glycine
LAP4	L-2-amino-4-phosphonobutyric acid
DCM	Dichloromethane
DDQ	2,3-dichloro-5,6-dicyanobenzoquinone
DIBAL	Diisobutylaluminum hydride
DIEA	*N,N*-Diisopropylethylamine
DMAP	4-Dimethylaminopyridine
DMF	Dimethylformamide
DMP	Dess-Martin periodinane
DMPK	Drug Metabolism Pharmacokinetics
DMSO	Dimethylsulfoxide
EC$_{50}$	Concentration required for 20% of maximal receptor activation
EDCI	*N*-(3-Dimethylaminopropyl)-*N′*-ethylcarbodiimide hydrochloride
ER	Endoplasmic reticulum
ESI	Electrospray ionization
EtOAc	Ethyl acetate
EtOH	Ethanol
FRET	Förster Resonance Energy Transfer

f_u	Fraction unbound
GABA	Gamma-aminobutyric acid
GIRK	G protein-coupled inwardly-rectifying potassium channel
Glu	Glutamate
GPCR	G protein-coupled receptor
HATU	1-[Bis(dimethylamino)methylene]-1*H*-1,2,3-triazolo[4,5-*b*]pyridinium 3-oxid hexafluorophosphate
HCl	Hydrochloric acid
HPLC	High-performance liquid chromatography
HRMS	High-resolution mass spectrometry
HTS	High-throughput screen
HWE	Horner-Wadsworth-Emmons
IBX	2-Iodoxybenzoic acid
IC_{50}	Concentration required for 50% inhibition of maximal receptor response
IP_3	Inositol trisphosphate
KHMDS	Potassium hexamethyldisilazide
K_p	Partition coefficient
LCMS	Liquid chromatography mass spectrometry
LHMDS	Lithium hexamethyldisilazide
LRMS	Low-resolution mass spectrometry

LUMO	Lowest unoccupied molecular orbital
MeCN	Acetonitrile
MeOH	Methanol
mGlu	Metabotropic glutamate receptor
MOM	Methoxymethyl acetal
MS	Mass spectrometry
NAL	Neutral allosteric ligand
NAM	Negative allosteric modulator
n-BuLi	*n*-Butyllithium
NEt_3	Triethylamine
NHMDS	Sodium hexamethyldisilazide
NMDA	*N*-methyl-D-aspartate
NMR	Nuclear magnetic resonance
NRPS	Non-ribosomal peptide synthetase
PAM	Positive allosteric modulator
PCP	Phencyclidine
PGP	P-glycoprotein
PHCCC	*N*-Phenyl-7-(hydroxyimino)cyclopropa[*b*]chromen-1a-carboxamide
PIP2	Phosphatidylinositol 4,5-bisphosphate
PKA	Protein kinase A
PKS	Polyketide synthase
PLC	Phospholipase C

PMB	*para*-Methoxy benzyl
PPTS	Pyridinium *p*-toluenesulfonate
RT	Room temperature
SAR	Structure-activity relationship
SCG	Superior cervcal ganglion
SFC	Supercritical fluid chromatography
T3P	Propylphosphonic anhydride
TBAF	Tetrabutylammonium fluoride
TBS	*tert*-Butyldimethyl silyl
TBSCl	*tert*-Butyldimethylsilyl chloride
TBSOTf	*tert*-Butyldimethylsilyl trifluoromethanesulfonate
Teoc	2-(Trimethylsilyl)ethoxycarbonyl
TES	Triethylsilyl
TFA	Trifluoroacetic acid
THF	Tetrahydrofuran
TLC	Thin-layer chromatography
TMS	Trimethylsilyl
Tol	Toluene
VFD	Venus flytrap domain
VUID	Vanderbilt University identification number

Challenges in the Discovery and Optimization of Metabotropic Glutamate 2/4 Heterodimer Positive Allosteric Modulators

Introduction

Metabotropic Glutamate Receptor Structure and Function

The metabotropic glutamate (mGlu) receptors are G protein-coupled receptors (GPCRs) that are widely distributed throughout the central nervous system (CNS). While the exact number varies, more than 800 GPCRs have been identified in humans and comprise ~4% of our genome[1-4]. GPCRs also comprise a large portion of targets for Food and Drug administration (FDA) approved drugs; 475 drugs approved by the FDA target 108 different GPCRs[5,6]. Additionally, approximately 20% of ongoing clinical trials also target GPCRs[7], emphasizing their prevalence and importance in the field of medicine. This is due to the fact that GPCRs play a number of key, and diverse, roles in human biology. Activation of GPCRs elicit hundreds, if not thousands, of secondary messaging cascades that result in a myriad of different cellular effects[8,9], but broadly play roles in our senses (smell, sight, taste)[10], behavior[9], homeostasis[11], hormonal signaling[12], and immune system regulation[13]. GPCRs are split into 6 classes, based on sequence homology and function, of which mGlus are a member of Class C. This family is characterized by a large extracellular, *N*-terminus domain, which is termed the Venus flytrap domain (VFD) for mGlus (**Figure 1.1[14]**). This name arises from the way that its two lobes "bite" down on glutamate to induce receptor activation. When the VFD activates, a large conformational change occurs which is propagated through the structurally rigid cysteine-rich domain (CRD), comprised of 9 cysteine residues, of which 8 form disulfide bridges with the other protomer of the mGlu obligate dimer[15]. The 9th cysteine forms a disulfide bridge with the VFD, which allows for it to propagate the structural changes in the VFD upon glutamate binding down through to the seven-transmembrane domain (7TD)[15]. Structural rearrangement of the transmembrane domains results in the heterotrimeric G protein breaking apart into Gβγ and Gα subunits, which then can participate in secondary messenger cascades and exert a number of intracellular changes[15]. The mGlus are also constitutive dimers, in which a disulfide bridge between cysteine residues in unstructured loops near the VFD between the two monomers covalently links the two protomers[15]. However, recent studies have shown that this disulfide bond is relatively unimportant for dimerization, as mutations of the cysteine residues to other amino acids only results in a small reduction in receptor function[16]. Further mutational studies indicate that the main energetic impetus for dimerization lies on the back (non-ligand binding portion) side of the upper lobe of the VFD, which contains hydrophobic residues that form a hydrophobic pocket with the hinge region of a second mGlu monomer[16]. Mutations of any of these hydrophobic residues to more polar amino acids results in severe reductions in receptor activation[16]. In addition, mutations that weaken this hydrophobic interface resulted in a receptor with a higher affinity for glutamate and more spontaneous activation in the absence of agonist as compared to the wild-type, suggesting that this interface is important

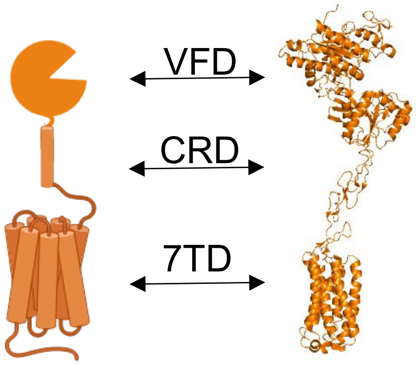

Figure 1.1[14] Structural and schematic representation of a generic mGlu monomer with structural features labeled.

for stabilizing the receptor in its non-active state[16].

There are 8 members of the mGlu family, $mGlu_{1\text{-}8}$, that are separated based on sequence homology, G protein signaling, and ligand binding. Group 1 consists of $mGlu_{1,5}$, group 2 consists of $mGlu_{2,3}$, and group 3 is made up of $mGlu_{4,6,7,8}$, $mGlu_6$ is localized to the retina of the eye, whereas the other group III receptors are widely expressed in the CNS. Group 1 is coupled to $G_{\alpha q}$, wherein activation of the receptor results in the release of the $G_{\alpha q}$ subunit from the heterotrimeric G protein. $G_{\alpha q}$ activates phospholipase C (PLC), which cleaves phosphatidylinositol 4,5-biphosphate (PIP2) into diacyl glycerol (DAG) and isolitol 1,4,5-triphosphate (IP_3), the latter of which is cytosolic and activates a number of receptors[15,17]. Importantly, it activates endoplasmic reticulum (ER) bound calcium channels, which allows for influx of calcium ions into the cytosol[18]. Assays for $G_{\alpha q}$ coupled receptors can take advantage of this signaling cascade by loading the cell with calcium sensitive dyes, which allows measure of the release of calcium ions as a proxy for measurement of receptor activation[19]. Group 2 and 3 are both coupled to $G_{\alpha i}$, where the interaction of the G protein with adenylate cyclase (AC) results in a reduced activation of AC, which converts adenosine triphosphate (ATP) into cyclic adenosine monophosphate (cAMP). This reduction in cellular CAMP can have a myriad of intracellular effects, including impacts on cellular ion channels and the ser/thr-speific protein kinase A (PKA) family of protein kinases[20-22]. Gi/o GPCRs can also directly affect ion channels via the βγ subunits and this may be even more important in modulating synaptic transmission than changes in cAMP.

mGlus and Schizophrenia

Schizophrenia is a mental disorder that affects approximately 1% of the US population and the cost of this disease was estimated to be $25-102 billion in 2013[23,24]. Symptoms of schizophrenia are separated into three main clusters: positive symptoms are those commonly associated with this disease, including hallucinations, delusions, and paranoia; negative symptoms are those that affect mood and behavior, including reduced expression of emotions and reduced pleasure from everyday life; and finally, cognitive symptoms include difficulty taking information and applying it to various situations. Today, numerous antipsychotics are on the market for treating this disease[25]. However, most are only able to treat the positive symptoms and have deleterious side effects that can cause difficulties with patient compliance[26-30]. Negative and cognitive symptoms represent a large unmet need for this patient population, and addressing these symptoms could greatly improve the quality of life for those who suffer from this condition.

Schizophrenia is associated with genetic mutations across a number of proteins, and the direct causes and pathology of the disease are not well understood[31,32]. However, a correlation with glutamatergic signaling was observed in the 1960s when recreational phencyclidine (PCP) users were admitted into clinics exhibiting symptoms similar to those observed in schizophrenic patients[33-37]. PCP is an *N*-methyl-D-aspartate (NMDA) receptor antagonist, which is an ionotropic glutamate receptor that allows flux of positive ions in response to ligand binding (glutamate, glycine, and/or aspartate). Additionally, NMDA knockdown mice (~5-10% expression level, knockouts are non-viable) exhibit increased hyperlocomotion and stereotypies, which are behaviors correlated with the positive symptoms of schizophrenia[38,39]. This phenotype could be rescued by gene therapy in mouse models[40], which means that potentiation of signaling at NMDA receptors could provide a therapeutic benefit. While direct NMDA agonists can cause excitotoxicity[41-43], which led to the hypothesis that modulation of upstream signaling pathways for NMDA receptors could have therapeutic potential for this disease.

Numerous studies have shown the efficacy of molecules that potentiate group II mGlu receptor activity in animal models of schizophrenia, including a number of tool compounds and clinical trials. It has been shown that group II non-selective agonists had efficacy in models of this disease in $mGlu_3$ knockout mice, but not in $mGlu_2$ knockouts, indicating that the efficacy of these agonists lies in their activity at $mGlu_2$.

Orthosteric and Allosteric Ligands

Most commercial drugs are act through an orthosteric mechanism, which means that they target the same binding site as the endogenous ligand for the targeted receptor[44-48]. The nature of endogenous ligands can vary vastly in nature and size, from small neurotransmitters for CNS receptors to large peptides, such as hormones. However, synthetic orthosteric ligands come with a number of caveats that can require rigorous medicinal chemistry efforts to overcome. Because orthosteric ligands result in sustained receptor activation or deactivation, chronic dosing can result in diminishing results as receptors become desensitized and internalized[49-52]. This means that the orthosteric drug can lose efficacy over time. For example, a number of drugs of abuse, such as heroin, hydrocodone, oxycodone and morphine are opioid receptor agonists that require increasing doses to achieve the same effect over chronic administration due to receptor desensitization[53-55]. Additionally, as orthosteric binding sites are highly conserved within receptor families, subtype selectivity can be elusive, which can complicate the interpretation of pharmacology if multiple receptors are being simultaneously activated or inhibited[56,57]. Finally, for CNS drug discovery, many orthosteric ligands are very polar (L-glutamate, gamma-aminobutyric acid (GABA), etc) or charged (acetylcholine) and mimics of these molecules must overcome this polarity for them to be sufficiently able to cross the blood brain barrier (BBB) for CNS indications[58].

Because of these challenges in orthosteric drug discovery, allosteric modulation has become a burgeoning area for medicinal chemistry efforts[44-47,56,57]. Allosteric pockets are located in areas of the protein outside of the orthosteric ligand binding pocket and molecules that interact with these allosteric sites can have a myriad of effects (**Figure 1.2**). Pure positive allosteric modulators (PAMs) can increase the potency and efficacy of the endogenous ligand, but do not result in signaling in the absence of agonist. Potentiation is accomplished by stabilizing an active conformation of the receptor, which can improve affinity, efficacy, or both. Agonist-PAMs (or ago-PAMs) are capable of activating the target in the absence of the orthosteric agonist, but also potentiates the receptor activation upon interaction with the orthosteric ligand. Negative allosteric modulators (NAMs) reduce the effect

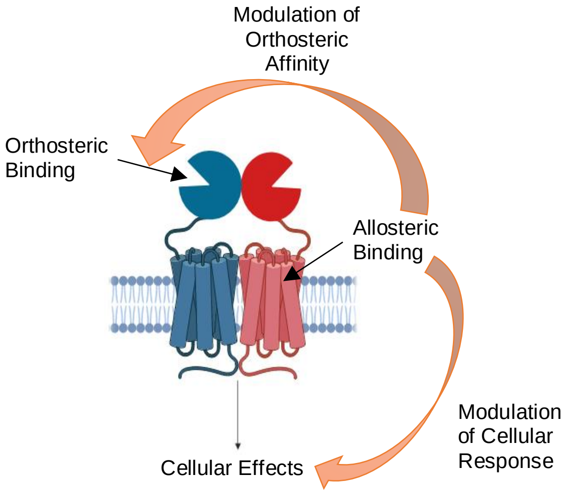
Modulation of Orthosteric Affinity
Orthosteric Binding
Allosteric Binding
Modulation of Cellular Response
Cellular Effects

Figure 1.2[59] Location of orthosteric and allosteric binding sites, along with the effects of allosteric modulators on orthosteric affinity and efficacy.

of the receptors orthosteric ligand by stabilizing an inactive conformation of the target. Additionally, neutral allosteric ligands (NALs) have no impact on signaling through the orthosteric site, but can block the effect of other allosteric ligands that bind in the same pocket.

The first major group of allosteric drugs was the benzodiazepine class, which have sedative, anxiolytic, and amnesic effects, and act by enhancing the effect of (GABA) at GABA receptors[60-62]. Recent drug discovery campaigns have had success in the clinic with allosteric modulators, first with cincacalcet, a calcium-sensing receptor PAM that was approved in 2004[63] (**Figure 1.3**). This was followed by the CCR5 NAM maraviroc, which is used in HIV treatment to help prevent entry of the virus into human cells[64,65]. The relatively low number of allosteric modulators in the clinic may have several explanations. Structure-activity relationships (SAR) in allosteric modulation can often be very complicated; subtle changes can completely ablate activity, or even result in mode switches (i.e-from PAM to NAM)[66]. The structure of allosteric pockets can also be vastly different between species, which can complicate the translation of data from animal models to human disease and the clinic[67]. Finally, allosteric modulators are typically extremely lipophilic, relying on hydrophobic interactions within the allosteric pocket, which can cause the drug to

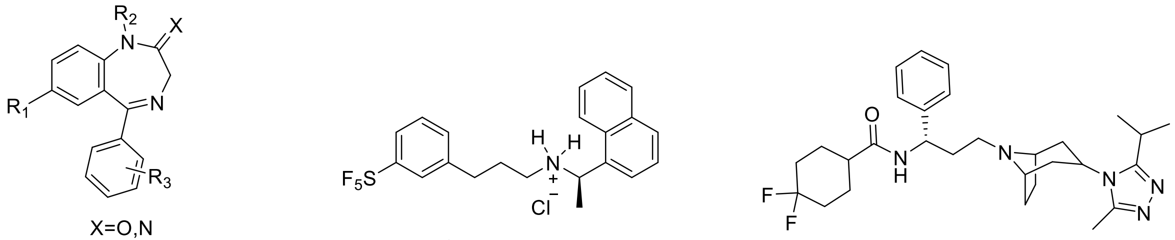

Benzodiazapines
GABA PAMs

Cincalcet
Calcium-Sensing Receptor PAM
Amgen

Maraviroc
CCR5 NAM
Pfizer

Figure 1.3 Structures and targets of commercially available allosteric drugs.

deposit into fatty tissues, along with other undesired pharmacokinetic effects[68]. Driving down the lipophilicity of these allosteric modulators can be very challenging. However, despite these challenges, allosteric compounds can function as invaluable tool compounds for achieving subtype selectivity and teasing apart complicated pharmacology within a family of receptors.

Metabotropic Glutamate Receptor Heterodimers

As mentioned previously, mGlus exist as constitutive dimers and were historically thought to exist exclusively as homodimeric receptors. However, heterodimeric receptors are known throughout the family of GPCRs, including GABA receptors, sweet taste receptors, and umami taste receptors[69-71]. Additionally, a number of mGlus are colocalized in certain brain regions, which suggests that heterodimerization is possible[72-75]. The first evidence for formation of these heteromers was shown by Doumezane *et al* in 2011, in which SNAP and CLIP tags were genetically fused to the extracellular N-terminus of all of the mGlus, with the exception of $mGlu_6$[76]. These tags are suicide inhibitors, meaning they covalently bind to the SNAP and CLIP enzymes and can be linked to specific substrates to label cysteines in the CLIP/SNAP active site. This allows for direction of Lumi4, a Förster resonance energy transfer (FRET) donor, and Green, a FRET acceptor, specifically to different mGlu monomers. Using this technology, heterodimer signaling can be specifically isolated by expressing the FRET donor and acceptor on different mGlus. In this study, each of the 49 possible SNAP/CLIP tagged proteins were expressed and it was determined that Group I mGlus are able to heterodimerize with each other, while Group II and III mGlus are capable of heterodimerizing in both an intra- and intergroup manner. Logically, this makes sense as it prevents monomers with different G-protein coupling from heterodimerizing. Additionally, Group I mGlus are almost always located postsynaptically, whereas Group II and Group III are typically presynaptic, meaning that the cellular localization of these proteins potentially plays a role in their heterodimerization[77].

Metabotropic Glutamate 2/4 Heterodimers in Vitro

Using the knowledge that functional heterodimers can form between group II and group III mGlus, the mGlu$_2$/mGlu$_4$ (denoted from here on as mGlu$_{2/4}$) heterodimer was explored as a means of better understanding the functional and pharmacological characteristics of this receptor. This combination was chosen in part due to the ability to pharmacologically manipulate each monomer of the heterodimer separately, using the group II selective orthosteric agonist DCGIV and the group III selective agonist L-AP4. It was discovered that selective agonists alone were unable to activate the heterodimer, but administration of both selective agonists, or use of glutamate, allowed for full receptor response by activating both monomers of the heterodimer[78].

However, these initial studies were performed *in vitro* via heterologous expression in neurons from rat superior cervical ganglion (SCG), which do not express mGlu receptors. Additionally, the heterodimer was formed by expression of both mGlu$_2$ and mGlu$_4$, which means there are likely three cell populations expressed in the cell: mGlu$_2$ and mGlu$_4$ homodimers, along with the desired heterodimer. The presence of the two homodimer populations complicates the interpretations derived from these studies. The use of means to selectively isolate signaling from the heterodimer alone also complicate interpretation, as alterations to the native proteins make relevance to living systems more complicated. While strong evidence was shown to support the existence of mGlu$_{2/4}$ heterodimers under these conditions, the relevance of this receptor in living systems had not yet been shown.

Metabotropic Glutamate 2/4 Heterodimers in Vivo

An interesting dichotomy has been observed with regards to mGlu$_4$ PAMs in which some scaffolds have efficacy in models of anxiety disorders, while other PAMs have no effect in these assays[78-81]. Anxiolytic type activity is typically associated with mGlu$_2$ potentiation[82-84], leading to the hypothesis that mGlu$_2$ and mGlu$_4$ may form a functional heterodimeric complex. Using co-immunoprecipitation with antibodies against mGlu$_2$ and mGlu$_4$ respectively, the Niswender lab showed that anti-mGlu$_4$ antibodies were capable of precipitating mGlu$_2$ protein (and vice versa) both in cell lines expressing the heterodimer and in native tissues, indicating that there is a physical interaction between the two proteins[85]. Additionally, using two structurally distinct mGlu$_4$ PAMs, it was observed that the effects of glutamate in mGlu$_{2/4}$ cell lines were potentiated by VU0155041, but not by *N*-phenyl-7-(hydroxyamino)cyclopropa[*b*]chromen-1a-carboxamide (PHCCC) (**Figure 1.4**).

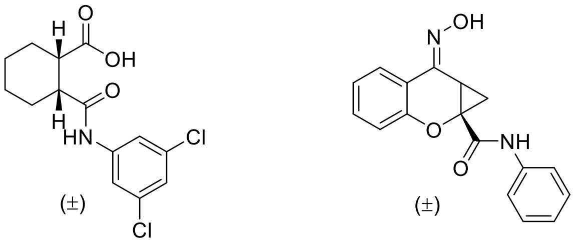

VU0155041 (**1.1**)
Dual mGlu$_4$/mGlu$_{2/4}$ PAM

PHCCC (**1.12**)
Selective mGlu$_4$ PAM

Figure 1.4 Structures of dual PAM VU0155041 and selective mGlu$_4$ PAM PHCCC.

Through electrophysiology and co-immunoprecipitation studies, the mGlu$_{2/4}$

heterodimer has been shown to be localized presynaptically to corticostriatal synapses, where cortical signaling is converted into changes in synaptic plasticity across the striatum[86-89]. These changes can have impacts on motor learning, habit formation, and cognition[87-90]. Additionally, this region of the basal ganglia is associated with numerous psychiatric diseases, such as schizophrenia, autism spectrum disorder, obsessive-compulsive disorder, and major depressive disorder[91]. A selective mGlu$_{2/4}$ PAM could allow one to selectively modulate glutamatergic signaling in this region and give great insight into the role(s) of this receptor under both normal physiological conditions and in models of schizophrenia. However, the lack of a selective mGlu$_{2/4}$ PAM has prevented more detailed studies into the specific roles that these heterodimeric complexes play in modulating neuronal signaling.

mGlu$_{2/4}$ Heterodimer Ligand Selectivity

As mentioned above, PHCCC is active at mGlu$_{4}$ homodimers, but not at the mGlu$_{2/4}$ heterodimer. This indicates that there are structural differences between the heterodimer and homodimer that could be exploited to potentially synthesize a selective mGlu$_{2/4}$ PAM. Though no modeling or structural work has been done specifically at the heterodimer, potentially due to the complexity that would be involved in trying to model the effects of the protein-protein interactions on the shape of the allosteric pocket, previous modeling studies indicate that there are two binding pockets within the mGlu$_{4}$ allosteric pocket[92]. One pocket lies higher in the protein, occupying a region that is closer to the extracellular space. The second pocket extends deeper into the protein, and these modeling studies indicate that this deeper pocket is more amenable to more linear, planar molecules like PHCCC. Modeling with VU041, which has a cyclohexane ring that can exist in a chair conformation and occupy a larger conformational space, showed that it was restricted to the shallow $mGlu_{2/4}$ allosteric pocket. These modeling studies indicate that flexible, sterically encumbered $mGlu_4$ PAMs are likely to be active at both the $mGlu_4$ homodimer and $mGlu_{2/4}$ heterodimer, while planar, linear, aromatic PAMs are more likely to be selective for $mGlu_4$ homodimers.

Conclusion

There is ample evidence for the existence of an $mGlu_{2/4}$ heterodimer both *in vitro* and *in vivo*. Electrophysiology and co-immunoprecipitation assays indicate that this receptor may be localized to corticostriatal synapses, an area of the brain strongly associated with behavior gating. Additionally, potentiation of $mGlu_2$ is associated with anxiolytic type activity, meaning that potentiation of $mGlu_2$ in this region of the brain may be efficacious in ameliorating symptoms of schizophrenia. A potent, selective, and CNS penetrant PAM targeting the $mGlu_{2/4}$ heterodimer would be vital for furthering the evidence toward the existence of these heterodimeric receptors and to help tease out the exact role(s) that this receptor performs in biological symptoms. One of the goals of this thesis was to use medicinal chemistry techniques to synthesize a selective $mGlu_{2/4}$ heterodimer PAM to enhance the study of this unique receptor.

Materials and Methods

General synthetic methods and instrumentation

All NMR spectra were recorded on a 400 MHz AMX Bruker NMR spectrometer. ^{1}H and ^{13}C chemical shifts are reported in δ values in ppm downfield with the deuterated solvent as the internal standard. Data are reported as follows: chemical shift, multiplicity (s = singlet, d = doublet, t = triplet, q = quartet, b = broad, m = multiplet), integration, coupling constant (Hz). Low-resolution mass spectra were obtained on an Agilent 6120 or 6150 with ESI source. Method A: MS parameters were as follows: fragmentor: 70, capillary voltage: 3000 V, nebulizer pressure: 30 psig, drying gas flow: 13 L/min, drying gas temperature: 350 ºC. Samples were introduced via an Agilent 1290 UHPLC comprised of a G4220A binary pump, G4226A ALS, G1316C TCC, and G4212A DAD with ULD flow cell. UV absorption was generally observed at 215 nm and 254 nm with a 4 nm bandwidth. Column: Waters Acquity BEH C18, 1.0 x 50 mm, 1.7 um. Gradient conditions: 5% to 95% CH_3CN in H_2O (0.1% TFA) over 1.4 min, hold at 95% CH_3CN for 0.1 min, 0.5 mL/min, 55ºC. Method B: MS parameters were as follows: fragmentor: 100, capillary voltage: 3000 V, nebulizer pressure: 40 psig, drying gas flow: 11 L/min, drying gas temperature: 350 ºC. Samples were introduced via an Agilent 1200 HPLC comprised of a degasser, G1312A binary pump, G1367B HP-ALS, G1316A TCC, G1315D DAD, and a Varian 380 ELSD (if applicable). UV absorption was generally observed at 215 nm and 254 nm with a 4 nm bandwidth. Column: Thermo Accucore C18, 2.1 x 30 mm, 2.6 µm. Gradient conditions: 7% to 95% CH_3CN in H_2O (0.1% TFA) over 1.6 min, hold at 95% CH_3CN for 0.35 min, 1.5 mL/min, 45 ºC. High-resolution mass spectra were obtained on an Agilent 6540 UHD Q-TOF with ESI source. MS parameters were as follows: fragmentor: 150, capillary voltage: 3500 V, nebulizer pressure: 60 psig, drying gas flow: 13 L/min, drying gas temperature: 275 ºC. Samples were introduced via an Agilent 1200 UHPLC comprised of a G4220A binary pump, G4226A ALS, G1316C TCC, and G4212A DAD with ULD flow cell. UV absorption was observed at 215 nm and 254 nm with a 4 nm bandwidth. Column: Agilent Zorbax Extend C18, 1.8 µm, 2.1 x 50 mm. Gradient conditions: 5% to 95% CH_3CN in H_2O (0.1% formic acid) over 1 min, hold at 95% CH_3CN for 0.1 min, 0.5 mL/min, 40 ºC. For compounds that were purified on a Gilson preparative reversed-phase HPLC, the system comprised of a 333 aqueous pump with solvent selection valve, 334 organic pump, GX-271 or GX-281 liquid handler, two column switching valves, and a 155 UV detector. UV wavelength for fraction collection was userdefined, with absorbance at 254 nm always monitored. Method: Phenomenex Axia-packed Luna C18, 30 x 50 mm, 5 µm column. Mobile phase: CH_3CN in H_2O (0.1% TFA). Gradient conditions: 0.75 min equilibration, followed by user-defined gradient (starting organic percentage, ending organic percentage, duration), hold at 95% CH_3CN in H_2O (0.1% TFA) for 1 min, 50 mL/min, 23 ºC. Solvents for extraction, washing and chromatography were HPLC grade. All reagents were purchased from Aldrich Chemical Co. and were used without purification.

mGlu Receptor Thallium Flux Assays

Cell lines: Polyclonal rat $mGlu_2$/HEK/GIRK, rat $mGlu_4$/HEK/GIRK and rat $mGlu_4$/$mGlu_2$ HEK/GIRK cells were used for these studies. For dye loading, media was exchanged with Assay Buffer (HBSS containing 20 mM HEPES, pH 7.4) using an ELX405 microplate washer (BioTek), leaving 20 µL/well, followed by addition of 20 µL/ well 2× FluoZin-2 AM (164 nM final) indicator dye (Life Technologies, prepared as a DMSO stock and mixed in a 1:1 ratio with pluronic acid F-127) in Assay Buffer. After a 1 h incubation at room temperature, dye was exchanged with Assay Buffer, leaving 20 µL/well, and allowed to sit for 15 minutes. Thallium flux was measured at room temperature using a Functional Drug Screening System 7000 (FDSS 7000, Hamamatsu). Baseline readings were taken (2 images at 1 Hz; excitation, 470 ± 20 nm; emission, 540 ± 30 nm), and test compounds (2×) were added in a 20µL volume and incubated for 140 s before the addition of 10 µL of Thallium Buffer with or without agonist (5×). Data were collected for an additional 2.5 min and analyzed using using Dotmatics software (Bishops Stortford, Hertz, UK) using a four parameter logistical curve fit. For direct GIRK assays, methods were performed as described previously.[93]

In-Vitro DMPK Methods- Intrinsic Clearance in Liver Microsomes

Hepatic microsomes (0.5 mg/mL) and 1 µM test compound were incubated in 100 mM potassium phosphate pH 7.4 buffer with 3 mM $MgCl_2$ at 37 ºC with constant shaking. After a 5 min preincubation, the reaction was initiated by addition of NADPH (1 mM). At selected time intervals (0, 3, 7, 15, 25, and 45 min), 50 µL aliquots were taken and subsequently placed into a 96-well plate containing 150 µL of cold acetonitrile with internal standard (50 ng/mL carbamazepine). Plates were then centrifuged at 3000 rcf (4 ºC) for 10 min, and the supernatant was transferred to a separate 96-well plate and diluted 1:1 with water for LC/MS/MS analysis. The in vitro half-life ($T_{1/2}$, min, Eq. 1), intrinsic clearance (CL_{INT}, mL/min/kg, Eq. 2) and subsequent predicted hepatic clearance (CL_{HEP}, mL/min/kg, Eq. 3) were determined employing the following equations:

(1) $$T_{1/2} = \frac{Ln(2)}{k}$$

where k represents the slope from linear regression analysis of the natural log percent remaining of test compound as a function of incubation time

(2) $$CL_{int} = \frac{0.693}{in\ vitro\ T_{1/2}} x\ \frac{mL\ incubation}{mg\ microsomes}\ x\ \frac{45\ mg\ microsomes}{gram\ liver}\ x\ \frac{45^{a}\ gram\ liver}{kg\ body\ wt}$$

[a] species specific scale up factors

(3) $$CL_{hep} = \frac{Q_h \cdot CL\ int}{Q_h + CL\ int}$$

where Q_h = hepatic blood flow in each species.

Plasma Protein Binding

The protein binding of each compound was determined in plasma via equilibrium dialysis employing HTDialysis Teflon dialysis chamber and cellulose membranes (MWCO 12-14 K) (HTDialysis LLC, Gales Ferry, CT). Plasma was added to the 96-well plate containing test compound and mixed thoroughly for a final concentration of 5 µM. Subsequently, 150 µL of the plasma-compound mixture was transferred to the dialysis chamber, with an accompanying 150 µL of phosphate buffer (25 mM, pH 7.4) on the other side of the membrane. The device plate was sealed and incubated for 4 hours at 37 ºC with shaking. At completion, aliquots from each chamber were diluted 1:1 with either plasma (for the buffer sample) or buffer (for the plasma sample) and transferred to a new 96-well plate, at which time ice-cold acetonitrile containing internal standard (50 ng/mL carbamazepine) (2 volumes) was added to extract the matrices. The plate was centrifuged (3000 rcf, 10 min) and supernatants transferred and diluted 1:1 (supernatant: water) into a new 96 well plate, which was then sealed in preparation for LC/MS/MS analysis. Each compound was assayed in triplicate within the same 96-well plate. Fraction unbound was determined using the following equation:

$$F_u = \frac{Conc_{buffer}}{Conc_{plasma}}$$

Brain Homogenate Binding

The binding of each compound was determined in brain homogenate via equilibrium dialysis employing HTDialysis Teflon dialysis chamber and cellulose membranes (MWCO 12-14 K) (HTDialysis LLC, Gales Ferry, CT). Brain tissue homogenate was prepared by diluting one volume whole brain tissue with three volumes of phosphate buffer (25 mM, pH 7.4). The mixture was then subjected to mechanical homogenization employing a Mini-Beadbeater™ and 1.0 mm Zirconia/Silica Beads (BioSpec Products). Brain homogenate spiked with test compound and mixed thoroughly for a final concentration of 5 µM. Subsequently, 150 µL of the brain homogenate-compound mixture was transferred to the dialysis chamber with an accompanying 150 µL of phosphate buffer (25 mM, pH 7.4) on the other side of the membrane. The block was sealed and incubated for 6 hours at 37 ^{o}C with shaking. At completion, aliquots from each side of the chamber were diluted 1:1 with either brain homogenate (to the buffer side) or buffer (to the brain homogenate side) in a new 96 well plate, at which time ice-cold acetonitrile containing internal standard (50 ng/mL carbamazepine) was added to extract the matrices. The plate was centrifuged (3000 rcf, 10 min) and supernatants transferred and diluted 1:1 (supernatant: water) into a new 96 well plate, which was then sealed in preparation for LC/MS/MS analysis. Each compound was assayed in triplicate within the same 96-well plate. Fraction unbound was determined using the following equation:

$$F_{u,tissue} = \frac{1/D_f}{\left(\frac{1}{F_{u,hom}} - 1\right) + 1/D_f}$$

Where $F_{u,hom}$ represent the measured fraction unbound in the diluted homogenate and D_f represents dilution factor.

LC/MS/MS Analysis of Samples from In Vitro Assays

Samples were analyzed via electrospray ionization (ESI) on an AB Sciex API-4000 (Foster City, CA) triple-quadrupole instrument that was coupled with Shimadzu LC-10AD pumps (Columbia, MD) and a Leap Technologies CTC PAL auto-sampler (Carrboro, NC). Analytes were separated by gradient elution using a Fortis C18 3.0 x 50 mm, 3 µm column (Fortis Technologies Ltd, Cheshire, UK) thermostated at 40 ^{o}C. HPLC mobile phase A was 0.1% formic acid in water (pH unadjusted), mobile phase B was 0.1% formic acid in acetonitrile (pH unadjusted). The gradient started at 10% B after a 0.2 min hold and was linearly increased to 90% B over 1.2 min; held at 90% B for 0.1 min and returned to 10% B in 0.1 min followed by a re-equilibration (0.9 min). The total run time was 2.5 min and the HPLC flow rate was

0.5 mL/min. The source temperature was set at 500 ºC and mass spectral analyses were performed using multiple reaction monitoring (MRM), with transitions specific for each compound utilizing a Turbo-Ionspray® source in positive ionization mode (5.0 kV spray voltage).

In-Vivo PK Methods

All rodent PK experiments were conducted in accordance with the National Institute of Health regulations of animal care covered in Principles of Laboratory Animal Care (National Institutes of Health publication 85-23, revised 1985) and were approved by the Institutional Animal Care and Use Committee.

Discrete Rat PK and Tissue Distribution Studies

For discrete rat pharmacokinetic experiments, compounds were formulated in 10% EtOH/60% PEG400/30% saline (IV, 0.2 mg/kg) and in 10% Tween 80 in 0.5% MC (PO, 10 mg/kg) and dosed via the jugular vein to two dual-cannulated (carotid artery and jugular vein) adult male Sprague– Dawley rats (IV) or by oral gavage (PO). Whole blood collections via the carotid artery were performed at 0.033, 0.117, 0.25, 0.5, 1, 2, 4, 7, and 24 hours post dose and plasma samples prepared for bioanalysis. Tissue distribution studies were performed by formulating the compound in 10% Tween 80 in 0.5% MC and dosing via intraperitoneal injection (30 mg/kg) to male SD rats (n = S36 3-4 per time point). At 1 hr post dose, animals were euthanized and decapitated, blood was collected via cardiac puncture, CSF was obtained, and the brains were removed, thoroughly washed in cold phosphate-buffered saline, and immediately frozen on dry ice.

Plasma and Brain Sample Preparation

Plasma was separated by centrifugation (4000 rcf, 4 ºC) and stored at –80 ºC until analysis. On the day of analysis, frozen whole brains were weighed and diluted with 1:3 (w/w) parts of 70:30 isopropanol:water. The mixture was then subjected to mechanical homogenation employing a Mini-Beadbeater™ and 1.0 mm Zirconia/Silica Beads (BioSpec Products) followed by centrifugation. The sample extraction of plasma (20 μL), brain homogenate (20 μL), or CSF (where appropriate, 20 μL) was performed by a method based on protein precipitation using three volumes of ice-cold acetonitrile containing an internal standard (50 ng/mL carbamazepine). The samples were centrifuged (3000 rcf, 5 min) and supernatants transferred and diluted 1:1 (supernatant: water) into a new 96-well plate, which was then sealed in preparation for LC/MS/MS analysis.

LC/MS/MS Bioanalysis of Samples from In Vivo Assays

In vivo samples were analyzed via electrospray ionization (ESI) on an AB Sciex API-4000 (Foster City, CA) triple-quadrupole instrument that was coupled with Shimadzu LC-10AD pumps (Columbia, MD) and a Leap Technologies CTC PAL auto-sampler (Carrboro, NC). Analytes were separated by gradient elution using a Fortis C18 3.0 x 50 mm, 3 μm column (Fortis Technologies Ltd, Cheshire, UK) thermostated at 40 ºC. HPLC mobile phase A was 0.1% formic acid in water (pH unadjusted), mobile phase B was 0.1% formic acid in acetonitrile (pH unadjusted). The source temperature was set at 500 ºC and mass spectral analyses were performed using multiple reaction monitoring (MRM), with transitions specific for each compound utilizing a Turbo-Ionspray® source in positive ionization mode (5.0 kV spray voltage). The calibration curves were constructed, and linear response was obtained by spiking known amounts of test compound in blank brain homogenate or plasma. All data were analyzed using AB Sciex Analyst software v1.5.1. The final PK parameters were calculated by noncompartmental analysis using Phoenix (version 6.2) (Pharsight Inc., Mountain View, CA).

Challenges in the Development of a Selective mGlu$_{2/4}$ Heterodimer PAM

Initial Screen of mGlu$_4$ PAMs

A catalog of ~2,000 internally synthesized mGlu$_4$ PAMs was screened against the heterodimer receptor, with counter-screens against both mGlu$_2$ and mGlu$_4$ homodimers to probe scaffold selectivity. mGlu$_4$ PAMs were chosen, as opposed to mGlu$_2$ PAMs, due to the fact that we were able to measure the amount of mGlu$_4$ homodimer transfected in our cell lines by use of PHCCC. Adjustment of the amount of mGlu$_4$ transfected into the cell lines allowed for expression of a majority amount of heterodimer with a minimal expression of mGlu$_4$ homodimer. In contrast, we were unable to reduce the level of mGlu$_2$ homomers, limiting our ability to probe the activity of mGlu$_2$ PAMs due to a contaminating signal.

From numerous active compounds, VU0155041 (**1.1**) was chosen as a preliminary lead due to its similar potencies at both the heterodimer and mGlu$_4$ homodimer. This compound was first reported several years ago[94,95], and showed efficacy in *in vivo* models of Parkinson's disease, which is typical of mGlu$_4$

activation[96]. Soon after this report, Lundbeck published data on their work on Lu AF21934[97], which is the primary carboxamide congener of VU041. Though the potency and efficacy remain relatively unchanged, the replacement of the carboxylic acid with an uncharged congener in physiological systems allowed for a large improvement in brain penetrance, making it a more useful tool compound. Though the initial report indicated that SAR around this scaffold was steep, we hypothesized that the fact that the heterodimer exhibits different ligand selectivity relative to $mGlu_4$ homodimers means that the allosteric pocket must be different in shape. Because the allosteric pocket is different, it was worth treating it as a new receptor and fully interrogating the SAR.

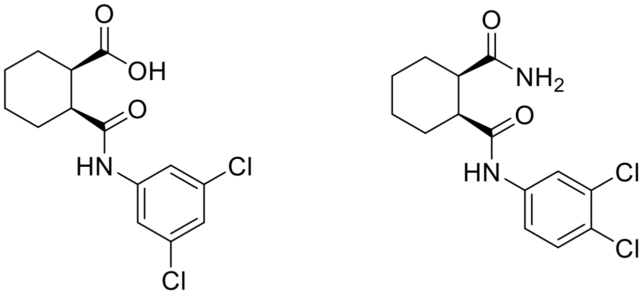
O
OH
O
HN
Cl
Cl
O
NH2
O
HN
Cl
Cl

VU0155041 (**1.1**)

LU AF21934 (**1.3**)

Figure 1.5 Initial screening hit (**1.1**) and structurally similar scaffold (**1.3**) with superior brain penetration.

SAR of VU041

Analogs of VU041 were synthesized in a rapid fashion from commercially available anhydrides following **scheme 1.1**. Briefly, the anhydride and

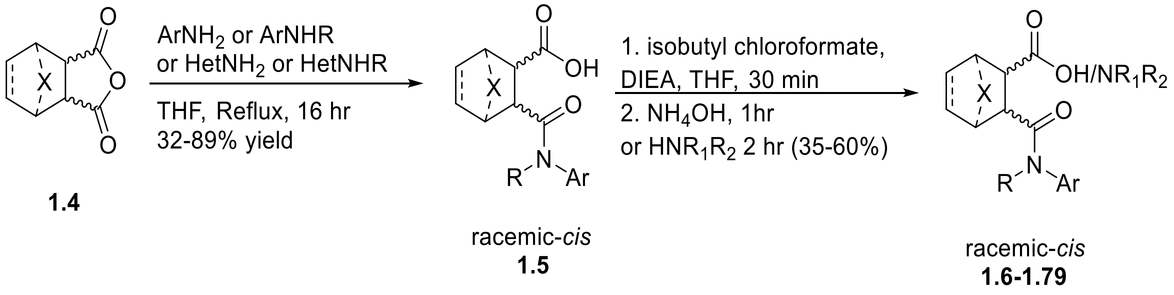
O
X
O
O
1.4
ArNH2 or ArNHR
or HetNH2 or HetNHR
THF, Reflux, 16 hr
32-89% yield
O
OH
X
O
R N Ar
racemic-cis
1.5
1. isobutyl chloroformate,
DIEA, THF, 30 min
2. NH4OH, 1hr
or HNR1R2 2 hr (35-60%)
O
OH/NR1R2
X
O
R N Ar
racemic-cis
1.6-1.79

Scheme 1.1: Route to synthesis of VU0155041 analogs.

corresponding amine were refluxed overnight in THF to give the carboxylic acid-amide intermediate. This compound proved somewhat non-trivial to convert to the corresponding amide, due to the propensity for this molecule to cyclize upon itself to form an imide if the acid was too activated or the initial amine nucleophile was too electron rich. Screening of several amide coupling reagents led to the discovery that formation of a mixed anhydride using isobutyl chloroformate and Hunig's base, followed by quenching with concentrated ammonium hydroxide for primary carboxamide congeners, or another amine nucleophile for further analogs. This resulted in a mixture of carboxylic acid and primary carboxamide, which was ideal as both analogs could be submitted for testing in our assay. Over 100 analogs were synthesized around the VU041 scaffold, revealing steep SAR that was observed in previous medicinal chemistry efforts. Initial modifications focused on changes to the substituents on the aniline ring used in the anhydride opening. No changes made to the aniline ring provided compounds that were superior in potency to the original hit, though some trends could be teased out from the data found. Halogens in the 3 and 4 positions of the aniline provided compounds that were active, with chlorine (**1.9, 1.10**) and bromine (**1.60**) being the most favorable. Converting from the 3,4-dichloroaniline to either the 2-amino-4,5-dichloropyridine (**1.58**) or 5-amino-2,3-dichloropyridine (**1.59**) also did not improve potency. The *N*-methyl analog of LUAF21934 also completely ablated activity, indicating that the secondary amide protons may play important roles in the activity of these compounds.

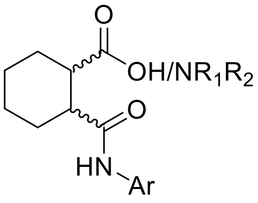

racemic-*cis*

Table 1.1. Structure for aryl analogs of VU0155041 **1.6-1.59** and associated potency and efficacy data from 10-point CRC-format screen at rat mGlu$_{2/4}$ cell lines. Tl^+ flux responses for each compound are reported as a percentage of the maximum response. VU number denotes the compound identifier assigned by Vanderbilt University. Data represent the mean of at least 3 replicate experiments with similar results.

Ar	**OH/NH$_2$**	**Compound Number**	**VUID**	**mGlu$_{2/4}$ EC$_{50}$ (μM)**	**mGlu$_{2/4}$ %Glu Max**
3,5-Cl, 4-F	OH	**1.6**	VU6006812	>10	58
3-Me, 4-F	OH	**1.7**	VU6006829	Inactive	
3-Cl	NH$_2$	**1.8**	VU6008057	2.9	31
4-Cl	NH$_2$	**1.9**	VU6008058	>10	58
3,5-Cl	NH$_2$	**1.10**	VU6008059	4.01	52
2,4-Cl	NH$_2$	**1.11**	VU6008061	Inactive	
3,4,5-F	NH$_2$	**1.12**	VU6008206	>10	30

3-Me, 4-F	NH_2	**1.13**	VU6008208	Inactive	
3-Cl, 4-CF_3	NH_2	**1.14**	VU6008924	>10	48
3-Me, 4-Cl	NH_2	**1.15**	VU6008926	Inactive	
3-Me, 4-Cl	NH_2	**1.16**	VU6008927	>10	33
3-Me, 4-OMe	NH_2	**1.17**	VU6008928	Inactive	
3-F, 4-CF_3	NH_2	**1.18**	VU6008930	>10	28
3-CF_3, 4-Cl	NH_2	**1.19**	VU6008931	Inactive	
3-CF_3, 4-Cl	OH	**1.20**	VU6008932	>10	35
3-F, 4-Cl	NH_2	**1.21**	VU6008933	>10	49
3-F, 4-Cl	OH	**1.22**	VU6008934	Inactive	
3-OMe, 4-CN	NH_2	**1.23**	VU6008935	Inactive	

3-OMe, 4-CN	OH	**1.24**	VU6008936	Inactive	
3-F, 4-F	OH	**1.25**	VU6008937	Inactive	
3-Cl, 4-OCF_3	NH_2	**1.26**	VU6008938	Inactive	
3-Cl, 4-OCF_3	OH	**1.27**	VU6008939	>10	40
3-F, 4-Me	OH	**1.28**	VU6008940	Inactive	
3-OMe, 4-Cl	NH_2	**1.29**	VU6008941	>10	33
3-OMe, 4-Cl	OH	**1.30**	VU6008942	Inactive	
3-CF_3, 4-Me	NH_2	**1.31**	VU6008944	Inactive	
3-CF_3, 4-Me	OH	**1.32**	VU6008945	Inactive	
3-Cl, 4-Me	NH_2	**1.33**	VU6008946	>10	28
3-Cl, 4-Me	OH	**1.34**	VU6008947	Inactive	

3-F, 4-OCF$_3$	NH$_2$	**1.35**	VU6008948	>10	23
3-F, 4-OCF$_3$	OH	**1.36**	VU60084949	Inactive	
3-CN, 4-Me	NH$_2$	**1.37**	VU6008951	Inactive	
3-Me, 4-CN	NH$_2$	**1.38**	VU6008954	Inactive	
3-CF$_3$, 5-CF$_3$	OH	**1.39**	VU6008955	Inactive	
3-Cl, 5-CF$_3$	OH	**1.40**	VU6008957	Inactive	
3-Cl, 5-CN	OH	**1.41**	VU6008959	Inactive	
3-CF$_3$, 5-CF$_3$	NH$_2$	**1.42**	VU6008955	Inactive	
3-OMe, 4-CF$_3$	OH	**1.43**	VU6008966	Inactive	
3-CN, 4-OMe	OH	**1.44**	VU6008967	Inactive	
3-CF$_3$, 4-F	NH$_2$	**1.45**	VU6008968	Inactive	

3-CF_3, 4-F	OH	**1.47**	VU6008969	Inactive
3-OMe, 4-Me	NH_2	**1.48**	VU6008970	Inactive
3-OMe, 4-Me	OH	**1.49**	VU6008971	Inactive
3-CN, 4-Cl	OH	**1.50**	VU6008972	Inactive
2,2-difluoro, 1,3-dioxole	NH_2	**1.51**	VU6008973	Inactive
2,2-difluoro, 1,3-dioxole	OH	**1.52**	VU6008974	Inactive
3-CF_3, 4-OMe	NH_2	**1.53**	VU6008975	Inactive
3-CF_3, 4-OMe	OH	**1.54**	VU6008976	Inactive
3-CN, 4-F	NH_2	**1.55**	VU6008977	Inactive
3-CN, 4-F	OH	**1.56**	VU6008978	Inactive
3-OMe, 4-F	OH	**1.57**	VU6008979	Inactive

2-N, 4,5-Cl	OH	**1.58**	VU6009645	Inactive	
3-N, 4,5-Cl	OH	**1.59**	VU6014324	>10	33
3-Br	NH_2	**1.60**	VU6014329	5.27	79

The modeling studies on $mGlu_4$ indicated the potential presence of some space in the binding pocket that was unoccupied by VU041 extending from the carboxylic acid portion of the molecule. Attempts to occupy this space through synthesis of substituted amides on the northern portion of the molecule proved ineffective, though the reason for the discrepancy between the modeling studies and obtained information is unknown.

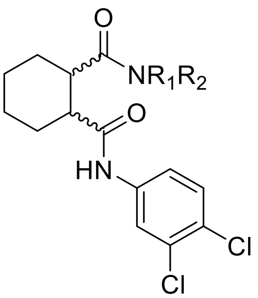

Table 1.2. Structure for amide analogs of VU0155041 **1.60-1.71** and associated potency and efficacy data from 10-point CRC-format screen at rat $mGlu_{2/4}$ cell lines. Tl^+ flux responses for each compound are reported as a percentage of the maximum response. VU number denotes the compound identifier assigned by Vanderbilt University. Data represent the mean of at least 3 replicate experiments with similar results.

HNR_1R_2	Compound Number	VUID	$mGlu_{2/4}$ EC_{50} (μM)	$mGlu_{2/4}$ %Glu Max
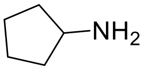	**1.60**	VU6009633	Inactive	
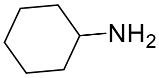	**1.61**	VU6009634	Inactive	
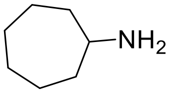	**1.62**	VU6009635	Inactive	
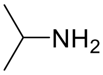	**1.63**	VU6009636	Inactive	
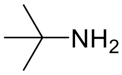	**1.64**	VU6008637	Inactive	
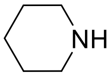	**1.65**	VU6009640	Inactive	
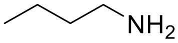	**1.66**	VU6009643	Inactive	
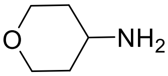	**1.67**	VU6009644	Inactive	
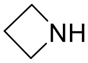	**1.68**	VU6009647	Inactive	
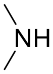	**1.69**	VU6009648	Inactive	

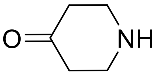	**1.70**	VU6009649	Inactive
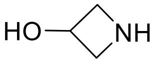	**1.71**	VU60014326	Inactive

With changes to the aniline ring and different amide substitutions proving ineffective in inducing potency or efficacy at the heterodimer, alterations were then made to the central core. Conversion of the *cis*-cyclohexane to the cyclohexene (**1.78**), *trans*-cyclohexane (**1.73**), or smaller ring sizes (**1.77**) resulted in a complete ablation of activity. We hypothesize that this is due to an induced fit model, where the conformation of the protein and the PAM may change such that they conform to fit each other and stabilize the active conformation. Restriction of this compound, either by rendering the ring less flexible with unsaturation or by changing the conformation with a *trans*-substitution, wherein both substituents can lie equatorial and the barrier to inversion is higher, resulted in ablation of activity. Additionally, we were able to confirm that the heterodimer also displayed an enantiomeric preference (**1.79**, **1.80**) by separation of racemic VU041 into the pure enantiomers using supercritical fluid chromatography (SFC).

Table 1.3. Structures for core analogs of VU0155041 **1.72-1.79** and associated potency and efficacy data from 10-point CRC-format screen at rat $\text{mGlu}_{2/4}$ cell lines. Stereocenters designated with * were resolved via chiral SFC separation and tested as single enantiomers of unknown configuration. Tl^+ flux responses for each compound are reported as a percentage of the maximum response. VU number denotes the compound identifier assigned by Vanderbilt University. Data represent the mean of at least 3 replicate experiments with similar results.

Structure	Compound Number	VUID	mGlu$_{2/4}$ EC$_{50}$ (µM)	mGlu$_{2/4}$ %Glu Max
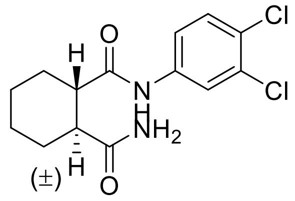	**1.72**	VU6009632	>10	51
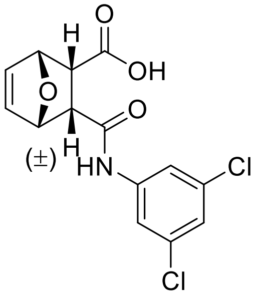	**1.73**	VU6007206	Inactive	
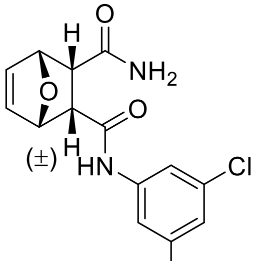	**1.74**	VU6008221	Inactive	
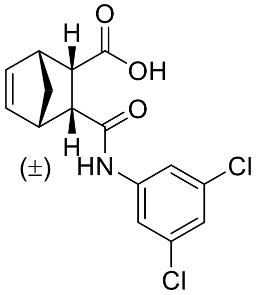	**1.75**	VU6007810	Inactive	
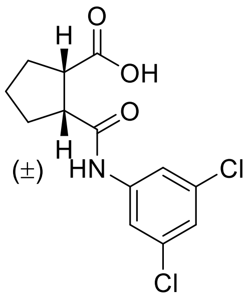	**1.76**	VU6009630	Inactive	

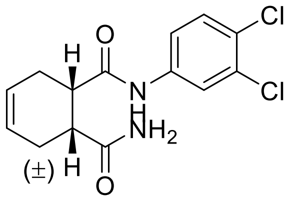	**1.77**	VU6009631	>10	44
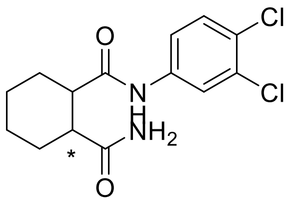	**1.78**	VU6008952	Inactive	
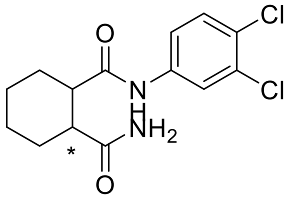	**1.79**	VU6008953	1.89	84

Screen of FDA Approved Drugs

Having determined that VU041 was an unproductive path towards synthesizing a selective mGlu$_{2/4}$ PAM, we decided to embark on a screening campaign in an attempt to discover a scaffold that was inherently selective for the heterodimer. A pilot screen was performed using a library of 1,152 structurally diverse drugs. Approved drugs make an ideal starting point for an SAR campaign due to the fact that they inherently have a good DMPK profile. This screening effort resulted in the

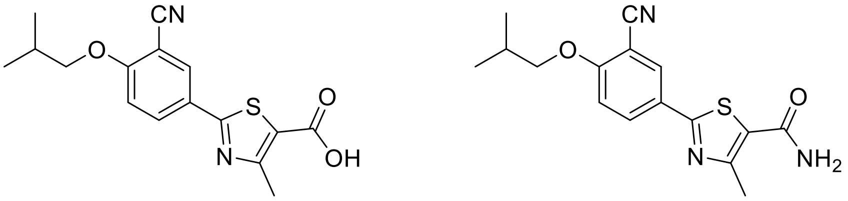

Febuxostat (1.80)
mGlu$_{2/4}$ EC$_{50}$= 3.38 μM
rat K$_p$= 0.03

VU6009638 (1.81)
mGlu$_{2/4}$ EC$_{50}$= 2.23 μM
rat K$_p$= 3.44

Figure 1.6. Initial hit (**1.80**) from a screen of FDA approved drugs and initial analog (**1.81**) with improved K$_P$.

discovery that Febuxostat (**1.80**), a xanthine-oxidase inhibitor used for the treatment of gout, had a weak activity of 3.38 μM, and displayed no activity against $mGlu_4$ in a G_{qi5} calcium assay. Unfortunately, this compound exhibited poor brain penetrance (K_p = 0.03), which was hypothesized to be due to the presence of the carboxylic acid moiety, which was a focus of our initial analog synthesis

Analogs were synthesized by a HATU-mediated coupling of commercially available Febuxostat (**1.80**) with various amines (**Scheme 1.2**). Conversion from the carboxylic acid to the primary carboxamide (VU6009638, **1.181**) proved to be a large improvement over the parent compound, increasing the potency to 2.2 μM and resulting in an ~100 fold improvement to the brain penetration (K_p = 3.44). Excitingly, when VU638 was screened against $mGlu_4$ in a calcium mobilization assay, it had no potentiation, which indicated that this chemotype had potential to be a selective 2/4 heterodimer PAM. However, when screened against HEK293 cell lines with a GIRK readout, this selectivity was lost. Next, this compound was screened against HEK293 cells that were not transfected with $mGlu_4$, $mGlu_2$, or $mGlu_{2/4}$, and activity was observed, which indicated that these compounds were direct GIRK activators. While VU638 was inactive in cell lines expressing GIRK2 homodimers, it was efficacious against GIRK1 containing cells lines (GIRK1/2, GIRK1/4).

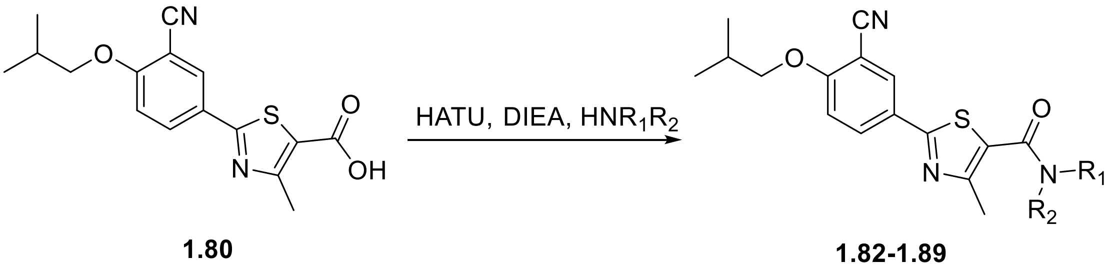

Scheme 1.2: Route to synthesis of Febuxostat analogs.

Despite this setback, a small library of amide analogs was synthesized and screened to determine their activity against the 2/4 heterodimer and to determine if we were able to modulate activity between GIRK and mGlu receptors. Excitingly, three compounds were found to be active against the heterodimer, VU6009964, VU6009958, and VU6009967, with corresponding activities of 5.2, 2.3, and 0.76 μM (35, 24 and 28% Glu max, **Table 1.4**). Initial screen against GIRK expressing cell lines proved promising, with indication of direct GIRK activation. However, these analogs proved to be weak potentiators of $mGlu_{2/4}$, and additionally, were not selective due to comparable activity at $mGlu_2$ homodimers (4.8 μM 73% Glu max, 2.4 μM 53% Glu max, 0.77 μM 57% Glu max). Due to our inability to determine the amount of $mGlu_2$ homodimer in our cell lines, and comparable activities between the $mGlu_{2/4}$ and $mGlu_2$ cell lines, it is likely that this activity is mostly driven by $mGlu_2$ homodimers. With this in mind, the secondary and tertiary amides of **1.80** are better characterized as $mGlu_2$ PAMs. In addition, the elimination of the carboxylic acid from these compounds proved detrimental to the favorable DMPK properties of these compounds, with high predicted hepatic clearance in both human and rat liver microsomes (human CL_{hep} >14 mL/min/kg, rat CL_{hep} >62 mL/min/kg). Due to these complications, the further development of this chemotype as $mGlu_{2/4}$ heterodimer PAMs was not pursued.

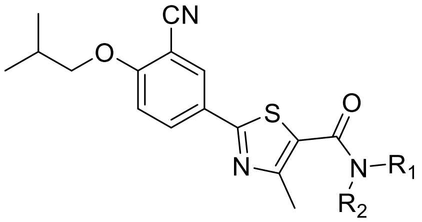

Table 1.4. Structures for amide analogs of Febuxostat **1.82-1.89** focused on amide synthesis for improvement of brain penetration and potency/efficacy over the original hit. Associated potency and efficacy data from 10-point CRC-format screen at rat mGlu$_{2/4}$ cell lines. Tl$^+$ flux responses for each compound are reported as a percentage of the maximum response. VU number denotes the compound identifier assigned by Vanderbilt University. Data represent the mean of at least 3 replicate experiments with similar results.

NR$_1$R$_2$	**Compound Number**	**VUID**	**mGlu$_{2/4}$ EC$_{50}$**	**mGlu$_{2/4}$ % Glu max**
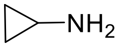	**1.82**	VU6009940	Inactive	
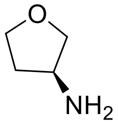	**1.83**	VU6009942	Inactive	
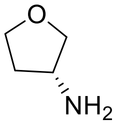	**1.84**	VU6009944	Inactive	
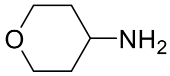	**1.85**	VU6009953	5.29	35
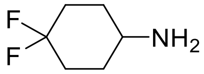	**1.86**	VU6009958	2.03	24
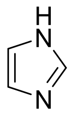	**1.87**	VU6009962	Inactive	

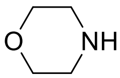	**1.88**	VU6009964	>10	57
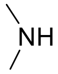	**1.89**	VU6009967	0.76	28

High-Throughput Screening Campaign

In order to discover new chemical matter that could result in a selective PAM for the $mGlu_{2/4}$ heterodimer, a high-throughput screening (HTS) campaign was commenced. This was run using the VICB collection of ~100,000 compounds and were run a single-point format, meaning a single 10 μM concentration of compound was tested to determine efficacy. First, compounds were screened against the heterodimer, then active compounds were tested in cell lines expressing either $mGlu_2$ or $mGlu_4$ homodimers to determine the selectivity of these compounds. However, due to the length of time that is required for an HTS campaign, active hits in the heterodimer cell line with attractive scaffolds for medicinal chemistry were resynthesized along with small libraries of analogs to both determine the selectivity and if there was any SAR around the new chemotype. The results of this work are detailed below.

VU6010417

The first hit explored was azetidinyl 1,2,4-oxadiazole VU6010417, which was an attractive scaffold for medicinal chemistry due to the ease of access to diverse analogs. It was synthesized by a one pot microwave mediated condensation reaction between commercially available benzamidoximes (**1.90-1.91, Scheme 1.3**) with 1-Boc-azetidine-3-carboxylic acid to yield Boc-protected 1,2,4-oxadiazole (**1.93-1.94**). Next, Boc-deprotection with trifluoroacetic acid gave the free amine in 45% over the two steps. Finally, HATU-mediated amide coupling with thiophene-2-carboxylic acid gave VU6010417 in 17% yield. Using this synthetic strategy, a diverse library of compounds was synthesized by varying the substituent on the Eastern arene (3-Cl and 3-CF_3), utilizing various 5-membered heterocyclic acids in the HATU-coupling reaction with the intermediate azetidine, and by varying the nature of the central ring to determine the necessity of the azetidine for activity.

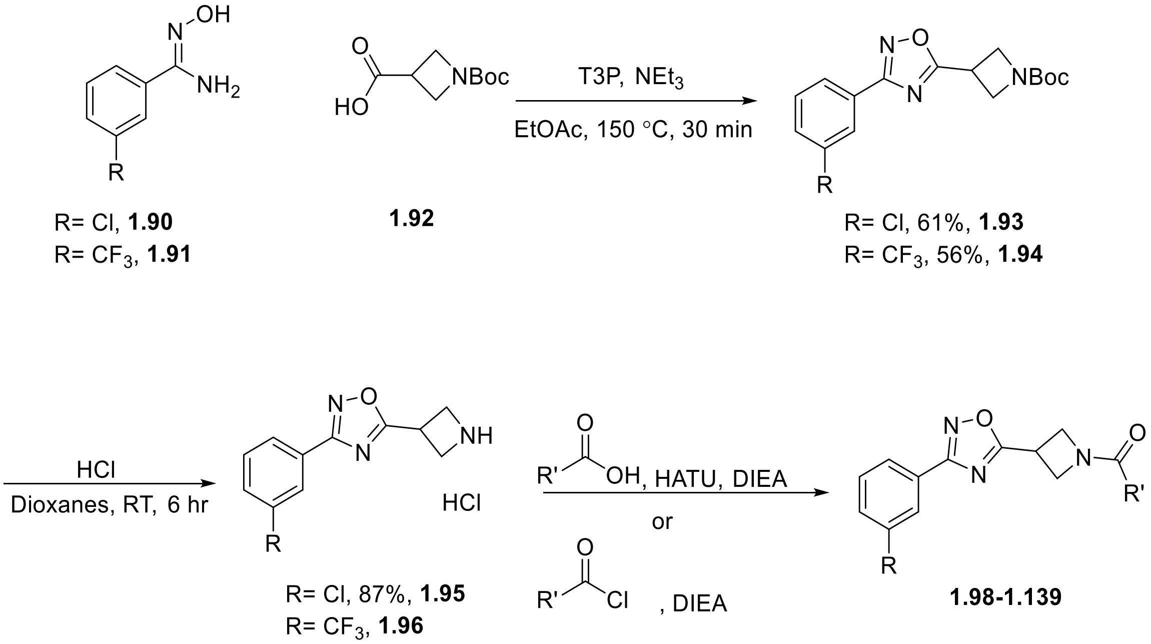

R= Cl, 1.90
R= CF3, 1.91
1.92
T3P, NEt3
EtOAc, 150 °C, 30 min
R= Cl, 61%, 1.93
R= CF3, 56%, 1.94
HCl
Dioxanes, RT, 6 hr
HCl
R= Cl, 87%, 1.95
R= CF3, 1.96
HATU, DIEA
or
, DIEA
1.98-1.139

Scheme 1.3: Route for rapid synthesis of analogs of VU6010417 focusing on aryl amide analogs of the Eastern aryl ring.

The initial hit exhibited a potency of 2.11 μM and 99% Glu max, which was a promising start for analog synthesis and optimization. Moving the thiophene substitution from the 2- to the 3-position resulted in a similar potency of 2.02 μM, but a drastic decrease in efficacy to 60% Glu max. Surprisingly, conversion of the 5-membered heterocycle to an oxazole, thiazole, and furan provided compounds that were either greater than 10 μM or exhibited diminished activity in comparison to the original hit. Because thiophenes are considered to be bioisosteres of phenyl rings, the thiophene was replaced with a phenyl ring to determine if this analog had better interactions with the target protein. However, this strategy also proved inefficacious, with both the chloro and trifluoromethyl analogs exhibiting potencies greater than 10 μM, though they did exhibit good efficacy at 108% Glu max for the chloro analog and 101% Glu max for the trifluoromethyl. Replacement of the chlorine of the aryl ring to the trifluoromethyl group resulted in an increase in potency to 1.10 μM and a massive increase in efficacy, 156% Glu max. Excitingly, an additional 4 analogs exhibited activities greater than the parent compound. Addition of a fluorine atom to the three position of the thiophene proved favorable, almost doubling the potency to 1.14 μM and 103% Glu max. Interestingly, a 2-carboxy-3-methly furan substituent gave the best overall potency of 1.02 μM and 94% Glu max. A 2-cyclopropyl-3-carboxyl substituted furan exhibited a potency of 1.28 μM and 85% Glu max, which corresponds with analogs seen before wherein the 3-substituted furan was superior to the 2-substitution. Finally, 3-carboxy-5-methyl thiophene resulted in a potency of 1.13 μM and 56% Glu max. Of special focus in these analogs was substituents in the 2 and 5 positions of these heterocycles, as these are hot spots for metabolism, and substituting these positions can block this metabolism and give a better DMPK profile.

Unfortunately, analysis of these compounds in cell lines expressing mGlu$_2$ homodimer revealed that these analogs were also able to potentiate activity at these receptors. Additionally, the potency and efficacy at the homodimer were much better than at the heterodimer, typically being twice as potent at the homodimeric receptor and with improved efficacy as well. The two best analogs, VU6017122 and VU6017139, were submitted for DMPK analysis, and exhibited moderate clearance in both human and rat. Both analogs exhibited poor free fraction, at less than 1% (0.4% and 0.5% respectively). Surprisingly, there was a drastic difference in the brain penetration for these two analogs, with VU122 having a moderate K$_p$ of 0.99 and VU139 having a favorable distribution into the brain of 2.44.

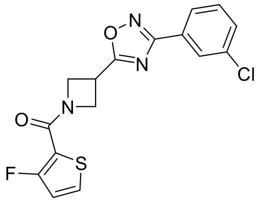

VU6017122
EC$_{50}$ mGlu$_2$= 402 nM
59% Glu$_{max}$

EC$_{50}$ mGlu$_{2/4}$= 1.14 μM
103% Glu$_{max}$

Human CL$_{Hep}$= 10.7 (51.2% max) mL/min/kg
Rat CL$_{Hep}$= 57.1 (67.3% max) mL/min/kg
f$_u$=0.4%
K$_p$=0.99

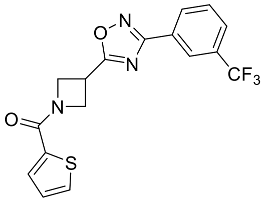

VU6017139
EC$_{50}$ mGlu$_2$= 496 nM
85% Glu$_{max}$

EC$_{50}$ mGlu$_{2/4}$= 1.10 μM
156% Glu$_{max}$

Human CL$_{Hep}$= 13.6 (65% max) mL/min/kg
Rat CL$_{Hep}$= 53.5 (63.1% max) mL/min/kg
f$_u$=0.5%
K$_p$=2.44

Figure 1.7. DMPK properties of two of the best analogs synthesized around the VU6010417 scaffold. These compound exhibited moderate clearance, poor free fraction, and moderate to good brain penetration.

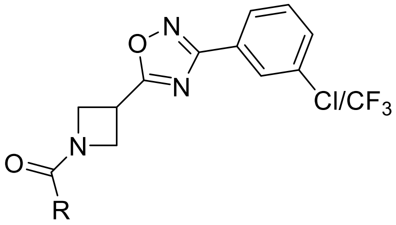

Table 1.5. Structures for azetidinyl amide analogs **1.97-1.134** of VU6010417 focused on amide synthesis for improvement of potency and efficacy, along with analysis of selectivity for mGlu$_{2/4}$. Asociated potency and efficacy data from 10-point CRC-format screen at rat mGlu$_{2/4}$ cell lines. Tl$^+$ flux responses for each compound are reported as a percentage of the maximum response. VU number denotes the compound identifier assigned by Vanderbilt University. Data represent the mean of at least 3 replicate experiments with similar results.

R	Cl/CF$_3$	Compound Number	VUID	mGlu$_{2/4}$ EC$_{50}$ (μM)	mGlu$_{2/4}$ %Glu Max	mGlu$_2$ EC$_{50}$ (μM)	mGlu$_2$ %Glu Max
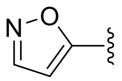	Cl	**1.97**	VU0531026	Inactive		Inactive	
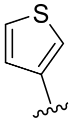	Cl	**1.98**	VU0531042	2.02	60	1.16	92
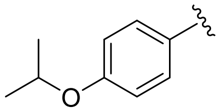	CF$_3$	**1.99**	VU0531089	>10	48	>10	60
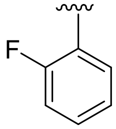	CF$_3$	**1.100**	VU0531090	>10	44	>10	82
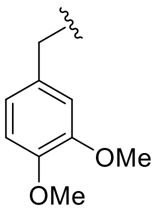	CF$_3$	**1.101**	VU0531097	>10	50	>10	84
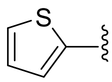	Cl	**1.102**	VU6010417	2.50	55	1.89	123

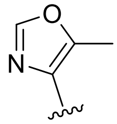	Cl	**1.103**	VU6010418	>10	40	4.85	65
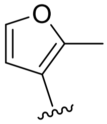	Cl	**1.104**	VU6010419	2.31	75	1.95	112
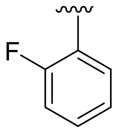	Cl	**1.105**	VU6010420	6.94	36	2.85	59
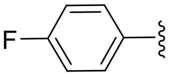	Cl	**1.106**	VU6010421	9.01	62	2.63	91
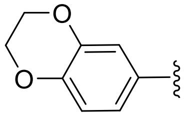	Cl	**1.107**	VU6010422	>10	30	3.09	54
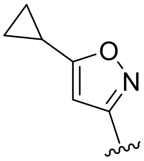	Cl	**1.108**	VU6010423	>10	26	6.68	47
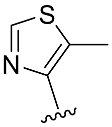	Cl	**1.109**	VU6010424	>10	30	3.33	55
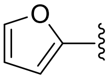	Cl	**1.110**	VU6010754	5.63	46	5.19	62
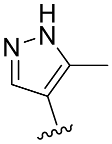	Cl	**1.111**	VU6010755	>10	29	>10	45
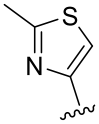	Cl	**1.112**	VU6010756	>10	34	4.77	47
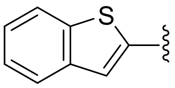	Cl	**1.113**	VU6010757	Inactive		Inactive	

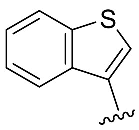	Cl	**1.114**	VU6010758	Inactive		Inactive	
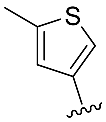	Cl	**1.115**	VU6010759	5.37	48	4.40	87
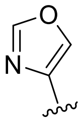	Cl	**1.116**	VU6010760	>10	36	>10	46
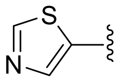	Cl	**1.117**	VU6010761	>10	52	>10	73
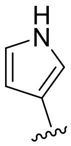	Cl	**1.118**	VU6010762	7.41	44	4.15	55
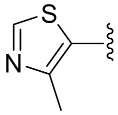	Cl	**1.119**	VU6010763	>10	23	4.09	39
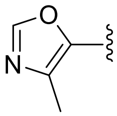	Cl	**1.120**	VU6010764	1.13	56	0.91	71
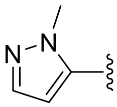	Cl	**1.121**	VU6010765	>10	30	>10	58
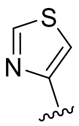	Cl	**1.122**	VU6010766	>10	33	>10	51
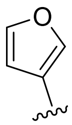	Cl	**1.123**	VU6010767	5.21	55	3.59	58
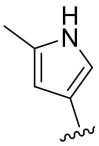	Cl	**1.124**	VU6010768	>10	50	8.64	62

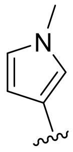	Cl	**1.125**	VU6010769	>10	55	>10	90
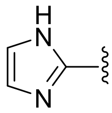	Cl	**1.126**	VU6010770	Inactive		Inactive	
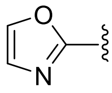	Cl	**1.127**	VU6010771	>10	48	6.42	69
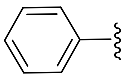	Cl	**1.128**	VU6017115	8.81	43	6.25	108
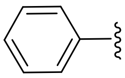	CF_3	**1.129**	VU6017116	4.92	37	2.42	84
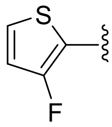	Cl	**1.130**	VU6017122	0.71	35	0.90	81
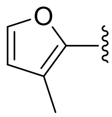	Cl	**1.131**	VU6017126	1.43	56	1.02	94
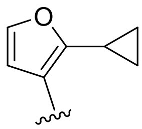	Cl	**1.132**	VU6017127	2.94	54	1.28	85
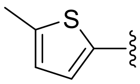	Cl	**1.133**	VU6017138	3.33	43	2.64	93
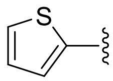	CF_3	**1.134**	VU6017139	0.496	85	1.10	156

Despite these setbacks for this chemotype as $mGlu_{2/4}$ heterodimer PAMs, further analog synthesis was pursued to explore its potential as an $mGlu_2$ PAM. Though these analogs exhibited moderate DMPK values, the subnanomolar potency of some analogs led us to want to pursue further analog synthesis. It was hypothesized that the azetidine moiety may potentially be a source of metabolic liability due to its relatively low chemical stability, especially under acidic conditions. Replacement of the azetidine with a pyrrolidine (**1.130**) and piperidine (**1.131**) moieties resulted in complete ablation of activity. Additionally, changing from the 3-substituted azetidine to the 2-substituted analog (**1.132**) resulted in inactive compounds. Synthesis of uncyclized analogs, both with 1 (**1.133**) and 2 (**1.134**) carbons between the 1,2,4-oxadiazole and the amine, resulted in compounds that were low potency, though exhibited moderate efficacy at 56% Glu max.

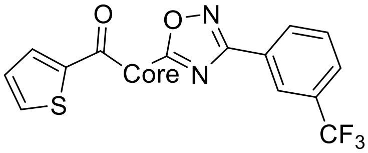

Table 1.6. Structures for azetidine replacement analogs **1.135-1.139** of VU6010417 for the improvement of clearance, free fraction, and selectivity. Associated potency and efficacy data from 10-point CRC-format screen at rat $mGlu_{2/4}$ cell lines. Tl^+ flux responses for each compound are reported as a percentage of the maximum response. VU number denotes the compound identifier assigned by Vanderbilt University. Data represent the mean of at least 3 replicate experiments with similar results.

Core	Compound Number	VUID	$mGlu_{2/4}$ EC_{50} (µM)	$mGlu_{2/4}$ %Glu Max	$mGlu_2$ EC_{50} (µM)	$mGlu_2$ %Glu Max
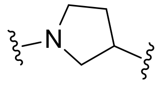	**1.135**	VU6017144	2.44	56	3.09	83
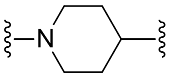	**1.136**	VU6017145	>10	39	>10	78

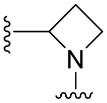	**1.137**	VU6017146	>10	37	>10	44
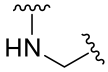	**1.138**	VU6017147	>10	60	>10	57
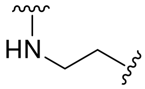	**1.139**	VU6017149	>10	63	>10	69

VU6010427

The next hit of interest was 1,3,4-oxadiazole VU6010427 (VU427), which again had a scaffold amenable to rapid analog synthesis and was a novel chemotype for potentiation of mGlu receptors. First, condensation of commercially available 4-methyl-benzhydrazide with cyanogen bromide gave known intermediate amino-1,3,4-oxadiazole (**1.142**)[98,99]. Next, amide formation with substituted benzoic acids via a HATU-mediated amide coupling gave the final compound (**1.143-1.153**). Using this synthetic route, a small library of 11 analogs of the aryl carboxylic was synthesized to explore the selectivity of this scaffold. Interestingly, as observed in the work around VU041, this scaffold also was most potent with a chlorine substituent (**1.145**), which may indicate that these two scaffolds bind in a similar

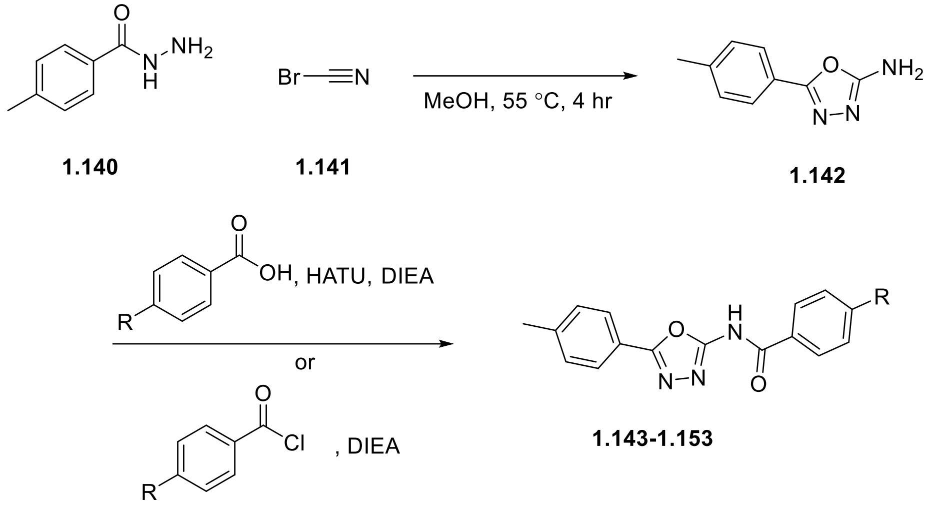

Scheme 1.4: Synthetic route for the synthesis of Eastern aryl replacements for VU6010427.

manner. Unfortunately, it was more potent at the $mGlu_4$ homodimer than at the $mGlu_{2/4}$ heterodimer (259 nM, 102% Glu max vs 386 nM 120% Glu max, respectively). Of interest, however, is that this was the first scaffold we observed that was active in cells expressing all three receptor populations, though the potency and efficacy were diminished at $mGlu_2$. From the data we have obtained, it is difficult to determine if this is due to off-target potentiation of GIRK proteins, as seen in Febuxostat, or if this compound is able to potentiate $mGlu_2$, $mGlu_4$, and $mGlu_{2/4}$. These compounds are currently being studied in the Weaver lab, where it has been determined that there is an off-target effect that is causing a false positive in our assays. Though the exact identity of the target is not yet known, we know that it is a protein that allows for thallium flux outside of GIRK activation.

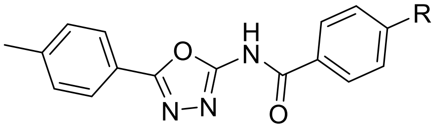

Table 1.7. Varied aryl substitution analogs of the Eastern ring on scaffold VU6010427, along with selectivity data across all three cell lines (both homodimers and heterodimer). Associated potency and efficacy data from 10-point CRC-format screen at rat mGlu$_{2/4}$ cell lines. Tl$^+$ flux responses for each compound are reported as a percentage of the maximum response. VU number denotes the compound identifier assigned by Vanderbilt University. Data represent the mean of at least 3 replicate experiments with similar results.

R	**Compound Number**	**VUID**	**mGlu$_{2/4}$ EC$_{50}$ (μM)**	**mGlu$_{2/4}$ %Glu Max**	**mGlu$_2$ EC$_{50}$ (μM)**	**mGlu$_2$ %Glu Max**	**mGlu$_4$ EC$_{50}$ (μM)**	**mGlu$_4$ %Glu Max**
F	**1.143**	VU6010425	2.04	113	1.52	96	2.65	96
CF$_3$	**1.144**	VU6010426	>10	73	>10	67	>10	42
Cl	**1.145**	VU6010427	1.60	87	1.80	83	3.76	83
OCF$_3$	**1.146**	VU6010428	>10	77	>10	86	>10	52
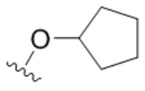	**1.147**	VU6010429	Inactive		Inactive		Inactive	
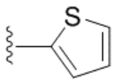	**1.148**	VU6010430	>10	55	>10	55	>10	25
CN	**1.149**	VU6010431	>10	23	>10	32	>10	18

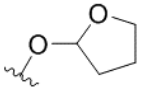	**1.150**	VU6010432	Inactive		Inactive		Inactive	
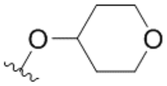	**1.151**	VU6010433	Inactive		Inactive		Inactive	
CHF_2	**1.152**	VU6010434	>10	57	>10	63	>10	35
H	**1.153**	VU6010435	>10	48	>10	60	>10	20

VU0495443

The next hit synthesized was aryl pyridone scaffold VU0495443. Synthesis began with methyl 6-hydroxynicotinate, which was alkylated with 3-(trifluoromethyl)benzyl bromide in DMF provided the desired *N*-alkylated material in 64% yield (**Scheme 1.5**). Saponification gave the necessary acid in 33% yield, which

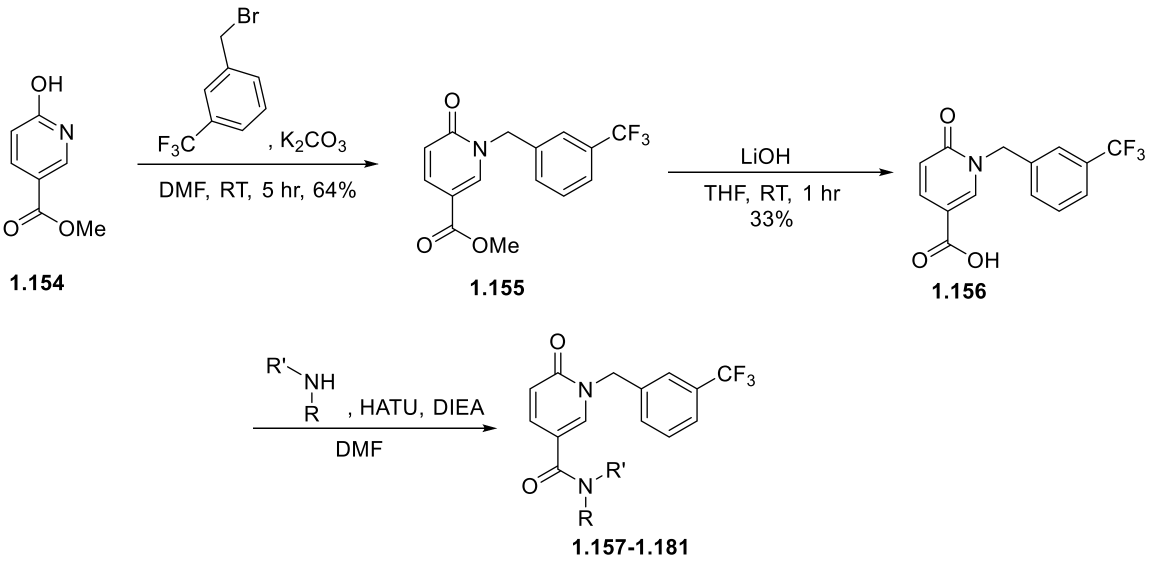
1.154
, K_2CO_3
DMF, RT, 5 hr, 64%
1.155
LiOH
THF, RT, 1 hr
33%
1.156
, HATU, DIEA
DMF
1.157-1.181

Scheme 1.5: Synthesis of southern aryl analogs of VU0495443 **1.157-1.181**.

was followed by HATU-mediated amide couplings with varying substituted benzoic acids gave analogs (**1.157-1.181**). As seen with previous heterodimer scaffolds, VU443 exhibited very steep SAR, with most structural modifications exhibiting no activity altogether. The initial hit, the 2-methyl carboxylate (**1.159**), exhibited modest activity at 8.5 μM and 42% Glu max. Keeping with electron withdrawing groups in the 2-position, the 2-trifluoromethoxybenzene analog (**1.162**) was synthesized, which almost doubled the potency to 5.38 μM and 43% Glu max. Interestingly, cyclization of the amide onto the benzene ring by amide coupling with indoline (**1.161**) was the most potent analog synthesized at 3.50 μM and 40% Glu max at the heterodimer. Unfortunately, this scaffold was equally or more potent at the $mGlu_2$ homodimer, which precluded it from further optimization.

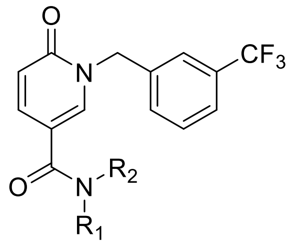

Table 1.8. Southern amide analogs **1.157-1.181** of VU0429553 focused on understanding potency/efficacy at $mGlu_{2/4}$ and selectivity against a $mGlu_2$ homodimer cell line. Associated potency and efficacy data from 10-point CRC-format screen at rat $mGlu_{2/4}$ cell lines. Tl^+ flux responses for each compound are reported as a percentage of the maximum response. VU number denotes the compound identifier assigned by Vanderbilt University. Data represent the mean of at least 3 replicate experiments with similar results.

NR_1R_2	Compound Number	VUID	$mGlu_{2/4}$ EC_{50} (μM)	$mGlu_{2/4}$ %Glu Max	$mGlu_2$ EC_{50} (μM)	$mGlu_2$ %Glu Max
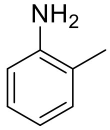	**1.157**	VU0495433	Inactive		Inactive	
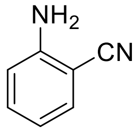	**1.158**	VU0495439	Inactive		Inactive	

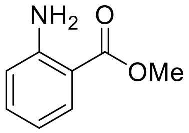	**1.159**	VU0495443	4.48	65	8.48	42
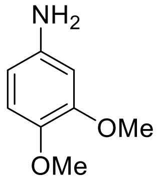	**1.16**	VU0495445	Inactive		Inactive	
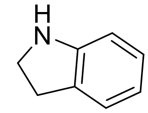	**1.161**	VU0495454	3.5	40	3.44	61
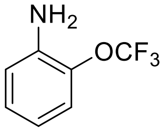	**1.162**	VU6010548	5.38	43	4.5	66
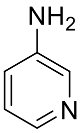	**1.163**	VU6010549	Inactive		Inactive	
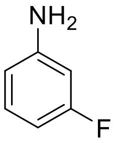	**1.164**	VU6010552	Inactive		Inactive	
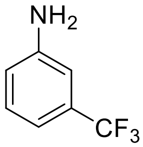	**1.165**	VU6010553	Inactive		Inactive	
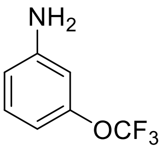	**1.166**	VU6010554	Inactive		Inactive	

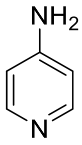	**1.167**	VU6010555	Inactive	Inactive
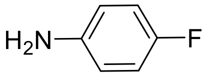	**1.168**	VU6010556	Inactive	Inactive
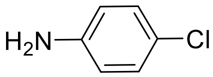	**1.169**	VU6010557	Inactive	Inactive
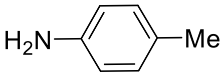	**1.170**	VU6010558	Inactive	Inactive
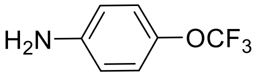	**1.171**	VU6010560	Inactive	Inactive
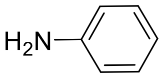	**1.172**	VU6010561	Inactive	Inactive
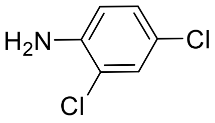	**1.173**	VU6010562	Inactive	Inactive
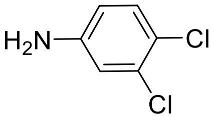	**1.174**	VU6010563	Inactive	Inactive
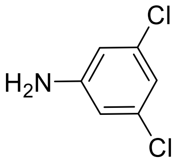	**1.175**	VU6010564	Inactive	Inactive

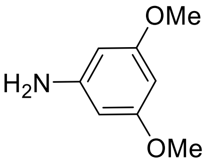	**1.176**	VU6010565	Inactive	Inactive	
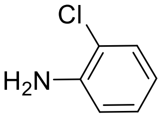	**1.177**	VU6010566	Inactive	Inactive	
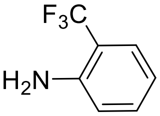	**1.178**	VU6010567	Inactive	Inactive	
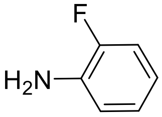	**1.179**	VU6010568	Inactive	Inactive	
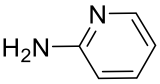	**1.180**	VU6010569	Inactive	Inactive	
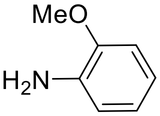	**1.181**	VU6010570	Inactive	>10	55

VU6009122

Due to its exceptional potency and interesting chemical structure, the positive control used in mGlu$_2$ screening, *N*-(4′-cyano[1,1′-biphenyl]-3-yl)-*N*-(3-pyridinylmethyl)-ethanesulfonamide hydrochloride (CBiPES), was explored for its selectivity. Analogs were synthesized according to the route shown in **scheme 1.6**. Briefly, Suzuki cross-coupling between 3-iodoaniline and 4-cyanobenzene boronic accomplished by first refluxing the intermediate aniline and varying benzaldehydes in methanol, followed by cooling and reduction via addition of sodium borohydride. Quench and workup of this material gave the crude product in sufficient purity to accomplish sulfonamide formation by addition of pyridine and ethanesulfonyl acid gave known intermediate (**1.184**) in 70% yield[100]. Next, reductive amination was chloride to the crude residue in DCE, giving desired materials in 5-20% yield. We primarily focused on the pyridine portion of this molecule to determine if there was SAR around this molecule and if there was any inherent selectivity. There was some texture to the SAR around the pyridine ring, with addition of a fluorine and methoxy group to this position being tolerated, though the fluorine was superior. Conversion of the pyridine ring to a pyrimidine was done to allow for any rotational conformational of the ring to have a nitrogen present in the meta position, which would hypothetically mean that there are more rotations of that ring in which favorable interactions with the protein are present. However, the pyrimidine analog did not prove to be superior to the original hit. Replacement of the pyridine ring with a thiazole resulted in a compound ~2 weaker than the original hit. Finally, replacement of the pyridine nitrogen with a fluorine atom, to mimic the electron withdrawing nature of the pyridine while removing the hydrogen bond acceptor, resulted in a completely inefficacious compound in either cell line. This combined with the good potency of the thiazole gives strong evidence that a basic

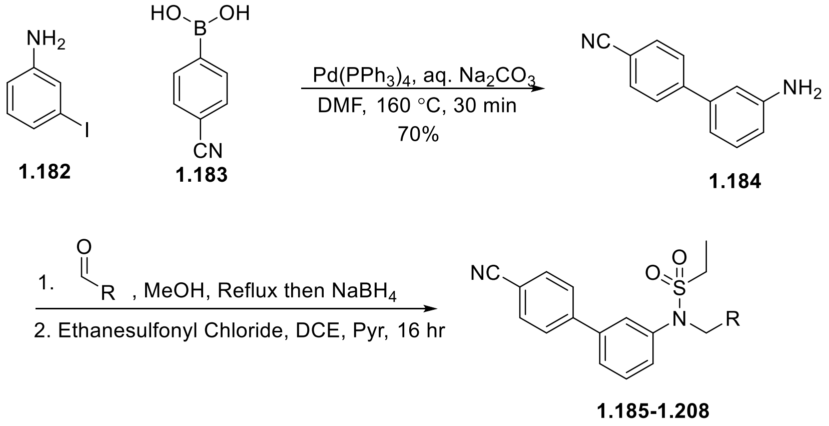

Scheme 1.6: Synthesis of benzylamine analogs of mGlu$_2$ PAM CBiPES **1.185-1.208**.

nitrogen on this portion of the molecule was required for activity.

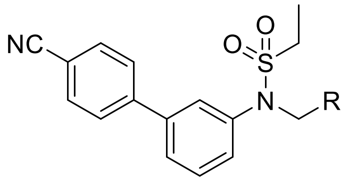

Table 1.9. Structures of benzylamine analogs of VU6009122 for the determination of scaffold selectivity against mGlu$_2$ and initial analysis of potency and efficacy. Associated potency and efficacy data from 10-point CRC-format screen at rat mGlu$_{2/4}$ cell lines. Tl$^+$ flux responses for each compound are reported as a percentage of the maximum response. VU number denotes the compound identifier assigned by Vanderbilt University. Data represent the mean of at least 3 replicate experiments with similar results.

R	**Compound Number**	**VUID**	**mGlu$_{2/4}$ EC$_{50}$ (nM)**	**mGlu$_{2/4}$ %Glu Max**	**mGlu$_2$ EC$_{50}$ (nM)**	**mGlu$_2$ %Glu Max**
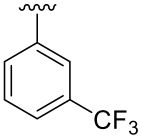	**1.185**	VU6012561	Inactive		Inactive	
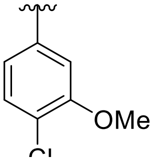	**1.186**	VU6012571	Inactive		Inactive	
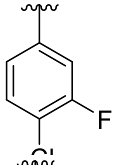	**1.187**	VU6012573	Inactive		Inactive	
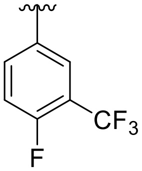	**1.188**	VU6012574	Inactive		Inactive	
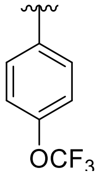	**1.189**	VU6012577	Inactive		Inactive	
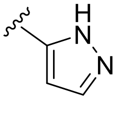	**1.19**	VU6012578	Inactive		Inactive	

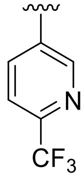	**1.191**	VU6012579	Inactive		Inactive	
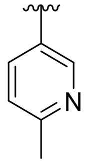	**1.192**	VU6012583	Inactive		Inactive	
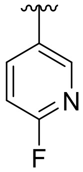	**1.193**	VU6012584	424	66	230	83
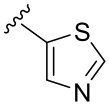	**1.194**	VU6012586	157	74	108	92
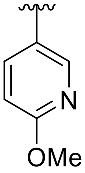	**1.195**	VU6012588	>10,000	50	4,490	73
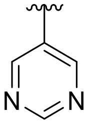	**1.196**	VU6012589	246	69	148	89
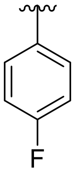	**1.197**	VU6012590	Inactive		Inactive	
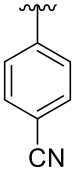	**1.198**	VU6012591	Inactive		Inactive	
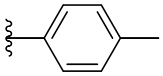	**1.199**	VU6012592	Inactive		Inactive	

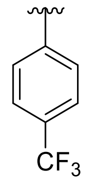	**1.200**	VU6012593	Inactive	Inactive
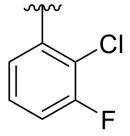	**1.201**	VU6012594	Inactive	Inactive
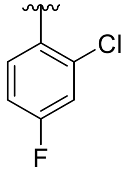	**1.202**	VU6012595	Inactive	Inactive
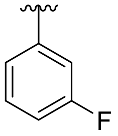	**1.203**	VU6012596	Inactive	Inactive
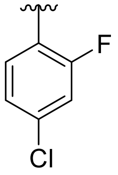	**1.204**	VU6012597	Inactive	Inactive
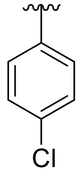	**1.205**	VU6012598	Inactive	Inactive
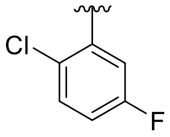	**1.206**	VU6012599	Inactive	Inactive
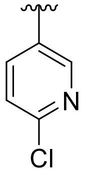	**1.207**	VU6012600	Inactive	Inactive
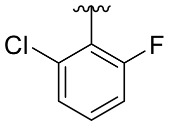	**1.208**	VU6012601	Inactive	Inactive

Using the same chemistry as shown in **scheme 1.6**, but replacing ethanesulfonyl chloride with trifluoroethylsulfonyl chloride allowed for synthesis of compounds **1.209-1.210**. While these analogs retained the good potency of the parent compound (**1.194**), the conversion to the trifluoroethyl sulfonamide resulted in a large decrease in the efficacy for this scaffold.

Table 1.10. Structures of two trifluoroethyl sulfonamide analogs, wherein the conversion from ethyl to trifluoroethyl caused a drastic drop in efficacy. Associated potency and efficacy data from 10-point CRC-format screen at rat mGlu$_{2/4}$ cell lines. Tl$^+$ flux responses for each compound are reported as a percentage of the maximum response. VU number denotes the compound identifier assigned by Vanderbilt University. Data represent the mean of at least 3 replicate experiments with similar results.

R	Compound Number	VUID	mGlu$_{2/4}$ EC$_{50}$ (nM)	mGlu$_{2/4}$ %Glu Max
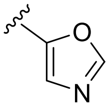	**1.209**	VU6013343	126	44
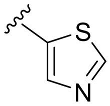	**1.210**	VU6013344	413	35

Despite the poor selectivity of this scaffold, several of the best compounds were taken on for DMPK analysis. All three compounds exhibited high predicted hepatic clearance in both rat and human. While VU6012584 showed good free fraction in both human and rat, the other two showed an undesirable very high fraction unbound, which can allow for higher metabolism and clearance. This chemotype also exhibited moderate K_p values of 0.57 and 0.44 (**1.196** was not run in the K_p study). However, due to the unselective nature of this compound and no evidence of the SAR being able to engender selectivity, we moved on to a new chemotype.

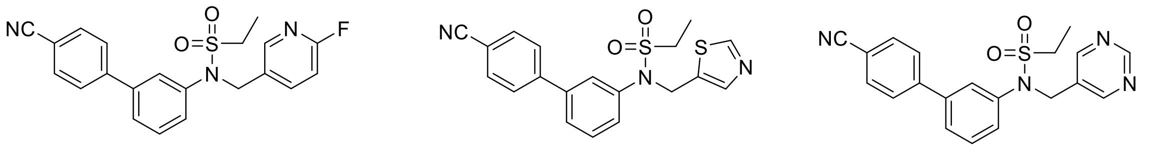

VU6012584 (1.193)
Human CL_{Hep}= 19.4 mL/min/kg
Rat CL_{Hep}= 65.8 mL/min/kg
$f_{u\ human}$= 4.6%
$f_{u\ rat}$= 6.8%
K_p=0.57

VU6012586 (1.194)
Human CL_{Hep}= 20.1 mL/min/kg
Rat CL_{Hep}= 67.5 mL/min/kg
$f_{u\ human}$= 12.5%
$f_{u\ rat}$= 15%
K_p=0.44

VU6012589 (1.196)
Human CL_{Hep}= 20.4 mL/min/kg
Rat CL_{Hep}= 67.3 mL/min/kg
$f_{u\ human}$= 23%
$f_{u\ rat}$= 29.4%

Figure 1.8. DMPK properties of analogs **1.193**, **1.194**, and **1.196**. **1.193** exhibited good free fraction, and both **1.193** and **1.194** had moderate K_P values (there was insufficient material to test **1.196**). However, both **1.194** and **1.195** had very high free fractions, which can allow for higher metabolism. This may contribute to the very high clearance across all three analogs.

Completion of HTS Screen

Met with disappointment with our initial efforts towards synthesizing a selective PAM for the $mGlu_{2/4}$ heterodimer, we elected to allow the HTS screen to complete. Compounds were initially screened in cells expressing the heterodimer, and then active compounds were counterscreened in cells expressing $mGlu_2$ or $mGlu_4$ homodimers to determine the selectivity of the hits. The screen found 216 active compounds, which were then distributed into 4 categories: pan-activators (61) compounds, $mGlu_2$ and $mGlu_{2/4}$ potentiators (141), $mGlu_4$ and $mGlu_{2/4}$ potentiators (12) and compounds selective for $mGlu_{2/4}$ (2) (**Figure 1.9**). Due to the chemical liability of acyl thioureas (especially to hydrolysis), our initial interest focused on VU0503424.

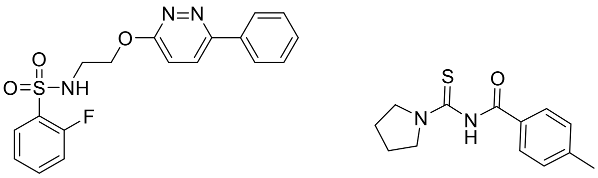

VU0503424 (1.211)
VU0507341 (1.212)

Figure 1.9. Structures of two hits from the HTS screen that exhibited some selectivity of the $mGlu_{2/4}$ heterodimer over $mGlu_2$ and $mGlu_4$ with single point screening at 10 μM.

VU0503424

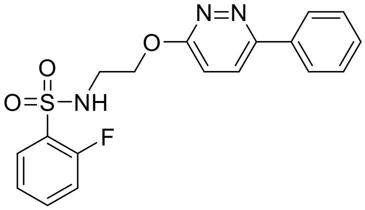

VU0503424 (1.211)
36% $Glu_{2/4\ max}$
21% $Glu_{2\ max}$
26% $Glu_{4\ max}$

Figure 1.10. Structure of **1.211** and related single-point efficacy from the HTS screen.

The single-point data for compounds VU0503424 can be seen in **Figure 1.10**. Screening this compound at 10 µM revealed that this compound seemed to be moderately selective at 36% Glu max, as compared to 21% at $mGlu_2$ and 26% at $mGlu_4$, although the efficacy was noted as weak. However, a preference in activity at high concentrations led us to explore this scaffold to determine if the potency and efficacy could be improved to yield selective PAMs.

Modular synthesis of this scaffold allowed for rapid access to diversity on both ends of this chemotype. Starting from 2,6-dichloropyridazine, SN_{Ar} with the sodium salt of ethanolamine formed by sodium hydride allowed access to known intermediate (**1.213**) in 48% yield[101]. From here, the synthesis was split into two parts depending on which part of the molecule was the focus. For diversifying the sulfonamide, microwave-mediated Suzuki coupling with phenylboronic acid gave intermediate (**1.217**) in 35% yield. Finally, sulfonamide formation with diverse sulfonyl chlorides gave desired analogs (**1.218-1.243**) in good yields. For access to diversity on the aryl pyridazine substituent, again from intermediate (**1.213**), sulfonamide formation with 2-fluorosulfonyl chloride gave intermediate (**1.215**) in 90% yield. Next, Suzuki-coupling with diverse boronic acids gave analogs (**1.244-**

1.265) in 10-30% yield.

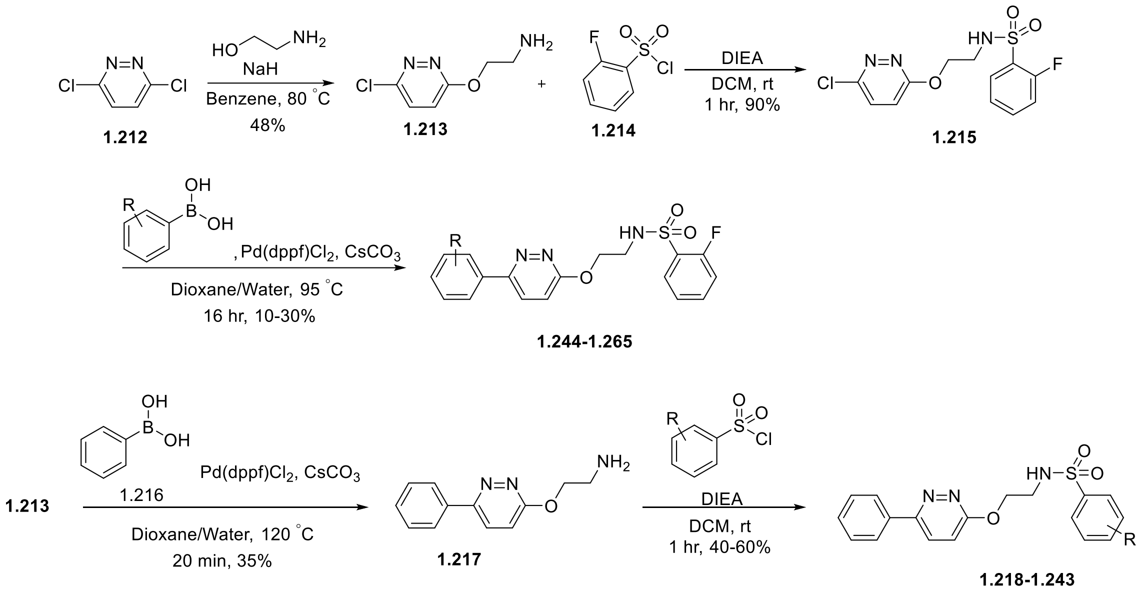

HO
NH2
NaH
Benzene, 80 °C
48%
DIEA
DCM, rt
1 hr, 90%
1.212
1.213
1.214
1.215
, Pd(dppf)Cl2, CsCO3
Dioxane/Water, 95 °C
16 hr, 10-30%
1.244-1.265
1.213
1.216
Pd(dppf)Cl2, CsCO3
Dioxane/Water, 120 °C
20 min, 35%
1.217
DIEA
DCM, rt
1 hr, 40-60%
1.218-1.243

Scheme 1.7: Divergent routes for synthesis of pyridazine analogs **1.218-1.265**.

Using this this divergent synthesis, a series of 56 analogs was synthesized. SAR around this scaffold was exceptionally steep (**Table 1.11**). On the sulfonamide moiety, fluorines were tolerated in both the 2 and 4 position. Around the aryl pyridazine, electron withdrawing groups were best tolerated, with the 3-chloro analog being the most potent compound (5.31 µM and 37% Glu max). Though the potency was measurable, the efficacy was still below the threshold for what is typically considered a PAM. Efficacy was improved in analogs **1.263** and **1.242** to 64 and 52% respectively, though this resulted in compounds that had potencies of 10 µM or greater.

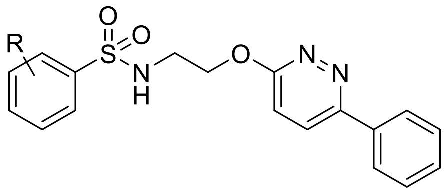

Table 1.11. Structures of VU0503424 analogs focusing on sulfonamide substitutions to determine selectivity and establish requirements for potency and efficacy. Associated potency and efficacy data from 10-point CRC-format screen at rat $mGlu_{2/4}$ cell lines. Tl^+ flux responses for each compound are reported as a percentage of the maximum response. VU number denotes the compound identifier assigned by Vanderbilt University. Data represent the mean of at least 3 replicate experiments with similar results.

R	Compound Number	VUID	$mGlu_{2/4}$ EC_{50} (μM)	$mGlu_{2/4}$ %Glu Max
3-Me	**1.218**	VU0503417	Inactive	
3,4-OMe	**1.219**	VU0503421	Inactive	
2-F	**1.220**	VU0503424	>10	41
3-Cl	**1.221**	VU0503432	Inactive	
3,4-Cl	**1.222**	VU6013362	Inactive	
3,5-Cl	**1.223**	VU6013363	Inactive	
4-CF_3	**1.224**	VU6014106	Inactive	
4-Cl	**1.225**	VU6014107	Inactive	

3-OMe	**1.226**	VU6014108	Inactive	
2-OCF_3	**1.227**	VU6014109	Inactive	
H	**1.228**	VU6014110	>10	39
3-Me, 4-Cl	**1.229**	VU6014111	Inactive	
4-Me	**1.230**	VU6014112	Inactive	
3,4-F	**1.231**	VU6014113	Inactive	
2-CN	**1.232**	VU6014114	Inactive	
2-OMe	**1.233**	VU6014115	Inactive	
2-CF_3	**1.234**	VU6014116	>10	52
2-Me	**1.235**	VU6014117	>10	44
2-Cl	**1.236**	VU6014118	>10	35

3-CN	**1.237**	VU6014120	Inactive	
4-CN	**1.238**	VU6014121	Inactive	
3-OCF_3	**1.239**	VU6014122	Inactive	
3-CF_3	**1.240**	VU6014123	Inactive	
3-F	**1.241**	VU6014124	>10	42
4-F	**1.242**	VU6014125	9.67	52
4-OCF_3	**1.243**	VU6014126	Inactive	

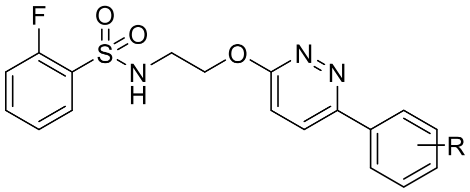

Table 1.12. Structures of VU0503424 analogs of the Eastern aryl ring substitution. Associated potency and efficacy data from 10-point CRC-format screen at rat $mGlu_{2/4}$ cell lines. Tl^+ flux responses for each compound are reported as a percentage of the maximum response. VU number denotes the compound identifier assigned by Vanderbilt University. Data represent the mean of at least 3 replicate experiments with similar results.

R	**Compound Number**	**VUID**	**mGlu$_{2/4}$ EC$_{50}$ (μM)**	**mGlu$_{2/4}$ %Glu Max**
4-OMe	**1.244**	VU0503458	Inactive	
2-F	**1.245**	VU6013118	Inactive	
2-Cl	**1.246**	VU6013119	Inactive	
2-Me	**1.247**	VU6013120	Inactive	
2-CF_3	**1.248**	VU6013121	Inactive	
2-OMe	**1.249**	VU6013122	Inactive	
2-OCF_3	**1.250**	VU6013123	Inactive	
3-F	**1.251**	VU6013124	Inactive	
3-Cl	**1.252**	VU6013125	5.31	37
3-Me	**1.253**	VU6013126	>10	37

3-CF_3	**1.254**	VU6013127	Inactive	
3-OMe	**1.255**	VU6013128	Inactive	
3-OCF_3	**1.256**	VU6013129	Inactive	
3-CN	**1.257**	VU6013130	Inactive	
3-N	**1.258**	VU6013131	Inactive	
4-F	**1.259**	VU6013132	Inactive	
4-Cl	**1.260**	VU6013133	Inactive	
4-Me	**1.261**	VU6013134	1.57	31
4-CF_3	**1.262**	VU6013135	Inactive	
4-OCF_3	**1.263**	VU6013136	>10	64
4-CN	**1.264**	VU6013137	Inactive	

4-N	**1.265**	VU6013138	Inactive

In an effort to improve the potency of the most efficacious compound, VU136, a series of poly-fluorinated sulfonamides was synthesized both to determine if the potency of this scaffold could be improved and to measure the selectivity of this scaffold. From the poly-fluorine walk, the 2,4-fluorosulfonamide (VU6014334, **1.271**, EC_{50} $mGlu_{2/4}$= 2.77 µM, 52% Glu max) was the most optimal analog synthesized in this effort, with moderate potencies and efficacy. However, when screening against both homodimer cell lines, it was discovered that this compound was active at both homodimeric receptors (EC_{50} $mGlu_2$= 618 nM, 38% Glu max; EC_{50} $mGlu_4$= 1.13 µM, 55% Glu max). However, due to the lack of selectivity of this scaffold and the steep SAR encountered in our efforts to optimize it, work on this scaffold was terminated.

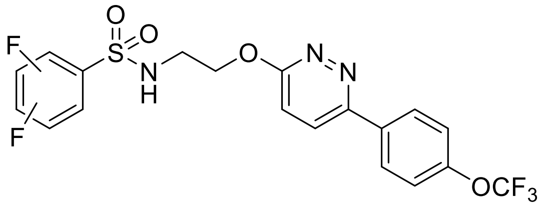

Table 1.13. Polyfluorinated analogs of VU0503424 synthesized in an effort to improve potency. Associated potency and efficacy data from 10-point CRC-format screen at rat $mGlu_{2/4}$ cell lines. Tl^+ flux responses for each compound are reported as a percentage of the maximum response. VU number denotes the compound identifier assigned by Vanderbilt University. Data represent the mean of at least 3 replicate experiments with similar results.

R	Compound Number	VUID	$mGlu_{2/4}$ EC_{50} (µM)	$mGlu_{2/4}$ %Glu Max	$mGlu_2$ EC_{50} (µM)	$mGlu_2$ %Glu Max	$mGlu_4$ EC_{50} (µM)	$mGlu_4$ %Glu Max
3,5-F	**1.266**	VU6014323	Inactive		Inactive		Inactive	
2,5-F	**1.267**	VU6014330	Inactive		Inactive		Inactive	

2,6-F	**1.268**	VU6014331	>10	41	Inactive		Inactive	
3,4-F	**1.269**	VU6014332	Inactive		Inactive		Inactive	
3,4,5-F	**1.270**	VU6014333	Inactive		Inactive		Inactive	
2,4-F	**1.271**	VU6014334	2.77	46	0.618	38	1.13	55

VU0507341

Our attention next turned to the second hit, VU0507341, which had a less ideal scaffold for medicinal chemistry efforts due to the potential reactivity of the core. Indeed, looking through literature precedent around acylthioureas of this type, a number of studies are observed to have this moiety central to the core of their molecules. However, these studies also have the goal of cytotoxicity (breast cancer cell lines, insecticides), which would mean that the toxicity of this core would need to be dialed out before *in vivo* studies could be performed. Additionally, it is possible that the potential cytotoxicity of this core could interfere with the *in vitro* assays used to measure potency and efficacy in our lab. Nonetheless, due to it being one of the two somewhat selective hits from our HTS screening campaign, it was determined that it was worth exploring this scaffold briefly.

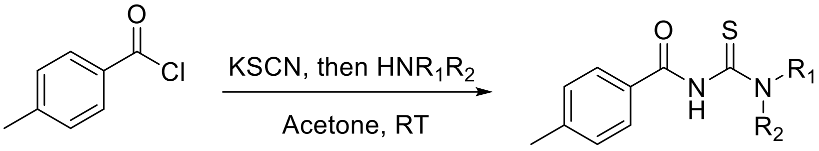

1.272

1.273-1.282

Scheme 1.8: 1-pot synthetic scheme for the synthesis of diverse thiourea analogs of VU0507341.

Synthesis of analogs of VU0507341 was accomplished by addition of potassium thiocyanate to commercial 4-methylbenzoyl chloride to form the acyl thiocyanate. This was then followed by addition of the desired amine to form the thiourea in 4-35% yield (**scheme 1.8**). Initial SAR focused around modifications to the pyrrolidine ring. Cleavage of the pyrollidine to the diethylamide resulted in a good increase in potency. Additionally, switching to the primary amine using cyclopropylamine resulted in a compound with low potency, suggesting that the tertiary amide is better for activity. Aromatization to the pyrrole resulted in a slight decrease in potency at the $mGlu_4$ homodimer, but an increase at the heterodimer. While ring expansion to the 6-membered piperidine ring resulted in an inactive compound, a phenyl piperazine motif showed good efficacy (**1.274**, EC_{50} $mGlu_4$=825 nM, Glu Max=112%, EC_{50} $mGlu_{2/4}$= 804 nM, Glu max=88%). Surprisingly, the urea formed from R-2-methylpiperidine was highly potent (**1.281**, EC_{50} $mGlu_4$=268 nM, Glu Max=106%, EC_{50} $mGlu_{2/4}$= 185 nM, Glu max=91%), which was especially interesting in comparison to the inactivity of piperidine itself. This phenomenon is a good display of the so-called “magic methyl” effect in medicinal chemistry, which corresponds to a number of chiral moieties (i.e- fluorine, amino, etc) can have a drastic effect on the potency of a molecule. This can be due to a number of factors, including changing the rotational energy around bonds and disturbing the planarity of a biaryl system by substitution of the 2-position of either ring. In this case, the methyl group is likely locking the conformation of the piperidine ring into a shape that is ideal for interaction with a hydrophobic region of the molecules target. Additionally, the methyl group protruding from the ring can have additional non-polar interactions. Though there was interesting SAR surrounding this structure, the similarity in the potencies between $mGlu_4$ and $mGlu_{2/4}$ (this series has not yet been tested on $mGlu_2$ homomers) and the nature of this scaffold has led us to believe that this chemotype is likely a GIRK-activator, or some similar ion channel that can allow for non-selective thallium flux, and thus, efforts around this scaffold have been terminated until $mGlu_2$ and GIRK screening can be performed.

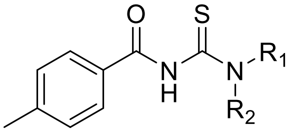

Table 1.14. Thiourea analogs of acyl thiourea VU0507341. Associated potency and efficacy data from 10-point CRC-format screen at rat $mGlu_{2/4}$ cell lines. Tl^+ flux responses for each compound are reported as a percentage of the maximum response. VU number denotes the compound identifier assigned by Vanderbilt University. Data represent the mean of at least 3 replicate experiments with similar results.

HNR_1R_2	Compound Number	VUID	$mGlu_{2/4}$ EC_{50} (nM)	$mGlu_{2/4}$ %Glu Max	$mGlu_4$ EC_{50} (nM)	$mGlu_4$ %Glu Max
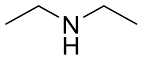	**1.273**	VU6019677	8,280	77	4,370	95
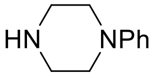	**1.274**	VU6019678	804	88	825	112
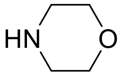	**1.275**	VU6019687	Inactive		Inactive	
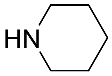	**1.276**	VU6019688	>10,000	66	>10,000	90

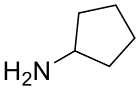	**1.277**	VU6019689	>10,000	33	>10,000	52
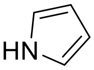	**1.278**	VU6019691	3,180	73	6,080	103
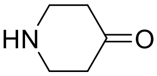	**1.279**	VU6019692	Inactive		>10,000	31
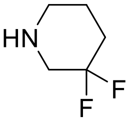	**1.28**	VU6019694	4,300	73	6,200	89
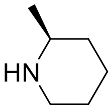	**1.281**	VU6019695	268	106	185	91
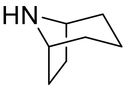	**1.282**	VU6019696	>10,000	83	>10,000	101

VU0544412

Turning our attention back to the mGlu$_4$/mGlu$_{2/4}$ dual activating hits, we were intrigued by the structure of thiazepane VU0544412. Additionally, there were 3 different aryl analogs of this scaffold that showed up as hits from the HTS screen, which was exciting because it gave strong evidence that this scaffold was a true hit instead of a false positive (though this does not rule out it being a GIRK activator). Finally, we believed that VU0544412 could potentially occupy a similar chemical space to the earlier VU041 scaffold, as both have flexible core structures and prefer halogens in the three position.

Synthesis of VU412 was performed according to a procedure reported in the literature. First, Michael addition of L-cysteine onto methyl acrylate using triethylamine as a base gave the Michael adduct in good yields. Next, intramolecular cyclization was accomplished by diluting the intermediate in 7M ammonia/methanol for 7 days. Workup of this reaction by acid base extraction gave the known thiazepane carboxylic acid core[102]. Analogs were then synthesized by a HATU mediated amide coupling reaction with various anilines (**Scheme 1.9**).

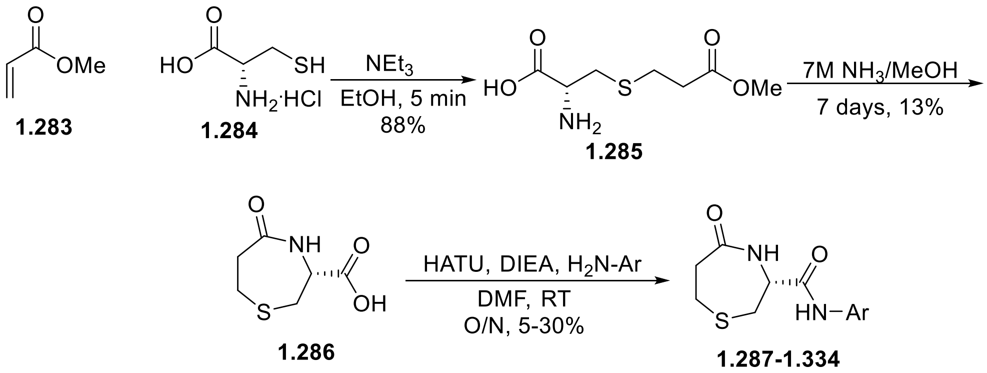
OMe
1.283
HO
SH
NH2·HCl
1.284
NEt3
EtOH, 5 min
88%
HO
S
OMe
NH2
1.285
7M NH3/MeOH
7 days, 13%
NH
S
OH
1.286
HATU, DIEA, H2N-Ar
DMF, RT
O/N, 5-30%
NH
S
HN−Ar
1.287-1.334

Scheme 1.9: Synthesis of thiazepine VU0544412 analogs from L-cysteine and methyl acrylate.

The initial hit, VU0544412 (**1.288**), had a potency of 772 nM and 106% Glu max, making it the most active compound synthesized in this project. Further halogen analogs showed that chlorines were favored in the three and in both the three and five positions (**1.299** and **1.313**), but the 3,4-dichloroaniline analog (**1.291**) was devoid of activity. Addition of a fluorine to the 4-position of the 3,5-dichloroaniline (**1.314**) resulted in a slight boost in potency.

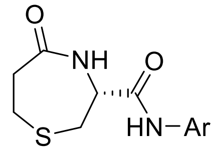

Table 1.15. Amide analogs of thiazepine VU0544412 focused on understanding necessities for activity and similarities to favorable activity for VU0544841. Associated potency and efficacy data from 10-point CRC-format screen at rat $mGlu_{2/4}$ cell lines. Tl^+ flux responses for each compound are reported as a percentage of the maximum response. VU number denotes the compound identifier assigned by Vanderbilt University. Data represent the mean of at least 3 replicate experiments with similar results.

HNAr	Compound Number	VUID	$mGlu_{2/4}$ EC_{50} (nM)	$mGlu_{2/4}$ %Glu Max
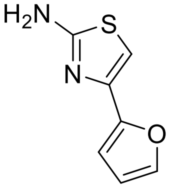	**1.287**	VU0544376	Inactive	
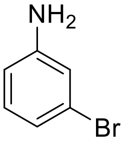	**1.288**	VU0544412	772	106
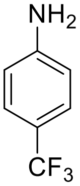	**1.289**	VU0544413	>10,000	37
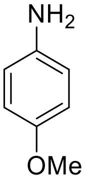	**1.290**	VU0544414	Inactive	
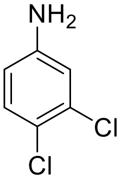	**1.291**	VU0544423	>10,000	57

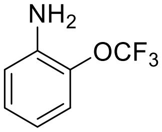	**1.292**	VU0544478	Inactive	
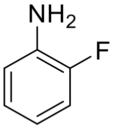	**1.293**	VU6014291	Inactive	
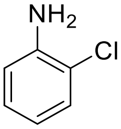	**1.294**	VU6014292	Inactive	
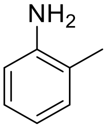	**1.295**	VU6014293	Inactive	
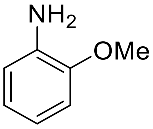	**1.296**	VU6014294	Inactive	
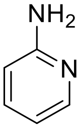	**1.297**	VU6014295	Inactive	
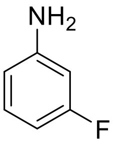	**1.298**	VU6014296	>10,000	84

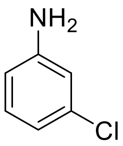	**1.299**	VU6014297	518	111
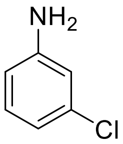	**1.300**	VU6014298	>10,000	63
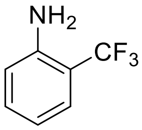	**1.301**	VU6014336	Inactive	
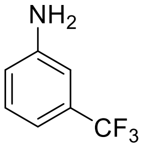	**1.302**	VU6014337	>10,000	55
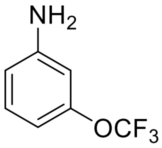	**1.303**	VU6014338	>10,000	51
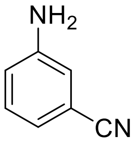	**1.304**	VU6014339	>10,000	52
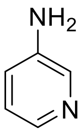	**1.305**	VU6014340	Inactive	
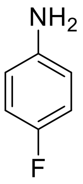	**1.306**	VU6014341	Inactive	

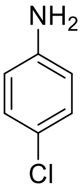	**1.307**	VU6014342	Inactive	
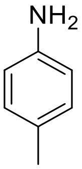	**1.308**	VU6014343	Inactive	
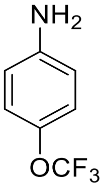	**1.309**	VU6014344	Inactive	
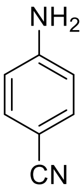	**1.310**	VU6014345	Inactive	
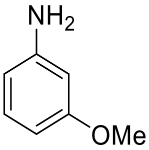	**1.311**	VU6015336	Inactive	
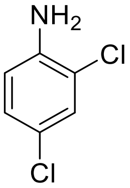	**1.312**	VU6015337	Inactive	
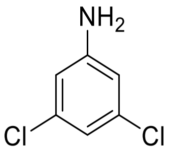	**1.313**	VU6015338	632	112

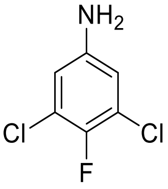	**1.314**	VU6015340	580	95
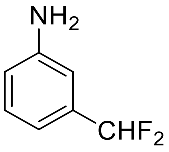	**1.315**	VU6018804	Inactive	
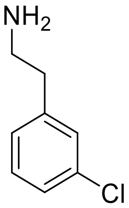	**1.316**	VU6018806	Inactive	
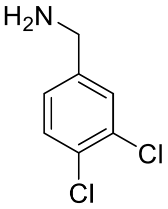	**1.317**	VU6018807	Inactive	
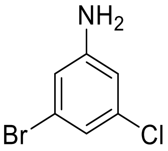	**1.318**	VU6022296	638	105
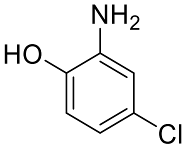	**1.319**	VU6022297	Inactive	
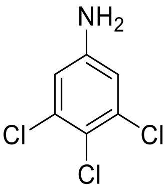	**1.320**	VU6022298	2,090	55

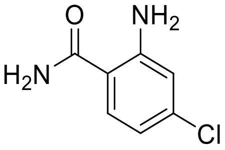	**1.321**	VU6022792	Inactive	
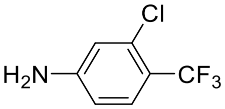	**1.322**	VU6022793	1,790	37
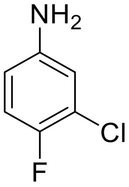	**1.323**	VU6022794	3,170	174
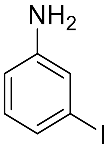	**1.324**	VU6022795	>10,000	156
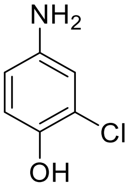	**1.325**	VU6022796	Inactive	
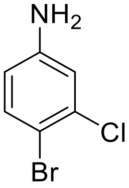	**1.326**	VU6022797	3,550	90
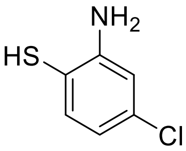	**1.327**	VU6022798	Inactive	

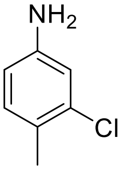	**1.328**	VU6022699	>10,000	53

Next, all possible combinations of 3,5-dihaloamides were synthesized to determine what the ideal combination of halogen substitutions was for this scaffold (**1.329-1.334**). As can be seen with analogs **1.318** and **1.333**, the addition of a bromine to the arene ring resulted in a massive boost to potency, with both the 3-bromo-5-chloro and 3,5-dibromo analogs resulting in compounds that were in the double-digit nanomolar range.

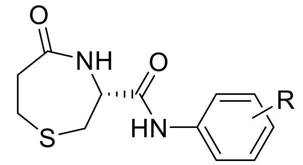

Table 1.16. 3,5-dihalogenated aniline analogs were explored to understand the most ideal halogen combination for potency and efficacy, and to better understand the trends in this series. Associated potency and efficacy data from 10-point CRC-format screen at rat $mGlu_{2/4}$ cell lines. Tl^+ flux responses for each compound are reported as a percentage of the maximum response. VU number denotes the compound identifier assigned by Vanderbilt University. Data represent the mean of at least 3 replicate experiments with similar results.

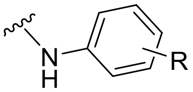	Compound Number	VUID	$mGlu_{2/4}$ EC_{50} (nM)	$mGlu_{2/4}$ %Glu Max	$mGlu_4$ EC_{50} (nM)	$mGlu_4$ %Glu Max
3,5-F	**1.329**	VU6023806	8,400	138	8,920	119
3-Cl, 5-F	**1.330**	VU6023811	904	144	278	114
3-Br, 5-F	**1.331**	VU6023808	992	118	351	119

3-I, 5-F	**1.332**	VU6023809	1,410	99	558	100
3,5-Cl	**1.313**	VU6015338	632	112		
3-Br, 5-Cl	**1.318**	VU6022296	63.8	105	32.8	109
3,5-Br	**1.333**	VU6023810	78.2	107	35.3	114
3-I, 5-Br	**1.334**	VU6023812	274	75	115	100

This trend in halogen potency tracks well with the one observed in halogen bonding, where the ability to halogen bond increases with the size of the halogen. Halogen bonding is a phenomenon where a heteroatom's (typically oxygen) lone pairs can interact with and stabilize the σ^* orbital from the halogen-carbon bond on the arene. This LUMO becomes lower in energy as the halogen size increases and the bonds get longer and weaker. However, the iodo-analog exhibits poor potency even though it is the best halogen at hydrogen-bonding, but this can be explained by the fact that the iodine atom is susceptible to oxidation or other means of decomposition, and is also extremely large and can disrupt favorable interactions with the protein through steric clashing.

Because of the high potency of this molecule, it was tested for DMPK properties to determine if this chemotype could potentially be a good tool compound as a dual mGlu$_4$/mGlu$_{2/4}$ activator. However, this molecule displays poor pharmacological characteristics (**Figure 1.11**). The 3-chloro analog (**1.299**) was moderately cleared in human (9.4 mL/min/kg), but highly cleared in rat (63.6 mL/min/kg). Additionally, the amount of this compound crossing the blood brain barrier into the brain was below the limit of quantitation (BLQ) in our system. Therefore, there is no quantifiable K$_P$, which is a major liability for this scaffold. This is partially believed to be due to the amino-acid like nature of this chemotype, in which the two amides are spaced such that they mimic the same spacing seen in proteins. This is likely making this a target of a P-glycoprotein (PGP) transporter, which are transporters that have evolved to move molecules across cell membranes. PGP in the BBB plays a large role in keeping substrates out of the brain, which is part of the reason that CNS targets can be difficult to target.

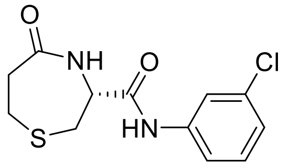

VU6014297 (1.299)
EC$_{50}$ mGlu$_{2/4}$= 518 nM
Glu$_{max}$= 111%

EC$_{50}$ mGlu$_4$= 148 nM
Glu$_{max}$ = 120%

Human CL$_{Hep}$= 9.4 (45% max) mL/min/kg
CL$_{Hep}$ rat= 63.6 (75% max) mL/min/kg
Brain (ng/g)= BLQ
K$_p$= N/A

Figure 1.11. DMPK properties of VU6014297, exhibiting moderate to high clearance and no brain penetration.

To date, the enantiomer of several of the most active compounds has been synthesized to determine the optimal stereochemistry for activity. In addition, the azapine analog of the thiazepane, with removal of the sulphur from the seven-membered core, has been synthesized to determine if the oxygen atom from the sulphoxide impeded activity and the sulphur can be removed with a less bulky equivalent. Future work should be focused on replacing the sulphur atom with an oxygen, which would be a more metabolically stable and less potentially reactive. For ameliorating the PGP substrate liability, inverse amides could prevent recognition by the efflux protein, though synthesis of the reverse amide is difficult due to the thermal instability of this compound, preventing Curtius rearrangements, and the potential instability of the hemiaminal species.

Conclusions

This subchapter has detailed our initial efforts towards synthesizing a small molecule PAM that was selective for the $mGlu_{2/4}$ heterodimer over both the $mGlu_2$ and $mGlu_4$ homodimers and the challenges that came along during this effort. The initial scaffold, VU041, faced very steep SAR and we were not able to improve the potency, efficacy, or selectivity over the hit compound. Work on scaffolds derived from HTS efforts resulted in a number of novel scaffold chemotypes, which resulted in the discovery of several compounds that showed activity at the $mGlu_{2/4}$ heterodimer and either $mGlu_2$, $mGlu_4$, or all three receptor populations. This last category of compounds were investigated as direct GIRK activators, or for activation of a separate protein altogether that allowed for non-mGlu receptor mediated thallium flux in our assays. Faced with these selectivity challenges, and, after the synthesis of over 400 compounds and no evidence of sufficient differentiation between the allosteric binding pocket in the heterodimer over the homodimer, we decided that a new approach would be necessary.

Tethering Strategy

Background

While it is theoretically possible to synthesize small molecules that are selective for a heterodimer of interest, selectivity is reliant on a structural change in the binding pocket upon heterodimerization. Additionally, without robust structural information, it can be difficult to determine if there is such a change in the binding pocket, and if selectivity is achievable at all. Finally, as shown by numerous studies into mGlu heterodimers, activation of only one monomer of an mGlu heteromer is insufficient for full receptor activation, which means that it may be difficult to obtain a robust signal from a heteromer with a monovalent ligand[16,55,57,65,71,]. One method for solving these issues is the synthesis of a bivalent ligand, which contains a ligand that can each individually bind to one half of the monomer[103,104]. Beginning with the pioneering work of Portoghese *et al* on bivalent ligands for the mGlu$_5$/Mu-opioid heterodimer[3], the synthesis of heterodimeric probes for the selective targeting of heterodimer receptors has become a burgeoning field in the realm of medicinal chemistry[105-118]. These ligands rely on a phenomenon known as avidity, the additive effect of multiple affinities[119]. One molecule binding to half of the receptor results in a local environment in which the other ligand has a very high concentration, which results in a high probability of activation of both monomers simultaneously.

These bivalent ligands do suffer from some limitations, mainly that they are often very large in size (>1,000 Da), which results in very non-drug like pharmacology. For example, the Portoghuese lab found it necessary to use an intrathecal (into the spinal column) injection to administer their $mGlu_5$/Mu-opioid tethered ligand in mice. Additionally, while these tethered ligands are designed with the intent of delivering both molecules simultaneously, there is the potential of negative allosteric interactions resulting in decreased affinity for the second ligand. Finally, these ligands are non-trivial to design and synthesize. They require high structural knowledge of the monovalent ligands, as it is required that either a functional group already on the molecule is utilized to attach the linker or the molecule must be functionally modified in such a way to allow for attachment of this linker. The linker must also be attached in such a location such that it minimally impacts the receptor-ligand interactions. Next, a number of linker lengths must be synthesized to determine the ideal spacing between the two ligands such that they can interact with the protein simultaneously. This can also result in some issues, as longer linker lengths can result in long hydrophobic chains that can impact aqueous solubility.

Despite these limitations and difficulties, the successful synthesis of a bivalent ligand can provide crucial information about receptor activation. An ideal bivalent ligand will produce a concentration response curve (CRC) that exhibits two EC/IC_{50}s: a low concentration one in which one molecule interacts with each receptor and a second, higher concentration curve in which two separate molecules bind simultaneously (**Figure 1.12**). Operating in concentrations that elicit the low concentration response, one can potentially selectively elicit a response from a heterodimeric receptor population. This information can provide strong evidence of the existence of these heterodimeric receptors *in vivo*, as it is hard to prove a heterodimer exists without a crystal structure, which is very difficult given the size and flexibility of GPCRs.

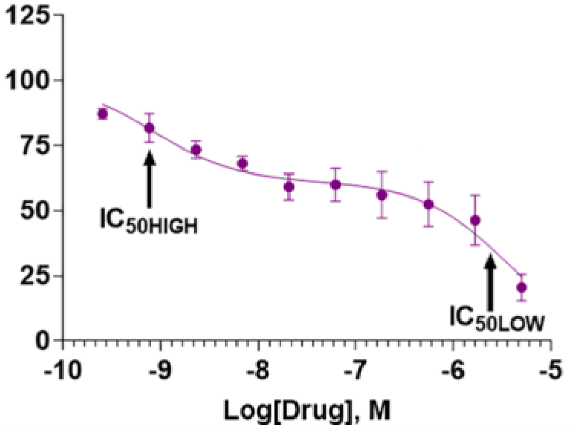

Figure 1.12. CRC of a tethered antagonist exhibiting a biphasic curve due to bisactivation with one molecule in low concentrations (IC_{50HIGH}) and two molecules bidning simultaneously (IC_{50LOW})[120].

mGlu$_{2/4}$ Tethered Ligand

The inspiration for synthesizing a tethered ligand for this receptor stemmed from data reported by Pin *et al*[121]. In this report, they used a FRET based assay in which the FRET donor and acceptor were placed on $mGlu_2$ and $mGlu_4$, respectively. The VFDs of each receptor shift away from one other, resulting in a quenching of the FRET signal. Using a concentration

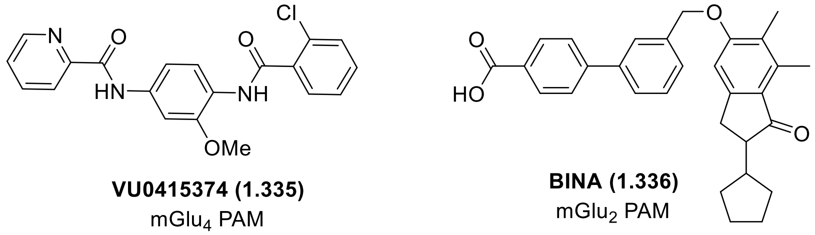

VU0415374 (1.335)
$mGlu_4$ PAM

BINA (1.336)
$mGlu_2$ PAM

Figure 1.13. Structures of PAMs VU0415374 and BINA that exhibited enhanced activation at $mGlu_{2/4}$ cell lines in the presence of a submaximal concentration of glutamate.

of PAM to elicit a submaximal receptor response, they showed that co-administration of the mGlu$_2$ PAM biphenyl-indanone A (BINA) and mGlu$_4$ PAM VU374 resulted in a more than additive receptor response, suggesting that both PAMs acting simultaneously results in superior receptor activation (**Figure 1.13**). This finding is especially interesting given that VU374 has previously been shown to be inactive at the heterodimer alone. It has a long, linear, planar structure that makes it amenable to the deep pocket in mGlu$_4$ that is hypothesized to be inaccessible in the heterodimer. Though the authors make note of this interesting phenomenon, they do not offer an explanation or thoughts as to why VU374 is active upon co-administration with an mGlu$_2$ PAM. It is possible that upon full activation of mGlu$_2$ in the presence of BINA that the movement of the mGlu$_2$ monomer can effect changes that allow for opening of the deep pocket in mGlu$_4$. More studies need to be done to rationalize this phenomenon, but the evidence that the two PAMs have an additive effect was sufficient for us to move forward in synthesizing bivalent ligands derived from them.The initial SAR around BINA showed that changes to the aryl carboxylic acid region of the molecule were tolerated, whereas few modifications to the indanone core were tolerated[120]. While the carboxylic acid could theoretically be converted to an ester or amide as a means of attaching a linker, the high conservation of this group in the 3 and 4 positions of the arene suggested that it plays a role in this molecule's potency. Fortunately, the initial report also gave strong evidence for a good location for the location of the linker. A BINA analog in which the carboxylic acid is moved to the three position (**1.337**) had an activity of 69 nM and 118% Glu max as compared to the parent compound with 111 nM and 114% Glu max (**Figure 1.14**). With the acid in this position, changing the hydrogen in the

4 position to a hydroxyl group (**1.338**) resulted in little change in potency (62 nM and 113% Glu max). Alkylating the alcohol to a methoxy group (**1.339**) resulted in only a slight decrease in potency, meaning that placing a linker on a hydroxy in the 4 position may allow for the molecule to maintain potency while also having the second ligand attached.

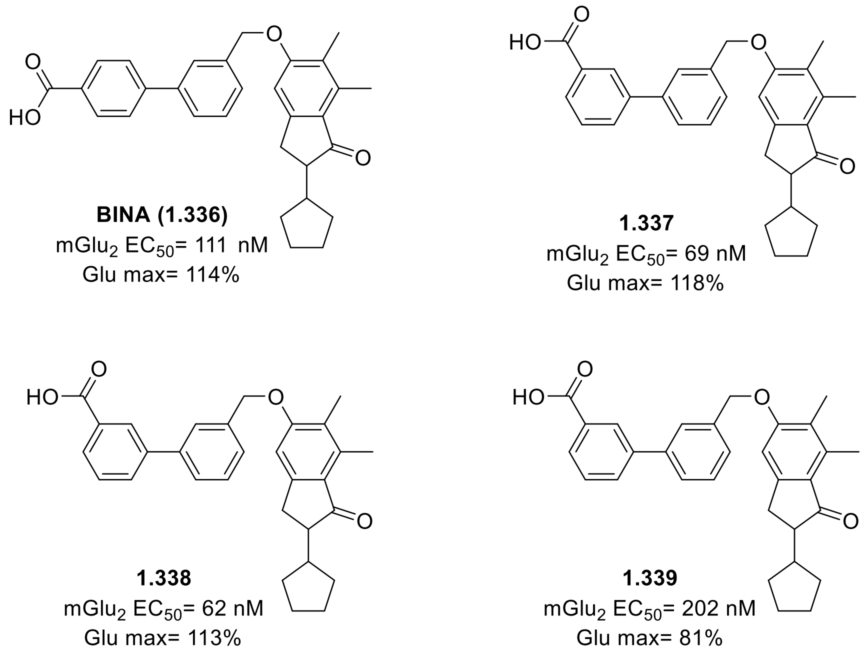

BINA (1.336)
mGlu$_2$ EC$_{50}$= 111 nM
Glu max= 114%

1.337
mGlu$_2$ EC$_{50}$= 69 nM
Glu max= 118%

1.338
mGlu$_2$ EC$_{50}$= 62 nM
Glu max= 113%

1.339
mGlu$_2$ EC$_{50}$= 202 nM
Glu max= 81%

Figure 1.14. BINA analogs from the published report indicate that a 4-OH group may be amenable for attachment of a linker[122].

Unfortunately, the SAR for VU374 was less helpful for ligand design than for BINA. The changes made to VU374 indicate that the pyridine ring tolerated very little change, which means that it is likely important for protein interactions. SAR on the far arene ring was much more tolerated, indicating that this side of the molecule may be solvent facing. Additionally, computational studies also modeled the pyridine ring binding deep into the allosteric pocket, while the chlorobenzene ring was closer to the top of

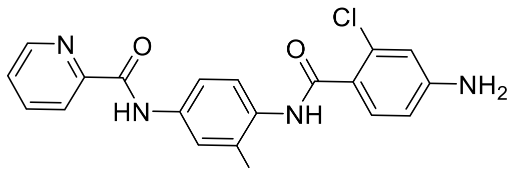

Figure 1.15. Structure of VU374 analog modified for linker attachment.

the protein. However, there was no indication of what functional group could be appended without large changes to the compound's potency. Based off of the computational studies, the 4 position was chosen to attach an amine that could be acylated to attach the linker (**Figure 1.15**).

With the design of both PAMs in hand, focus was next shifted to the design of the linker portion. While no dual allosteric bivalent ligand for two family C GPCRs has been synthesized to date, the mGlu$_5$/Mu-opioid tether contains an mGlu$_5$ NAM. While there is not necessarily an overlap between the location of the allosteric pocket between mGlus, especially between families where there is little sequence homology, the tether length used in their study was thought to be potentially the most similar to our system. Thus, a library of tethers was designed using diamines of various lengths to establish tethered ligands that were centered around the tether length of 22 atoms. To achieve this, it was decided that VU374 would be extended by reaction with glycolic anhydride, which extends this portion of the molecule by 6 atoms and also adds an ether linkage that will help with aqueous solubility. For BINA, it was decided that the hydroxyl group would be alkylated with *tert*-butyl bromoacetate to extend this linker by 3 atoms and also add a functional handle to

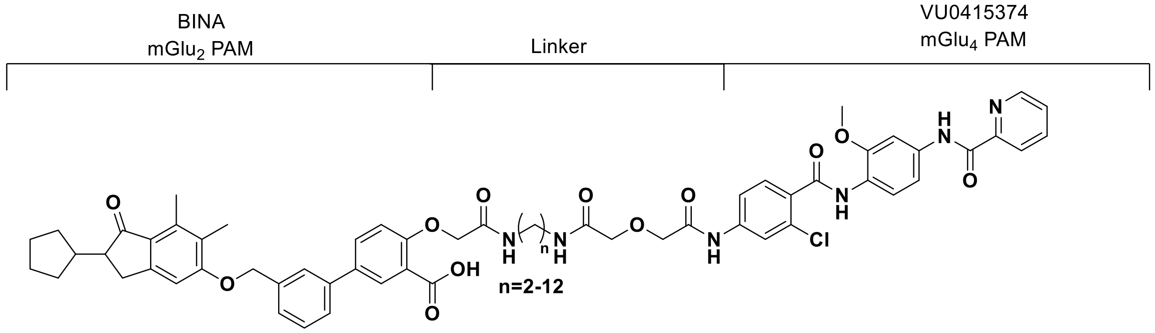

Figure 1.16. Design of mGlu$_{2/4}$ linked compounds utilizing homologated diamines to modulate the spacing between the two PAMs.

add boc-protected diamines to before boc-deprotection and addition of the second PAM.

Tether Synthesis- BINA

Though the synthesis of BINA is reported in the literature, there are no spectra or experimentals included in the report. Therefore, the synthesis of BINA was performed mostly according to this route, with changes made to accommodate the tether. First, Friedal-Crafts acylation with the acyl chloride derived from cyclopentylacetic acid provided the desired adduct in 85% yield. Mannich reaction of the resulting ketone with dimethylamine hydrochloride and *para*-formaldehyde in acetic acid followed by dilution in DMF and reflux gave the enone in 96% yield. Nazarov cyclization in concentrated sulfuric acid resulted in the desired cyclization product in 78% yield. Next, demethylation of the methoxy group was mediated by aluminum chloride in refluxing toluene for 1 hour, which gave the phenol, which was taken on crude for an S_N2 reaction with 3-pinacolboranebenzyl bromide and Suzuki coupling with methyl 5-bromosalicylate gave **1.350** in 47% yield over the three steps. Alkylation of the resulting phenol with *tert*-butyl bromoacetate gave the desired adduct in 89% yield, which allowed for selective deprotection of the *tert*-butylcarboxylate with TFA in 90% yield. This route gives the desired adduct in good yields in a very scalable 9 step synthesis.

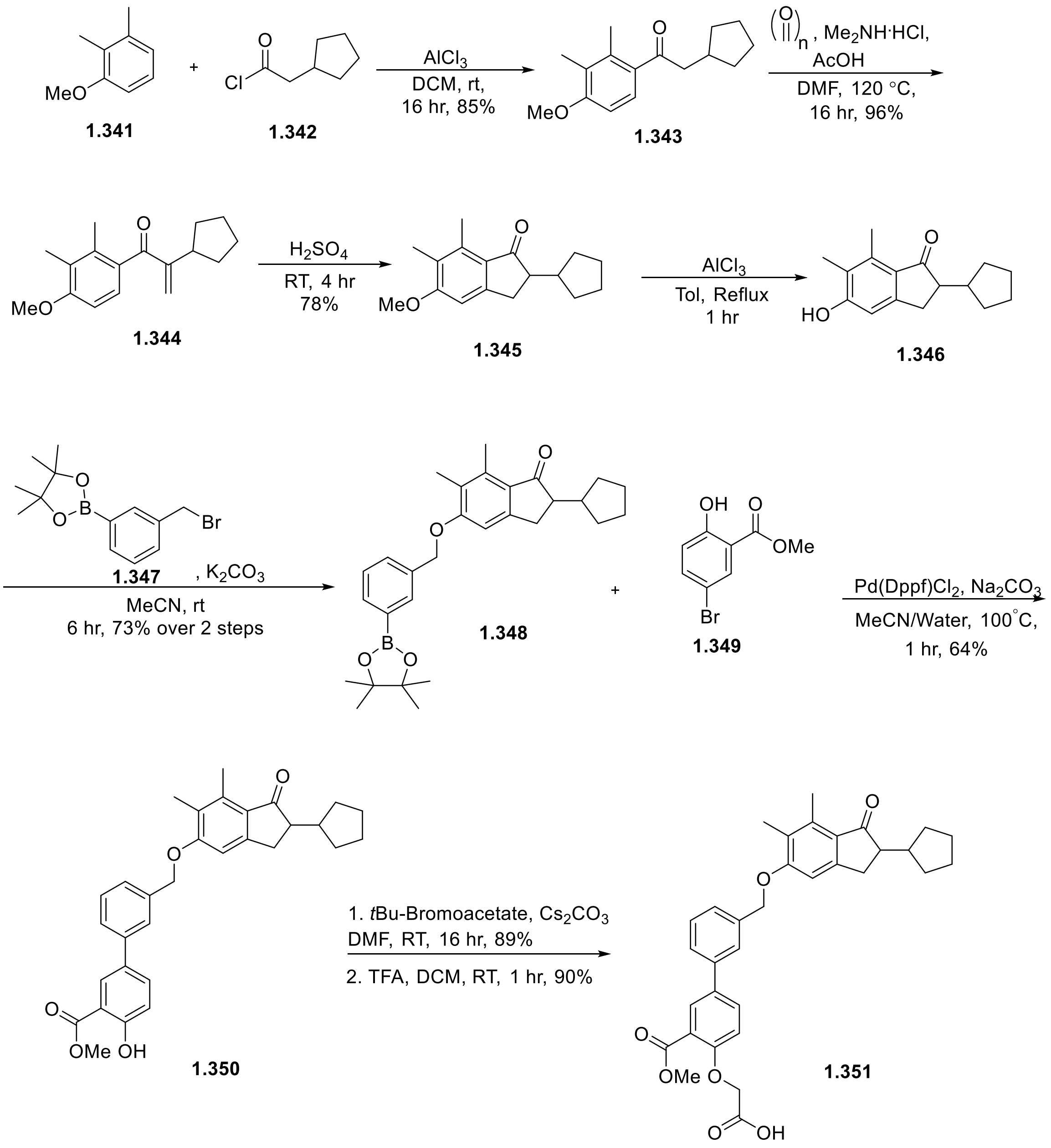
MeO
1.341
+
Cl
O
1.342
AlCl$_3$
DCM, rt,
16 hr, 85%
MeO
O
1.343
(O)$_n$, Me$_2$NH·HCl,
AcOH
DMF, 120 °C,
16 hr, 96%
MeO
O
1.344
H$_2$SO$_4$
RT, 4 hr
78%
MeO
O
1.345
AlCl$_3$
Tol, Reflux
1 hr
HO
O
1.346
O
B
O
Br
1.347
, K$_2$CO$_3$
MeCN, rt
6 hr, 73% over 2 steps
O
O
B
O
O
1.348
+
OH
O
OMe
Br
1.349
Pd(Dppf)Cl$_2$, Na$_2$CO$_3$
MeCN/Water, 100°C,
1 hr, 64%
O
O
O
OMe OH
1.350
1. *t*Bu-Bromoacetate, Cs$_2$CO$_3$
DMF, RT, 16 hr, 89%
2. TFA, DCM, RT, 1 hr, 90%
O
O
O
OMe O
O
OH
1.351

Scheme 1.10: Route for synthesis of BINA analog **1.351**.

Tether- VU374

The synthesis of the VU374 portion of the tether began with bis Boc-protection of 2-methoxy-4-nitro aniline in quantitative yield. While reversing the nitro and amino group in the central core to achieve the synthesis would be simpler, the cost of this compound was prohibitive (100x more expensive) for scaling up and made the Boc-protection route more efficient. Reduction of the nitro group with hydrogen and palladium on carbon allowed for amide coupling with the HCl salt of 2-pyridinecarbonyl chloride in 14% yield over the three steps. Boc-deprotection with TFA resulted in the free aniline in 65%, which was followed by the addition of 2-chloro-4-nitrolcarbonyl chloride. This gave the VU374 core in 92% yield, and then was followed by an iron mediated nitro reduction. This helped avoid hydrodehalogenation that occurred when palladium on carbon and hydrogen were used. Finally, acylation of the resulting aniline using glycolic anhydride gave the extended VU374 analog in 20% yield over 2 steps.

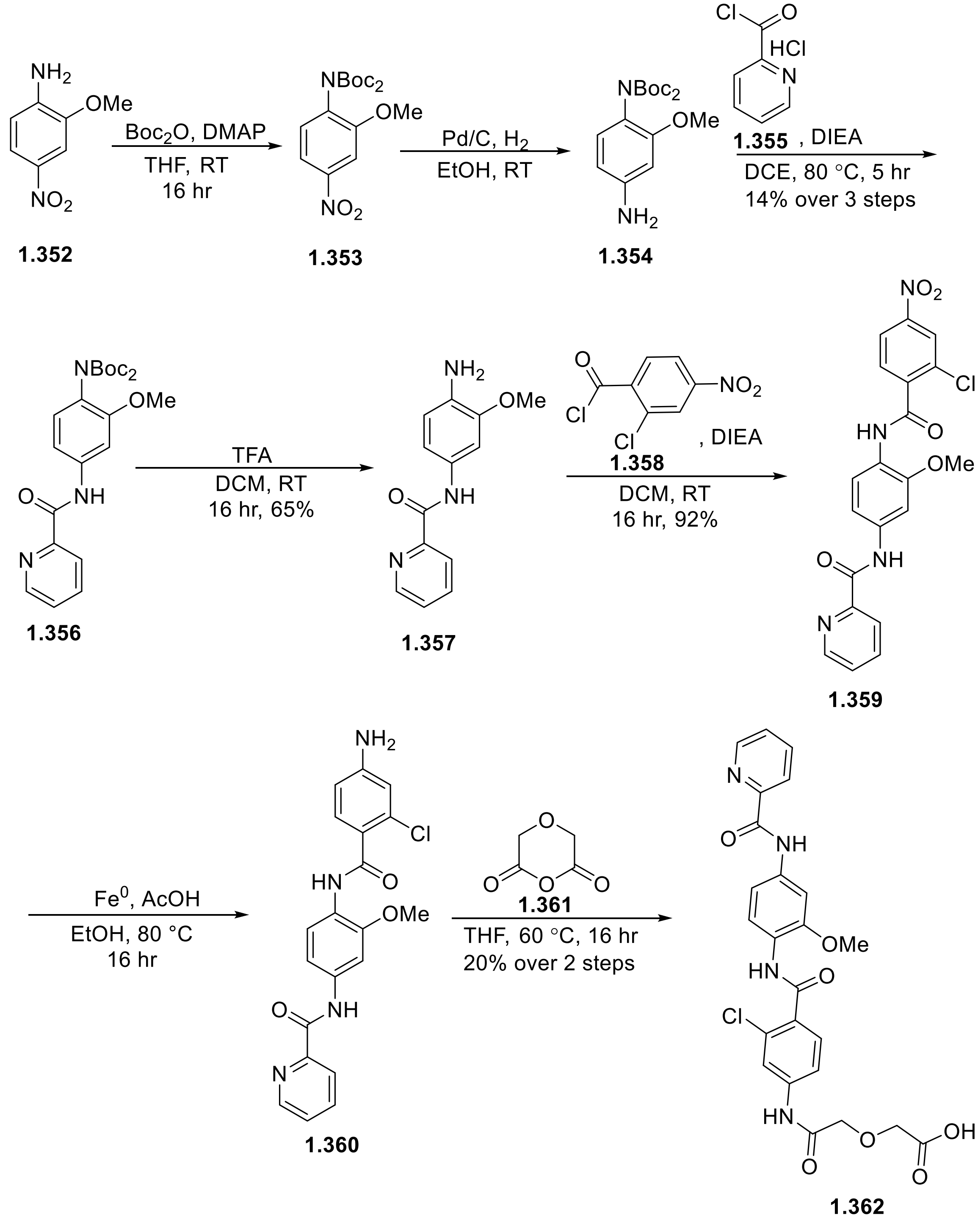
NH2
OMe
NO2
1.352
Boc2O, DMAP
THF, RT
16 hr
NBoc2
OMe
NO2
1.353
Pd/C, H2
EtOH, RT
NBoc2
OMe
NH2
1.354
Cl
O
HCl
N
1.355 , DIEA
DCE, 80 °C, 5 hr
14% over 3 steps
NBoc2
OMe
O
NH
N
1.356
TFA
DCM, RT
16 hr, 65%
NH2
OMe
O
NH
N
1.357
O
Cl
Cl
NO2
1.358
, DIEA
DCM, RT
16 hr, 92%
NO2
Cl
HN
O
OMe
O
NH
N
1.359
Fe0, AcOH
EtOH, 80 °C
16 hr
NH2
Cl
HN
O
OMe
O
NH
N
1.360
O
O
O
O
1.361
THF, 60 °C, 16 hr
20% over 2 steps
N
O
NH
OMe
HN
O
Cl
HN
O
O
OH
O
1.362

Scheme 1.11: Synthetic scheme used to achieve the synthesis of VU374 analog **1.362**.

Tether- Synthesis

To achieve the synthesis of the final tethered ligands, monoprotected boc-diamines were required to connect the BINA and VU374 analogs. These were synthesized according to known procedures using excess diamine in the presence of Boc anhydride in chloroform. Workup of this crude reaction and water washes resulted in crude Boc-diamines that were sufficiently pure for further transformations. First, HATU-mediated amide coupling between Boc- diamine gave the crude BINA amide with the linker chain attached. Saponification to reveal the free carboxylic acid was followed by Boc-deprotection using HCl in dioxanes to precipitate the HCl salt of the primary amine. These steps were performed without purification. Amide coupling of this amine with the VU374 analog in DMF using HATU followed by preparative reverse-phase HPLC gave the desired tethered ligands in 2-12% yields, which gave sufficient quantities for biological testing.

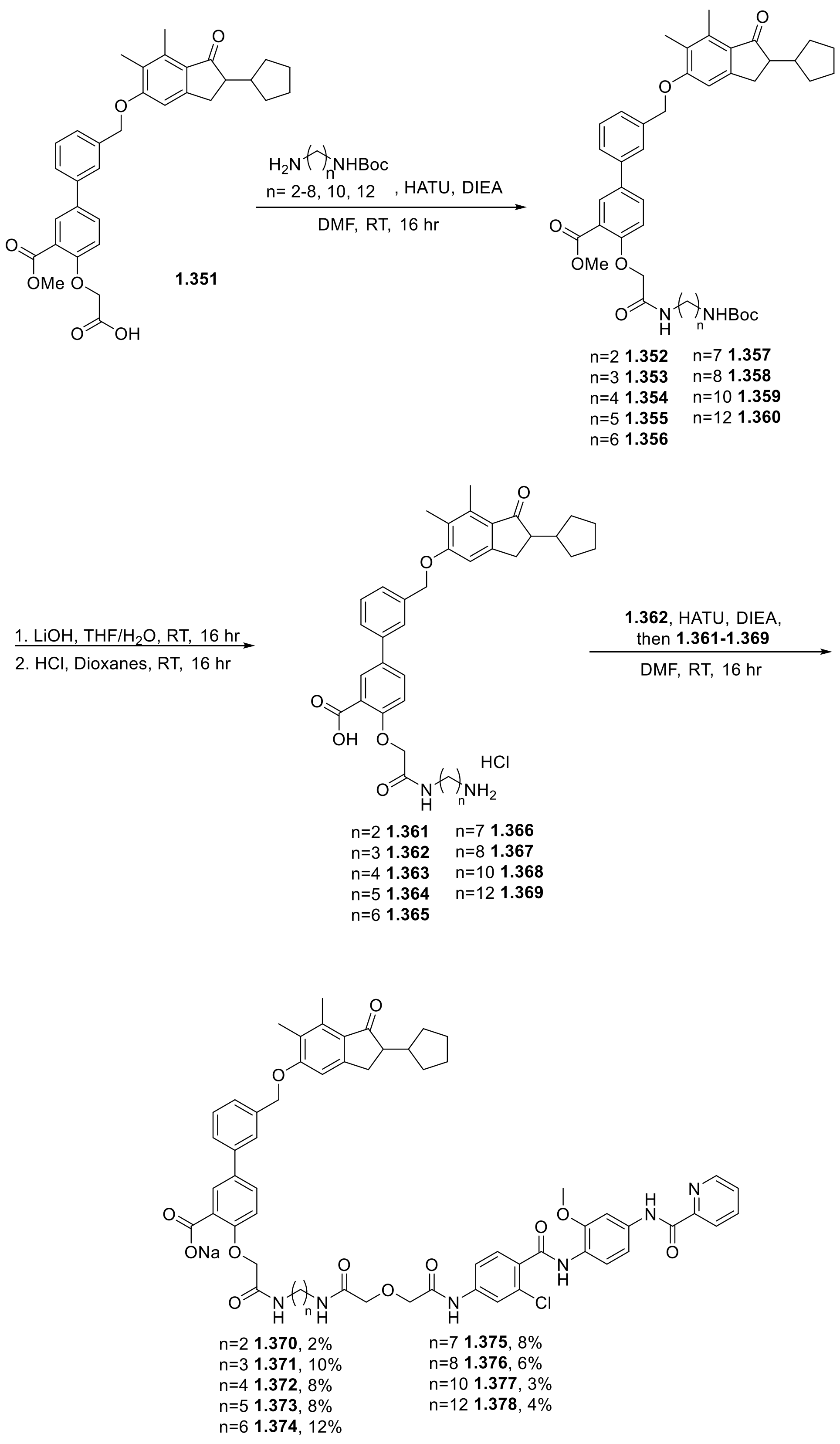
1.351
H2N( )nNHBoc
n= 2-8, 10, 12 , HATU, DIEA
DMF, RT, 16 hr
n=2 1.352
n=3 1.353
n=4 1.354
n=5 1.355
n=6 1.356
n=7 1.357
n=8 1.358
n=10 1.359
n=12 1.360
1. LiOH, THF/H2O, RT, 16 hr
2. HCl, Dioxanes, RT, 16 hr
HCl
n=2 1.361
n=3 1.362
n=4 1.363
n=5 1.364
n=6 1.365
n=7 1.366
n=8 1.367
n=10 1.368
n=12 1.369
1.362, HATU, DIEA,
then 1.361-1.369
DMF, RT, 16 hr
n=2 1.370, 2%
n=3 1.371, 10%
n=4 1.372, 8%
n=5 1.373, 8%
n=6 1.374, 12%
n=7 1.375, 8%
n=8 1.376, 6%
n=10 1.377, 3%
n=12 1.378, 4%

Scheme 1.12: Final steps utilized to achieve the synthesis of 9 linkers of varying spacing.

Tether-Pharmacology

The screening of these tethered ligands resulted in very complicated, somewhat opaque data. The tethered ligands were active across all three cell populations used in this study, both homomers and the heterodimer. This was actually very exciting because it indicates that the modifications made to each PAM did not render the PAMs inactive, which means that the tether of ideal length should work with our ligand design. When these compounds were screened in just the heterodimer cell line, some very interesting results were observed. As can be seen in **Figure 1.17**, there are some trends that can be observed. The intermediate linker lengths of 3-7 show a flattened CRC, whereas the linker lengths of 2, 8, 10, and 12 seem to display curves that are more typical in these assays. The steepness of the CRC is measured by the Hill coefficient for these assays, where numbers of 1 or greater are typical for standard CRCs. However, the flattened CRCs exhibit diminished Hill coefficients, from which one can at least determine that there is some differential effects in the heterodimer cell line versus each homodimer. Unfortunately, due to the presence of homomer populations in the heterodimer cell line, it is difficult to definitively determine if this flattening is due to our tethered ligand acting as desired, or if there is some role that the heteromer populations are playing in making these curves different. One thing that is interesting to note is that the curves for the 7 and 8 carbon linkers seem to display the biphasic curve that is indicative of a functioning tethered ligand. However, due to the complications arising from the population of homomers and heteromers in our heterodimer cell line, few conclusions that can be derived from our assay results. For this reason, we collaborated with the lab of Jonathan Javitch at Columbia, who utilized an assay developed in their lab for measuring signaling from heterodimeric receptors[123]. This assay is called complemented donor-acceptor resonance energy transfer (CODA-RET) and, per the name, relies on complementation between the two monomers in a heterodimeric protein. In this assay, a C or N-terminal fragment of luciferase is fused to the C-terminus of each monomer of the desired heterodimer. Thus, the protein is only functional in a heterodimeric complex, wherein the complementary fragments can come together and isolating the signal to heterodimers over the respective homomers. This luciferase protein acts as a bioluminescence resonance energy transfer (BRET) donor for a BRET acceptor protein, mVenus, fused to the Gα subunit of the GPCR. Receptor activation results in a conformational change that brings the BRET acceptor and donor together in space, resulting in a high BRET state. Thus, BRET signaling in this assay can be used to quantify receptor activation specifically from heterodimeric proteins.

Using the linkers of length n= 5, 10, 12 (**1.373**, **1.377**, **1.378, Figure 1.18**), it was shown that these PAMs were functional at homodimeric cell lines, but showed no significant potentiation versus vehicle in cell lines expressing the $mGlu_{2/4}$ heterodimer. These data highlight the fact that, while our cell line is perhaps the most biologically relevant compared to assays that utilize modified proteins to isolate heterodimer signaling, the lack of selectivity in signaling has greatly complicated data interpretation and clarity.

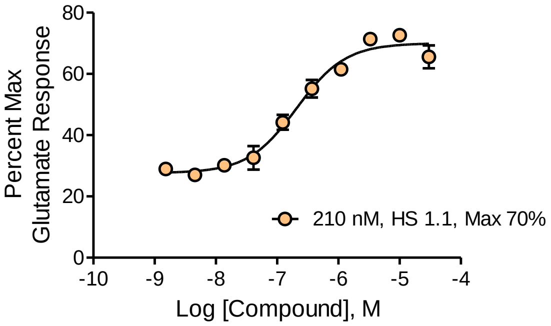
VU6023979 (2 carbon)

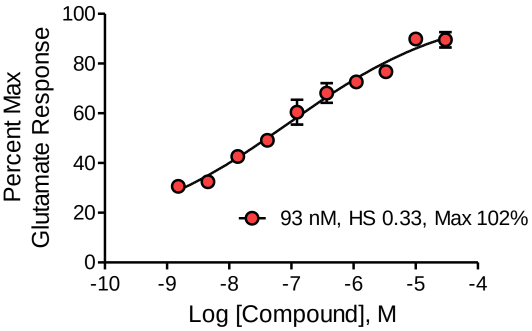
VU6023798 (3 carbon)

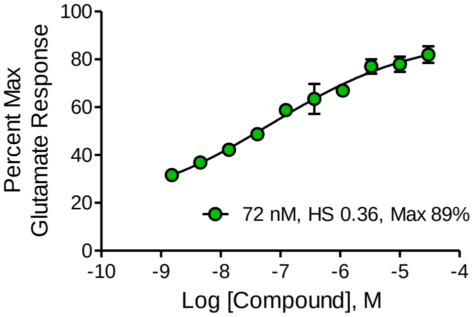
VU6023799 (4 carbon)

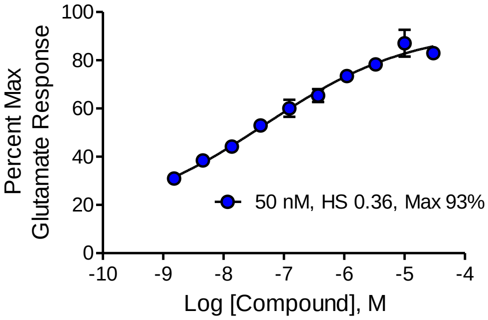
VU6023800 (5 carbon)

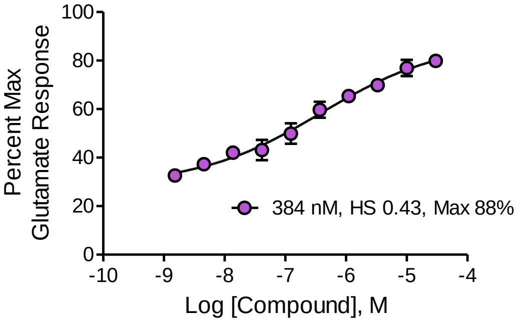
VU6023801 (6 carbon)

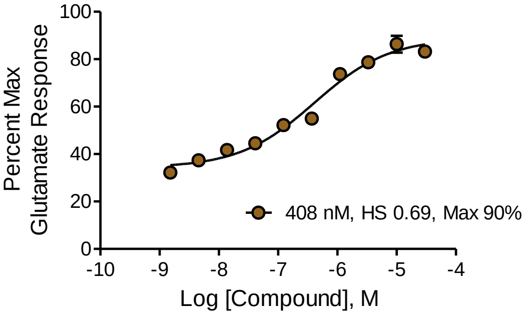
VU6023802 (7 carbon)

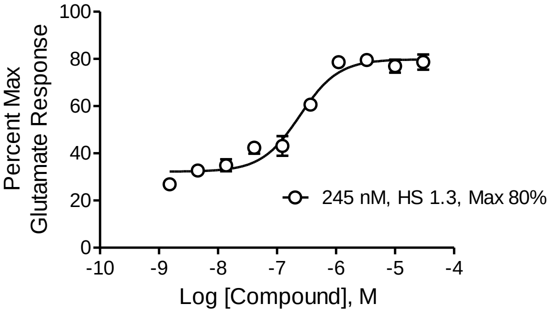
VU6023803 (8 carbon)

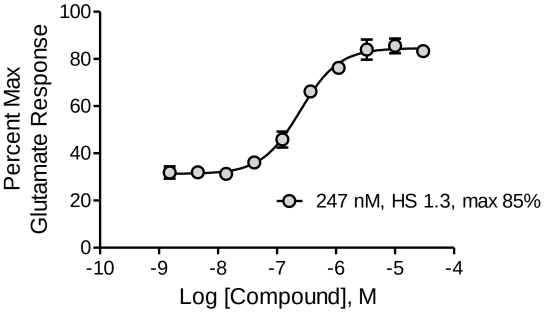
VU6023804 (10 carbon)

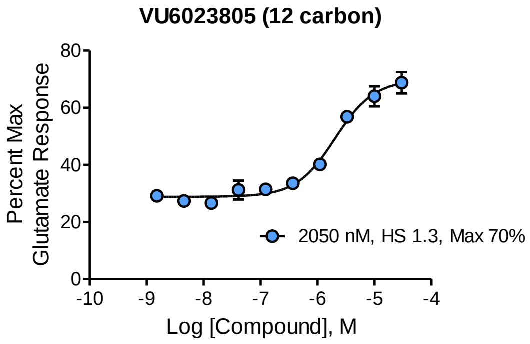

Figure 1.17. CRCs of each tethered ligand screened in cells expressing the mGlu$_{2/4}$ heterodimer exhibiting varying potencies and hill coefficients. Carbon spacers 3-7 have reduced Hill slopes, which was thought to be potentially indicative of dimeric interaction.

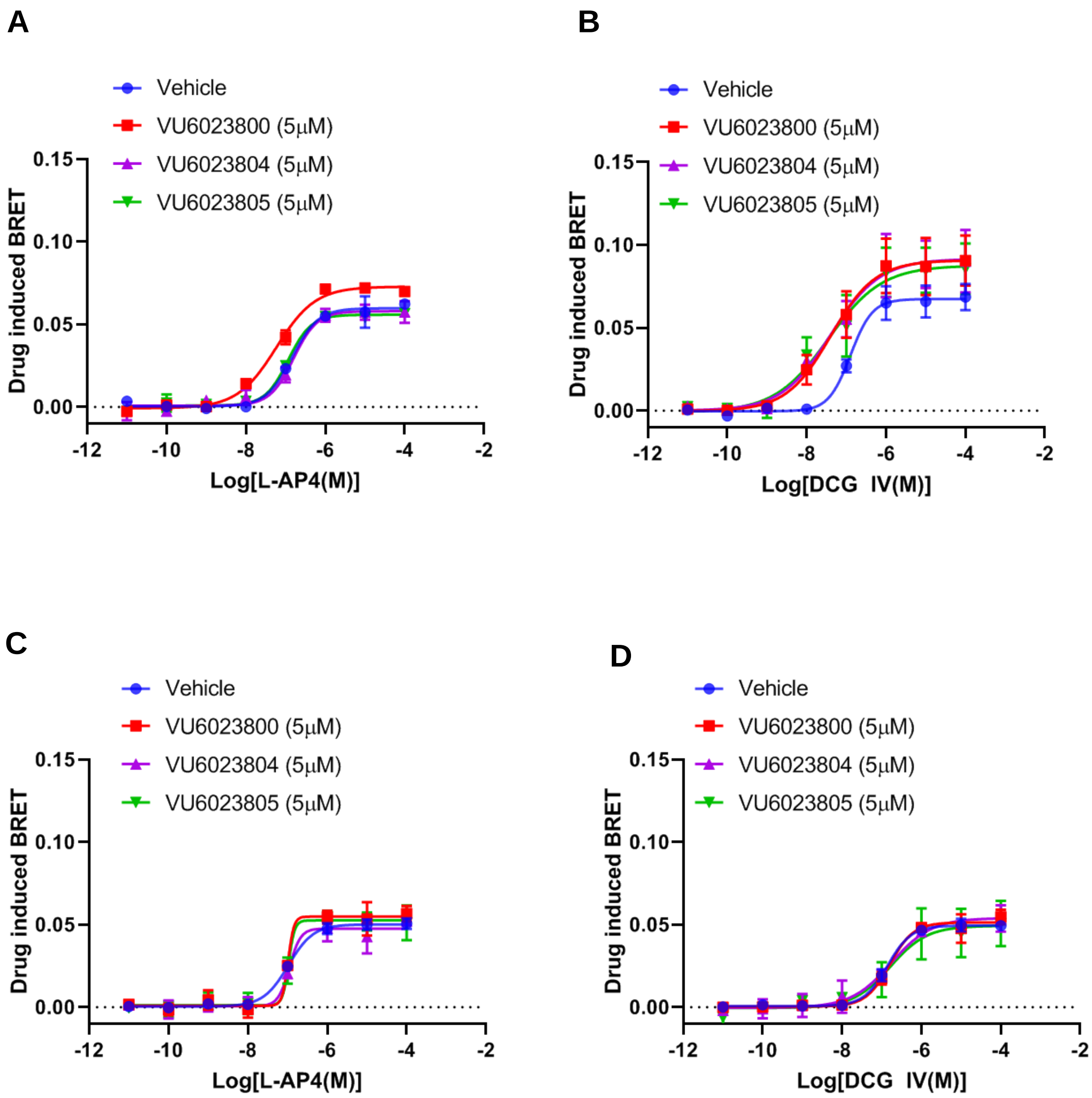

Figure 1.18. Data courtesy of the Javitch lab using DCG-IV, an agonist selective for mGlu$_2$ in this assay, and L-AP$_4$, selective for mGlu$_4$ activation. **A**. VU6023800 (VU800) acts as a PAM at mGlu$_4$ homodimers, while VU6023804 (VU804) and VU6023805 (VU805) do not. **B.** All 3 tethered ligands potentiate at mGlu$_2$ homodimers. **C**,**D**. None of the tested compounds show significant efficacy versus vehicle in mGlu$_{2/4}$ cell lines, indicating that there is no significant heterodimeric activation using these ligands.

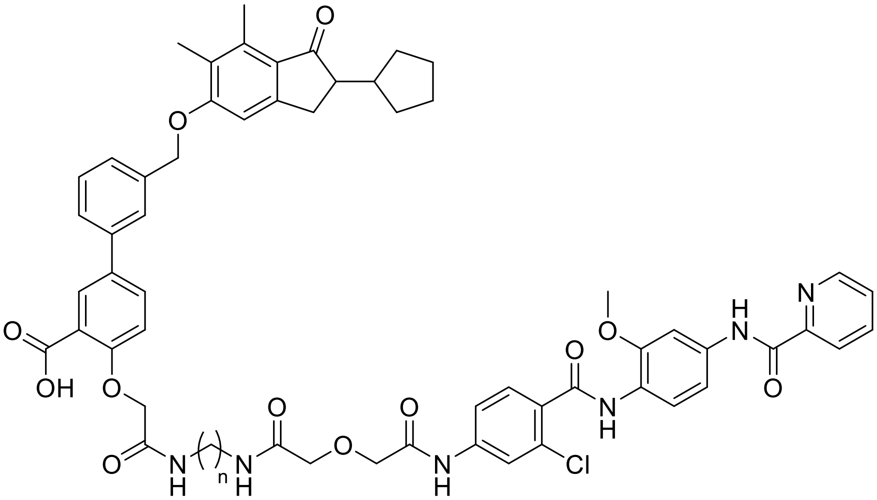

Table 1.17. 3,5-dihalogenated aniline analogs were explored to understand the most ideal halogen combination for potency and efficacy, and to better understand the trends in this series. Associated potency and efficacy data from 10-point CRC-format screen at rat mGlu$_{2/4}$ cell lines. Tl$^+$ flux responses for each compound are reported as a percentage of the maximum response. VU number denotes the compound identifier assigned by Vanderbilt University. Data represent the mean of at least 3 replicate experiments with similar results.

n	Compound Number	VUID	mGlu$_{2/4}$ EC$_{50}$ (nM)	mGlu$_{2/4}$ % Glu max	mGlu$_2$ EC$_{50}$ (nM)	mGlu$_2$ % Glu max	mGlu$_4$ EC$_{50}$ (nM)	mGlu$_4$ % Glu max
2	**1.370**	VU6023797	210	70	281	92	657	104
3	**1.371**	VU6023798	93	102	54	100	38	114
4	**1.372**	VU6023800	50	93	98	98	33	113
5	**1.373**	VU6023799	72	89	92	102	35	110

6	**1.374**	VU6023801	384	88	62	102	79	86
7	**1.375**	VU6023802	408	90	122	101	772	82
8	**1.376**	VU6023803	245	80	94	97	642	90
10	**1.377**	VU6023804	247	85	134	102	372	89
12	**1.378**	VU60023805	2,050	70	1,180	102	1,850	80

Summary, Conclusions, and Future Directions

In summary, 9 tethered ligands were synthesized utilizing $mGlu_2$ and $mGlu_4$ PAMs, with varying linker lengths to probe the distance between the allosteric pockets in the $mGlu_{2/4}$ heterodimer. These ligands were then tested in our GIRK cell-based assay which resulted in complex and opaque pharmacology. The data derived from these studies is hard to interpret due to the presence of $mGlu_2$ and $mGlu_4$ heteromers present in the heterodimer cell lines. However, differential pharmacology within the series hints at some difference between the tether lengths, where the extreme short and long lengths exhibited behavior that would indicate the two PAMs in the tether were acting as if they were monovalent. The intermediate lengths exhibited flattened CRCs, though it is again hard to discern why due to the multiple factors at hand. Due to these difficulties and concerns, the ligands were sent to the Javitch lab at Columbia University. Using their assay which is selective for heterodimer signaling, it was determined that the three compounds we sent for testing did not function as a heterodimeric ligand using agonists selective for each monomer of the heterodimer. This assay will be retried in the future with glutamate as an agonist, due to the fact that the literature reports that activation of both sides of the heterodimer are necessary for activity. These data highlight the difficulties that were incurred due to the nature of how we were expressing the $mGlu_{2/4}$ heterodimer. While our system was the most native in terms of its signaling pathways, the presence of $mGlu_2$ and $mGlu_4$ homodimers convolutes the data discovered in these assays. Assay optimization could be done to utilize cell lines that can isolate heterodimer signaling (i.e- FRET or CODA-RET based complimentarity assays), which would allow for a clearer picture of what receptor(s) PAMs are interacting with. Future directions for this project would be to test the remaining linker lengths to determine if any of them are an ideal length for bivalent activity. Additionally, the PAMs could be further modulated to test shorter and longer linker lengths to determine the ideal spacer length for use in this system. In terms of the discovery of a single small molecule PAM that may have more ideal DMPK properties than a tethered ligand, an HTS screen utilizing a cell line selective for $mGlu_{2/4}$ signaling (i.e- FRET or BRET) could be utilized to discover scaffolds that may be inherently selective for the heterodimer. Introducing selectivity to a scaffold is an inherently difficult task, further complicated by the lack of understanding of the $mGlu_{2/4}$ allosteric pocket, on either the $mGlu_2$ or $mGlu_4$ PAM, so starting with a scaffold that is selective would be ideal.

Experimental Methods

General synthetic methods and instrumentation

All NMR spectra were recorded on a 400 MHz AMX or 600 MHz AV-II Bruker NMR spectrometer. ^{1}H and ^{13}C chemical shifts are reported in δ values in ppm downfield with the deuterated solvent as the internal standard. Data are reported as follows: chemical shift, multiplicity (s = singlet, d = doublet, t = triplet, q = quartet, b = broad, m = multiplet), integration, coupling constant (Hz). Low-resolution mass spectra were obtained on an Agilent 6120 or 6150 with ESI source. Method A: MS parameters were as follows: fragmentor: 70, capillary voltage: 3000 V, nebulizer pressure: 30 psig, drying gas flow: 13 L/min, drying gas temperature: 350ºC. Samples were introduced via an Agilent 1290 UHPLC comprised of a G4220A binary pump, G4226A ALS, G1316C TCC, and G4212A DAD with ULD flow cell. UV absorption was generally observed at 215 nm and 254 nm with a 4 nm bandwidth. Column: Waters Acquity BEH C18, 1.0 x 50 mm, 1.7 um. Gradient conditions: 5% to 95% CH_3CN in H_2O (0.1% TFA) over 1.4 min, hold at 95% CH_3CN for 0.1 min, 0.5 mL/min, 55ºC. Method B: MS parameters were as follows: fragmentor: 100, capillary voltage: 3000 V, nebulizer pressure: 40 psig, drying gas flow: 11 L/min, drying gas temperature: 350ºC. Samples were introduced via an Agilent 1200 HPLC comprised of a degasser, G1312A binary pump, G1367B HP-ALS, G1316A TCC, G1315D DAD, and a Varian 380 ELSD (if applicable). UV absorption was generally observed at 215 nm and 254 nm with a 4 nm bandwidth. Column: Thermo Accucore C18, 2.1 x 30 mm, 2.6 um. Gradient conditions: 7% to 95% CH_3CN in H_2O (0.1% TFA) over 1.6 min, hold at 95% CH_3CN for 0.35 min, 1.5 mL/min, 45ºC. High-resolution mass spectra were obtained on an Agilent 6540 UHD Q-TOF with ESI source. MS parameters were as follows: fragmentor: 150, capillary voltage: 3500 V, nebulizer pressure: 60 psig, drying gas flow: 13 L/min, drying gas temperature: 275 ºC. Samples were introduced via an Agilent 1200 UHPLC comprised of a G4220A binary pump, G4226A ALS, G1316C TCC, and G4212A DAD with ULD flow cell. UV absorption was observed at 215 nm and 254 nm with a 4 nm bandwidth. Column: Agilent Zorbax Extend C18, 1.8 µm, 2.1 x 50 mm. Gradient conditions: 5% to 95% CH_3CN in H_2O (0.1% formic acid) over 1 min, hold at 95% CH_3CN for 0.1 min, 0.5 mL/min, 40ºC. For compounds that were purified on a Gilson preparative reversed-phase HPLC, the system comprised of a 333 aqueous pump with solvent selection valve, 334 organic pump, GX-271 or GX-281 liquid handler, two column switching valves, and a 155 UV detector. UV wavelength for fraction collection was user defined, with absorbance at 254 nm always monitored. Method: Phenomenex Axia-packed Luna C18, 30 x 50 mm, 5 µm column. Mobile phase: CH_3CN in H_2O (0.1% TFA). Gradient conditions: 0.75 min equilibration, followed by user-defined gradient (starting organic percentage, ending organic percentage, duration), hold at 95% CH_3CN in H_2O (0.1% TFA) for 1 min, 50 mL/min, 23ºC. Solvents for extraction, washing and chromatography were HPLC grade. All reagents were purchased from Aldrich Chemical Co. and were used without purification.

General Procedure for Compounds 1.5-1.79.

To a solution of 6 (0.13 mmol, 1 eq) in THF (0.5 mL, 0.26M) in a 1-dram vial at room temperature aniline/ heterocyclic amine (0.13 mmol, 1 eq) was added in one portion. The vial was sealed and the mixture heated to reflux for 16 hours to yield crude 1.5.

For compounds 1.6-1.79, after cooling to room temperature, N,N-Diisopropylethylamine (0.143 mmol, 1.1 eq) and isobutyl chloroformate (0.143 mmol, 1.1 eq) were added and the reaction was stirred for 30 minutes at room temperature. For primary carboxamide congeners, ammonium hydroxide (1mL) was added and the reaction was stirred for an additional hour at room temperature. For substituted amide analogs, desired amine (0.26, 2 eq) was added instead of ammonium hydroxide and stirring was continued for an additional 2 hours. The reaction was then diluted with ether (1mL), the layers were separated and the aqueous layer was extracted with ether (3x2mL). The organic layers were passed through a phase separator and concentrated in vacuo, and then crude product was purified using preparative HPLC (30x50mm column, MeCN/0.1% TFA:Water, 4 min gradient) to yield desired compounds 1.6-1.79

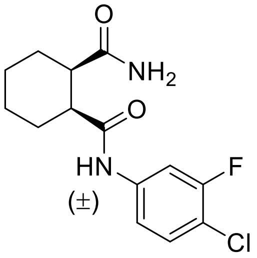

(1S,2R)-*N*1-(4-chloro-4-fluorophenyl)cyclohexane1,2-dicarboxamide (1.21). White solid, 24% yield. ^{1}H NMR (400 MHz, DMSO) δ 10.0 (s, 1H), 7.82 (dd, *J* = 12.5, 2.0 Hz, 1H), 7.49 (t, *J* = 9.1 Hz, 1H), 7.35 (dd, *J* = 9.1, 2.0 Hz, 1H), 7.09 (bs, 1H), 6.75 (bs, 1H), 2.85 (m, 1H), 2.51 (m, 1H), 2.21-2.10 (m, 1H), 2.09-2.00 (m, 1H), 1.77-1.64 (m, 3H), 1.61-1.50 (m, 1H), 1.46-1.29 (m, 2H); ^{13}C NMR (100 MHz, DMSO) δ 175.5, 173.5, 156.9 (d, J_{CF} = 243.5 Hz), 140.3 (d, J_{CF} = 10.2 Hz), 130.2, 115.9 (J_{CF} = 3.1), 112.0 (d, J_{CF} = 17.8), 107.0 (d, J_{CF} = 26.2 Hz), 43.3, 42.6, 27.4, 25.8, 24.0, 22.2. LCMS: 0.867 min; M+H= 299.2; >99% at 215 and 254 nm.

General Procedure for Compounds 1.82-1.89.

To a solution of 9 (0.06 mmol, 1 eq) in DMF (0.5 mL) in a 1-dram vial, HATU (0.126 mmol, 2 eq) and N,NDiisopropylethylamine (0.190 mmol, 3 eq) were added. The reaction was stirred for 10 minutes, then amine (0.076 mmol, 1.2 eq) was added and the reaction was stirred for 8 hours at room temperature. The crude reaction mixture was diluted with water (1.5mL) and extracted with DCM (3x2mL) and the organics were passed through a phase separator and concentrated in vacuo. Crude product was purified using preparative HPLC (30x50mm column, MeCN/0.1% TFA:Water, 4 min gradient) to yield desired compounds **1.82-1.89**.

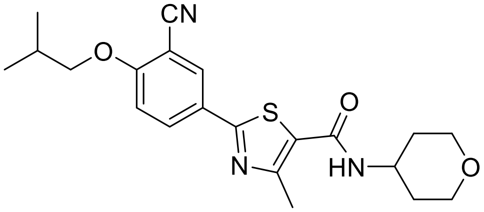

2-(3-cyano-4-iosbutoxyphenyl)-4-methyl-*N*-(tetrahydro-2H-pyran-4-yl)thiazole-5-carboxamide (1.85).

Yellow solid, 63% yield. ^{1}H NMR (400MHz, CDCl$_3$) δ 8.11 (d, *J* = 2.2 Hz, 1H), 8.04 (dd, *J* = 8.6, 2.2 Hz, 1H), 6.99 (d, *J* = 8.6 Hz, 1H), 5.72 (d, *J* = 7.5 Hz, 1H), 4.16 (m, 1H), 4.00 (m, 2H), 3.89 (d, *J* = 6.6 Hz, 2H), 3.52 (td, *J* = 11.6, 1.5 Hz, 2H), 2.71 (s, 3H), 2.19 (sep, *J* = 6.6 Hz, 1H), 1.97-2.05 (m, 2H), 1.58 (qd, *J* = 11.6, 4.1 Hz, 2H), 1.08 (d, *J* = 6.6 Hz, 6H); ^{13}C NMR (100 MHz, CDCl$_3$) δ 164.6, 162.5, 161.1, 132.6, 132.1, 126.1, 125.9, 115.6, 112.8, 103.1, 75.9, 66.9, 46.7, 33.3, 28.3, 19.2, 17.6. LCMS: 1.043 min; M+H= 400.2; >99% at 215 and 254 nm.

General Procedure for tert-butyl 3-[3-(3-chlorophenyl)-1,2,4-oxadiazol-5-

yl]azetidine-1-carboxylate and tert-butyl 3-[3-[3-(trifluoromethyl)phenyl]-1,2,4-oxadiazol-5-yl]azetidine-1-carboxylate (1.93-1.94).

To a solution of 3-chloro-*N′*-hydroxybenzenecarboximidamide or 3-(trifluoromethyl)benzamidoxime (1 eq), T3P (2.5 eq), and triethylamine (3 eq) in ethyl acetate (0.2 M) in a microwave vial was added 1-Boc-azetidine-3-carboxylic acid (1 eq). The vial was capped and the reaction was heated to 150 °C via microwave irradiation for 30 minutes. After cooling to room temperature, the reaction was washed with saturated ammonium chloride, then extracted with EtOAc (3x), and the organics were pooled, passed through a phase separator and concentrated *in vacuo*. Crude product was purified using Teledyne ISCO Combi-Flash system (0-50% EtOAc/Hex) to yield desired products.

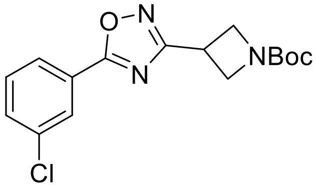

3-[3-(3-chlorophenyl)-1,2,4-oxadiazol-5-yl]azetidine-1-carboxylate (1.93).

Yellow oil, 61%. ^{1}HNMR (400 MHz, CDCl$_3$) δ 7.98 (t, *J* = 1.7, 1H), 7.87 (dt, *J* = 7.6, 1.3 Hz, 1H), 7.40-7.37 (m, 1H), 7.32 (t, *J* = 7.7 Hz, 1H), 4.31 (t, *J* = 8.8 Hz, 2H), 4.24 (dd, *J* = 8.7, 6.0 Hz, 2H), 4.05-3.92 (m, 1H), 1.40 (s, 9H); ^{13}CNMR (100 MHz, CDCl$_3$) δ 179.4, 167.5, 155.8, 134.9, 131.3, 130.2, 128.2, 127.4, 125.5, 80.1, 53.2, 28.3, 25.7.

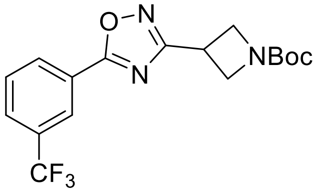

tert-butyl 3-[3-[3-(trifluoromethyl)phenyl]-1,2,4-oxadiazol-5-yl]azetidine-1-

carboxylate (1.94).

Yellow oil, 57%. ^{1}HNMR (400 MHz, CDCl$_3$) δ 8.36 (bs, 1H), 8.27 (d, *J* = 7.8 Hz, 1H), 7.75 (t, *J* = 7.84 Hz, 1H), 7.63 (d, *J* = 7.84 Hz, 1H), 4.39 (t, *J* = 4.4 Hz, 2H), 4.32 (dd, *J* = 8.6, 6.0 Hz, 2H), 4.06 (tt, *J* = 7.4, 6.0 Hz, 1H), 1.46 (s, 9H); ^{13}CNMR (100 MHz, CDCl$_3$) 179.8, 167.8, 156.1, 131.4 (q, *J* = 32.8 Hz), 130.7, 139.7, 128.1 (q, *J* = 3.7 Hz), 127.6, 124.6 (q, *J* = 3.8 Hz), 123.9 (q, *J* = 270.7 Hz), 80.5, 53.3, 28.5, 25.9.

General Procedure for 5-(azetidin-3-yl)-3-(3-chlorophenyl)-1,2,4-oxadiazole hydrochloride and 5-(azetidin-3-yl)-3-[3-(trifluoromethyl)phenyl]-1,2,4-oxadiazole hydrochloride (1.95-1.96).

To a solution of **1.93** or **1.94** (1 eq) in 1,4-Dioxane (0.37 M) was added 4M HCl/Dioxane slowly. The reaction was stirred for 6 hours, at which point LCMS analysis indicated full conversion of starting material to desired product and a precipitate had formed. The precipitate was isolated *via* vacuum filtration, washing with ether and hexanes, to yield the desired product as a white solid.

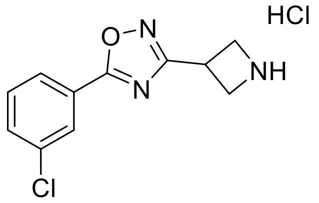

5-(azetidin-3-yl)-3-(3-chlorophenyl)-1,2,4-oxadiazole hydrochloride (1.95).

White solid, 75% yield. ^{1}HNMR (400 MHz, DMSO) δ 9.70 (bs, 1H), 9.43 (bs, 1H), 8.03-7.98 (m, 2H), 7.76-7.68 (m, 1H), 7.64 (t, *J* = 7.8 Hz, 1H), 4.59 (m, 1H), 4.42-4.25 (m, 4H); ^{13}CNMR (100 MHz, DMSO) δ 178.6, 166.6, 134.0, 131.6, 131.4, 127.9, 126.5, 125.6, 48.2, 28.1.

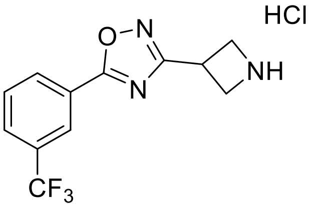

5-(azetidin-3-yl)-3-[3-(trifluoromethyl)phenyl]-1,2,4-oxadiazole hydrochloride (1.96).

White solid, 30% yield. ^{1}HNMR (400 MHz, DMSO) δ 9.63 (bs, 2H), 8.34 (d, *J* = 7.8 Hz, 1H), 8.27 (s, 1H), 8.02 (d, *J* = 7.9 Hz), 7.87 (t, *J* = 7.8 Hz, 1H), 4.60-4.49 (m, 1H), 4.41-4.29 (m, 4H); ^{13}CNMR (100 MHz, DMSO) δ 178.9, 166.6, 130.9, 130.4 (q, *J* = 32.2), 128.4 (q, *J* = 3.54), 127.0, 123.7 (q, *J* = 270.7), 123.3 (q, *J* = 3.9), 48.4, 28.2.

General Procedure for 1.98-1.139.

To a solution of substituted benzoic acid (1 eq) in DMF (0.2 M) at room temperature was added HATU (2 eq) and DIEA (4 eq). This mixture was stirred for 10 minutes before the addition of **1.95** or **1.96**. The reaction was allowed to stir overnight, then diluted with water (1 mL) and extracted with DCM (3x2 mL). The organics were passed through a phase separator then purified by Gilson HPLC to yield desired compounds.

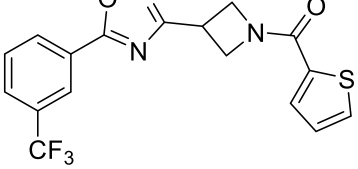

[3-[3-(3-chlorophenyl)-1,2,4-oxadiazol-5-yl]azetidin-1-yl]-(3-fluoro-2-thienyl)methanone (1.130).

Clear oil, 40% yield. ^{1}HNMR (400 MHz, $CDCl_3$) δ 8.38 (s, 1H), 8.29 (d, *J* = 7.8 Hz, 1H), 7.79, (d, *J* = 8.1 Hz, 1H), 7.65 (t, *J* = 7.8 Hz, 1H), 7.58-7.55 (m, 2H), 7.15-7.12 (m, 1H), 4.99-4.54 (m, 4H), 4.28 (tt, *J* = 7.5, 6.0 Hz, 1H); ^{13}CNMR (100 MHz, $CDCl_3$) δ 179.2, 167.9, 163.2, 136.0, 131.8 (q, *J* = 32.7 Hz), 131.0, 130.8, 130.8, 129.8, 128.2 (q, *J* = 3.7 Hz), 127.9, 127.4, 124.7 (q, *J* = 3.8), 123.9 (q, *J* = 271 Hz), 26.7.

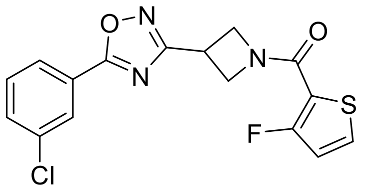

2-thienyl-[3-[3-[3-(trifluoromethyl)phenyl]-1,2,4-oxadiazol-5-yl]azetidin-1-yl]methanone (1.134).

Clear oil, 5%. ^{1}HNMR (600 MHz, $CDCl_3$) δ 8.01 (t, *J* = 1.7 Hz, 1H), 7.99 (dt, *J* = 4.4, 1.1 Hz, 1H), 7.51-7.48 (m, 1H), 7.44 (t, *J* = 7.9 Hz, 1H), 7.42 (t, *J* = 5.5 Hz, 1H), 6.83 (d, *J* = 5.5 Hz, 1H), 4.87-4.52 (m, 4H), 4.23 (tt, *J* = 7.7, 6.2 Hz, 1H); ^{13}CNMR (125 MHz, $CDCl_3$) δ 179.1, 167.9, 156.0 (d, *J* = 222 Hz) 135.2, 131.7, 130.4, 129.7 (d, *J* = 8.3 Hz), 128.3, 127.8, 125.8, 118.2 (d, *J* = 22.7 Hz), 115.9 (d, *J* = 12.8 Hz), 26.6, 26.5 ppm.

General Procedure for the synthesis of 1.143-1.181.

To a solution of 5-(p-tolyl)-1,3,4-oxadiazol-2-amine (1 eq) in DMF (0.05 eq) at room temperature was added DIEA (3 eq) and substituted acyl chloride (1.2 eq) or carboxylic acid (1.2 eq) and HATU (1.1 eq). The reaction was stirred overnight at room temperature, then diluted with water (2 mL) and extracted with DCM (3x2mL).

The organics were passed through a phase separator then concentrated under a constant stream of air and purified using Gilson HPLC to yield desired material in 2-20% yield.

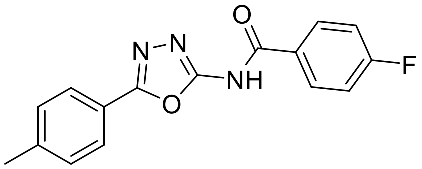

4-fluoro-N-[5-(p-tolyl)-1,3,4-oxadiazol-2-yl]benzamide (1.143).

White solid, 11% yield. ^{1}HNMR (600 MHz, DMSO) δ 8.16-8.09 (m, 2H), 7.86 (d, *J* = 7.9 Hz, 2H), 7.45-7.38 (m, 4H), 2.40 (s, 3H); ^{13}CNMR (125 MHz, DMSO) δ 165.3 (d, *J* = 208 Hz), 161.9, 158.1, 142.4, 131.7 (d, *J* = 7.5 Hz), 130.5, 129.2 (d, *J* = 10.8 Hz), 126.5, 121.1, 116.2 (d, *J* = 18.1 Hz), 21.6.

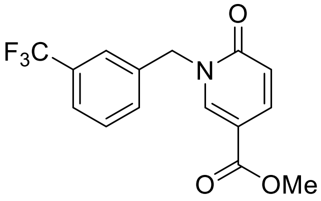

methyl 6-oxo-1-[[3-(trifluoromethyl)phenyl]methyl]pyridine-3-carboxylate (1.154).

To a solution of methyl 6-hydroxynicotinate (300 mg, 1.96 mmol) in DMF (9.8 mL) at 23 °C was added potassium carbonate (412 mg, 2.94 mmol) and 3-(trifluoromethyl)benzyl bromide (359 μL, 2.35 mmol). The reaction was stirred for 5 hours, at which point LCMS analysis indicated full conversion to desired product. The reaction was diluted with water (10 mL) and extracted with DCM (3x10 mL). The organics were washed with water (2x20 mL), then passed through a phase separator and concentrated *in vacuo*. Crude product was purified using Teledyne ISCO Combi-Flash system (solid loading, 12G column, 0-50% EtOAc/Hex) to yield

methyl 6-oxo-1-[[3-(trifluoromethyl)phenyl]methyl]pyridine-3-carboxylate (390 mg,1.25 mmol, 63.96% yield) as a white solid. ^{1}HNMR (400 MHz, $CDCl_3$) δ 8.21 (d, *J* = 2.4 Hz, 1H), 7.82 (dd, *J* = 9.6, 2.5 Hz, 1H), 7.56 (bs, 1H), 7.53 (d, *J* = 7.7 Hz, 1H), 7.48 (d, *J* = 7.7 Hz, 1H), 7.44 (q, *J* = 7.6 Hz, 1H), 5.18 (s, 2H), 3.80 (s, 3H); ^{13}CNMR (100 MHz, $CDCl_3$) δ 164.5, 162.3, 142.7, 138.9, 136.7, 131.5, 131.3 (q, *J* = 31.5 Hz), 129.6, 125.3 (q, *J* = 3.7 Hz), 124.9 (q, *J* = 3.7 Hz), 123.9 (q, *J* = 276 Hz), 120.2, 110.4, 52.6, 52.2.

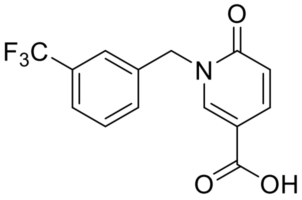

6-oxo-1-[[3-(trifluoromethyl)phenyl]methyl]pyridine-3-carboxylic acid (1.155). To a solution of methyl 6-oxo-1-[[3-(trifluoromethyl)phenyl]methyl]pyridine-3-carboxylate (390 mg, 1.25 mmol) in THF (6 mL) at 23 °C was added lithium hydroxide (6 mL, 6 mmol) and the reaction was stirred for 1 hour, at which point LCMS analysis indicated product formation. The organics were removed *in vacuo*, then the aqueous was acidifed with 2M HCl and extracted with ether (2x5 mL), DCM (2x5 mL) and EtOAc (2x10 mL). The organics were passed through a phase separator then concentrated *in vacuo* to yield 6-oxo-1-[[3-(trifluoromethyl)phenyl]methyl]pyridine-3-carboxylic acid (122 mg,0.41 mmol, 33% yield) as a white solid. ^{1}HNMR (400 MHz, DMSO) δ 8.68 (d, *J* = 2.4 Hz, 1H), 7.82 (dd, *J* = 9.5, 2.5 Hz, 1H), 7.73 (bs, 1H), 7.65 (d, *J* = 7.0 Hz, 1H), 7.63-7.55 (m, 2H), 6.46 (d, *J* = 9.5 Hz, 1H), 5.28 (s, 2H). ^{13}CNMR (100 MHz, $CDCl_3$) δ 165.3, 161.6, 144.0, 139.4, 138.3, 131.9, 129.8, 129.2 (q, *J* = 31.5 Hz), 124.6 (q, *J* = 3.7 Hz), 124.5 (q, *J* = 3.6 Hz), 124.1 (q, *J* = 271 Hz), 120.0, 118.9, 110.4, 51.5.

General Procedure for the synthesis of 1.157-1.181.

To a solution of 6-oxo-1-[[3-(trifluoromethyl)phenyl]methyl]pyridine-3-carboxylic acid (1 eq) in DCM (0.03M) was added PYCLU (2 eq) and DIEA (2 eq). The reaction was stirred for 15 minutes before addition of amine (1 eq) and the reaction was heated to 100 °C for 30 minutes using microwave irradiation. The reaction was quenched by addition of water (2mL) then extracted with DCM (3x4mL) and the organics were passed through a phase separator and concentrated under a stream of constant air. Crude product was purified using Gilson HPLC to yield desired materials in 8-47% yield.

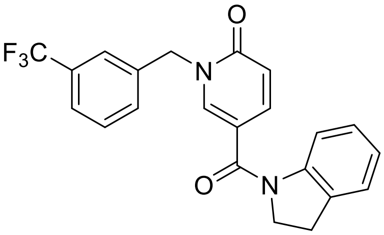

5-(indoline-1-carbonyl)-1-(3-(trifluoromethyl)benzyl)pyridin-2(1H)-one (1.161). White solid, 45% yield. ^{1}HNMR (400 MHz, $CDCl_3$) δ 7.85 (d, *J* = 2.4 Hz, 1H), 7.62-7.56 (m, 3H), 7.54 (d, *J* = 7.7, 1H), 7.50 (q, *J* = 7.6 Hz, 1H), 7.22 (d, *J* = 7.3 Hz), 7.11 (t, *J* = 7.3 Hz, 1H), 7.03 (t, *J* = 7.3 Hz, 1H), 6.66 (d, *J* = 9.4 Hz, 1H), 5.22 (s, 2H), 4.10 (t, *J* = 8.1 Hz, 2H), 3.12 (t, *J* = 8.1 Hz, 2H); ^{13}CNMR (100 MHz, $CDCl_3$) δ 164.8, 162.3, 142.3, 140.2, 138.8, 136.7, 132.7, 131.9, 131.6 (q, *J* = 32.3 Hz), 129.8, 127.5, 125.5 (q, *J* = 3.7 Hz), 125.4, 125.2 (qq, *J* = 3.7), 124.5, 123.9 (q, *J* = 271 Hz), 120.4, 116.8, 116.2, 52.6, 50.9, 28.4.

General Procedure for 1.185-1.210.

To a solution of 4-(3-aminophenyl)benzonitrile (1 eq) in methanol (0.2M) at room temperature was added corresponding aldehyde (1.6 eq) and the reaction was heated to 60 °C for 2 hours. After cooling to room temperature, sodium borohydride (2 eq) was added and the reaction was stirred an additional hour at room temperature, then diluted with water (5mL) and extracted with DCM (3x8mL). The organics were passed through a phase separator and concentrated *in vacuo*, then the resulting crude intermediate was dissolved in THF (0.2M) and to this solution was added pyridine (1 eq) and ethanesulfonyl chloride (1.2 eq) for **1.185-1.208** or 2,2,2-trifluoroethylsulfonyl chloride (1.2 eq) for **1.209-1.210**. The reaction was heated to 60 °C overnight, then cooled to room temperature and diluted with water (3mL) and extracted with ether (3x3mL). The organics were pooled, passed through a phase separator and concentrated under a constant stream of air, then purified using Gilson HPLC to give desired materials in 2-45% yield.

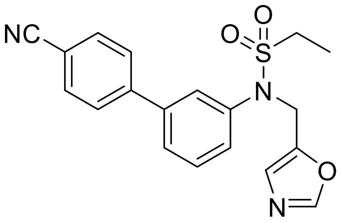

***N*-(4'-cyano-[1,1'-biphenyl]-3-yl)-*N*-(thiazol-5-ylmethyl)ethanesulfonamide (1.194)**. Brown solid, 45% yield. ^{1}HNMR (400 MHz, $CDCl_3$) δ 8.73 (s, 1H), 7.69 (d, *J* = 8.4 Hz, 2H), 7.58 (t, *J* = 7.1 Hz, 3H), 7.55-7.50 (m, 1H), 7.47 (d, *J* = 7.8 Hz, 1H), 7.45 (t, *J* = 1.8 Hz, 1H), 7.35-7.28 (m, 1H), 5.13 (s, 2H), 3.10 (q, *J* = 7.4 Hz, 2H), 1.42 (t, *J* = 7.4 Hz, 3H); ^{13}CNMR (100 MHz, $CDCl_3$) δ 154.5, 144.2, 143.3, 140.9, 139.3, 134.1, 132.8, 130.4, 128.6, 128.4, 127.9, 127.4, 118.8, 111.7, 53.6, 47.6, 46.6, 8.2.

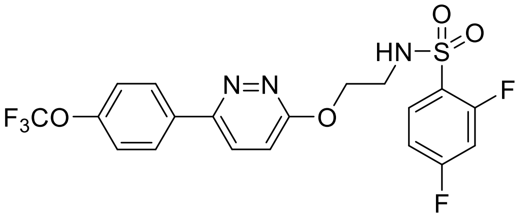

2,4-difluoro-*N*-[2-[6-[4-(trifluoromethoxy)phenyl]pyridazin-3-yl]oxyethyl]benzenesulfonamide (1.217).

To a solution of 2-(6-chloropyridazin-3-yl)oxyethanamine (882 mg, 5.08 mmol) in DCM (25.403mL) at 23 ^oC was added DIEA (1.77 mL, 10.16 mmol, 2 eq) and 2,4-difluorobenzenesulfonyl chloride (1296 mg, 6.1 mmol, 1.2 eq). The reaction was stirred for 2 hours at this temperature, then diluted with water (20mL) and the layers were separated, the aqueous was extracted with DCM (2x20mL), then the organics were pooled, dried over magnesium sulfate, filtered, and concentrated *in vacuo*. Crude product was purified using Teledyne ISCO Combi-Flash system (solid loading, 12G column, 0-60% EtOAc/Hex) to yield N-[2-(6-chloropyridazin-3-yl)oxyethyl]-2,4-difluoro-benzenesulfonamide (763 mg, 2.18 mmol, 43% yield) as a tan solid. ^{1}HNMR (400 MHz, DMSO) δ 8.31 (t, *J* = 5.6 Hz, 1H), 7.91-7.81 (td, *J* = 8.6, 6.4 Hz, 1H), 7.75 (d, *J* = 9.2 Hz, 1H), 7.49-7.41 (m, 1H), 7.24 (td, *J* = 8.4, 2.0 Hz, 1H), 7.13 (d, *J* = 9.2 Hz, 1H), 4.39 (t, *J* = 5.3 Hz, 2H), 3.36 (q, *J* = 7.0 Hz, 2H); ^{13}CNMR (100 MHz, DMSO) δ 166.0 (d, *J* = 11.8 Hz), 163.9, 163.5 (d, *J* = 11.7), 160.2 (d, *J* = 13.5 Hz), 157.6 (d, *J* = 13.2), 150.8, 131.6, 131.5 (d, *J* = 11.3), 125.5 (dd, *J* = 57.2, 3.65 Hz), 120.8, 112.2 (dd, *J* = 86.7, 3.41 Hz), 105.9 (t, *J* = 25.9 Hz), 65.8, 41.4.

To a solution of *N*-[2-(6-chloropyridazin-3-yl)oxyethyl]-2,4-difluoro-benzenesulfonamide (100 mg, 0.29 mmol, 1 eq) in 1,4-dioxane (0.14M) in a 2-5 mL microwave vial was added aqueous sodium carbonate (2M, 429 μL, 0.86 mmol, 3 eq), 4-trifluoromethoxyphenylboronic acid (71 mg, 0.34 mmol, 1.2 eq) and tetrakis(triphenylphosphine)palladium(0) (17 mg, 0.01 mmol, 0.05 eq). The vial was sealed and heated to 120 °C for 30 minutes using microwave irradiation. After cooling to room temperature, the reaction mixture was filtered through a plug of celite, washing with EtOAc (3x10mL). The layers were separated and the aqueous was extracted with EtOAc (3x5mL), then the organics were pooled, dried over magnesium sulfate, filtered, and concentrated *in vacuo*. Crude product was purified using Gilson HPLC (55-85% 0.1% aq. TFA/MeCN) to yield 2,4-difluoro-N-[2-[6-[4-(trifluoromethoxy)phenyl]pyridazin-3-yl]oxyethyl]benzenesulfonamide (88 mg, 0.19 mmol, 65%) as a white solid. ^{1}HNMR (400 MHz, $CDCl_3$) δ 8.01-7.95 (m, 2H), 7.93 (td, *J* = 8.5, 6.2 Hz, 1H), 7.75 (d, *J* = 9.2 Hz), 7.31 (d, *J* = 8.3 Hz, 2H), 6.99 (d, *J* = 9.2 Hz, 1H), 6.97-6.92 (m, 1H), 6.89-6.82 (m, 1H), 5.73 (t, *J* = 6.0 Hz, 1H), 4.62 (t, *J* = 5.1 Hz, 2H), 3.55 (q, *J* = 5.2 Hz, 2H); ^{13}CNMR (100 MHz, $CDCl_3$) δ 167.1 (d, *J* = 11.6 Hz), 164.6 (d, *J* = 11.5 Hz), 163.8, 160.9 (d, *J* = 12.8 Hz), 158.4 (d, *J* = 12.8 Hz), 154.6, 150.5, 134.6, 132.0 (d, *J* = 9.9 Hz), 128.2, 127.5, 125.0 (dd, *J* = 56.0, 3.65 Hz), 121.4, 120.6 (d, *J* = 256 Hz), 118.0, 112.1 (dd, *J* = 86.6, 3.50 Hz), 105.7 (t, *J* = 25.4 Hz), 66.0, 42.7.

General Procedure for the synthesis of 1.273-1.282.

To a solution of *p*-toluoyl chloride (1 eq) in acetone (0.19M) was added potassium thiocyanate (1.65 eq) and the reaction was stirred for 30 minutes at room temperature. Next, the corresponding amine (2 eq) was added and the reaction was stirred overnight, then diluted with water (2mL) and extracted with DCM (3x3mL). The organics were passed through a phase separator, then concentrated under a stream of constant air and crude product was purified using Gilson HPLC to yield desired material in 5-39% yield.

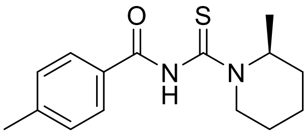

N-(cyclopentylcarbamothioyl)-4-methyl-benzamide (1.281).

Pink oil, 32% yield. ^{1}HNMR (400 MHz, $CDCl_3$) δ 8.33 (bs, 1H), 7.73 (d, *J* = 8.2 Hz, 2H), 7.27 (d, *J* = 8.0 Hz, 2H), 3.36-3.27 (m, 1H), 2.40 (s, 3H), 1.99-1.88 (m, 1H), 1.78-1.61 (m, 5H), 1.36 (d, *J* = 7.0 Hz, 3H); ^{13}CNMR (100 MHz, $CDCl_3$) δ 178.5, 163.4, 143.9, 130.0, 129.7, 128.0, 54.9, 47.3, 30.0, 25.8, 21.7, 18.3, 15.5.

General Procedure for the synthesis of 1.287-1.334.

To a solution of (3R)-5-oxo-1,4-thiazepane-3-carboxylic acid (1 eq) in DMF (0.2M) was added HATU (2 eq) and DIEA (3 eq). The reaction was stirred for 15 minutes, then the corresponding aniline/amine nucleophile was added and the reaction was stirred overnight at room temperature. The reaction was then diluted with water (2mL) and extracted with DCM (3x2mL), then the organics were pooled, passed through a phase separator and concentrated *in vacuo*. Crude product was purified using Gilson HPLC to yield desired material in 5-48% yield.

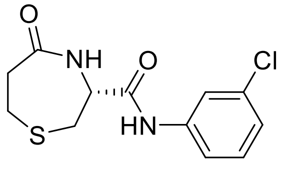

(3R)-*N*-(3-chlorophenyl)-5-oxo-1,4-thiazepane-3-carboxamide (1.299).

Yellow oil, 48%. ^{1}HNMR (400 MHz, DMSO) δ 10.40 (s, 1H), 7.80 (t, *J* = 2.0 Hz, 1H), 7.48-7.44 (m, 1H), 7.36 (t, *J* = 8.0 Hz, 1H), 7.17-7.13 (m, 1H), 7.13-7.09 (m, 1H), 4.54-4.48 (m, 1H), 3.03 (dd, *J* = 14.4, 2.2 Hz, 1H), 2.95 (dd, *J* = 14.4, 8.2 Hz, 1H), 2.90-2.73 (m, 3H), 2.72-2.68 (m, 2H); ^{13}CNMR (100 MHz, $CDCl_3$) δ 174.3, 168.1, 134.0, 133.1, 130.1, 123.5, 119.1, 118.0, 57.8, 40.3, 33.9, 23.5.

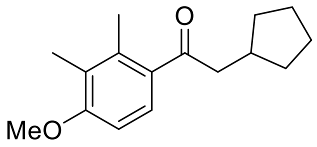

1-methoxy-2,3-dimethylbenzene (1.341).

To a solution of cyclopentyl acetic acid (6.2 g, 48.4 mmol, 1 eq) was added thionyl chloride (16.5 mL, 226.4 mmol, 4.7 eq) and the reaction was heated to reflux for 1 hour. After cooling to room temperature, the reaction was concentrated *in vacuo*, then the resulting residue was dissolved in DCM (242 mL, 0.2M) and placed in an ice bath. Next, 2,3-dimethylanisole (8.0 mL, 58 mmol, 1.2 eq) and aluminum chloride (6.45 g, 48 mmol, 1 eq) were added and the reaction was allowed to slowly warm to room temperature overnight. The reaction was quenched by pouring over crushed ice, then the layers were separated and the aqueous was extracted with DCM (3x50 mL). The organics were pooled, dried over magnesium sulfate, filtered, and concentrated *in vacuo*, then crude product was purified using Teledyne ISCO Combi-Flash system (liquid loading, 120g, 0-5% EtOAc/Hex) to yield 2-cyclopentyl-1-(4-methoxy-2,3-dimethyl-phenyl)ethanone (10.2 g, 41.2 mmol, 85%) as a yellow oil. ^{1}HNMR (400 MHz, $CDCl_3$) δ 7.43 (d, *J* = 8.6 Hz, 1H, 1H), 6.71 (d, *J* = 8.6 Hz, 1H), 3.84 (s, 3H), 2.87 (d, *J* = 7.2 Hz, 2H), 2.36 (s, 3H), 2.35-2.25 (m, 1H), 2.17 (s, 3H), 1.88-1.79 (m, 2H), 1.69-1.57 (m, 2H), 1.57-1.48 (m, 2H), 1.22-1.10 (m, 2H); ^{13}CNMR (100 MHz, $CDCl_3$) δ 205.2, 159.4, 137.9, 132.9, 127.2, 126.7, 106.6, 55.6, 48.4, 36.7, 32.7, 25.1, 17.1, 11.8.

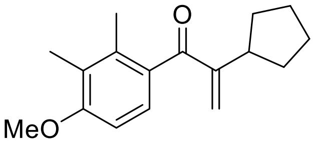

2-cyclopentyl-1-(4-methoxy-2,3-dimethyl-phenyl)prop-2-en-1-one (1.344). To a solution of 1-methoxy-2,3-dimethylbenzene (10.2 g, 41 mmol, 1 eq) and paraformaldehyde (9.3 g, 103 mmol, 2.5 eq) in acetic acid (10 mL) was added dimethylamine hydrochloride (15.1 g, 186 mmol, 4.5 eq) and the reaction was heated to 80 °C for 16 hours, at which point LCMS analysis indicated full conversion to Mannich intermediate. The reaction was then diluted with DMF (60 mL, 0.69M) and the reaction was heated to 120 °C for an additional 16 hours. After cooling to room temperature the reaction was diluted with water (60mL) and extracted with DCM (3x100mL). The organics were pooled, dried over magnesium sulfate, filtered, and concentrated *in vacuo*, then crude product was purified using Teledyne ISCO Combi-Flash system (liquid loading, 120g, 0-5% EtOAc/Hex) to yield 2-cyclopentyl-1-(4-methoxy-2,3-dimethyl-phenyl)prop-2-en-1-one (10.3g, 40 mmol, 96%) as a yellow oil. ^{1}HNMR (400 MHz, $CDCl_3$) δ 7.12 (d, *J* = 8.5 Hz, 1H), 6.69 (d, *J* = 8.5 Hz, 1H), 5.78 (s, 1H), 5.53 (s, 1H), 3.83 (s, 3H), 3.10 (p, *J* = 8.4 Hz), 1H), 2.23 (s, 3H), 2.16 (s, 3H), 2.03-1.92 (m, 2H), 1.79-1.68 (m, 2H), 1.49-1.38 (m, 2H); ^{13}CNMR (100 MHz, $CDCl_3$) δ 201.2, 158.8, 154.2, 136.9, 132.8, 127.4, 126.1, 124.7, 106.5, 55.6, 40.6, 31.9, 25.0, 17.2, 11.7.

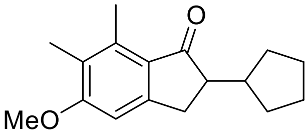

2-cyclopentyl-5-methoxy-6,7-dimethyl-indan-1-one (1.345).

A solution of 2-cyclopentyl-1-(4-methoxy-2,3-dimethyl-phenyl)prop-2-en-1-one (10.3 g, 40 mmol, 1 eq) in sulfuric acid (48 mL) was stirred for 4 hours at room temperature, then quenched by pouring the reaction mixture over crushed ice. The resulting mixture was extracted with ether (3x100 mL), then the organics were pooled, dried over magnesium sulfate, filtered, and concentrated *in vacuo* to yield 2-cyclopentyl-5-methoxy-6,7-dimethyl-indan-1-one (8.0 g, 31.0 mmol, 78%) as a yellow oil in sufficient purity for further transformations. An analytical sample was obtained using flash chromatography. ^{1}HNMR (400 MHz, $CDCl_3$) δ 6.64 (s, 1H), 3.81 (s, 3H), 3.02 (dd, J = 17.0, 7.8 Hz, 1H), 2.68 (dd, J = 17.0, 3.7 Hz, 1H), 2.62-2.56 (m, 1H), 2.54 (s, 3H), 2.33-2.20 (m, 1H), 2.06 (s, 3H), 1.92-1.83 (m, 1H), 1.64-1.50 (m, 3H), 1.50-1.44 (m, 2H), 1.41-1.29 (m, 1H), 1.08-0.97 (m, 1H); ^{13}CNMR (100 MHz, $CDCl_3$) δ 208.0, 162.4, 154.9, 138.2, 127.7, 125.1, 104.2, 55.4, 51.1, 41.3, 30.7, 29.6, 28.2, 25.3. 25.2, 13.7, 10.8.

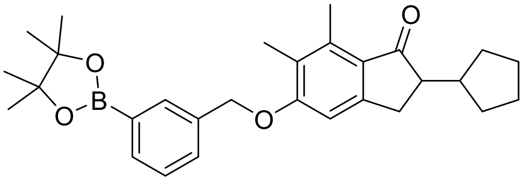

2-cyclopentyl-6,7-dimethyl-5-[[3-(4,4,5,5-tetramethyl-1,3,2-dioxaborolan-2-yl)phenyl]methoxy]indan-1-one (1.348).

To a solution of 2-cyclopentyl-5-methoxy-6,7-dimethyl-indan-1-one (716 mg, 2.77 mmol, 1 eq) in Toluene (13.9 mL, 0.2M) at room temperature was added aluminum chloride (1.1 g, 8.31 mmol, 3 eq). The reaction was heated to 110 °C for one hour, then cooled to room temperature, then was poured over crushed ice. After the ice had melted, the resulting solution was extracted with ether (3x75mL) and the organics were pooled, dried over magnesium sulfate, filtered, and concentrated *in vacuo* to yield 2-cyclopentyl-5-hydroxy-6,7-dimethyl-indan-1-one as a red/pink solid that was taken on without further purification.

A solution of 2-cyclopentyl-5-hydroxy-6,7-dimethyl-indan-1-one (390 mg, 1.6 mmol, 1 eq), 3-bromomethylphenylboronic acid pinacol ester (521 mg , 1.76 mmol, 1.1 eq eq), and cesium carbonate (576 mg, 1.76mmol, 1.1 eq) at 23 ^{o}C in DMF (7.981mL) was stirred overnight. The reaction was quenched by addition of water (10mL) and extracted with DCM (3x10mL). The organics were pooled, dried over magnesium sulfate, filtered, and concentrated *in vacuo*. Crude product was purified using Teledyne ISCO Combi-Flash system (solid loading, 12G column, 0-40% EtOAc/Hex) to yield 2-cyclopentyl-6,7-dimethyl-5-[[3-(4,4,5,5-tetramethyl-1,3,2-dioxaborolan-2-yl)phenyl]methoxy]indan-1-one (537 mg,1.17 mmol, 73% yield) as a bright red oil. ^{1}HNMR (400 MHz, $CDCl_3$) δ 7.87 (bs, 1H), 7.81 (d, *J* = 7.3 Hz, 1H), 7.58 (d, *J* = 7.8 Hz, 1H), 7.44 (t, *J* = 7.5 Hz, 1H), 6.76 (s, 1H), 5.13 (s, 2H), 3.12-3.01 (m, 1H), 2.76-2.66 (m, 2H), 2.62 (s, 3H), 2.39-2.28 (m, 1H), 2.19 (s, 3H), 1.99-1.89 (m, 1H), 1.69-1.49 (m, 6H), 1.37 (s, 12H), 1.13-1.02 (m, 1H); ^{13}CNMR (100 MHz, $CDCl_3$) δ 208.5, 161.7, 155.0, 138.8, 136.1, 134.6, 133.7, 130.3, 128.3, 128.2, 125.8, 105.7, 84.1, 70.3, 51.4, 41.5, 30.9, 29.8, 28.3, 25.5, 25.4, 25.0, 14.1, 11.4.

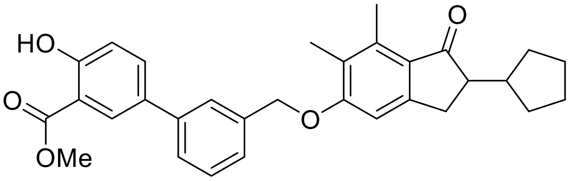

methyl 5-[3-[(2-cyclopentyl-6,7-dimethyl-1-oxo-indan-5-yl)oxymethyl]phenyl]-2-hydroxy-benzoate (1.350).

To a solution of 2-cyclopentyl-6,7-dimethyl-5-[[3-(4,4,5,5-tetramethyl-1,3,2-dioxaborolan-2-yl)phenyl]methoxy]indan-1-one (2.2 g, 4.76 mmol, 1 eq) in a mixture of MeCN (18 mL) and Water (9 mL) was added methyl 5-bromosalicylate (1.2 g, 5.23 mmol, 1.1 eq), sodium carbonate (1.02 g, 9.52 mmol, 2 eq), and dichloro[1,1'-bis(diphenylphosphino)ferrocene]palladium(ii) dichloromethane adduct (195 mg, 0.24 mmol, 0.05 eq). The reaction was heated to 100 ºC for 1 hour, then cooled to room temperature then filtered through a celite, washing with EtOAc (3x20 mL) and the resulting filtrates were concentrated *in vacuo*. Crude product was purified using Teledyne ISCO Combi-Flash system (lquid loading, 24G column, 0-30% EtOAc/Hex) to yield methyl 5-[3-[(2-cyclopentyl-6,7-dimethyl-1-oxo-indan-5-yl)oxymethyl]phenyl]-2-hydroxy-benzoate (1.5 g, 3.06 mmol, 64 % yield) as a sticky pink solid. ^{1}HNMR (400 MHz, $CDCl_3$) δ 10.79 (s, 1H), 8.09 (d, *J* = 1.6 Hz, 1H), 7.72 (d, *J* = 8.4 Hz, 1H), 7.62 (s, 1H), 7.54 (d, *J* = 7.3 Hz, 1H), 7.47 (t, *J* = 7.4 Hz), 7.42 (d, *J* = 7.3 Hz), 7.07 (d, *J* = 8.6 Hz, 1H), 6.80 (s, 1H), 5.18 (s, 2H), 3.98 (s, 3H), 3.13-3.02 (m, 1H), 2.78-2.66 (m, 2H), 2.63 (s, 3H), 2.40-2.28 (m, 1H0, 2.22 (s, 3H), 1.99-1.89 (m, 1H), 1.69-1.48 (m, 5H), 1.46-1.34 (m, 1H), 1.14-1.02 (m, 1H); ^{13}CNMR (100 MHz, $CDCl_3$) δ 208.5, 170.6, 161.6, 161.3, 155.0, 140.4, 138.9, 137.5, 134.5, 132.1, 129.3, 128.3, 126.4, 126.0, 125.7, 125.5, 18.3, 112.7, 105.7, 70.2, 52.5, 51.4, 41.5, 30.9, 29.8, 28.3, 25.5, 25.4, 14.1, 11.4.

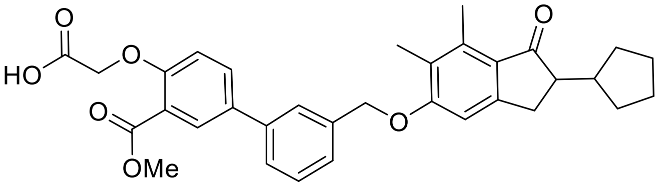

methyl 2-(2-tert-butoxy-2-oxo-ethoxy)-5-[3-[(2-cyclopentyl-6,7-dimethyl-1-oxo-indan-5-yl)oxymethyl]phenyl]benzoate (1.351).

To a solution of methyl 5-[3-[(2-cyclopentyl-6,7-dimethyl-1-oxo-indan-5-yl)oxymethyl]phenyl]-2-hydroxy-benzoate (300 mg, 0.62 mmol, 1 eq) and cesium carbonate (800 mg, 2.44 mmol, 3.9 eq) in DMF (3.10 mL, 0.2M) at 23 °C was added tert-butyl bromoacetate (0.23 mL, 1.55mmol, 2.5 eq). The reaction was stirred for 54 hours at room temperature, then diluted with water (30mL) and extracted with DCM (3x10mL). The organics were pooled, washed with water (2x15mL), and passed through a phase separator, then crude product was purified using Teledyne ISCO Combi-Flash system (solid loading, 12G column, 0-25% EtOAc/Hex) to yield methyl 2-(2-tert-butoxy-2-oxo-ethoxy)-5-[3-[(2-cyclopentyl-6,7-dimethyl-1-oxo-indan-5-yl)oxymethyl]phenyl]benzoate (332 mg, 0.55 mmol, 89% yield) as a pink foam. ^{1}HNMR (400 MHz, $CDCl_3$) δ 8.09 (d, *J* = 2.3 Hz, 1H), 8.08 (dd, *J* = 8.6, 2.4 Hz, 1H), 7.62 (bs, 1H), 7.54 (d, *J* = 7.5 Hz, 1H), 7.45 (t, *J* = 7.5 Hz, 1H), 7.41 (d, *J* = 7.5 Hz, 1H), 6.93 (d, *J* = 8.6 Hz, 1H), 6.79 (s, 1H), 5.17 (s, 2H), 4.65 (s, 2H), 3.93 (s, 3H), 3.11-3.01 (m, 1H), 2.76-2.64 (m, 2H), 2.62 (s, 3H), 2.38-2.25 (m, 1H), 2.21 (s, 3H), 1.97-1.86 (m, 1H), 167-1.51 (m, 5H), 1.49 (s, 10H), 1.43-1.35 (m, 1H), 1.13-1.01 (m, 1H); ^{13}CNMR (100 MHz, $CDCl_3$) δ 208.4, 167.5, 166.4, 161.6, 140.1, 138.8, 137.5, 134.0, 131.7, 130.6, 129.3, 128.3, 126.5, 126.1, 125.7, 125.6, 121.2, 114.2, 105.7, 82.6, 70.1, 66.8, 52.3, 51.3, 41.4, 30.9, 29.8, 28.3, 28.1, 25.5, 25.3, 14.0, 11.4.

To a solution of methyl 2-(2-tert-butoxy-2-oxo-ethoxy)-5-[3-[(2-cyclopentyl-6,7-dimethyl-1-oxo-indan-5-yl)oxymethyl]phenyl]benzoate (332 mg, 0.55 mmol) in DCM (2.5 mL) at 23 ^{o}C was added trifluoroacetic acid (2.5 mL). The reaction was stirred for 1 hour, then the organics were removed *in vacuo*. The resulting residue was diluted with water (10mL) and extracted with DCM (3x15mL). The organics were passed through a phase separator and concentrated *in vacuo* to yield 2-[4-[3-[(2-cyclopentyl-6,7-dimethyl-1-oxo-indan-5-yl)oxymethyl]phenyl]-2-methoxycarbonyl-phenoxy]acetic acid (271 mg,0.50 mmol, 90% yield) as an off-white solid. ^{1}HNMR (400 MHz, DMSO) δ 7.96 (d, *J* = 2.4 Hz, 1H), 7.81 (dd, *J* = 8.7, 2.4 Hz), 1H), 7.75 (bs, 1H), 7.61 (d, *J* = 7.5 Hz, 1H), 7.48 (t, *J* = 7.6 Hz, 1H), 7.44 (d, *J* = 7.6 Hz, 1H), 7.12 (d, *J* = 8.8 Hz, 1H), 7.01 (s, 1H), 5.23 (s, 2H), 4.83 (s, 2H), 3.83 (s, 3H), 3.04 (dd, *J* = 16.9, 7.6 Hz, 1H), 2.66-2.54 (m, 2H), 2.50 (s, 3H), 2.21-2.12 (m, 1H), 2.10 (s, 3H), 1.85-1.76 (m, 1H), 1.61-1.53 (m, 1H), 1.53-1.41 (m, 4H), 1.36-1.25 (m, 1H), 1.06-.95 (m, 1H); ^{13}CNMR (100 MHz, $CDCl_3$) δ 207.1, 169.8, 166.0, 160.9, 156.4, 154.7, 138.9, 137.6, 137.3, 132.3, 131.2, 129.2, 128.8, 127.3, 126.2, 125.8, 125.3, 124.7, 120.9, 114.2, 106.2, 69.5, 65.2, 52.0, 50.6, 40.8, 30.2, 29.2, 27.9, 25.0, 24.7, 13.4, 10.9.

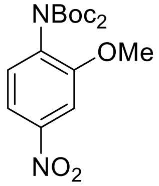

***tert*-butyl *N*-tert-butoxycarbonyl-N-(2-methoxy-4-nitro-phenyl)carbamate (1.353).**

To a solution of 2-methoxy-4-nitroaniline (3000 mg, 17.8 mmol) and 4-dimethylaminopyridine (1.07 g, 8.92 mmol, 0.5 eq) in THF (60 mL) at 23 ^oC was added di-tert-butyl dicarbonate (8.2 g, 37.47 mmol, 2.5 eq). The reaction was stirred for 5 hours then quenched by addition of saturated ammonium chloride (20mL), the layers were separated, and the aqueous was extracted with ether (3x25mL). The organics were pooled, dried over magnesium sulfate, filtered, and concentrated *in vacuo* to yield (5.4 g,15 mmol, 82% yield) as a yellow foam that was taken on without further purification.

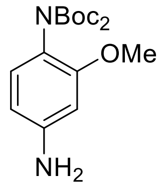

***tert*-butyl *N*-(4-amino-2-methoxy-phenyl)-N-tert-butoxycarbonyl-carbamate (1.354)**.

To a solution of tert-butyl N-tert-butoxycarbonyl-N-(2-methoxy-4-nitro-phenyl)carbamate (4.44 g, 12.03 mmol) in Ethanol (60 mL) at 23 ^oC was added palladium on activated carbon (443 mg) and the reaction was stirred under hydrogen atmosphere overnight. The reaction was filtered through a plug of celite then concentrated *in vacuo* to yield tert-butyl N-(4-amino-2-methoxy-phenyl)-N-tert-butoxycarbonyl-carbamate (3.9 g,11 mmol, 9577% yield) as a brown foam that was taken on without further purification.

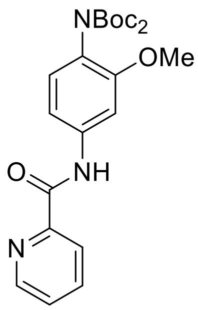

tert-butyl _N_-tert-butoxycarbonyl-N-[2-methoxy-4-(pyridine-2-carbonylamino)phenyl]carbamate (1.356).

A solution of tert-butyl N-(4-amino-2-methoxy-phenyl)-N-tert-butoxycarbonyl-carbamate (3.5 g, 10.3 mmol, 1 eq) in DCE (20 mL) at room temperature was added *N,N*-diisopropylethylamine (6.3 mL, 36 mmol, 3.5 eq) and picolinoyl chloride hydrochloride (2.2 g, 12 mmol, 1.2 eq). The reaction was heated to 80 °C for 5 hours, then the reaction was cooled to room temperature then diluted with water (50 mL) and extracted with DCM (3x50 mL). The organics were pooled, dried over magnesium sulfate, filtered, and concentrated *in vacuo*, then crude product was purified using Teledyne ISCO Combi-Flash system (solid loading, 40G column, 0-60% EtOAc/Hex) to yield tert-butyl N-tert-butoxycarbonyl-N-[2-methoxy-4-(pyridine-2-carbonylamino)phenyl]carbamate (640 mg,1.44 mmol, 14% yield) along with residual starting material. ^{1}HNMR (400 MHz, $CDCl_3$) δ 10.07 (bs, 1H), 8.59 (dq, *J* = 4.8, 0.7 Hz, 1H), 8.26 (dt, *J* = 4.4, 0.9 Hz, 1H), 7.91 (td, *J* = 7.7, 1.7 Hz, 1H), 7.75 (d, *J* = 2.1 Hz, 1H), 7.46 (ddd, *J* = 7.6, 4.8, 1.2 Hz, 1H), 7.10 (dd, *J* = 8.4, 2.1 Hz, 1H), 7.04 (d, *J* = 8.4 Hz, 1H), 3.85 (s, 3H), 1.38 (s, 18H); ^{13}CNMR (100 MHz, $CDCl_3$) δ 162.1, 155.0, 151.9, 149.7, 148.1, 138.4, 137.9, 129.2, 126.7, 124.7, 122.4, 111.0, 103.1, 82.2, 55.7, 28.0.

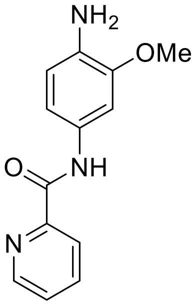

N-(4-amino-3-methoxy-phenyl)pyridine-2-carboxamide (1.357)

To a solution of tert-butyl N-tert-butoxycarbonyl-N-[2-methoxy-4-(pyridine-2-carbonylamino)phenyl]carbamate (805 mg, 1.82 mmol) in DCM (9 mL) was added trifluoroacetic acid (9 mL) and the reaction was stirred for 1 hour, at which point LCMS analysis indicated full conversion to desired product. The organics were concentrated *in vacuo* then the residue was quenched by addition of saturated sodium bicarbonate, and the resulting yellow mixture was extracted with DCM (3x15mL). The organics were pooled, dried over magnesium sulfate, filtered, and concentrated *in vacuo* to yield N-(4-amino-3-methoxy-phenyl)pyridine-2-carboxamide (287 mg, 1.18 mmol, 65% yield) as a waxy yellow solid. ^{1}HNMR (400 MHz, CDCl$_3$) δ 9.86 (s, 1H), 8.56 (d, *J* = 4.6 Hz, 1H0, 8.26 (d, *J* = 7.8 Hz, 1H), 7.86 (td, *J* = 7.7, 1.6 Hz, 1H), 7.56 (d, *J* = 2.1 Hz, 1H), 7.45-7.37 (m, 1H), 6.99 (dd, *J* = 8.3, 2.2 Hz, 1H), 6.69 (d, *J* = 8.3 Hz, 1H), 3.87 (s, 3H), 3.66 (bs, 2H); ^{13}CNMR (100 MHz, CDCl$_3$) δ 161.6, 150.2, 148.0, 147.4, 137.7, 133.1, 129.6, 126.6, 122.2, 114.8, 112.5, 103.7, 55.6.

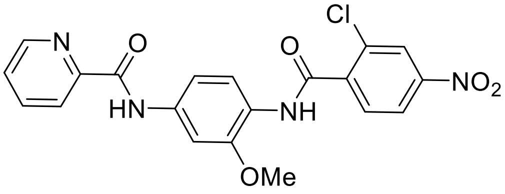

N-[4-[(2-chloro-4-nitro-benzoyl)amino]-3-methoxy-phenyl]pyridine-2-carboxamide (1.359).

To a solution of N-(4-amino-3-methoxy-phenyl)pyridine-2-carboxamide (1.35 g, 5.7 mmol, 1 eq) in DCM (29 mL, 0.2M) was added DIEA (2 mL, 11.5 mmol, 2 eq) and 2-chloro-4-nitrobenzoyl chloride (1.5 g, 6.88 mmol, 1.2 eq) dropwise. The reaction was stirred overnight at room temperature, then quenched by addition of water (30 mL) and the layers were separated and the aqueous layer was extracted with DCM (2x30 mL). The organic layers were pooled, dried over magnesium sulfate, filtered, and concentrated *in vacuo* to yield *N*-[4-[(2-chloro-4-nitro-benzoyl)amino]-3-methoxy-phenyl]pyridine-2-carboxamide (2.26 g,5.3 mmol, 92% yield) as a brown foam. Product was taken on without further purification. An analytically pure sample was obtained using Gilson HPLC. ^{1}HNMR (400 MHz, DMSO) δ 10.67 (s, 1H), 10.00 (s, 1H), 8.76 (d, *J* = 4.6 Hz, 1H), 8.38 (d, *J* = 1.8 Hz, 1H), 8.28 (dd, *J* = 8.4, 1.8 Hz, 1H), 8.18 (d, *J* = 7.7 Hz, 1H), 8.10 (t, *J* = 7.4 Hz, 1H), 7.88 (d, *J* = 8.7 Hz, 1H), 7.84 (d, *J* = 8.4 Hz, 1H), 7.73-7.66 (m, 1H), 7.61 (dd, *J* = 8.7, 1.4 Hz, 1H), 3.84 (s, 3H); ^{13}CNMR (100 MHz, DMSO) δ 163.6, 162.3, 151.0, 149.8, 148.4, 148.2, 142.6, 138.2, 136.8, 131.2, 130.1, 127.0, 124.4, 123.6, 122.3, 122.3, 122.1, 111.7, 104.1, 55.7.

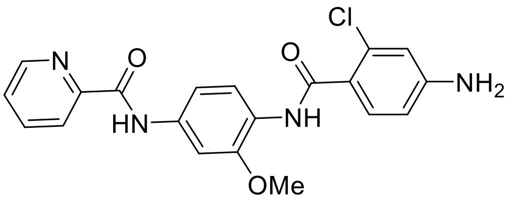

N-[4-[(4-amino-2-chloro-benzoyl)amino]-3-methoxy-phenyl]pyridine-2-carboxamide (1.360).

To a solution of N-[4-[(2-chloro-4-nitro-benzoyl)amino]-3-methoxy-phenyl]pyridine-2-carboxamide (1.3 g, 3.0 mmol, 1 eq) in ethanol (15 mL) at room temperature was added acetic acid (7.5 mL, 131 mmol, 44 eq) and iron (631 mg, 11.3 mmol, 3.8 eq). The reaction was heated to 100 ºC for 2 hours, at which point LCMS analysis indicated full conversion of starting material, so the reaction was cooled to room temperature and basified with 1M NaOH. The resulting dark red solution was extracted with EtOAc (3x80 mL) and the organics were pooled and concentrated *in vacuo* to yield a brown solid that was taken on without further purification assuming quantitative yield.

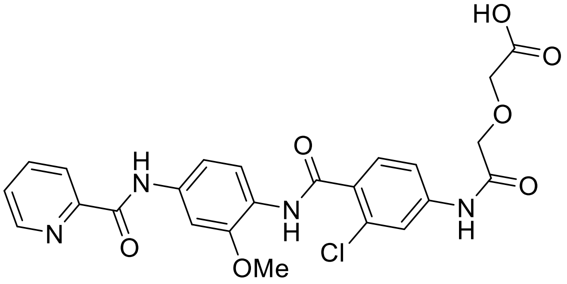

2-[2-[3-chloro-4-[[2-methoxy-4-(pyridine-2-carbonylamino)phenyl]carbamoyl]anilino]-2-oxo-ethoxy]acetic acid (1.362). To a solution of *N*-[4-[(4-amino-2-chloro-benzoyl)amino]-3-methoxy-phenyl]pyridine-2-carboxamide (1.2 g, 3.0 mmol, 1 eq) was added diglycolic anhydride (522 mg, 4.5 mmol, 1.5 eq) and the reaction mixture was heated to 60 °C overnight. After cooling, the resulting precipitate was isolated via vacuum filtration to yield 2-[2-[3-chloro-4-[[2-methoxy-4-(pyridine-2-carbonylamino)phenyl]carbamoyl]anilino]-2-oxo-ethoxy]acetic acid (354 mg, 0.69 mmol, 23% yield) as an orange solid. ^{1}HNMR (400 MHz, DMSO) δ 10.64 (s, 1H), 10.27 (s, 1H), 9.49 (s, 1H), 8.75 (d, *J* = 4.2 Hz, 1H), 8.18 (d, *J* = 7.7 Hz, 1H), 8.08 (t, *J* = 7.0 Hz, 1H), 7.93 (s, 1H), 7.87 (d, *J* = 8.6 Hz, 1H), 7.77 (s, 1H), 7.71-7.65 (m, 2H), 7.61-7.55 (m, 2H), 4.23 (s, 4H), 3.84 (s, 3H); ^{13}CNMR (100 MHz, DMSO) δ 171.7, 168.6, 164.3, 162.3, 150.8, 149.8, 148.4, 140.6, 138.2, 135.9, 131.1, 130.3, 130.0, 127.0, 126.2, 122.7, 122.3, 119.9, 117.7, 111.7, 104.1, 70.3, 68.0, 55.8.

General Procedure for the synthesis of 1.352-1.360.

To a solution of 2-[4-[3-[(2-cyclopentyl-6,7-dimethyl-1-oxo-indan-5-yl)oxymethyl]phenyl]-2-methoxycarbonyl-phenoxy]acetic acid (45 mg, 0.08 mmol, 1 eq) in DMF (0.5 mL, 0.17M) was added HATU (63 mg, 0.17 mmol, 2 eq) and DIEA (43.3 μL, 0.25 mmol, 3 eq) and the mixture was stirred for 30 minutes at room temperature. Next, the corresponding monoprotected *N*-boc diamine (0.12 mmol, 1.5 eq) was added and the reaction was stirred overnight, then diluted with water (2 mL) and extracted with DCM (3x2 mL). The organics were passed through a phase separator and concentrated under a stream of constant air to yield a red oil that was taken on without further purification assuming quantitative yield.

General Procedure for the synthesis of 1.361-1.369.

To a solution of **1.352-1.360** (0.083 mmol, 1 eq) in THF (0.25 mL, 0.33M) at room temperature was added 1M aqueous LiOH (0.25 mL, 0.25 mmol, 3 eq) and the reaction was stirred overnight. The organics were removed *in vacuo*, then the aqueous was acidified with 1M HCl, then extracted with DCM (3x4 mL) and the organics were passed through a phase separator and concentrated *in vacuo* and taken on for the next reaction without further purification.

The resulting residue was diluted in 1,4-dioxane (0.5 mL, 0.17M) at room temperature was added 4M HCl in 1,4-dioxane (0.5 mL, 2 mmol, 24 eq) and the reaction was stirred overnight. The organics were then concentrated *in vacuo* to yield crude **1.361-1.369** that were taken on without further purification assuming quantitative yield.

General Procedure for the synthesis of 1.370-1.378.

To a solution of 2-[2-[3-chloro-4-[[2-methoxy-4-(pyridine-2-carbonylamino)phenyl]carbamoyl]anilino]-2-oxo-ethoxy]acetic acid (36.5 mg, 0.07 mmol, 1 eq) in DMF (0.50 mL) was added HATU (27 mg, 0.07 mmol, 1 eq) and DIEA (12.4 µL, 0.07 mmol, 1 eq) and the mixture was stirred for 30 minutes. In separate vials, **1.361-1.369** were dissolved in DMF (0.50 mL) and DIEA (40 µL, 0.23 mmol, 3.2 eq) was added. The second solution was added to the first, and the reaction was stirred overnight at room temperature, then diluted with water (5 mL) and extracted with DCM (3x5 mL) and the organics were passed through a phase separator and concentrated *in vacuo*. Crude product was purified using Gilson HPLC (60-100% 0.1% aq. TFA/MeCN), then fractions containing desired materials were pooled, the TFA salt quenched by addition of saturated sodium bicarbonate (5 mL), then extracted with DCM (3x5 mL). The organics were passed through a phase separator and concentrated *in vacuo* to yield **1.370-1.378** as their corresponding sodium salts. Due to the size of these molecules and the high flexibility that could complicate NMRs, desired materials were characterized by LCMS analysis. Yields correspond to the yield over the final 4 steps.

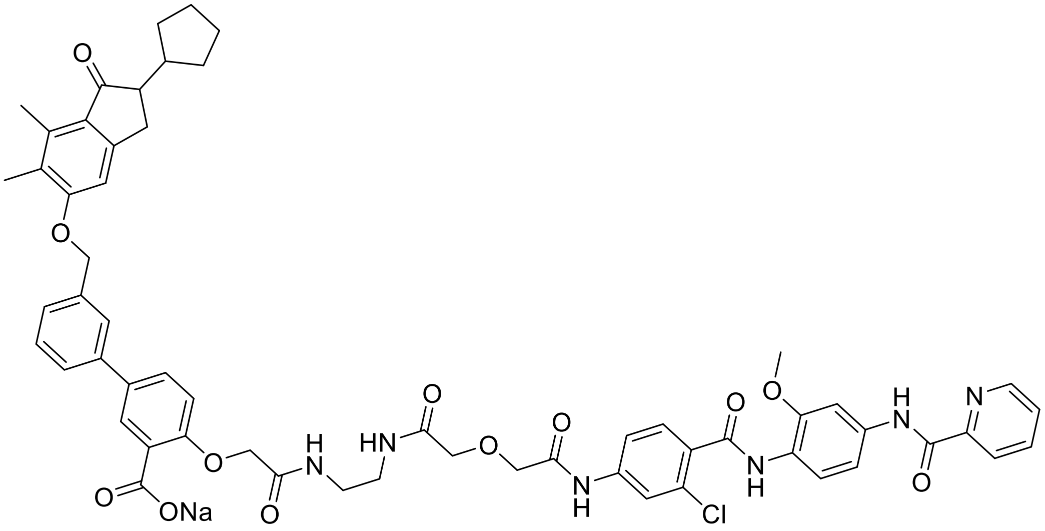

[2-[2-[2-[[2-[2-[3-chloro-4-[[2-methoxy-4-(pyridine-2-carbonylamino)phenyl]carbamoyl]anilino]-2-oxo-ethoxy]acetyl]amino]ethylamino]-2-oxo-ethoxy]-5-[3-[(2-cyclopentyl-6,7-dimethyl-1-oxo-indan-5-yl)oxymethyl]phenyl]benzoyl]oxysodium (1.370).

2% yield. LRMS calculated for $C_{58}H_{58}ClN_6O_{12}$ $[M+H]^+$: 1065.4, found: 1065.2

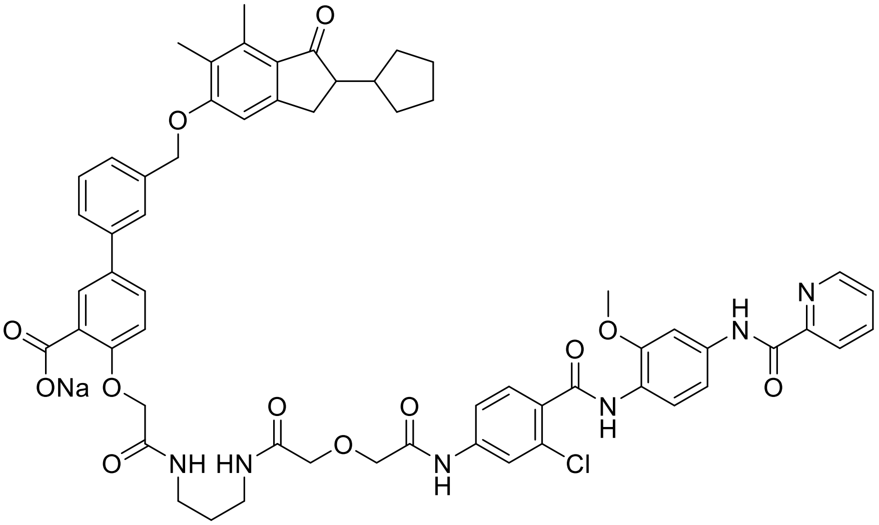

[2-[2-[3-[[2-[2-[3-chloro-4-[[2-methoxy-4-(pyridine-2-carbonylamino)phenyl]carbamoyl]anilino]-2-oxo-ethoxy]acetyl]amino]propylamino]-2-oxo-ethoxy]-5-[3-[(2-cyclopentyl-6,7-dimethyl-1-oxo-indan-5-yl)oxymethyl]phenyl]benzoyl]oxysodium (1.371).

10% yield. LRMS calculated for $C_{59}H_{60}ClN_6O_{12}$ $[M+H]^+$: 1079.4, found: 1079.2.

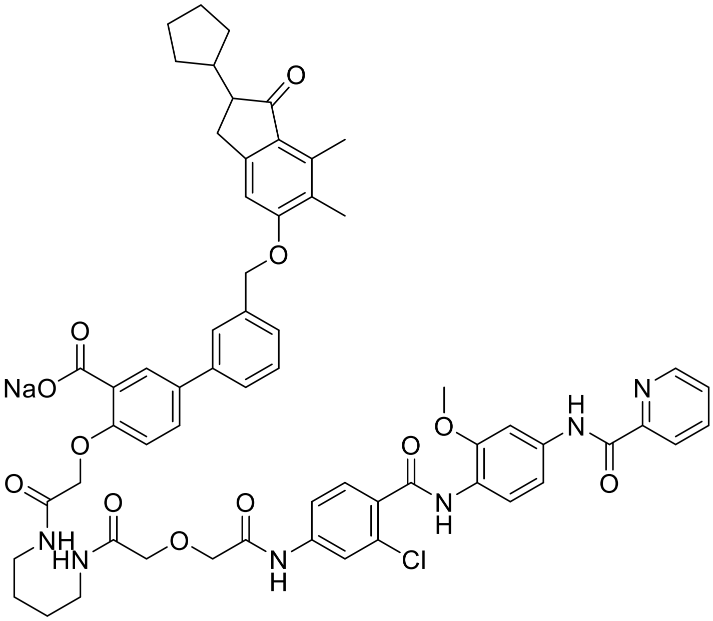

[2-[2-[4-[[2-[2-[3-chloro-4-[[2-methoxy-4-(pyridine-2-carbonylamino)phenyl]carbamoyl]anilino]-2-oxo-ethoxy]acetyl]amino]butylamino]-2-oxo-ethoxy]-5-[3-[(2-cyclopentyl-6,7-dimethyl-1-oxo-indan-5-yl)oxymethyl]phenyl]benzoyl]oxysodium (1.372).

8% yield. LRMS calculated for $C_{60}H_{62}ClN_6O_{12}$ $[M+H]^+$: 1092.4, found: 1093.2.

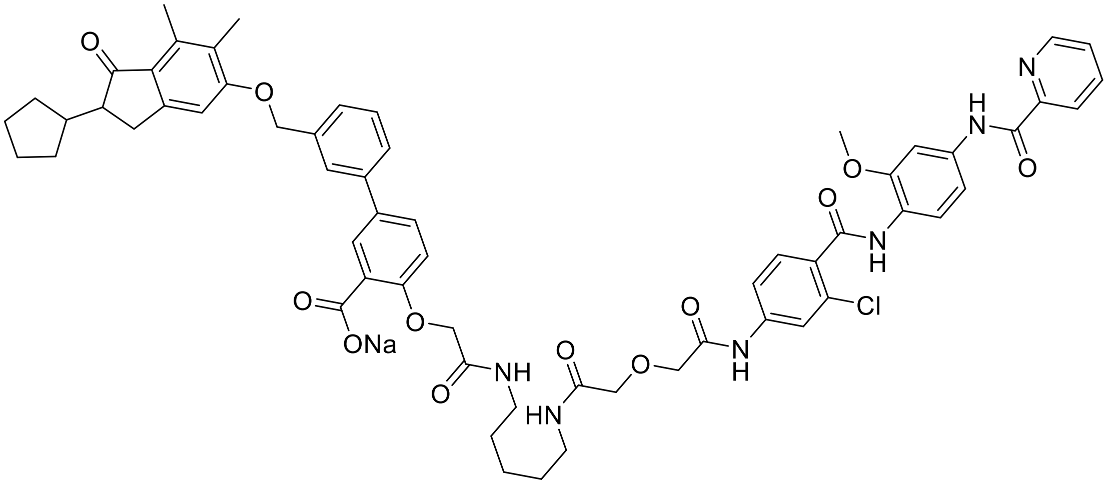

[2-[2-[5-[[2-[2-[3-chloro-4-[[2-methoxy-4-(pyridine-2-carbonylamino)phenyl]carbamoyl]anilino]-2-oxo-ethoxy]acetyl]amino]pentylamino]-2-oxo-ethoxy]-5-[3-[(2-cyclopentyl-6,7-dimethyl-1-oxo-indan-5-yl)oxymethyl]phenyl]benzoyl]oxysodium (1.373).

8% yield. LRMS calculated for $C_{61}H_{64}ClN_6O_{12}$ $[M+H]^+$: 1107.4, found: 1107.3.

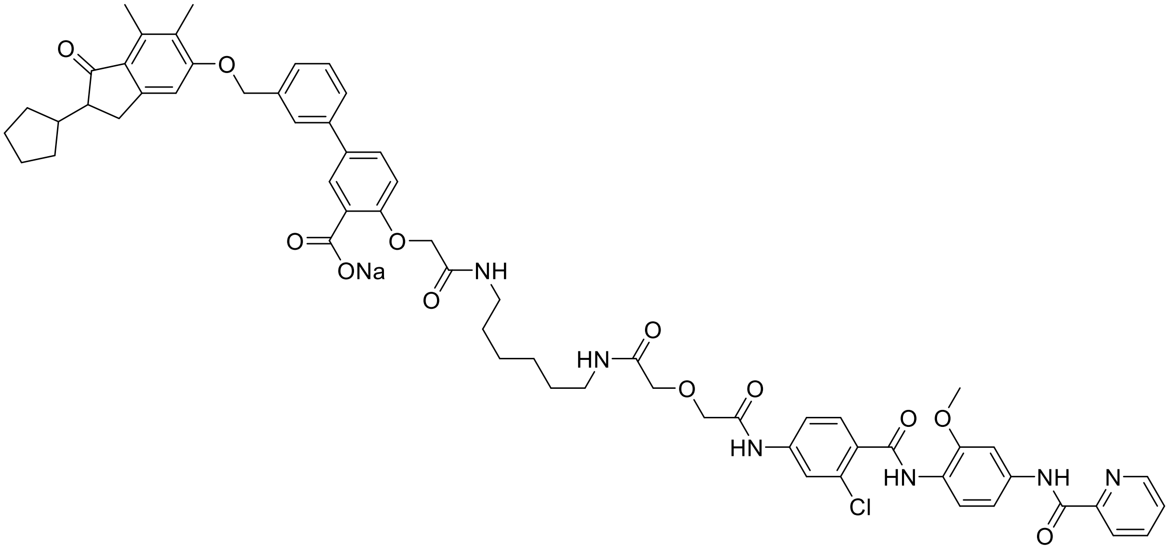

[2-[2-[6-[[2-[2-[3-chloro-4-[[2-methoxy-4-(pyridine-2-carbonylamino)phenyl]carbamoyl]anilino]-2-oxo-

ethoxy]acetyl]amino]hexylamino]-2-oxo-ethoxy]-5-[3-[(2-cyclopentyl-6,7-dimethyl-1-oxo-indan-5-yl)oxymethyl]phenyl]benzoyl]oxysodium (1.374).

12% yield. LRMS calculated for $C_{62}H_{66}ClN_6O_{12}$ $[M+H]^+$: 1121.4, found: 1121.2.

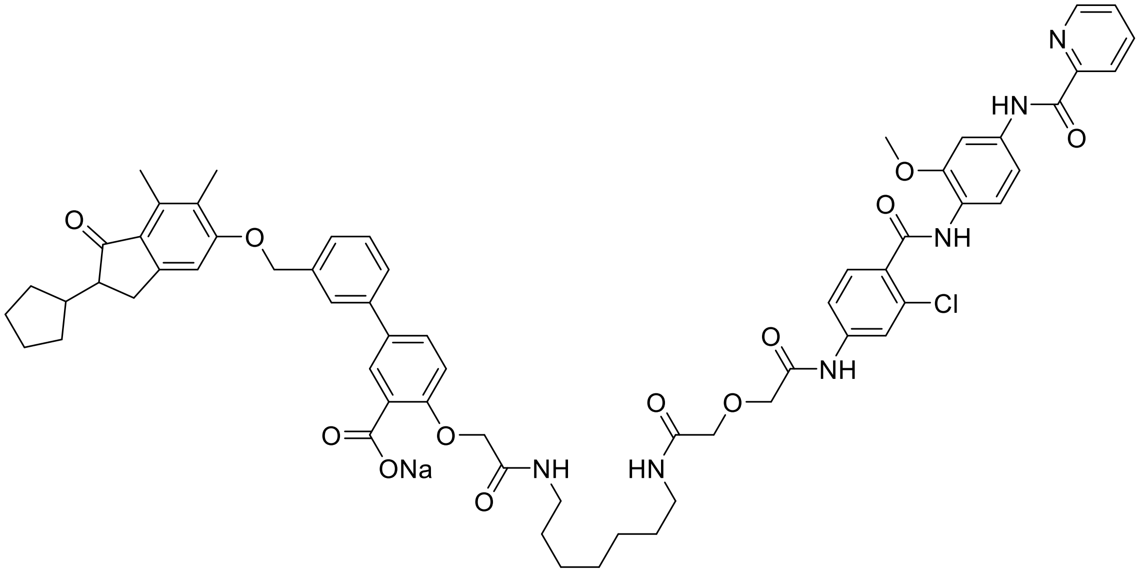

[2-[2-[7-[[2-[2-[3-chloro-4-[[2-methoxy-4-(pyridine-2-carbonylamino)phenyl]carbamoyl]anilino]-2-oxo-ethoxy]acetyl]amino]heptylamino]-2-oxo-ethoxy]-5-[3-[(2-cyclopentyl-6,7-dimethyl-1-oxo-indan-5-yl)oxymethyl]phenyl]benzoyl]oxysodium (1.375).

8% yield. LRMS calculated for $C_{63}H_{68}ClN_6O_{12}$ $[M+H]^+$: 1135.5, found: 1135.3.

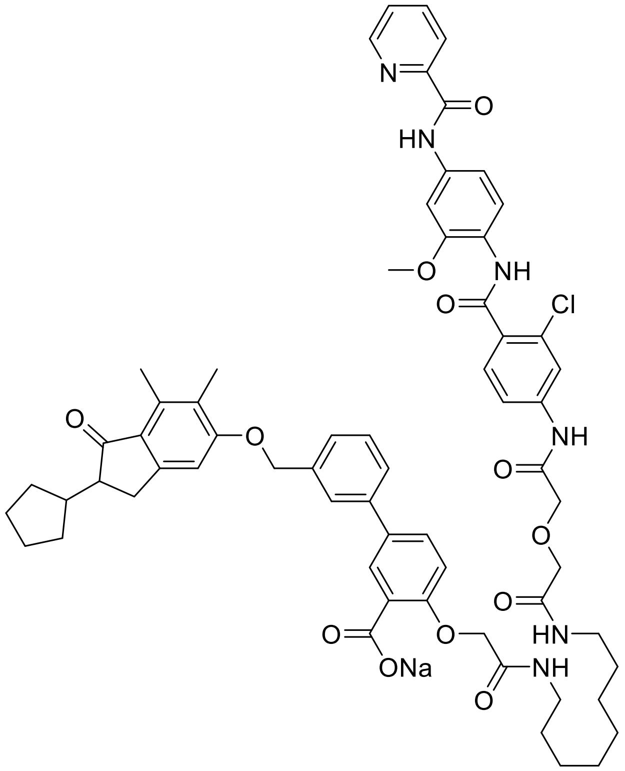

[2-[2-[8-[[2-[2-[3-chloro-4-[[2-methoxy-4-(pyridine-2-carbonylamino)phenyl]carbamoyl]anilino]-2-oxo-ethoxy]acetyl]amino]octylamino]-2-oxo-ethoxy]-5-[3-[(2-cyclopentyl-6,7-dimethyl-1-oxo-indan-5-yl)oxymethyl]phenyl]benzoyl]oxysodium (1.377).

6% yield. LRMS calculated for $C_{63}H_{68}ClN_6O_{12}$ $[M+H]^+$: 1149.5, found: 1149.3

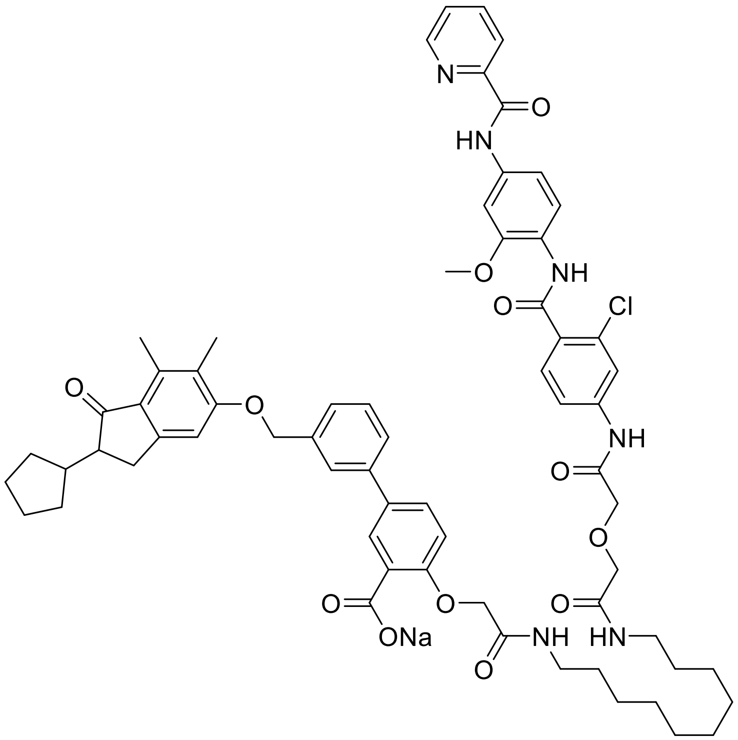

[2-[2-[10-[[2-[2-[3-chloro-4-[[2-methoxy-4-(pyridine-2-carbonylamino)phenyl]carbamoyl]anilino]-2-oxo-ethoxy]acetyl]amino]decylamino]-2-oxo-ethoxy]-5-[3-[(2-cyclopentyl-6,7-dimethyl-1-oxo-indan-5-yl)oxymethyl]phenyl]benzoyl]oxysodium (1.378).

2% yield. LRMS calculated for $C_{64}H_{70}ClN_6O_{12}$ $[M+H]^+$: 1177.5, found: 1177.5.

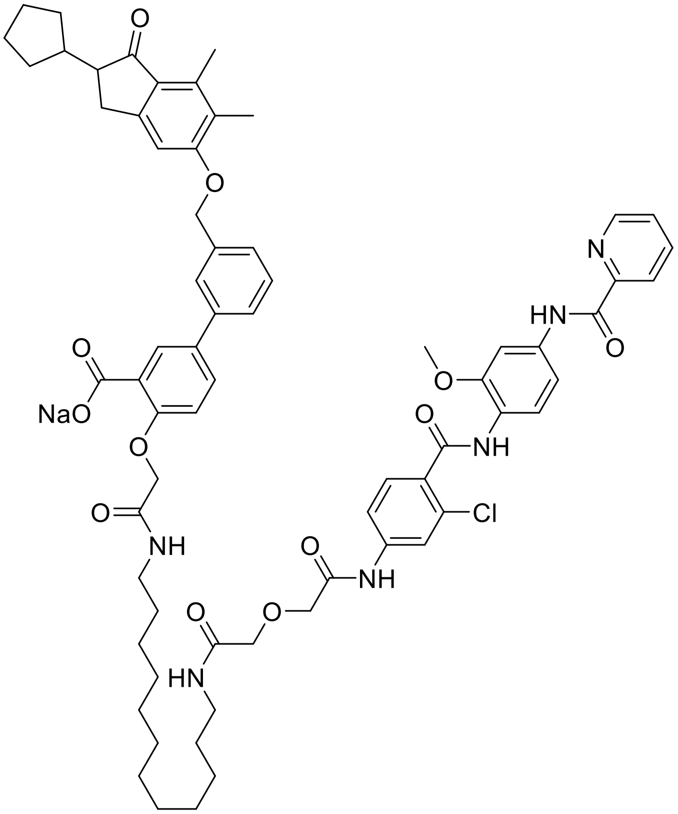

[2-[2-[12-[[2-[2-[3-chloro-4-[[2-methoxy-4-(pyridine-2-carbonylamino)phenyl]carbamoyl]anilino]-2-oxo-ethoxy]acetyl]amino]dodecylamino]-2-oxo-ethoxy]-5-[3-[(2-cyclopentyl-6,7-dimethyl-1-oxo-indan-5-yl)oxymethyl]phenyl]benzoyl]oxysodium (1.379).

4% yield. LRMS calculated for $C_{64}H_{70}ClN_6O_{12}$ $[M+H]^+$: 1205.5, found: 1205.3.

CHAPTER 2

Total Synthesis of Epi- And Pericoannosin A

Introduction

Natural Products In Medicine

Before the age of modern medicine, therapeutics were derived from natural sources, such as plants and animals. For example, salicylic acid containing fauna, such as willow and other plants rich in this natural product, have been known to be used since the time of ancient civilizations. The father of medicine, Hippocrates, mentions tea derived from salicylate containing plants as a means for treating fevers, and it was common in medicine throughout the Middle Ages[124,125]. Other famous natural product derived medicines include the Penicillin class of antibiotics, derived from the mold *Penicillum*[126], taxol, a microtubule inhibitors used in chemotherapies, was derived from the Pacific Yew[127], and the statins, which are used for the treatment of high cholesterol and were isolated from the fungus *Aspergillus terreus*[128] (**Figure 2.1**). Natural products comprised 34% of the drugs approved by the US Food and Drug Administration (FDA) from 1981-2010[129].

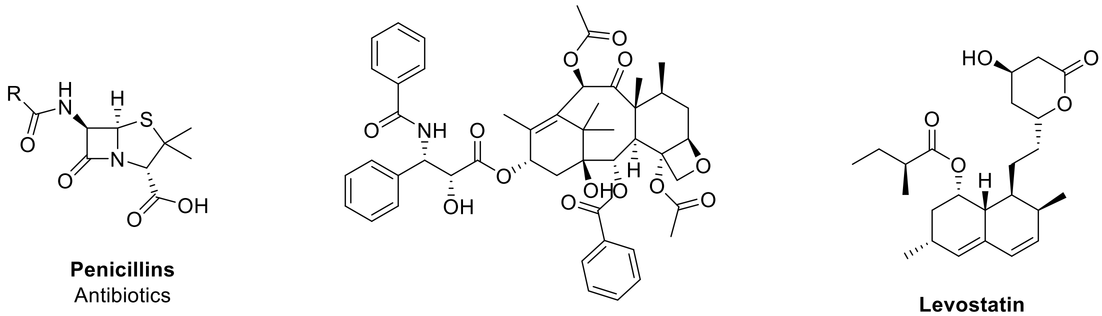

Penicillins
Antibiotics

Taxol
Chemotherapeutic

Levostatin
Cholesterol Lowering

Figure 2.1. Structure and medicinal uses of several natural products.

However, the use of natural products in drug discovery has waned considerably in recent years, especially in comparison to the last century[130]. This is for a number of reasons, including the fact that natural products can have complex structures that can make process scale synthesis difficult and/or expensive[131]. They can also exhibit complex pharmacology that can make it difficult to determine what proteins it is targeting and predict undesired side effects[132,133]. Additionally, natural products are not designed for use in human biology, which means they can have undesirable pharmacokinetic properties[134,135] that can be difficult to ameliorate without a good understanding of the molecules minimum pharmacophore, the portions of the molecule necessary for activity. Determination of the minimum pharmacophore for a complex natural product is not a trivial task[136,137].

For these reasons, recent drug discovery efforts have focused on the use of large compound libraries in HTS screens that can be screened against a single protein target, which has the advantage of accessing chemical matter that definitively interacts with the desired molecular target[138]. However, the success of these campaigns is heavily reliant on a strong understanding of the biological processes that cause a disease state and understanding of the role of one’s molecular target in this disease state[139-141]. A recent example of the importance of this understanding is the recent failure of a number of beta-secretase 1 (BACE1) inhibitors in clinical trials, which were efforts to prevent the formation of amyloid plaques that are associated with Alzheimer’s disease (AD)[142-144]. Many of these trials failed due to a lack of efficacy in phase II and/or III, meaning that there was an insufficient understanding of the role of BACE1 in AD. The discovery of natural product derived medicines often follows a more phenotypic process, in which it is discovered that an organism can elicit a biological effect, which means that one only has to find the molecule(s) that contribute to this effect. Additionally, HTS libraries can lack in the realm of chemical diversity, which is associated with higher rates of success in HTS screening efforts[145,165]. These caveats highlight the importance of natural products for the discovery of novel medicines.

Natural Products from Periconia sp. F-31

The medicinal plant graviola (*Annona muricata*) is found in numerous tropical areas throughout the world, including parts of the Americas, Asia, and Africa. Various parts of this flowering tree have been used in a number of traditional medicines for the treatment of inflammation, rheumatism, diabetes, hypertension, and parasitic infection[147-149]. Living in this plant is an endophytic fungus, *Periconia* sp. F-31, from which *in vitro* assays displayed antiviral, antitumor, and anti-inflammatory activities[150]. Analysis of these metabolites revealed a number of hybrid polyketide synthase (PKS)/non-ribosomal peptide synthetase derived compounds. The first family of natural products discovered were the periconiasins, which are metabolites form the cytochalasan family of natural products[151-153]. These compounds exhibited potent and selective cytotoxicity against HCT-8, a colon cancer cell line, and BGC-823, a gastric cancer cell line[151-153]. Five of these natural

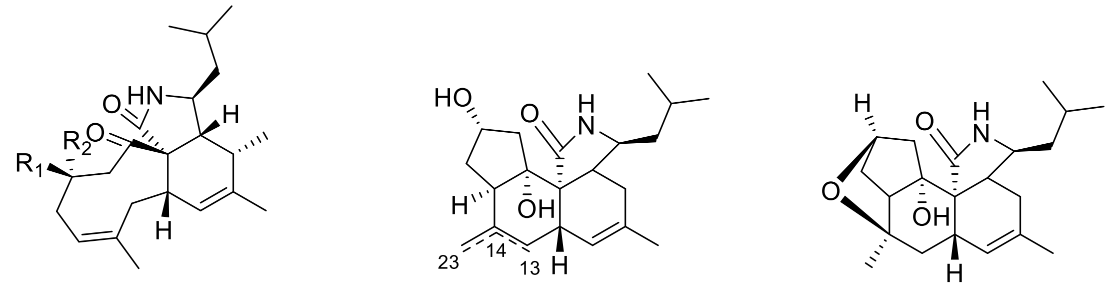
HN
O
R2
R1
H
HO
OH
23
14
13
N
O

Periconiasin A (**2.1**): R$_1$=H, R$_2$=OH
Periconiasin B (**2.2**): R$_1$=OH, R$_2$=H
Periconaisin C (**2.3**): R$_1$=R$_2$=O

Periconiasin E (**2.4**): Δ^{13}
Periconiasin F (**2.5**): Δ^{23}

Periconiasin D (**2.6**)

Figure 2.2. Structures of Periconiasins A-F isolated from fungus *Periconia* Sp. F-31.

products were synthesized in 2016, using a biomimetic strategy derived from the proposed biosynthetic pathway **(Figure 2.3)**[154].

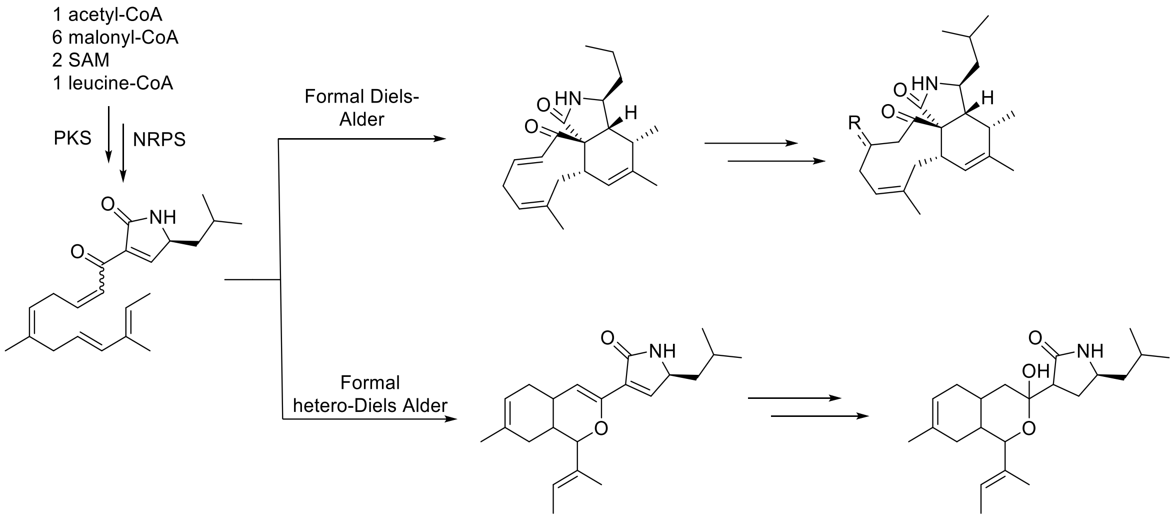
1 acetyl-CoA
6 malonyl-CoA
2 SAM
1 leucine-CoA
PKS
NRPS
Formal Diels-Alder
Formal hetero-Diels Alder
R
HN
NH
OH
O
H

Figure 2.3. Structures of biosynthesis for the formation of the periconiasins and pericoannosins.

A similar compound, Pericoannosin A, was discovered from isolation efforts in this species and was discovered to have a unique hexahydr-1*H*-isochromen-5-isobutylpyrrolidin-2-one skeleton hypothesized to be derived from a common biosynthetic intermediate to the periconiasins (**Figure 2.3, 2.4**)[153]. This was proposed to be derived from a similar pathway to the Periconiasins, but resulting from a slightly different sequence of cyclizations to arrive at this unique skeleton.

This cyclization sequence seems to be non-enzyme mediated, indicated by the discovery of Pericoannosin B, which is epimeric at every stereocenter besides the one derived from L-leucine. This unusual skeleton combined with the discovery of a weak anti-HIV activity of 69.6 µM along with no observable cytotoxicity led to a strong interest in developing a synthetic route for the synthesis of this natural product.

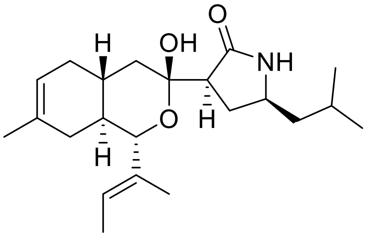

Pericoannosin A (**2.7**)

Figure 2.4. Structure of the natural product Pericoannosin A.

Previous Total Synthesis of Pericoannosin A

In 2017, Kalesse *et al.* reported their total synthesis of Pericoannosin A in a 15 step (18 steps from known compounds) longest linear sequence, with 27 total synthetic steps[155]. Their retrosynthesis was predicated on formation of the unique lactol moiety last, which could be formed from an aldol-oxidation sequence to form the necessary 1,3 dicarbonyl species. The protected lactam necessary for the aldol addition was readily available from Boc-L-leucine using known procedures. The aldehyde necessary for the aldol reaction could be synthesized from a homologation sequence, which was done after an asymmetric Diels-Alder cycloaddition to set the desired stereo- and regiochemistry of the cyclohexene ring. The Diels-Alder precursor was synthesized by a Horner-Wadsworth-Emmons (HWE) reaction of oxazolidinone **2.12** onto an aldehyde derived from the oxidative cleavage of **2.11**, which was accessed via an aldol reaction with commercially available tiglic aldehyde.

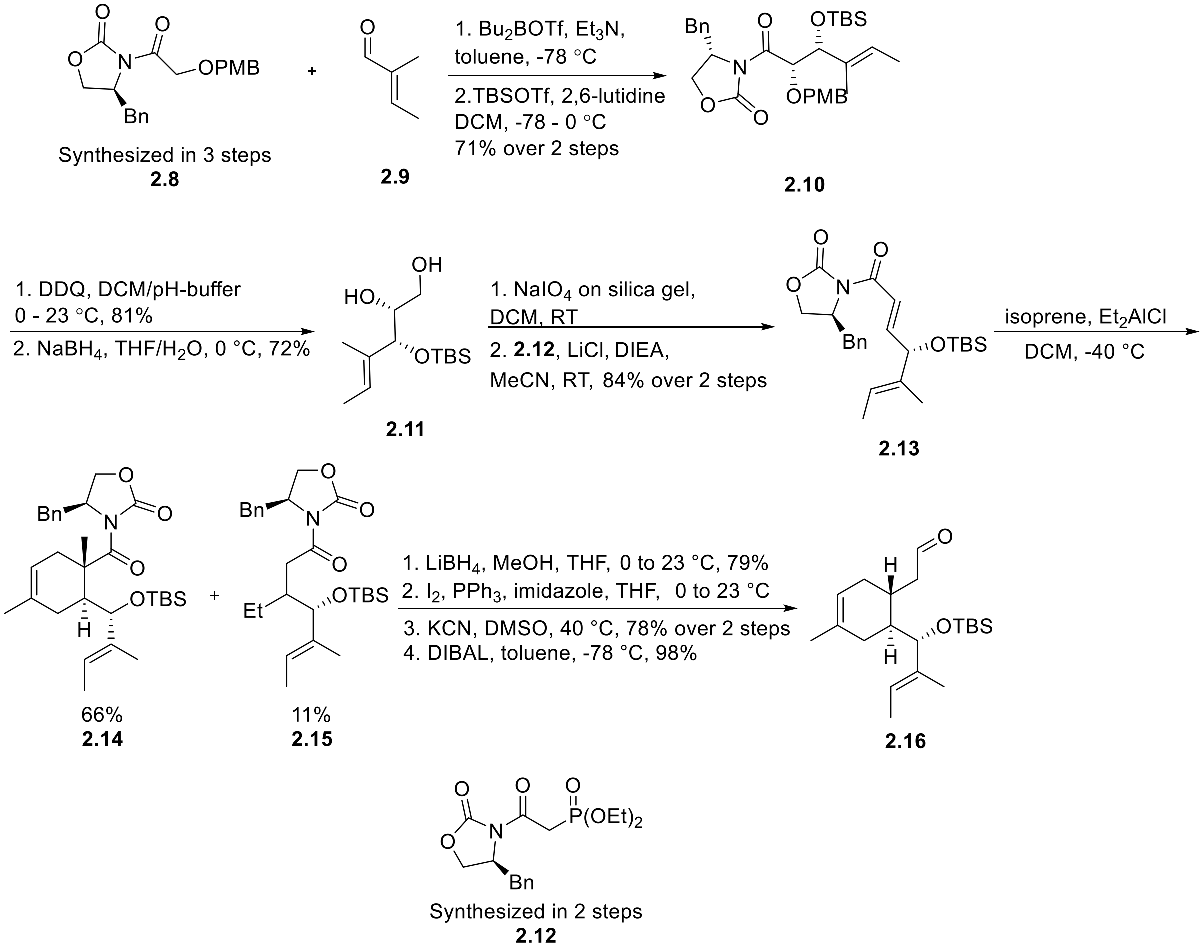
Synthesized in 3 steps
2.8
2.9
1. Bu$_2$BOTf, Et$_3$N, toluene, -78 °C
2.TBSOTf, 2,6-lutidine DCM, -78 - 0 °C
71% over 2 steps
2.10
1. DDQ, DCM/pH-buffer 0 - 23 °C, 81%
2. NaBH$_4$, THF/H$_2$O, 0 °C, 72%
2.11
1. NaIO$_4$ on silica gel, DCM, RT
2. 2.12, LiCl, DIEA, MeCN, RT, 84% over 2 steps
2.13
isoprene, Et$_2$AlCl
DCM, -40 °C
66%
2.14
11%
2.15
1. LiBH$_4$, MeOH, THF, 0 to 23 °C, 79%
2. I$_2$, PPh$_3$, imidazole, THF, 0 to 23 °C
3. KCN, DMSO, 40 °C, 78% over 2 steps
4. DIBAL, toluene, -78 °C, 98%
2.16
Synthesized in 2 steps
2.12

Scheme 2.1. Synthesis of intermediate **2.16** in the reported synthesis of Pericoannosin A.

In the forward sense, the total synthesis began with an Evan's aldol addition of oxazolidinone **2.8**, available in 3 known steps from glycolic acid mediated by dibutylboron trilfate, followed by silyl protection of the resulting alcohol in 71% overall yield over the two steps (**Scheme 2.1**). Next, PMB-deprotection with DDQ followed by reductive cleavage of the Evan's auxiliary yielded vicinal diol **2.11** in 72% overall yield. Periodate cleavage of the 1,2-diol yielded the aldehyde necessary for HWE addition with phosphonate **2.12**, a known compound synthesized in 2 steps by addition of (*S*)-4-benzyl-2-oxazolidinone to bromo acetylbromide followed by an Arbuzov reaction, which went in 84% over the two steps. The Diels-Alder cycloaddition of this intermediate with isoprene mediated by diethylaluminum chloride went in 66% yield as a single, desired diastereomer, along with 11% of an inseparable impurity that was identified as a Michael addition adduct with an ethyl group derived from the Lewis Acid. Reductive removal of the auxiliary with lithium borohydride yielded the primary alcohol, which allowed separation and isolation of the pure Diels-Alder adduct. Homologation of this alcohol was performed by Appel reaction with iodine, then displacement of the halide with potassium cyanide in 78% overall yield. DIBAL reduction of the resulting nitrile yielded the aldol precursor in 98% yield from **2.16**.

The lactam aldol partner was synthesized readily from Boc-L-leucine in a known procedure (**Scheme 2.2**). First, the amino acid was coupled with Meldrum's acid using EDCI and DMAP, followed by reductive removal of the carbonyl using sodium borohydride and acetic acid. Finally, refluxing in toluene resulted in the collapse of Meldrum's acid into a ketene intermediate, along with release of carbon dioxide and acetone. The Boc-protected amine then attacks the central, more electrophilic carbon of the ketene to form the 5-membered lactam. However, the Boc-lactam was found to be unproductive in the desired aldol reaction due to "acid-

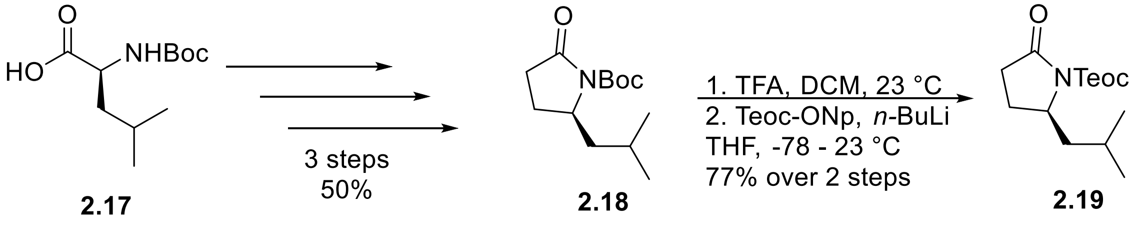

Scheme 2.2. Synthesis of enolate precursor **2.19** for aldol addition to **2.16.**

mediated elimination" of the silyl-ether, though at exactly what step is unclear. Thus, the Boc group was swapped for a Teoc protecting group by TFA deprotection of the amide, then reprotection using *n*-BuLi and Teoc-O-*p*-nitrophenol, in 77% yield.

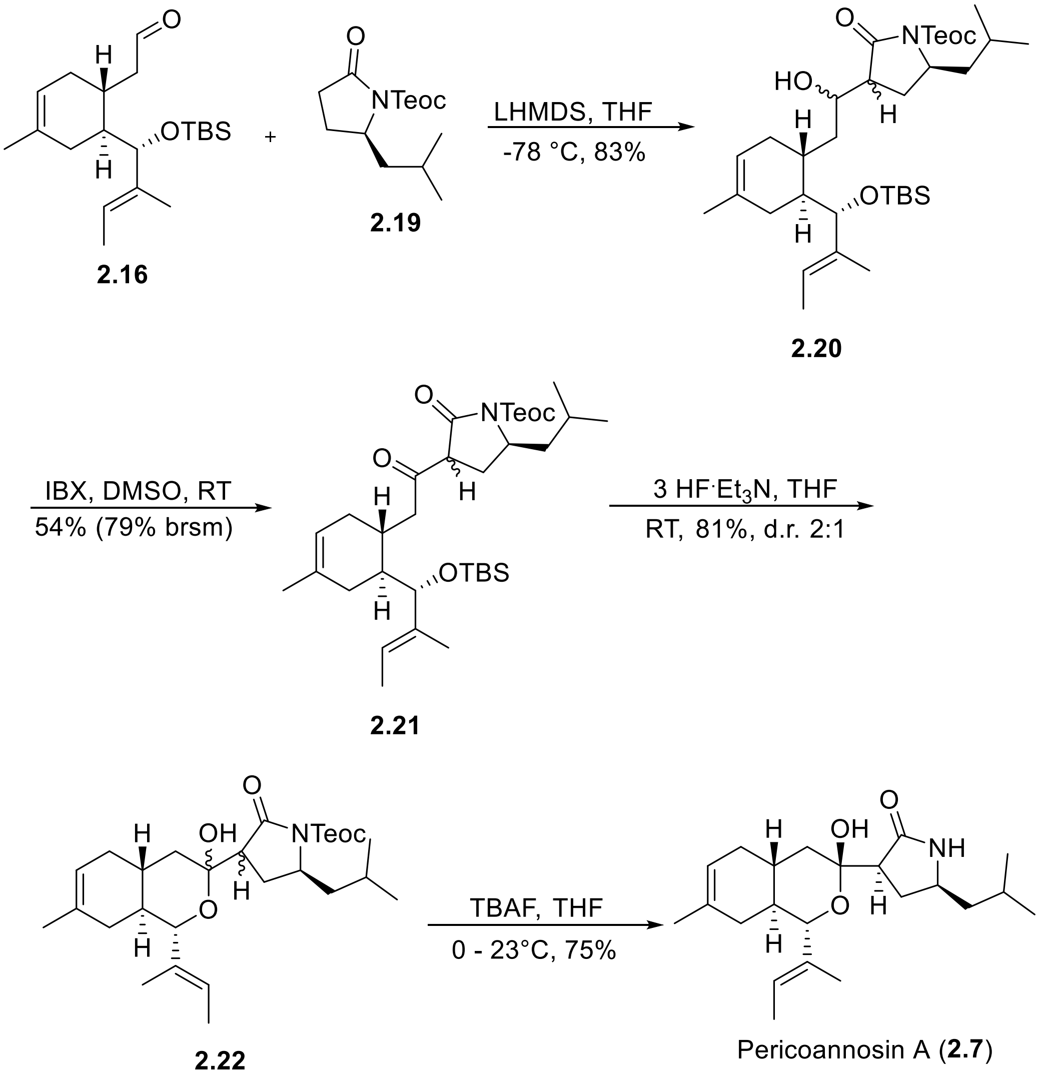
2.16
OTBS
2.19
NTeoc
LHMDS, THF
-78 °C, 83%
2.20
IBX, DMSO, RT
54% (79% brsm)
2.21
3 HF·Et3N, THF
RT, 81%, d.r. 2:1
2.22
TBAF, THF
0 - 23°C, 75%
Pericoannosin A (2.7)

Scheme 2.3. End game synthesis of Pericoannosin A in an 18 LLS and 27 overall step sequence.

The aldol condensation was performed using lithium hexamethyldisilizane (LHMDS) as the base, yielding a mixture of 4 inconsequential diastereomers in 83% yield (**Scheme 2.3**). IBX oxidation of the β-hydroxy amide to the 1,3 dicarbonyl yielded the desired material in 54%, with a yield of 79% brsm. Cyclization of this intermediate using triethylamine trihydrofluoride under dilute conditions gave lactol **2.22** in 81% yield, with a d.r. of 2:1. Finally, cleavage of the Teoc-protecting group and equilibration with an excess of TBAF yielded the natural product in a final yield of 75%, and in 5% overall yield for the total synthesis.

First Retrosynthesis of Pericoannosin A

Our first retrosynthesis of Pericoannosin A was done before the synthesis

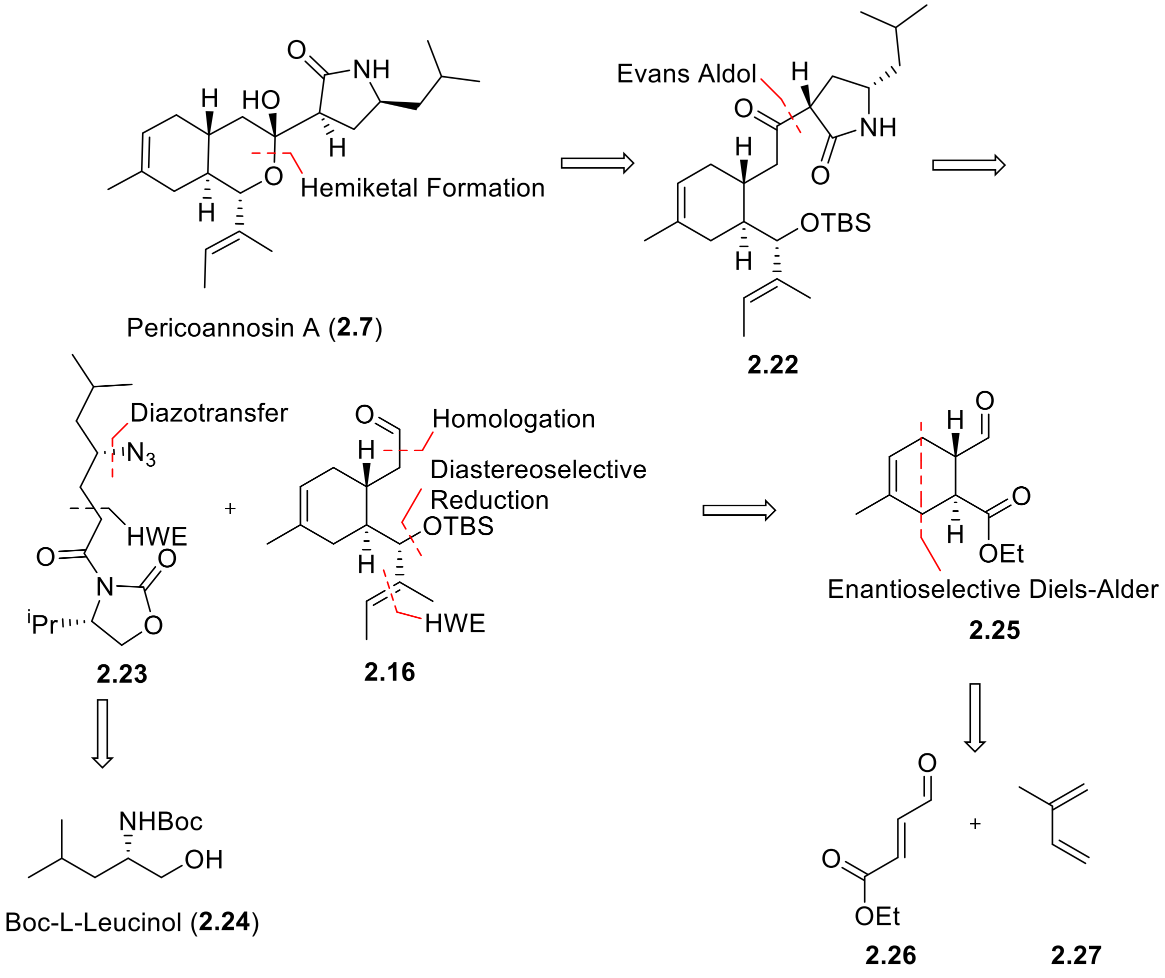
Hemiketal Formation
Pericoannosin A (2.7)
Evans Aldol
OTBS
2.22
Diazotransfer
N3
HWE
iPr
2.23
+
Homologation
Diastereoselective Reduction
OTBS
HWE
2.16
Enantioselective Diels-Alder
OEt
2.25
NHBoc
OH
Boc-L-Leucinol (2.24)
OEt
2.26
2.27

Scheme 2.4. Our retrosynthetic analysis of Pericoannosin A, coincidentally utilizing common intermediate **2.16**.

was published, and it is interesting to note the similarities and differences in the two retrosyntheses (**Scheme 2.4**). For our retrosynthesis, the last step would be cyclization to form the lactam, which would occur after a cyclization to yield the lactol moiety. This would then be separated into two fragments that would come together in an aldol reaction, azide **2.23** and aldehyde **2.16**, an intermediate that is common to both routes. The azide is accessible through known chemistry from Boc-L-leucine[155], and the aldehyde is accessible through a homologation sequence from an aldehyde. The southern portion of the molecule would be synthesized through a Weinreb ketone synthesis, followed by an asymmetric reduction and silyl protection, which are all possible from known intermediate **2.25**, which is synthesized by an asymmetric Diels-Alder of isoprene with commercially available aldehyde **2.26**.

First Generation Synthesis of Pericoannosin A

The organocatalyzed Diels-Alder cycloaddition of **2.26** with isoprene reported by Hayashi *et al* with commercial organocatalyst **2.32** went smoothly, yielding the desired adduct in similar yield and enantioselectivity (90% yield, 94% ee) to the literature report[157] (**Scheme 2.5**). Excitingly, this reaction also scaled nicely, with yield ranging from 75-90% to yield multigram quantities of the Diels-Alder adduct. With this material in hand, reduction with sodium borohydride went smoothly to yield the primary alcohol in 85% yield. At this stage, it was envisioned that a non-silyl protecting group would be used to allow for orthogonal deprotection in the presence of the TBS-silyl ether that would be introduced later. Protecting groups that are cleaved under acidic conditions (i.e-MOM) were avoided due to the lability of silyl protecting groups under acidic conditions. Thus, it was decided that a PMB-ether

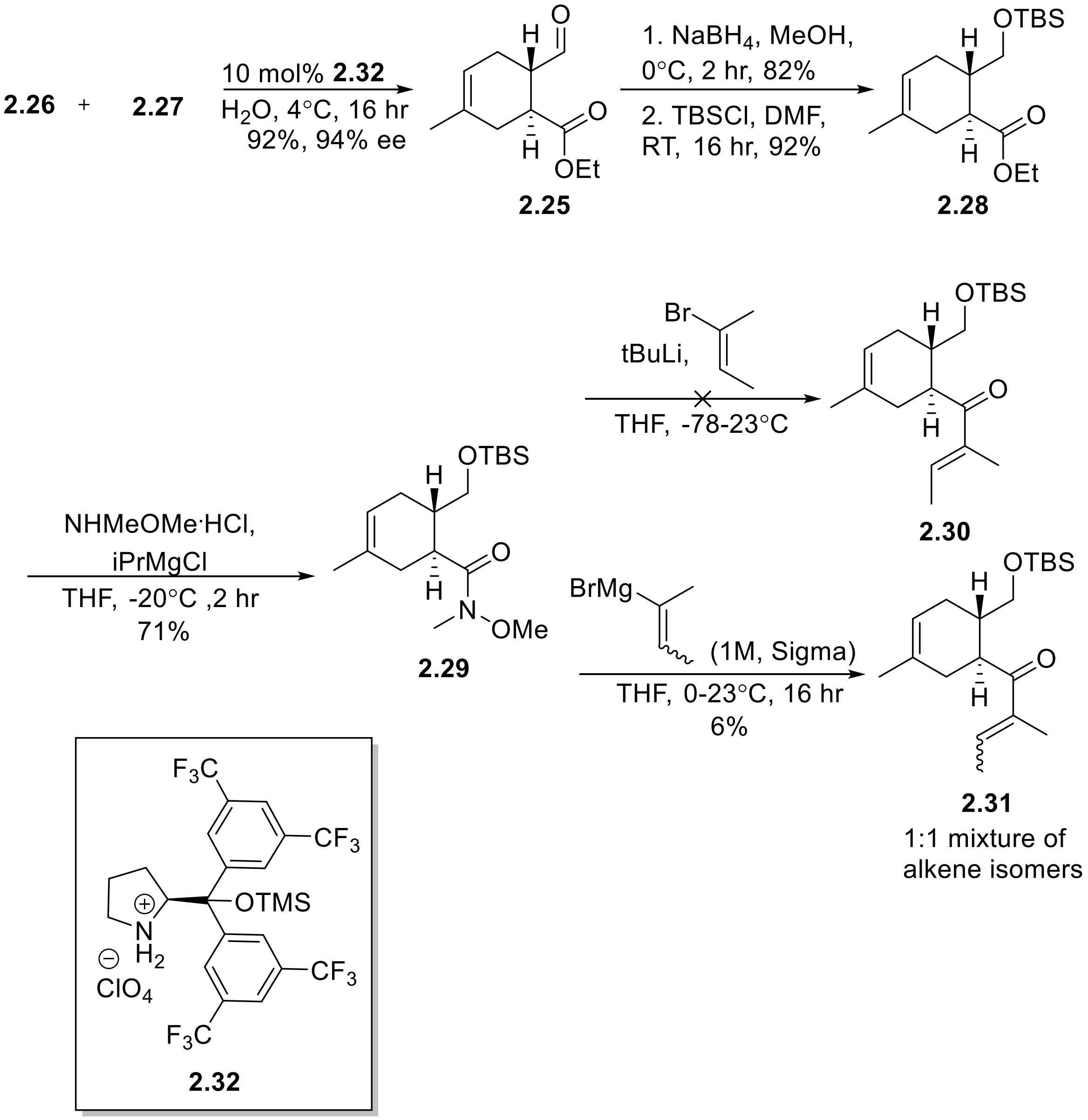
2.26 + 2.27
10 mol% 2.32
H_2O, 4°C, 16 hr
92%, 94% ee
2.25
1. $NaBH_4$, MeOH, 0°C, 2 hr, 82%
2. TBSCl, DMF, RT, 16 hr, 92%
2.28
NHMeOMe·HCl, iPrMgCl
THF, -20°C ,2 hr
71%
2.29
Br
tBuLi,
THF, -78-23°C
2.30
BrMg
(1M, Sigma)
THF, 0-23°C, 16 hr
6%
2.31
1:1 mixture of alkene isomers
2.32
H
O
OEt
OTBS
N
OMe
F_3C
CF_3
OTMS
H_2
ClO_4

Scheme 2.5. Failed synthesis of intermediate **2.31** through an attempted Weinreb ketone synthesis.

would be most desirable as the protecting group for the primary alcohol. Unfortunately, protection under extremely mild conditions, using the trifluoroacetimidate and catalytic amounts various lanthanide Lewis-Acids, resulted in degradation of the enantiomeric purity of the product. This result was somewhat surprising and disappointing, but it was figured that a mono-deprotection of the bis-silyl protected molecule could be performed at a later stage, so the primary alcohol was protected as the TBS-ether using TBSCl and imidazole, yielding the protected alcohol in 92% yield.

Conversion of the ethyl ester to the Weinreb amide using isopropyl magnesium chloride went smoothly, yielding the amide in 71% yield with no evidence of alpha-epimerization of the carbonyl. Unfortunately, addition of an organometallic reagent derived from the respective vinyl group was unproductive. Addition using the vinyl lithium reagent derived from the vinyl bromide and *t*BuLi resulted in no desired product, only basic elimination of the methoxy group from the Weinreb amide, a common side reaction for very basic nucleophiles[158]. The use of a commercial Grignard reagent resulted in a minute amount of conversion to the ketone, but revealed that the commercial reagent was a mixture of E and Z isomers.

To circumvent this roadblock, we decided to reverse the nucleophile and electrophile; instead of nucleophilic attack of the vinyl group onto the core scaffold, convert the cyclohexene into a nucleophile and use an electrophile to form the

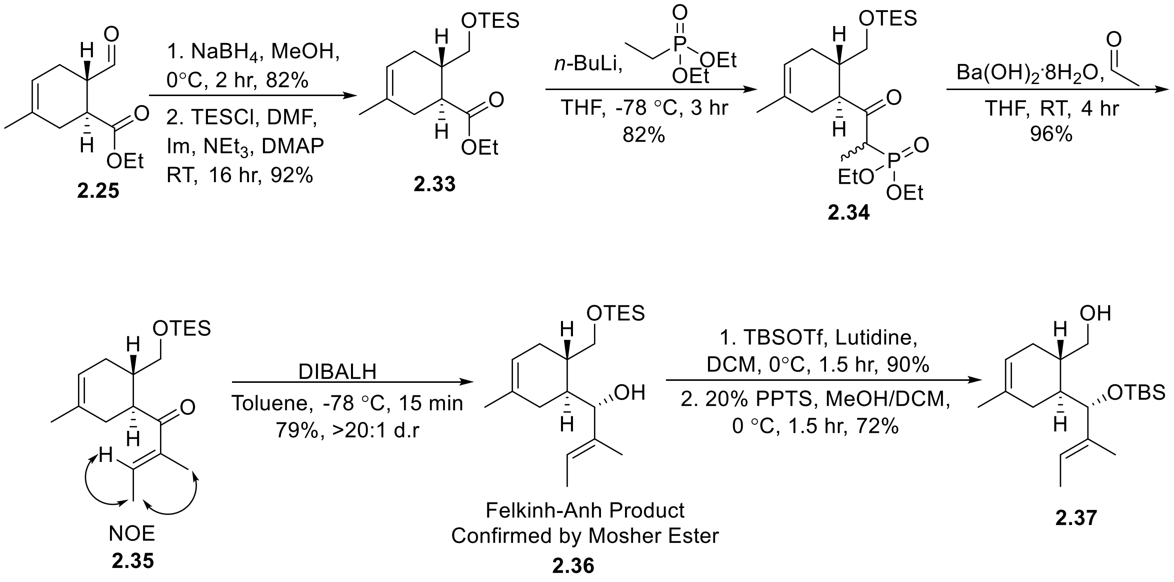

1. $NaBH_4$, MeOH, 0°C, 2 hr, 82%
2. TESCl, DMF, Im, NEt_3, DMAP RT, 16 hr, 92%
2.25
2.33
n-BuLi,
THF, -78 °C, 3 hr
82%
2.34
$Ba(OH)_2 \cdot 8H_2O$,
THF, RT, 4 hr
96%
NOE
2.35
DIBALH
Toluene, -78 °C, 15 min
79%, >20:1 d.r
Felkinh-Anh Product
Confirmed by Mosher Ester
2.36
1. TBSOTf, Lutidine, DCM, 0°C, 1.5 hr, 90%
2. 20% PPTS, MeOH/DCM, 0 °C, 1.5 hr, 72%
2.37

Scheme 2.6. Synthesis of **2.37**, an intermediate common to our and the published synthesis.

desired vinyl group (**Scheme 2.6**). To accomplish this, the ethyl ester was converted to a HWE reagent using lithiated ethyl ethylphosphonate, which proceeded in 89% yield. Due to the presence of methyl epimers and keto-enol tautomers, it was difficult to ascertain if any alpha epimerization had occurred. To our delight, using a slight excess of the phosphonate to help prevent vinylogous aldol chemistry, the HWE of this phosphonate with acetaldehyde using barium hydroxide as the base went smoothly to afford the α,β unstaturated carbonyl, which was confirmed to be the desired E olefin isomer by 1D nOe (**Appendix B**).

Asymmetric reduction of this enone was attempted using a number of conditions. Initially, a Corey-Bakshi-Shibata (CBS) reduction was envisioned[159-161]. However, this reduction was plagued by alkene hydroboration and little reduction product. It was then found that the Felkin-Anh model of nucleophilic attack would theoretically give the desired alcohol stereocenter[162-164]. This was first attempted using DIBAL at -78 °C for 1 hour, which gave only a moderate yield of the desired product, but, excitingly, as a single diastereomer. Mosher ester analysis of this reduction product revealed that the Felkin-Anh model did indeed predict the stereochemical outcome of the reaction. Reaction optimization revealed that the reaction was very rapid, with complete consumption of starting materials being observed within 5-20 minutes, depending on scale.

Next, protection of the allylic alcohol with TBSOTf under standard conditions gave the desired bis-silyl protected product. To our surprise, it was fairly difficult to perform mono-deprotection of this product. It seems that the allylic silyl-ether is more labile than one would expect a secondary TBS-protected alcohol to be, perhaps due to it being allylic or due to the relatively high steric strain it is under being located between the cyclohexene ring and the dimethyl vinyl group. However, it was found that catalytic camphor sulfonic acid (CSA) in methanol at 0 °C allowed for sufficiently selective mono-deprotection to yield the primary alcohol in variable yields of 40-50%. Due to the difficulty in deprotecting the bis-TBS ether, the primary alcohol protecting group was changed to a triethylsilyl (TES) protecting group, which is more labile than a TBS group and it was hypothesized that this would improve the efficiency of this synthetic step. Indeed, stirring the starting material with 0.2 equivalents of pyridinium *p*-toluenesulfonate (PPTS) in a 1:1 mixture of DCM and methanol for 30 minutes allowed for isolation of the pure primary alcohol in 72% yield in a 1 gram scale reaction.

At this point in the synthesis, the total synthesis of this natural product was published, revealing the similarities in our routes. Though we knew that future work would be necessary to differentiate our routes in the future, we were fortunate to be able to use optimized conditions that were published to help push toward late intermediates to try out the novel chemistries that our synthesis contained. Using the published conditions, the primary alcohol was homologated using Appel conditions, followed by displacement with potassium cyanide in DMSO. Unfortunately, the yields of the published could not be replicated (48 and 66%, respectively, versus 78% over the two steps in the literature report), but we were able to push sufficient quantities of material forward for further work. DIBAL reduction of the resulting nitrile yielded known aldehyde **2.16** in 53% yield, which matched the published material, additionally confirming the stereochemistry of the carbonyl reduction.

The synthesis of **2.23** was achieved according to the route described by Avery, *et al*[156]*.* Briefly, Boc-L-leucinol was oxidized using standard Parikh-Doering conditions to give the desired aldehyde in 87% yield, which was then homologated in an HWE olefination using triethyl ethylphosphonate and sodium hexamethyldisilazide (NHMDS) and hydrogenated under standard conditions to give **2.38** in good yields. Next, saponification followed by Boc-deprotection using HCl in dioxanes formed a white solid that could be isolated using air free filtration (product may form a hydrate that is more soluble in ether than the parent compound). Azide formation using the sulfuric acid salt of imidazole sulfonylazide[165] gave **2.40** in a moderate yield, which was followed by imide formation under standard conditions with *R*-ispropyl oxazolidinone to form desired intermediate **2.23** in a good yielding 7 step sequence.

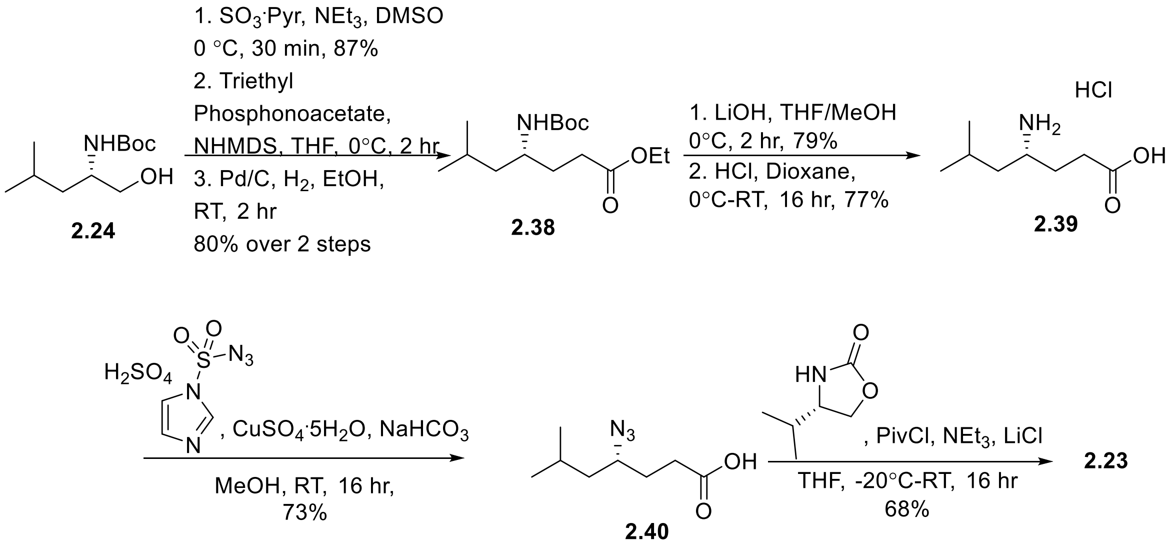
NHBoc
OH
2.24
1. SO3·Pyr, NEt3, DMSO
0 °C, 30 min, 87%
2. Triethyl
Phosphonoacetate,
NHMDS, THF, 0°C, 2 hr
3. Pd/C, H2, EtOH,
RT, 2 hr
80% over 2 steps
NHBoc
OEt
O
2.38
1. LiOH, THF/MeOH
0°C, 2 hr, 79%
2. HCl, Dioxane,
0°C-RT, 16 hr, 77%
HCl
NH2
OH
O
2.39
H2SO4
O
O
S
N3
N
N
, CuSO4·5H2O, NaHCO3
MeOH, RT, 16 hr,
73%
N3
OH
O
2.40
O
HN
O
, PivCl, NEt3, LiCl
THF, -20°C-RT, 16 hr
68%
2.23

Scheme 2.7. Synthesis of compound through a rapid, seven step sequence reported by Avery *et al*.

With intermediates **2.16** and **2.23** in hand, the aldol condensation was attempted using standard Evan's aldol conditions. Forming the boron enolate with dibutyl boron triflate, the desired aldol product could be obtained in moderate yields of 40-65%. With this product in hand, attempts to reduce the azide and cyclize to the lactam were attempted, with the vision of a final step formation and equilibration to simultaneously form the lactol and epimerize to the thermodynamically favored natural product. Unfortunately, numerous methods for reducing the azide produced either very little ($SnCl_2$, Staudinger reduction-PBu_3 or PPh_3, 5% yield) or no (Lindlar catalyst, Zn/NH_4Cl) product. This is hypothesized to be due to steric reasons, as the beta-hydroxy ketone will be rigidified by an intramolecular hydrogen bond. This results in the azide being blocked by the TBS silyl ether or the vinyl group on one side, and the carbonyl or isopropyl group of the oxazolidinone.

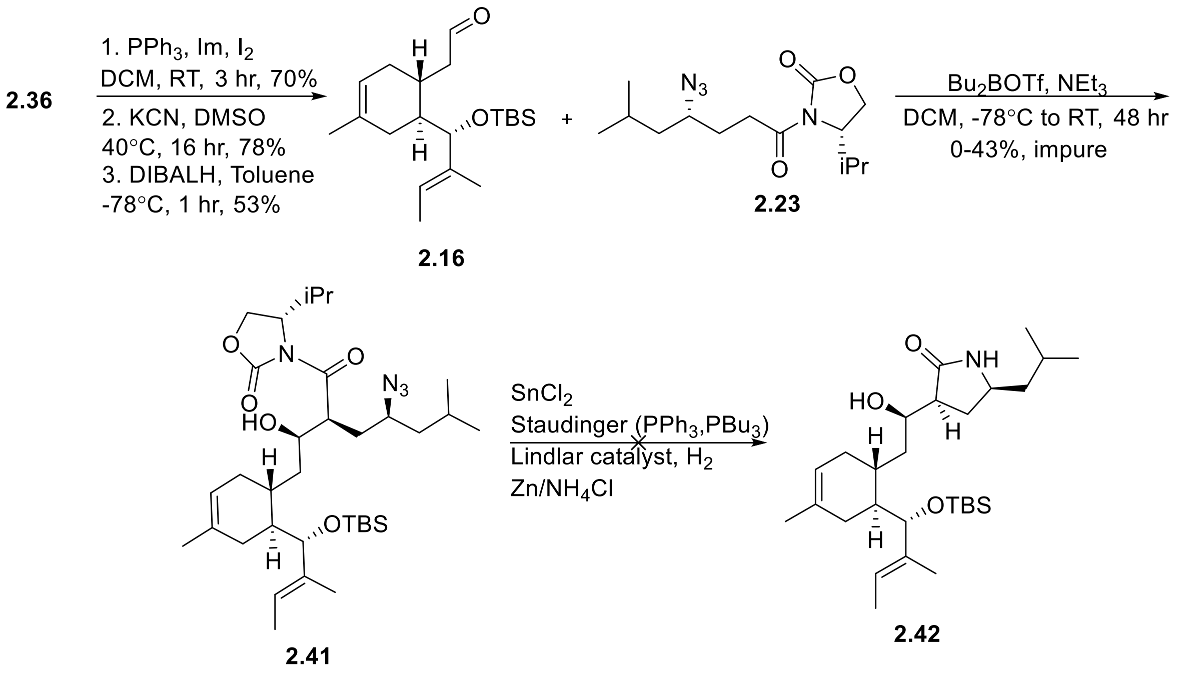

2.36
1. PPh_3, Im, I_2
DCM, RT, 3 hr, 70%
2. KCN, DMSO
40°C, 16 hr, 78%
3. DIBALH, Toluene
-78°C, 1 hr, 53%
H
O
OTBS
H
2.16
+
N_3
O
O
N
O
iPr
2.23
Bu_2BOTf, NEt_3
DCM, -78°C to RT, 48 hr
0-43%, impure
iPr
O
N
O
O
N_3
HO
H
OTBS
H
2.41
$SnCl_2$
Staudinger (PPh_3,PBu_3)
Lindlar catalyst, H_2
Zn/NH_4Cl
O
NH
HO
H
H
OTBS
H
2.42

Scheme 2.8. Synthesis of **2.41** and failed lactam synthesis through azide reduction.

To circumvent this obstacle in the synthesis, it was decided that the lactol would be formed first, which would remove much of the steric bulk surrounding the azide and allow for the desired reactions to occur. In the event, the beta-keto amide was oxidized using 4 equivalents of 2-ioxodybenoic acid (IBX) in DMSO to yield the 1,3 diketone in 78% yield. Due to the presence of diastereomers and keto-enol tautomers, this product was not characterized further, but pushed onto the next step.

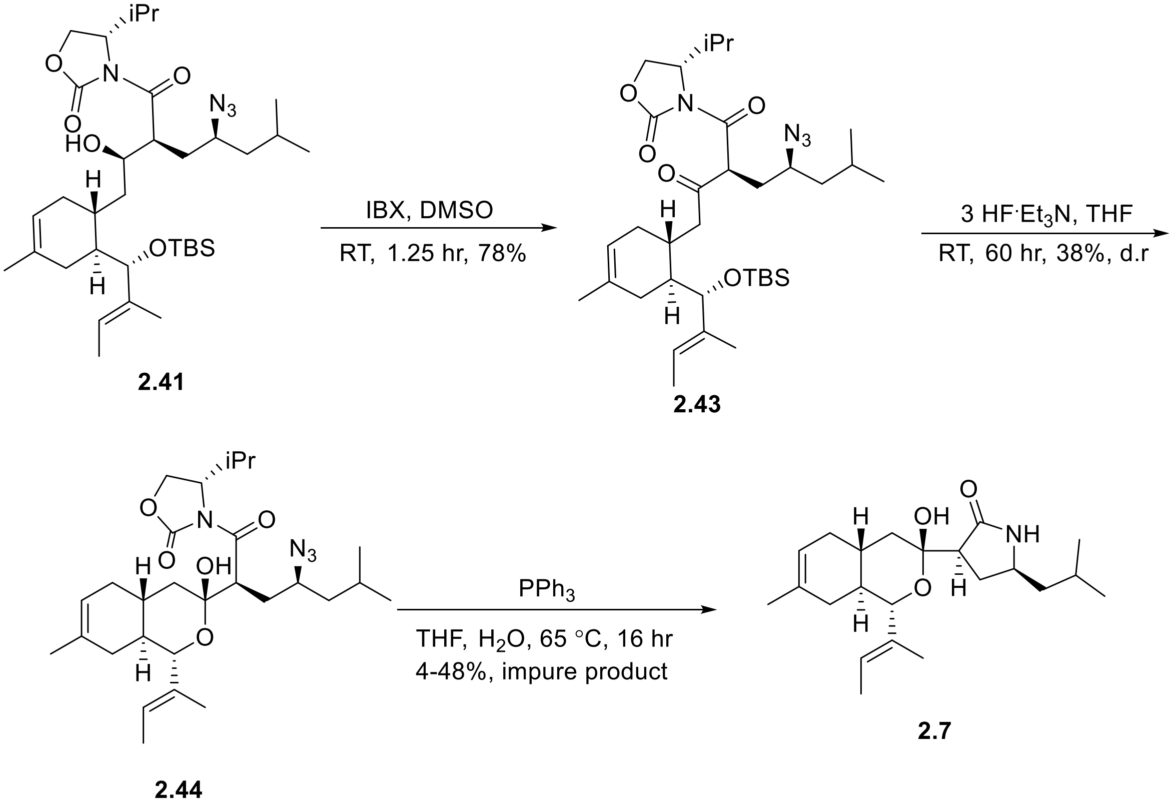

Scheme 2.9. Unsuccessful attempts at the final steps for the synthesis of Pericoannosin A.

Cyclization of intermediate **2.43** to the lactol was accomplished using a large excess of triethylamine trihydrofluoride in THF, with stirring for 54 hours. This yielded a mixture of 2 diastereomers,that were taken on for the final cyclization to yield the natural product. In the event, the Staudinger reduction of azide **2.44** was performed using resin-bound triphenylphosphine, to simplify the workup, in a mixture of THF and water, first, at room temperature overnight, then at 60 °C for 8 hours, which allowed for full conversion of starting materials. Isolation of this product using column chromatography revealed an unknown impurity that could not be separated after several columns. However, it was thought that this route, with some optimization, would be sufficiently robust, combined with an improved synthetic scheme, for finishing the molecule and publication.

Second Generation Route for the Formal Total Synthesis of Pericoannosin A

While the first generation route towards the synthesis of Pericoannosin A was successful in bringing up late stage intermediates for the synthesis, there was significant room for improvement. The end of the synthesis could not be changed in a facile manner and was already efficient, so this part of the scheme was left untouched. One area of the synthesis that was found to be inefficient was the homologation sequence starting from the aldehyde. Ignoring the formation of the ketone, the homologation requires 6 synthetic steps, including a protection-deprotection sequence, and two reduction transformations (reduction of the aldehyde, reduction of the nitrile) to get to the desired aldehyde. This leaves a lot of room for improvement, and is where our efforts were first focused for optimization of the route. Routes for optimization were hypothesized from the aldehyde to get to the homologated aldehyde. This route would need to be able to withstand fairly aggressive reaction conditions in the lithated phosphonate addition and DIBAL reduction of the enone. Additionally, it would need to be more efficient than the previous 6 step synthesis. To this end, it was hypothesized that an olefination reaction of the aldehyde would be sufficiently orthogonal such that it could be run chemoselectively, not touching the ester (**Scheme 2.10**). Additionally, this terminal alkene would be inert to the reaction conditions that are intermediary to the formation of the homologated aldehyde. Finally, the alkene is a versatile functional handle, and could be transformed in a facile manner to the aldehyde using a selective hydroboration-oxidation, followed by an oxidation of the resulting primary alcohol. Selective hydroborations of terminal alkenes over more substituted alkenes is well precedented[166], and can be carried out using bulky boron reagents, such as 9-BBN, to only react with the desired alkene, along with reacting solely in an anti-Markovnikov fashion.

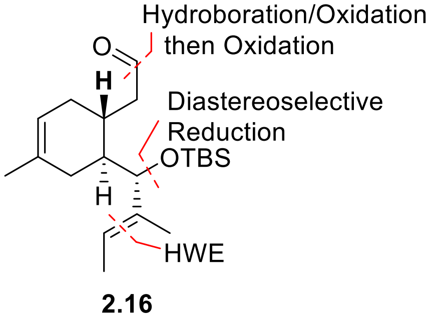
Hydroboration/Oxidation then Oxidation
O
H
Diastereoselective Reduction
OTBS
H
HWE

2.16

Scheme 2.10. Revised retrosynthesis toward intermediate **2.16**.

Starting from the Diels-Alder adduct used in the first generation route, olefination was first attempted using potassium *t*-butoxide and methytriphenylphosphonium bromide in THF, which gave the desired product in a moderate yield of 52%, but only 4:1 d.r. It was thought that these reaction conditions were too strongly basic, causing equilibration at the alpha position of the ester, which was confirmed by thermodynamic equilibration with DBU in toluene to yield the desired alkene as a single diastereomer. Thus, a non-basic Wittig olefination was attempted, which utilized trimethylsilyl (TMS) diazomethane and Wilkinson's catalyst to form a carbene that reacts with triphenylphosphine to form an intermediate that can react with isopropanol to give an ylide without addition of any base. This reaction proceeded smoothly to give the Wittig olefination product, albeit in moderate yields of 50-60%, but with a d.r. of >20:1 by NMR. While we were excited to be able to obtain the desired product without epimerization of the formed stereocenters, further optimization was done due the moderate yields and relative expense of TMS diazomethane and Wilkinson's catalyst that could potentially prohibit large scale synthesis of the desired intermediate.

Wittig olefination was next explored using different bases to form the ylide, LHMDS and KHMDS, for which an interesting salt effect was observed. Using KHMDS to form the ylide results in the formation of KBr, which has relatively low solubility in THF, and thus it was thought that the potassium would be unable to activate the ester for deprotonation, thus preventing epimerization and potential decomposition of the starting material. Lithium bromide, on the other hand, is very soluble in THF, and it was thought that the free lithium ion could potentially be detrimental to the reaction. However, the exact opposite was observed. While both olefinations proceeded in an improved yield of 65%, the d.r. using KHMDS was drastically lower, 10:1, than the olefination using LHMDS, which produced the desired material in >20:1 d.r. We were delighted to find, upon scaling up this reaction using LHMDS as the base, that we were able to obtain the desired product in 75% yield, with little to no impact on the enantiopurity of this intermediate.

Conditions[a]	Yield	d.r.
$Rh(PPh_3)_3Cl$, ^{i}PrOH, PPh_3, $TMSCHN_2$	65%	>20:1
CH_3PPh_3Br, KO^{t}Bu	55%	4:1
CH_3PPh_3Br, KHMDS	59%	10:1
CH_3PPh_3Br, LHMDS	73%	>20:1
CH_3PPh_3Br, LHMDS[b]	75%	>20:2

[a]Reactions were conducted on 100 mg (0.5 mmol) scales. [b]Reaction conducted on a 1 g (5 mmol) scale.

Table 2.1. Conditions explored for Wittig olefination of Diels Alder adduct **2.25** (**Scheme 2.11**).

Fortunately, the next several steps in the sequence proceeded in a similar manner to the initial route with minimal optimization (**Scheme 2.11**). Stirring the Wittig product with excess lithated ethyl ethylphosphonate producted the β-ketophosphonate in 81% yield, which was then reacted with acetaldehyde in the

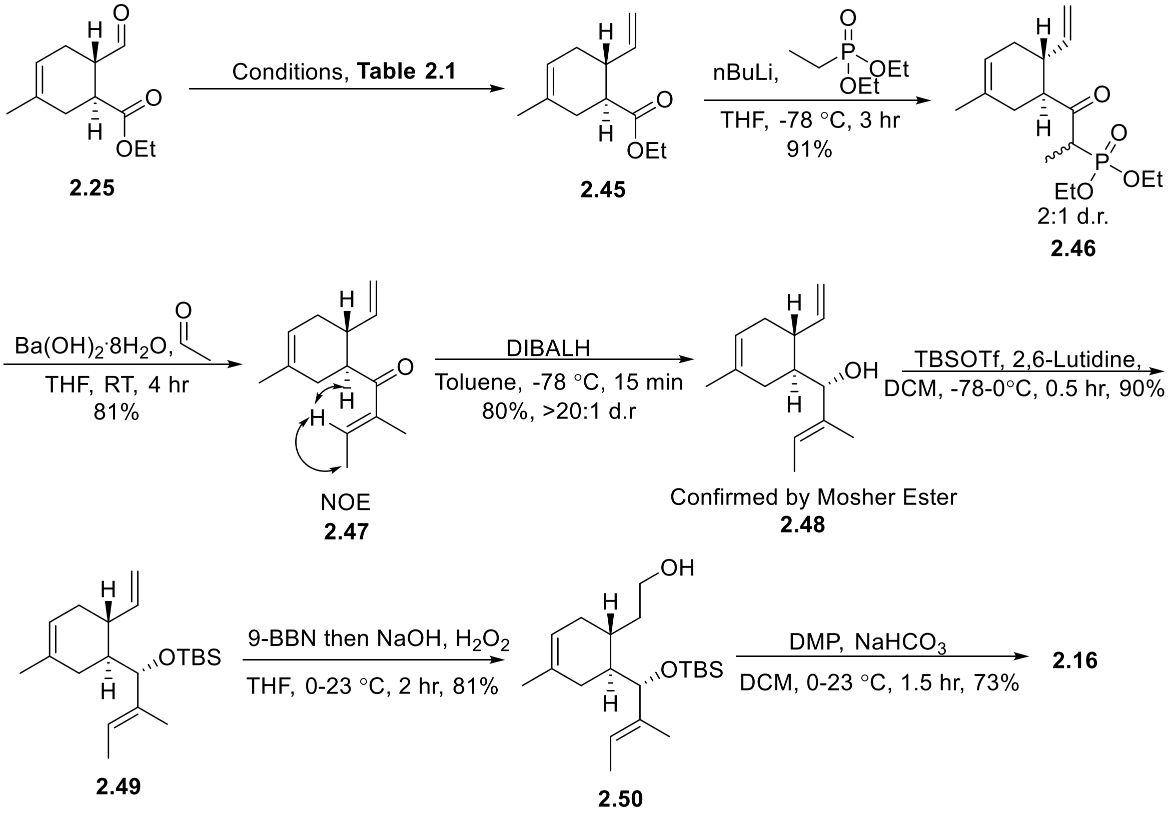
H
O
OEt
H
2.25
Conditions, Table 2.1
2.45
nBuLi,
OEt
THF, -78 °C, 3 hr
91%
2:1 d.r.
2.46
Ba(OH)2·8H2O,
THF, RT, 4 hr
81%
NOE
2.47
DIBALH
Toluene, -78 °C, 15 min
80%, >20:1 d.r
OH
Confirmed by Mosher Ester
2.48
TBSOTf, 2,6-Lutidine,
DCM, -78-0°C, 0.5 hr, 90%
OTBS
2.49
9-BBN then NaOH, H2O2
THF, 0-23 °C, 2 hr, 81%
2.50
DMP, NaHCO3
DCM, 0-23 °C, 1.5 hr, 73%
2.16

Scheme 2.11. Second generation synthesis of aldehyde **2.16**.

presence of barium hydroxide octahydrate to yield the enone in 81% yield. Reduction of the enone using DIBAL at -78 °C for 15 minutes in toluene proceeded in slightly lower yields than the first route. The undesired allylic alcohol epimer was also observed as a minor side product, but the two diastereomers were fortunately easily separable via column chromatography, enabling the synthesis of the allylic alcohol in 83% yield. TBS protection of this alcohol proceeded in 89% yield using TBSOTf and 2,6-lutidine in DCM. Selective hydroboration of the terminal alkene using a slight excess of 9-borabicyclo(3.3.1)nonane (9-BBN) in THF, followed by oxidation using hydrogen peroxide with 2M NaOH, yielded the desired primary alcohol in 81% yield. Oxidation of this alcohol using Dess-Martin Periodinane (DMP) in DCM buffered with sodium bicarbonate, to neutralize the acetic acid byproducts and protect the very sensitive allylic silyl ether, proceeded smoothly to give the known aldehyde in 73% yield.

Aldol Optimization and Attempted Completion of Synthesis

At this point in the synthesis, it became apparent that the initial Evan's aldol conditions using the boron enolate derived from dibutylboron triflate was not tenable for the completion of the synthesis. Even in the initial route, the yields of this reaction were inconsistent, either giving no desired product with some decomposition of starting materials, or about 45% yield. Either of these cases were not ideal for the completion of the synthesis, especially when the aldol was attempted using a number of different Evan's auxiliaries (Bn, Ph, iPr) and conditions (LHMDS, $TiCl_4$, Bu_2BOTf) with no major improvements in the yield of the reaction.

A model system for this aldol was developed utilizing isoveraldehyde, which was thought would be a good mimic for the steric bulk around the aldehyde used in the synthesis. Utilizing the boron enolate derived from oxazolidinone **2.23**, no productive yield of desired product was observed, even upon using a new bottle of the Lewis acid and freshly distilled base. Using the lithium enolate, however, resulted in good conversion to the aldol condensation product, which we thought was curious as these conditions did not work in the actual system. From here, we hypothesized that the issues plaguing this aldol reaction may be due to the large steric bulk surrounding the aldehyde from the Southern allylic alcohol and alkene. Our first attempt to ameliorate this was utilizing NHMDS as the base, as it was hypothesized that the sodium salt would be unable to form a closed transition state, and that the open transition state may allow production of product. However, these conditions also failed to yield any desired product. Because it would take significant retooling and optimization of the synthetic route to alter the sterics of the aldehyde used in the aldol reaction, we hypothesized that lowering the sterics around the nucleophile in the aldol could allow for productive reaction to occur.

To lower the steric bulk around of the nucleophile, we decided to focus on the two requirements that are necessary for the moiety attached to the carbonyl of the azide: it must be sufficiently activating to allow for the formation of an enolate, but also labile enough to function as a good leaving group upon reduction of the azide to allow formation of the lactam. An ideal candidate for this is the use of an ester, which has an acidic alpha proton for enolate formation and could be easily formed from the already known acid (**2.40**). Synthesis of the methyl ester was achieved by addition of TMS diazomethane, which gave the desired material in 92% yield

(**Scheme 2.12**). Next, aldol reaction mediated by LHMDS proceeded in a moderate yield of 47%, but with good recovery of starting material, which resulted in a yield of 76% based on recovered starting (brsm). Interestingly, no additional methyl ester was recovered, which indicated to us that this material was decomposing in some way before it was capable of participating in the aldol reaction. Analysis of the LCMS reports from this reaction indicated the presence of a dimer derived from a formal Claisen condensation of the methyl ester, which is known to occur with ester derived enolates at too high of temperatures. Lowering of the temperature to -98 °C showed no improvement in yield. We then thought that the formation of this byproduct could be the result of an improper order of addition, as we were initially adding the base to a solution of ester, which results in a small population of enolate in a large pool of unchanged ester and could facilitate this condensation reaction. Unfortunately,

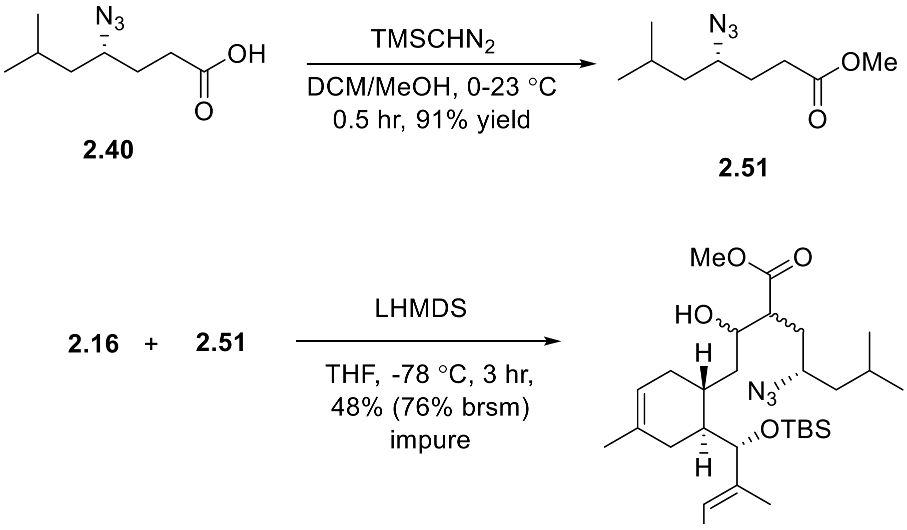

2.40

2.51

2.52

Scheme 2.12. Synthesis of enolate precursor **2.51** and subsequent aldol reaction.

adding a solution of ester to a solution of LHMDS resulted in no significant change in yield. Surprisingly, addition of 3 equivalents of enolate was also ineffective in improving the yield in this reaction. Switching the base from LHMDS to lithium diisopropyl amide (LDA) resulted in an aldol with similar efficacy in producing the desired product, but recovery of only trace amounts of starting aldehyde. This is presumably due to the increased basicity of diisopropylamine compared to hexamethyldisilizane resulting in decomposition of the sensitive starting aldehyde.

Several groups have reported that this formal Claisen condensation can be mediated not through a direct nucleophilic attack of an ester enolate onto an ester, but instead can occur by first formation of a ketene by decomposition of the lithium enolate with release of the methoxide anion[167-169]. However, prevention of this decomposition is typically ameliorated by lowering of the reaction temperature, which was already shown to be ineffective. Additionally, warm temperatures are typically needed for this ketene formation to occur, so it is most likely a result of a direct Claisen condensation that occurs concurrently or immediately after enolate formation[169]. Another means of preventing this mechanism of decomposition is to utilize a *tert*-butyl ester, which is more thermally stable than less sterically encumbered esters, but due to the poor electrophilicity of *tert*-butyl esters, it was hypothesized that this method would complicate the future lactam formation step. Nonetheless, the high recovery of unreacted starting material along with the relative ease of synthesis of the methyl ester portion of the reaction made this a useful synthetic step.

Next, the aldol product, which was isolated as a mixture of 4 diastereomers, was oxidized using IBX in DMSO to form the β-keto ester in 43% yield, with a yield of 57% brsm. Cyclization to the lactol with triethylamine trihydrofluoride proceeded in a good yield of 86%. Unfortunately, cyclization of this material to the natural product proved non-trivial. Staudinger reduction in toluene resulted in good conversion to the amine in 1 hour, but proved ineffective at enacting the desired cyclization. Isolation of this intermediate followed by stirring in methanol with potassium carbonate resulted in no change in starting material, while heating to reflux resulted in decomposition of starting material and little product formation. This was hypothesized to be due to the sensitivity of the lactol species, so we decided to rearrange the order of the final steps (**Scheme 2.13**). Cyclization of the aldol product under standard Staudinger conditions in THF smoothly converted to the lactam, as a mixture of 4 diastereomers, in 4-5 hours at 60 °C in 91% yield. There was no observation of the secondary amine intermediate by LCMS, meaning that lactam

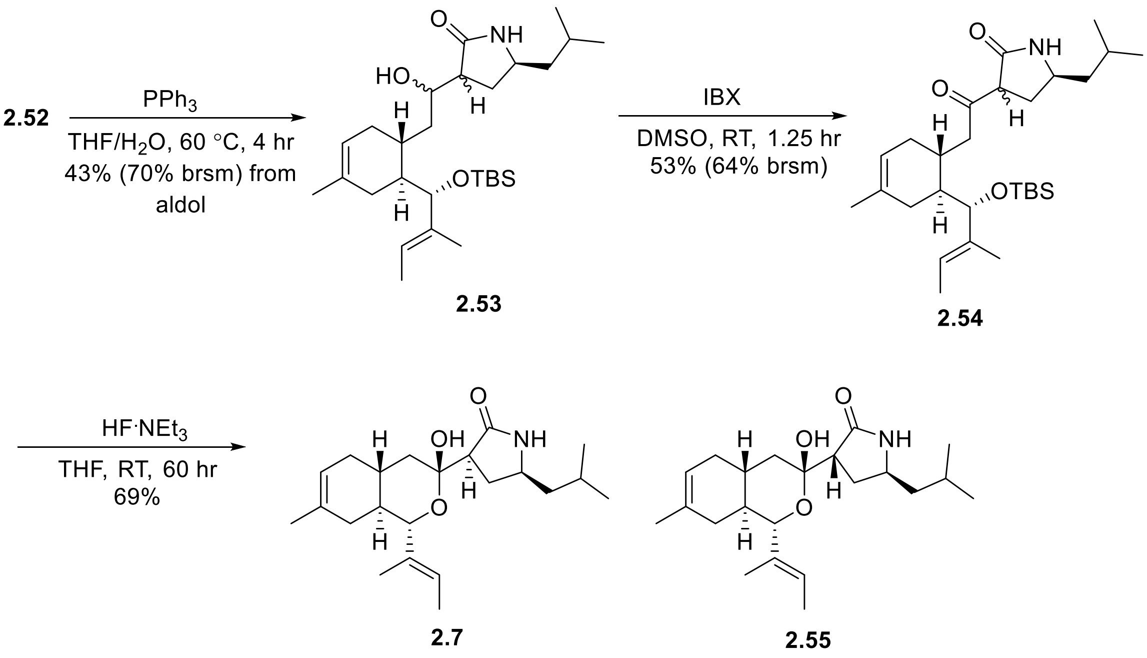

Mixture of 3:1 **2.7**:**2.53**

Scheme 2.13. End game synthesis of Pericoannosin A.

formation proceeded rapidly after completion of the reduction. IBX oxidation of the resulting material proceeded in 53% yield (64% brsm), which was followed by cyclization under the same conditions as before to yield **2.53** as a mixture of 2 diastereomers in 69% yield. At this point, equilibration using the conditions in the published synthesis was attempted to determine if our route was viable for producing the desired product. However, the use of TBAF in THF resulted in no appreciable change in the ratio of diastereomers. This is likely due to the fact that the Teoc protecting group may acidify the alpha proton of the amide, allowing for TBAF to equilibrate this position. With the remaining material, separation of the diastereomers by preparative TLC was attempted, which was unsuccessful in producing pure natural product.

Summary and Future Directions

In summary, this work represents both a formal total synthesis of Pericoannosin A that is a marked improvement over the published work, and a total synthesis of a mixture of epi- and Pericoannosin A. Arrival at common intermediate **2.16** in an 8 longest linear and total steps in 18.3% yield stands as a large improvement over the published work, which arrives at this intermediate in 14 longest linear step sequence and 16 overall steps, with poor atom economy. The use of an organocatalyzed asymmetric Diels-Alder cyclization sets 2 stereocenters that allow for the creation of the allylic stereocenter by structural induction, whereas the published synthesis utilizes two separate Evan’s oxazolidinone steps to establish all 3 stereocenters in **2.16**. The high yield and low step count of this formal synthesis make these chemistries ideal for the future synthesis of Pericoannosin A, or for similarly structured natural products.

This work has also established different reactions for the total synthesis of Pericoannosin A. An ester aldol followed by lactam cyclization allowed preparation of the Eastern lactam of the natural product. Unfortunately, the desired product was isolated as a mixture of two diastereomers that were very difficult to separate by flash chromatography and prep TLC. Future directions for this synthesis include exploring the separation of these diastereomers by reverse phase chromatography/HPLC or by supercritical fluid chromatography (SFC), which can utilize chiral columns for an improved separation[170-171]. Additionally, one could also explore ways of equilibrating the two diastereomers to the desired material. One method could potentially be a kinetic protonation, in which the enolate could be formed and quenched at cryogenic temperatures[172]. The proton would most likely preferentially come in opposite of the isobutyl group of the lactam due to sterics. However, the enolate formation would most likely be complicated due to the similar pKas of the lactam nitrogen and the alpha proton. Alternatively, according to the literature report, the product is also the thermodynamically favored product, so thermodynamic equilibration conditions using base could theoretically be used as well.

Experimental Methods

General Synthetic Methods and Instrumentation

All reagents and solvents were commercial grade and used as received. All reactions were carried out employing standard chemical technique under air, unless otherwise noted. Thin layer chromatography (TLC) was performed on glass-backed silica gel of 250 μm thickness. Visualization was accomplished with UV light and/or the use of $KMnO_4$ or *p*-anisaldehyde stain. Analytical HPLC 113 was performed on an Agilent 1200 LCMS with UV detection at 215 and 254 nm and electrospray ionization. MS parameters were as follows: capillary voltage: 3000V, nebulizer pressure: 40 psi, drying gas flow: 11 L/min, drying gas temperature: 350 °C. Samples were separated on an internal column (Thermo Accucore C18 2.1 x 30 mm, 2.6 μm) before ionization with the following solvent gradient: 7% to 95% MeCN in H_2O (0.1% TFA) over 1.6 min, hold at 95% MeCN for 0.35 min, 1.5 mL/min flow, 45 °C. Chromatography on silica gel was performed using Teledyne ISCO pre-packed silica gel columns using gradients of EtOAc/Hexanes or DCM/MeOH. ^{1}H and ^{13}C NMR spectra were recorded on Bruker DRX-400 (400 MHz) or AV-II 600 (600 MHz) instrument and chemical shifts are reported in ppm relative to residual solvent.

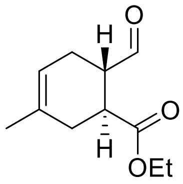

ethyl (1*S*,6*S*)-6-formyl-3-methyl-cyclohex-3-ene-1-carboxylate (2.25).

To a 100 mL round-bottom flask at 4 ^{o}C containing ethyl (E)-4-oxobut-2-enoate (3.53

mL, 28.1 mmol, 1 eq) and [bis[3,5-bis(trifluoromethyl)phenyl]-[(2S)-pyrrolidin-1-ium-2-yl]methoxy]-trimethyl-silane perchlorate (981 mg, 1.4 mmol, 0.05 eq) in water (30 mL) was added isoprene (8.43 mL, 84 mmol, 3 eq) with stirring. After 48 hours, the reaction mixture was quenched with saturated sodium bicarbonate (20 mL), then extracted with ether (3x75 mL), and the organic layers were dried over magnesium sulfate, filtered, and concentrated *in vacuo* onto silica gel. Crude product was purified using Teledyne ISCO Combi-Flash system (solid loading, 40G column, 0-25% Hex/EtOAc) to yield ethyl (1*S*,6*S*)-6-formyl-3-methyl-cyclohex-3-ene-1-carboxylate (5.2 g, 26.4 mmol, 94% yield) as a clear oil. **^{1}H-NMR (400 MHz, CDCl$_3$)** δ 9.67 (s, 1H), 5.38 (bs, 1H), 4.19-4.07 (m, 2H), 2.91-2.76 (m, 2H), 2.37-2.24 (m, 2H), 2.14-2.01 (m, 1H), 1.64 (s, 3H), 1.27-1.17 (m, 3H) ppm; **^{13}C-NMR (100 MHz, CDCl$_3$)** δ 202.8, 174.5, 133.0, 118.4, 60.9, 47.4, 39.8, 31.5, 24.3, 23.3, 14.3 ppm; **ESI-HRMS:** m/z calc for $C_{11}H_{19}O_3$ $[M+H]^+$: 197.1172, found: 197.1175; **$[\alpha]_D^{20}$** = +58.2 (c 1.0, CHCl$_3$); **R$_f$** = 0.24 (5% EtOAc/Hex).

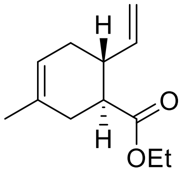

ethyl (1*S*,6*R*)-3-methyl-6-vinyl-cyclohex-3-ene-1-carboxylate (2.45).

To a suspension of methyltriphenylphosphonium bromide (2.01 g, 5.61 mmol, 1.1 eq) in THF (17 mL) at 0 °C was added LHMDS (1M in THF, 5.35 mL, 5.35 mmol, 1.05 eq) dropwise. The reaction was stirred for 40 minutes at this temperature, then cooled to -78 °C and a solution of ethyl (1*S*,6*S*)-6-formyl-3-methyl-cyclohex-3-ene-1-carboxylate (1 g, 5.10 mmol, 1 eq) was added slowly. The cooling bath was removed and the reaction was stirred for 10 minutes at this temperature before a solution of saturated NH_4Cl (30 mL) and ether (30 mL) were added. The layers were separated and the aqueous was extracted with ether (3x30 mL), then the organics were pooled, dried over magnesium sulfate, filtered, and concentrated *in vacuo*. Crude product was purified by column chromatography (EtOAc/Hex, 0-20%) to yield ethyl (1*S*,6*R*)-3-methyl-6-vinyl-cyclohex-3-ene-1-carboxylate (751 mg, 3.87 mmol, 75%) as a clear oil in >20:1 d.r. **^{1}H-NMR (400 MHz, $CDCl_3$)** δ 5.75-5.66 (m, 1H), 5.38 (m, 1H), 5.06 (dd, *J* = 17.1, 1.5 Hz, 1H), 4.97 (dd, *J* = 10.2, 1.7 Hz, 1H), 4.11 (qd, *J* = 7.1, 1.4 Hz, 2H), 2.49-2.41 (m, 2H), 2.32-2.26 (m, 1H), 2.15-2.09 (m, 2H, 1.95-1.87 (m, 1H), 1.67 (bs, 3H), 1.24 (t, *J* = 7.2 Hz, 3H) ppm; **^{13}C-NMR (100 MHz, $CDCl_3$)** δ 175.4, 140.8, 132.1, 119.8, 115.2, 60.2, 45.9, 40.9, 32.8, 31.2, 23.3, 14.5; **ESI-HRMS:** m/z calc for $C_{12}H_{18}O_2$ $[M+H]^+$: 195.1380, found: 195.1381; **$[\alpha]_D^{20}$** = +53.6 (c 0.65, $CHCl_3$); **R_f** = 0.48 (Hex:EtOAc 20:1).

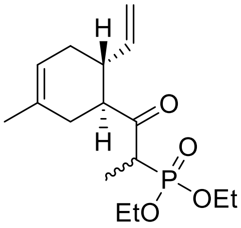

2-diethoxyphosphoryl-1-[(1*S*,6*R*)-3-methyl-6-vinyl-cyclohex-3-en-1-yl]propan-1-one (2.46).

To a solution of diethyl ethylphosphonate (1.28 g, 7.72 mmol, 3 eq) in THF (12.9 mL) at -78 °C was added *n*-BuLi (1.77M in Hex, 3.68 mL, 7.46 mmol) dropwise. The reaction was stirred for 1 hour at this temperature, then ethyl (1*S*,6*R*)-3-methyl-6-vinyl-cyclohex-3-ene-1-carboxylate (500 mg, 2.57 mmol, 1 eq) in THF

(3.2 mL) was added slowly and the reaction was stirred an additional 1.5 hours at the same temperature. The reaction was quenched by addition of saturated NH_4Cl (30 mL), then allowed to warm to room temperature and the mixture was extracted with ether (3x60 mL). The organics were dried over magnesium sulfate, filtered, and then concentrated *in vacuo* and crude product was purified using column chromatography (0-50% EtOAc/Hex) to yield 2-diethoxyphosphoryl-1-[(1*S*,6*R*)-3-methyl-6-vinyl-cyclohex-3-en-1-yl]propan-1-one (740 mg , 2.35 mmol, 91% yield) as a clear oil as a ~3:1 mixture of methyl diastereomers.

Analytical data are given for the mixture of diastereomers (signals are described as major (mj) and minor (mn) where it can be determined, otherwise given as a mix (mix)). **^{1}H-NMR (400 MHz, $CDCl_3$):** 5.64 (m, 1.36H, mix), 5.33 (m, 0.33H, mn), 5.27 (m, 1H, mj)**,** 4.99 (d, *J* = 17.2 Hz, 0.35H, mn), 4.93 (d, *J* = 17.1 Hz, 1H, mj), 4.88 (d, *J* = 10.2 Hz, 1.37H, mix), 4.05 (sep, *J* = 7.2 Hz, 5.7H, mix), 3.25 (qd, *J* = 26.0, 7.1 Hz, 0.40H, mn), 3.18 (qd, *J* = 26.5, 6.9 Hz, 1H, mj), 2.99 (td, *J* = 19.9, 5.5 Hz, 1.23H, mix), 2.53-2.43 (m, 0.32H, mn), 2.33-2.22 (m, 1.24H, mix), 2.22-2.14 (m, 1H, mj), 2.14-1.82 (m, 4.94H, mix), 1.59 (bs, 3.85H, mix), 1.26 (q, *J* = 7.3, 9H, mix), 1.17 (dd, *J* = 17.5, 7.0 Hz, 3.44H, mix), 0.85 (t, *J* = 7.2 Hz, 0.22H, mn) ppm; **^{13}C-NMR (100 MHz, $CDCl_3$)** δ 209.9 (d, *J* = 3.9 Hz, mj), 208.5 (d, *J* = 4.0 Hz, mn), 145.5 (mn), 141.1 (mn), 104.4 (mj), 132.8 (mj), 131.5 (mn), 120.5 (mn), 118.9 (mj), 115.9 (mj), 115.0 (mn), 62.7 (d, *J* = 6.8 Hz, mj), 62.6 (d, *J* = 6.9 Hz, mn), 62.5 (d, *J* = 6.8 Hz, mj), 62.4 (d, *J* = 6.8 Hz, mn), 53.3 (mj), 51.8 (mn), 49.7 (mj), 48.4 (mj), 46.6 (mn), 45.3 (mn), 43.1 (mj), 39.0 (mn), 33.3 (mn), 32.2 (mj), 31.8 (mj), 30.8 (mn), 23.3 (mj), 23.3 (mn), 16.5 (d, *J* = 5.3 Hz, mj), 16.4 (d, *J* = 5.8 Hz, mj), 11.5

(d, *J* = 6.5 Hz, mn), 9.8 (d, *J* = 6.1 Hz, mj) ppm; **ESI-HRMS:** m/z calc for $C_{16}H_{27}O_4P$ [M+H]$^+$: 315.1720, found: 315.1720; **R*f*** = 0.27 (Hex:EtOAc 2:1).

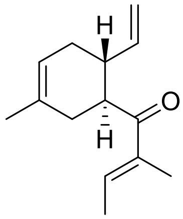

(E)-2-methyl-1-[(1*S*,6*R*)-3-methyl-6-vinyl-cyclohex-3-en-1-yl]but-2-en-1-one (2.47).

To a solution of 2-diethoxyphosphoryl-1-[(1*S*,6*R*)-3-methyl-6-vinyl-cyclohex-3-en-1-yl]propan-1-one (1.2 g, 3.84 mmol, 1.2 eq) in THF (16 mL) at 0 °C was added barium hydroxide octahydrate (1.01 g, 3.2 mmol, 1 eq) and acetaldehyde (180 µL, 3.2 mmol, 1 eq) at 0 °C. The reaction was warmed to room temperature overnight, then diluted with ether (60 mL) and filtered. The organics were removed *in vacuo*, then crude product was purified using column chromatography (0-60% EtOAc/Hex, high gradient used to recover excess starting material) to yield (E)-2-methyl-1-[(1*S*,6*R*)-3-methyl-6-vinyl-cyclohex-3-en-1-yl]but-2-en-1-one (528 mg, 2.58 mmol, 81% yield) as a clear oil. Olefin geometry was confirmed by 1D nOE analysis. **^{1}H-NMR (400 MHz, $CDCl_3$)** *δ* 6.70 (q, *J* = 6.4 Hz, 1H), 5.55 (m, 1H), 5.35 (m, 1H), 4.92 (d, *J* = 17.1 Hz, 1H), 4.83 (dd, *J* = 10.9, 1.0 Hz, 1H), 3.27 (td, *J* = 10.7, 5.3 Hz, 1H), 2.50-2.41 (m, 1H), 2.17-2.07 (m, 2H), 1.95-1.87 (m, 2H), 1.83 (d, *J* = 6.9 Hz, 3H), 1.72 (s, 3H), 1.62 (s, 3H) ppm; **^{13}C-NMR (100 MHz, $CDCl_3$)** *δ* 205.2, 141.0, 139.4, 136.9, 132.8, 119.8, 114.8, 44.9, 40.8, 34.5, 31.4, 23.3, 14.9, 11.2 ppm; **ESI-HRMS:** m/z calc for $C_{14}H_{20}O$ [M+H]$^+$: 205.1587, found: 205.1587; **$[\alpha]_D^{20}$**

= +63.8 (c 1.14, $CHCl_3$); **R_f** = 0.348 (Hex:EtOAc 50:1);

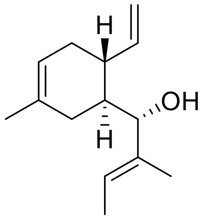

(E,1*S*)-2-methyl-1-[(1*S*,6*R*)-3-methyl-6-vinyl-cyclohex-3-en-1-yl]but-2-en-1-ol (2.48).

To a solution of (E)-2-methyl-1-[(1*S*,6*R*)-3-methyl-6-vinyl-cyclohex-3-en-1-yl]but-2-en-1-one (528 mg, 2.58 mmol, 1 eq) in Toluene (10.6 mL) at -78 ºC was added DIBAL (1M in toluene, 3.51 mL, 3.51 mmol, 1.34 eq) dropwise, turning the reaction yellow. The mixture was stirred for 5-15 minutes (monitored by TLC), then quenched by addition of methanol (3.5 mL) and saturated Rochelle's salt (20 mL), then allowed to warm to room temperature and diluted further with Rochelle's salt (75 mL) and ether (75 mL). The mixture was stirred vigorously at room temperature for 2 hours, forming two distinct layers, then the organics were separated and the aqueous was extracted with ether (3x50mL). The organics were pooled, dried over magnesium sulfate, filtered, and concentrated *in vacuo*, then crude product was purified using column chromatography (0-20% EtOAc/Hex) to yield (E,1*S*)-2-methyl-1-[(1*S*,6*R*)-3-methyl-6-vinyl-cyclohex-3-en-1-yl]but-2-en-1-ol (424 mg, 2.06 mmol, 80% yield) as a clear oil. **^{1}H-NMR (400 MHz, $CDCl_3$)** δ 5.95 (ddd, J = 17.5, 10.1, 8.0 Hz, 1H), 5.39 (q, J = 6.44 Hz, 1H), 5.32 (m, 1H), 5.11 (d, J = 17.2 Hz, 1H), 4.99 (dd, J = 10.4, 0.8 Hz, 1H), 3.87 (d, J = 8.8 Hz, 1H), 2.43 (p, J

= 7.3 Hz, 1H), 2.15 (m, 1H), 2.01-1.89 (m, 2H), 1.82-1.72 (m, 2H), 1.63-1.55 (m, 9H), 1.53-1.43 (m, 1H) ppm; **^{13}C-NMR (100 MHz, $CDCl_3$)** δ 144.1, 136.7, 132.6, 122.9, 119.3, 114.0, 80.8, 41.2, 39.9, 30.7, 23.8, 13.2, 10.7 ppm; **ESI-HRMS:** m/z calc for $C_{14}H_{21}$ $[M+H]^+[-H_2O]$: 189.1638, found: 189.1640; **$[\alpha]_D^{20}$** = +24.2 (c 1.21, $CHCl_3$); **R_f** = 0.296 (20:1 Hex:EtOAc);

Mosher ester analysis was performed as described by Hoye, *et al.*[173] Briefly, to a solution of (E,1*S*)-2-methyl-1-[(1*S*,6*R*)-3-methyl-6-vinyl-cyclohex-3-en-1-yl]but-2-en-1-ol (10 mg, 0.05 mmol) and (*R*)-(-)-alpha-methoxy-alpha-trifluoromethyl acetic acid {(*R*)-Mosher's acid} (35.18 mg, 0.15 mmol, 3.1 eq) in DCM (0.75 mL) at 23 °C was added 1,3-dicyclohexylcarbodiimide (31.0 mg, 0.15 mmol, 3.1 eq) and 4-dimethylaminopyridine (18.4 mg, 0.15 mmol, 3.1 eq). The reaction was stirred overnight at room temperature, then diluted with DCM (1 mL) and filtered through a plug of celite, washing with DCM (3x2 mL). The solvent was removed *in vacuo*, then crude product was purified using silica gel chromatography (0-10% EtOAc/Hex) to yield [(E,1*S*)-2-methyl-1-[(1*S*,6*R*)-3-methyl-6-vinyl-cyclohex-3-en-1-yl]but-2-enyl] (2*R*)-3,3,3-trifluoro-2-methoxy-2-phenyl-propanoate (20 mg, 0.047 mmol, 98% yield) as a clear oil. **^{1}H-NMR (400 MHz, $CDCl_3$)** δ 7.53-7.45 (m, 2H), 7.40-7.36 (m, 3H), 5.80 (ddd, *J* = 17.3, 10.1, 7.6 Hz, 1H), 5.58 (qd, *J* = 6.8, 1.1 Hz, 1H), 5.34 (m, 1H), 5.30 (d, *J* = 9.9 Hz, 1H), 4.99 (td, *J* = 17.1, 1.4 Hz, 1H), 4.94 (m, 1H), 3.54 (d, *J* = 1.0 Hz, 3H), 3.20 (m, 1H), 2.38-2.32 (m, 1H), 2.25-2.16 (m, 1H), 2.04-1.99 (m, 1H), 1.99-1.89 (m, 4H), 1.77-1.70 (m, 2H), 1.62-1.59 (m, 3H), 1.59-1.57 (m, 3H), 1.37 (s, 3H), 1.36-1.17 (m, 5H)

The *S*-Mosher ester product was synthesized in an analogous fashion using (*S*)-(-)-alpha-methoxy-alpha-trifluoromethyl acetic acid (16 mg, 0.038 mmol, 78%). **^{1}H-NMR (400 MHz, CDCl$_3$)** *δ* 7.52-7.47 (m, 2H), 7.42-7.35 (m, 3H), 5.75 (ddd, *J* = 17.2, 10.4, 7.5 Hz, 1H), 5.65 (qd, *J* = 6.7, 1.1 Hz, 1H), 5.37-5.31 (m, 2H), 4.89-4.87 (m, 1H), 4.87-4.82 (m, 1H), 3.53 (d, *J* = 1.1 Hz, 3H), 2.22-2.12 (m, 1H), 2.12-2.06 (m, 1H), 2.01-1.91 (m, 2H), 1.89-1.83 (m, 1H), 1.65 (dd, *J* = 6.8, 0.8 Hz, 3H), 1.57 (s, 3H), 1.56 (d, *J* = 9.4 Hz, 3H).

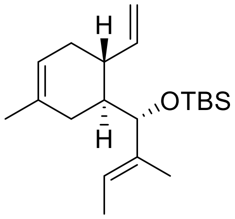

2-[(1*R*,6*S*)-6-[(E,1*S*)-1-[*tert*-butyl(dimethyl)silyl]oxy-2-methyl-but-2-enyl]-4-methyl-cyclohex-3-en-1-yl]ethanol (2.49).

To a solution of (E,1*S*)-2-methyl-1-[(1*S*,6*R*)-3-methyl-6-vinyl-cyclohex-3-en-1-yl]but-2-en-1-ol (101 mg, 0.49 mmol, 1 eq) in DCM (2.45 mL) at -78 ºC was added 2,6-lutidine (0.29 mL, 2.45 mmol, 2 eq) and tert-butyldimethylsilyl trifluoromethylsulfonate (0.21 mL, 0.93 mmol, 1.5 eq). This was then warmed to 0ºC for 30 minutes, at which point TLC analysis confirmed formation of desired product. The reaction was quenched by addition of water (5 mL) and the aqueous was extracted with DCM (3x5 mL). The organics were pooled, passed through a phase separator, and concentrated *in vacuo*, then crude product was purified using column chromatography (100% Hex) to yield tert-butyl-dimethyl-[(E,1S)-2-methyl-1-[(1*S*,6*R*)-3-methyl-6-vinyl-cyclohex-3-en-1-yl]but-2-enoxy]silane (141 mg,

0.44 mmol, 90% yield) as a clear oil. **^{1}H-NMR (400 MHz, CDCl$_3$)** δ 5.89 (ddd, *J* = 17.3, 10.2, 7.2 Hz, 1H), 5.34-5.26 (m, 2H), 5.02 (d, *J* = 17.3 Hz, 1H), 4.95 (d, *J* = 10.3 Hz, 1H), 3.86 (d, *J* = 9.6 Hz, 1H), 2.73-2.66 (m, 1H), 2.24-2.14 (m, 1H), 1.96-1.85 (m, 2H), 1.79-1.70 (m, 1H), 1.58 (d, *J* = 6.7 Hz, 3H), 1.56-1.51 (m, 6H), 0.87 (s, 10H), 0.01 (s, 3H), -0.06 (s, 3H) ppm; **^{13}C-NMR (100 MHz, CDCl$_3$)** δ 143.7, 137.7, 132.3, 122.2, 118.9, 112.9, 79.6, 41.2, 35.4, 28.0, 26.3, 26.1, 25.9, 24.2, 18.4, 13.2, 10.8, -2.7, -4.3, -5.1 ppm; **ESI-HRMS:** No peaks corresponding to desired material were observed by HRMS. **$[\alpha]_D^{20}$** = -14.50 (c 1.03, CHCl$_3$); **R$_f$** = 0.826 (100% Hexanes).

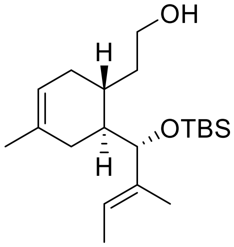

2-[(1*R*,6*S*)-6-[(E,1*S*)-1-[*tert*-butyl(dimethyl)silyl]oxy-2-methyl-but-2-enyl]-4-methyl-cyclohex-3-en-1-yl]ethanol (2.50).

To a solution of tert-butyl-dimethyl-[(E,1*S*)-2-methyl-1-[(1*S*,6*R*)-3-methyl-6-vinyl-cyclohex-3-en-1-yl]but-2-enoxy]silane (272 mg, 0.85 mmol) in THF (4.24 mL) at 0 °C was added 9-BBN solution (0.5M in THF, 3.39 mL, 1.7 mmol) dropwise. The reaction was warmed to room temperature and stirred for 30 minutes, at which point TLC analysis indicated consumption of starting materials. The reaction was again cooled to 0 °C and a premixed solution of hydrogen peroxide (30 wt%, 1.11 mL, 10.87 mmol) and aqueous sodium hydroxide (2M, 1.24 mL, 2.47 mmol) was added slowly. The reaction was warmed to room temperature and stirred for 1.5

hours, then diluted with brine (10 mL) and extracted with ether (3x15 mL). The organics were pooled, dried over magnesium sulfate, filtered, and concentrated *in vacuo*, then crude product was purified using column chromatography (0-20% EtOAc/Hex) to yield 2-[(1*R*,6*S*)-6-[(E,1*S*)-1-[tert-butyl(dimethyl)silyl]oxy-2-methyl-but-2-enyl]-4-methyl-cyclohex-3-en-1-yl]ethanol (234 mg, 0.69 mmol, 81% yield) as a clear oil. **^{1}H-NMR (400 MHz, CDCl$_3$)** *δ* 5.30-5.23 (m, 2H), 3.80 (d, *J* = 10.0 Hz, 1H), 3.72-3.63 (m, 2H), 2.21-2.12 (m, 2H), 1.94-1.85 (m, 1H), 1.76-1.65 (m, 2H), 1.65-1.61 (m, 1H), 1.59-1.52 (m, 9H), 1.50 (s, 3H), 0.85 (s, 9H), 0.00 (s, 3H), -0.07 (s, 3H) ppm; **^{13}C-NMR (100 MHz, CDCl$_3$)** *δ* 137.8, 131.6, 122.3, 118.9, 79.8, 61.8, 39.9, 37.0, 27.4, 26.5, 24.1, 18.4, 13.1, 10.5, -4.3, -5.1 ppm; **ESI-HRMS:** m/z calc for $C_{20}H_{38}O_2Si$ [M+Na]$^+$: 361.2533, found: 361.2539; **$[\alpha]_D^{20}$** = -13.60 (c 0.75, CHCl$_3$); **R$_f$** = 0.478 (15% Hexanes/EtOAc);

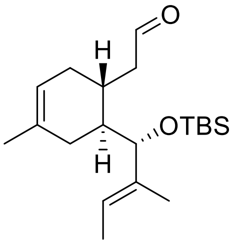

2-[(1*R*,6*S*)-6-[(E,1*S*)-1-[*tert*-butyl(dimethyl)silyl]oxy-2-methyl-but-2-enyl]-4-methyl-cyclohex-3-en-1-yl]acetaldehyde (2.16).

To a solution of 2-[(1*R*,6*S*)-6-[(E,1*S*)-1-[tert-butyl(dimethyl)silyl]oxy-2-methyl-but-2-enyl]-4-methyl-cyclohex-3-en-1-yl]ethanol (88 mg, 0.26 mmol, 1 eq) in DCM (1.73 mL) at 0 °C was added sodium bicarbonate (131 mg, 1.56 mmol, 6 eq) and Dess-Martin Periodinane (165 mg, 0.39 mmol, 1.5 eq). The reaction was warmed to room temperature and stirred for 1.5 hours, at which point TLC analysis indicated full consumption of starting materials and formation of a more non-polar spot. The reaction was diluted with water (2 mL) and extracted with EtOAc (3x4 mL) and the organics were passed through a phase separator and concentrated *in vacuo*. Crude product was purified using Teledyne ISCO Combi-Flash system (solid loading, 0-15% EtOAc/Hex) to yield 2-[(1*R*,6*S*)-6-[(E,1S)-1-[tert-butyl(dimethyl)silyl]oxy-2-methyl-but-2-enyl]-4-methyl-cyclohex-3-en-1-yl]acetaldehyde (64 mg, 0.19 mmol, 73% yield) as a clear oil.

^{1}H-NMR (400 MHz, CDCl$_3$) δ 9.50 (t, *J* = 2.0 Hz, 1H), 5.24-5.19 (m, 2H), 3.88 (d, *J* = 9.9 Hz, 1H), 2.85-2.77 (m, 1H), 2.33-2.24 (m, 1H), 2.10 (ddd, *J* = 16.3, 9.0, 2.2 Hz, 1H), 1.92 (ddd, *J* = 16.3, 5.4, 1.7 Hz, 1H), 1.77-1.59 (m, 4H), 1.53-1.49 (m, 6H), 1.45 (dd, *J* = 6.6, 0.9 Hz, 4H), 1.00 (s, 9H), 0.09 (s, 3H), 0.02 (s, 3H); **^{13}C-NMR (100 MHz, CDCl$_3$)** δ 200.9, 137.9, 131.5, 122.6, 118.9, 79.9, 48.3, 40.2, 27.5, 26.2, 25.0, 24.1, 18.5, 13.0, 10.5, -4.2, -5.0 ppm; **ESI-HRMS:** m/z calc for $C_{20}H_{36}O_2Si$ [M+Na]$^+$: 359.2377, found: 359.2380; **$[\alpha]_D^{20}$** = -21 (c 1.0, CHCl$_3$), lit: -31.5; **R$_f$** = 0.46 (5% EtOAc/Hex)

Analytical data are in accordance with the literature.

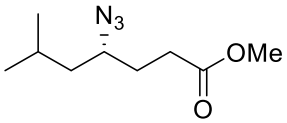

methyl (4*R*)-4-azido-6-methyl-heptanoate (2.51).

To a solution of (4*R*)-4-azido-6-methyl-heptanoic acid (383 mg, 2.07 mmol, 1 eq) in a mixture of DCM (5 mL) and Methanol (0.51 mL) at 0 ^oC was added (trimethylsilyl)diazomethane (2M in ether, 2.07 mL, 4.14 mmol, 2 eq) dropwise. The reaction was warmed to room temperature and stirred for 30 minutes, then concentrated *in vacuo* onto silica gel and crude product was purified using Teledyne ISCO Combi-Flash system (solid loading, 4G column, 0-20% EtOAc/Hex) to yield methyl (4*R*)-4-azido-6-methyl-heptanoate (369 mg,1.85mmol, 90% yield) as a clear oil. **^{1}H-NMR (400 MHz, CDCl$_3$)** *δ* 3.68 (s, 3H), 3.35 (sep, *J* = 4.8 Hz, 1H), 2.53-2.36 (m, 2H), 1.94-1.83 (m, 1H), 1.82-1.66 (m, 2H), 1.50 (ddd, *J* = 14.1, 8.6, 5.9 Hz, 1H), 1.30 (ddd, *J* = 13.8, 8.4, 5 Hz, 1H), 0.93 (dd, *J* = 6.6, 1.0 Hz, 6H); **^{13}C-NMR (100 MHz, CDCl$_3$)** *δ* 173.6, 60.3, 51.9, 43.5, 30.7, 30.0, 25.2, 23.0, 22.2; **ESI-HRMS:** m/z calc for $C_9H_{18}NO_2$ $[M+Na]^+$: 222.1213, found: 222.1212; **$[\alpha]_D^{20}$** = +16.7 (c 0.71, CHCl$_3$); **R*$_f$*** = 0.38 (20:1 Hex/EtOAc).

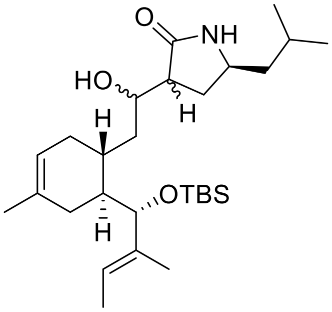

(5*S*)-3-[2-[(1*R*,6*S*)-6-[(E,1*S*)-1-[*tert*-butyl(dimethyl)silyl]oxy-2-methyl-but-2-enyl]-4-methyl-cyclohex-3-en-1-yl]-1-hydroxy-ethyl]-5-isobutyl-pyrrolidin-2-one (2.53).

To a solution of lithium bis(trimethylsilyl)amide (1M in THF, 121 µL, 0.65 mmol, 1.6 eq) in THF (4.18 mL) at -78 °C was added a solution of methyl (4R)-4-azido-6-methyl-heptanoate (121 mg, 0.61mmol, 1.5 eq) in THF (0.84 mL) dropwise. The resulting mixture was stirred for 1 hour at this temperature, then a solution of 2-[(1*R*,6*S*)-6-[(E,1*S*)-1-[tert-butyl(dimethyl)silyl]oxy-2-methyl-but-2-enyl]-4-methyl-cyclohex-3-en-1-yl]acetaldehyde (136 mg, 0.40 mmol, 1 eq) in THF (1.26 mL) was added dropwise and the reaction was stirred an additional 2 hours at this temperature, then quenched by addition of saturated ammonium chloride (5 mL). The reaction was allowed to warm to room temperature, then diluted with water (5mL) to dissolve remaining salts and extracted with EtOAc (3x15 mL). The organics were pooled, dried over magnesium sulfate, filtered, and concentrated *in vacuo*. Crude product was purified using Teledyne ISCO Combi-Flash system (solid loading, 4G column, 0-15% EtOAc/Hex) to yield 103 mg of an inseparable mixture of desired product and starting ester Claisen condensation product, along with 54 mg of desired starting material. **ESI-HRMS:** m/z calc for $C_{29}H_{53}N_3O_4Si$ $[M+Na]^+$: 558.3698, found: 558.3708; **R_f** = 0.49, 0.54 (10% EtOAc/Hex).

Glassware was not dried for this reaction. To a solution of crude methyl (4S)-4-azido-2-[2-[(1*R*,6*S*)-6-[(E,1*S*)-1-[tert-butyl(dimethyl)silyl]oxy-2-methyl-but-2-enyl]-4-methyl-cyclohex-3-en-1-yl]-1-hydroxy-ethyl]-6-methyl-heptanoate (32 mg, 0.06 mmol, 1 eq) in a mixture of THF (1.2 mL) and Water (0.40 mL) was added triphenylphosphine (47 mg, 0.18 mmol, 3 eq). The reaction was heated to 60 ^oC for 5 hours at which point full conversion to the desired product was observed. After cooling to room temperature, the remaining triphenylphosphine was oxidized by addition of 3% hydrogen peroxide (3 mL) and diluted with ether (3 mL). The layers were separated and the aqueous was extracted with ether (3x5 mL), then the organics were passed through a phase separator and concentrated *in vacuo*. Crude product was purified using Teledyne ISCO Combi-Flash system (solid loading, 4G column, 0-60% EtOAc/Hex). to yield (5*S*)-3-[2-[(1*R*,6*S*)-6-[(E,1*S*)-1-

[tert-butyl(dimethyl)silyl]oxy-2-methyl-but-2-enyl]-4-methyl-cyclohex-3-en-1-yl]-1-hydroxy-ethyl]-5-isobutyl-pyrrolidin-2-one (26 mg, 0.054 mmol, 43% yield over 2 steps, 70% brsm from the first reaction) as an oily solid. Characterization was performed on the most polar diastereomer. **^{1}H-NMR (400 MHz, CDCl$_3$)** δ 5.76 (s, 1H), 5.30-5.25 (m, 2H), 3.81 (d, *J* = 6.7 Hz, 1H), 3.70-3.63 (m, 1H), 2.57 (td, *J* = 5.7, 1.8 Hz, 1H), 2.44-2.36 (m, 1H), 2.25-2.18 (m, 2H), 1.98-1.93 (m, 1H), 1.91-1.83 (m, 1H), 1.74-1.70 (m, 2H), 1.63-1.61 (m, 1H), 1.60-1.57 (m, 6H), 1.52-1.50 (m, 3H), 1.50-1.47 (m, 2H), 1.43-1.39 (m, 1H), 1.39-1.34 (m, 1H), 1.32-1.27 (m, 2H), 0.92 (dd, *J* = 4.4, 0.9 Hz, 6H), 0.85 (s, 9H), 0.00 (s, 3H), -0.08 (s, 3H); **^{13}C-NMR (100 MHz, CDCl$_3$)** δ 178.5, 137.8, 131.5, 122.4, 118.9, 79.6, 67.8, 50.8; 46.4, 45.6, 39.2, 38.4, 27.2, 27.0, 26.6, 26.2, 26.1, 26.1, 25.5, 24.1, 23.2, 23.2, 22.4, 18.4, 13.2, 10.6, -4.3, -5.1; **ESI-HRMS:** m/z calc for $C_{22}H_{36}NO_2$ $[M+Na]^+$: 500.3530, found: 500.3542; **$[\alpha]_D^{20}$** = -14.7 (c 0.57, CHCl$_3$); **R_f** = 0.30, 0.40, 0.86, 0.90 (50% EtOAc/Hex).

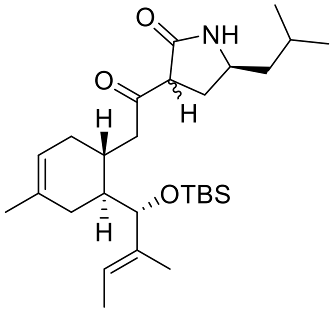

(5*S*)-3-[2-[(1*R*,6*S*)-6-[(E,1*S*)-1-[*tert*-butyl(dimethyl)silyl]oxy-2-methyl-but-2-enyl]-4-methyl-cyclohex-3-en-1-yl]acetyl]-5-isobutyl-pyrrolidin-2-one (2.54). Glassware was not dried for this reaction. To a solution of (5*S*)-3-[2-[(1*R*,6*S*)-6-[(E,1*S*)-1-[tert-butyl(dimethyl)silyl]oxy-2-methyl-but-2-enyl]-4-methyl-cyclohex-3-

en-1-yl]-1-hydroxy-ethyl]-5-isobutyl-pyrrolidin-2-one (40 mg, 0.08 mmol, 1 eq) in DMSO (0.80 mL) at room temperature was added 2-iodoxybenzoic acid (94 mg, 0.33 mmol, 4 eq) and the reaction was stirred for 1.25 hours. The reaction was quenched by addition of saturated sodium bicarbonate (5 mL), then diluted with EtOAc (5 mL). The layers were separated and the aqueous was extracted with EtOAc (3x5 mL) and the organics were passed through a phase separator. Crude product was purified using Teledyne ISCO Combi-Flash system (solid loading, 4G column, 0-100% EtOAc/Hex) to yield (5*S*)-3-[2-[(1*R*,6*S*)-6-[(E,1*S*)-1-[tert-butyl(dimethyl)silyl]oxy-2-methyl-but-2-enyl]-4-methyl-cyclohex-3-en-1-yl]acetyl]-5-isobutyl-pyrrolidin-2-one (21 mg, 0.044 mmol, 53% yield, 64% brsm) as a white solid. Due to the presence of keto-enol tautomers, the product was not further characterized. **R_f** = 0.32 (20% EtOAc/Hex).

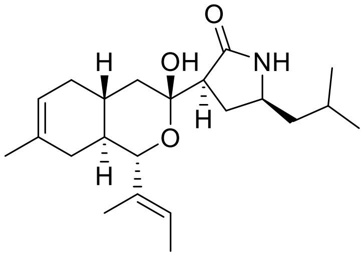

2.7

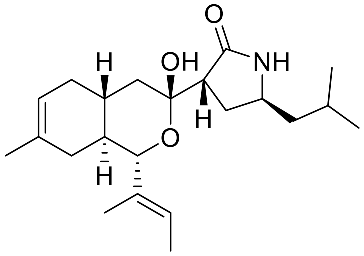

2.55

Pericoannosin A and Epi-Pericoannosin A (2.7, 2.55).

To a solution of (5*S*)-3-[2-[(1*R*,6*S*)-6-[(E,1*S*)-1-[tert-butyl(dimethyl)silyl]oxy-2-methyl-but-2-enyl]-4-methyl-cyclohex-3-en-1-yl]acetyl]-5-isobutyl-pyrrolidin-2-one (21 mg, 0.04 mmol) in THF (1.5 mL) at 23 °C in a 10 mL plastic conical tube was added triethylamine trihydrofluoride (1.5 mL, 9.2 mmol). The reaction was stirred for 60 hours at this temperature, then quenched by addition of saturated sodium bicarbonate (50 mL) and diluted with ether (35 mL). The layers were separated and the aqueous was extracted with ether (3x35 mL), then the organics were pooled, washed with brine (30mL), dried over magnesium sulfate, filtered, and concentrated *in vacuo*. Crude product was purified using Teledyne ISCO Combi-Flash system (solid loading, 4G column, 0-35% EtOAc/Hex) to yield **2.7** and **2.54** (11 mg,0.030 mmol, 69% yield) as a 3:1 mixture of diastereomers, with the desired being the major product.

For NMR analysis, “min” corresponds to minor peaks, “mix” corresponds to signals that cannot be distinguished from the two diastereomers.

^{1}H-NMR (600 MHz, $(CD_3)_2CO$) *δ* 7.16 (bs, 1H), 6.67 (d, *J* = 2.2, 1H), 5.58 (m, 0.31H, min), 5.43-5.38 (m, 1H), 5.38-5.36 (m, 0.34H, min), 5.36-5.33 (m, 1H), 4.03-4.00 (m, 0.16H, min), 3.99 (d, *J* = 10.1 Hz, 1H), 3.81 (t, *J* = 9.7 Hz, 0.32H, min), 3.70-3.63 (m, 1H), 3.61-3.57 (m, 0.30H, min), 2.90-2.84 (m, 0.33H, min), 2.56 (t, *J* = 9.8 Hz, 1H), 2.39-2.33 (m, 1H), 2.29-2.19 (m, 0.37H, min), 2.17-2.11 (m, 0.35H, min), 2.01-1.95 (m, 1H), 1.89-1.82 (m, 1H, mix), 1.82-1.79 (m, 1H, mix), 1.78-1.72 (m, 2H, mix), 1.72-1.66 (m, 1H), 1.67-1.64 (m, 3H), 1.62-1.59 (m, 6H, mix), 1.58-1.57 (m, 2H, mix), 1.54-1.47 (m, 2H), 1.39-1.23 (m, 4H, mix), 1.20 (td, *J* = 12.5, 1.8 Hz, 1H), 0.95-0.89 (m, 8H, mix); **^{13}C-NMR (150 MHz, $(CD_3)_2CO$)** *δ* 178.9, 171.9 (min), 159.4 (min), 159.3 (min), 135.4, 134.5 (min), 133.8, 133.3 (min), 124.8 (min), 124.8 (min), 122.9, 120.9, 120.9 (min), 82.1, 50.8, 50.7 (min), 49.7, 49.4 (min), 49.1 (min), 48.1 (min), 47.3, 41.0, 40.9 (min), 38.8, 38.5 (min), 34.3 (min), 34.2 (min), 33.4, 33.3 (min), 33.0, 32.7 (min), 32.7 (min), 31.9 (min), 31.5 (min), 31.5 (min), 30.9, 30.8, 30.3 (min), 25.6, 25.5 (min), 23.9, 23.8 (min), 23.2 (min), 23.2 (min), 23.2, 22.9, 22.8 (min), 13.2 (min), 13.1, 11.3, 10.9 (min), 10.9 (min). **ESI-HRMS:** m/z calc for $C_{20}H_{38}O_2Si$ $[M+Na]^+$: 384.2509, found: 361.2514. **R*f*** = 0.28 (33% EtOAc/Hex).

Analytical data of major peaks correspond with the literature data (**Figures 2.5, 2.6** and **Tables 2.2, 2.3)**.

NMR Comparison of Diastereomer Mixture with Authentic Sample

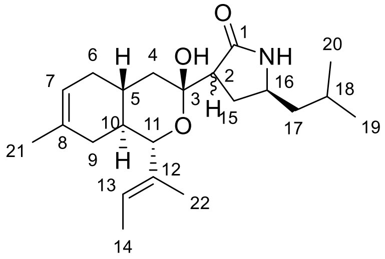

Table 2.2: Comparison of ^{1}H-NMR data.

No.	Natural Sample δ_H mult (*J* in Hz)	Synthetic Sample δ_H mult (*J* in Hz)
1		
2	2.56, t (10.2)	2.56, t (9.8)
3		
4	1.66, dd (12.6, 3.6)	1.72-1.66, mix
	1.20, dd (12.6, 11.2)	1.20, td (12.5, 1.8)
5	1.82, m	1.82-1.79, m
6	1.99, m	2.01-1.95, m
	1.61, nd	1.60-1.59, m
7	5.35, bs	5.36-5.33, m
8		
9	1.60, nd	1.60-1.59, m
	1.50, m	1.54-1.47, m
10	1.37, m	1.39-1.23, m
11	3.99, d (10.2)	3.99 (d, 10.1)
12		
13	5.41, m	5.43-5.38, m
14	1.58, nd	1.58-1.57, m
15	2.36, m	2.39-2.33, m
	1.80, m	1.82-1.79, m
16	3.67, m	3.70-3.63, m
17	1.51, m	1.54-1.47, m
	1.31, m	1.39-1.23, m
18	1.77, m	1.78-1.72, m
19	0.93, d (7.2)	0.95-0.89, m
20	0.92, d (7.2)	0.95-0.89, m
21	1.59, s	1.59-1.58, m
22	1.60, s	1.60-1.59, m
NH	nd	7.16, bs
OH	6.67, d, (2.4)	6.67, d, (2.2)

Dai, J. *et al*., authentic sample (600 MHz)

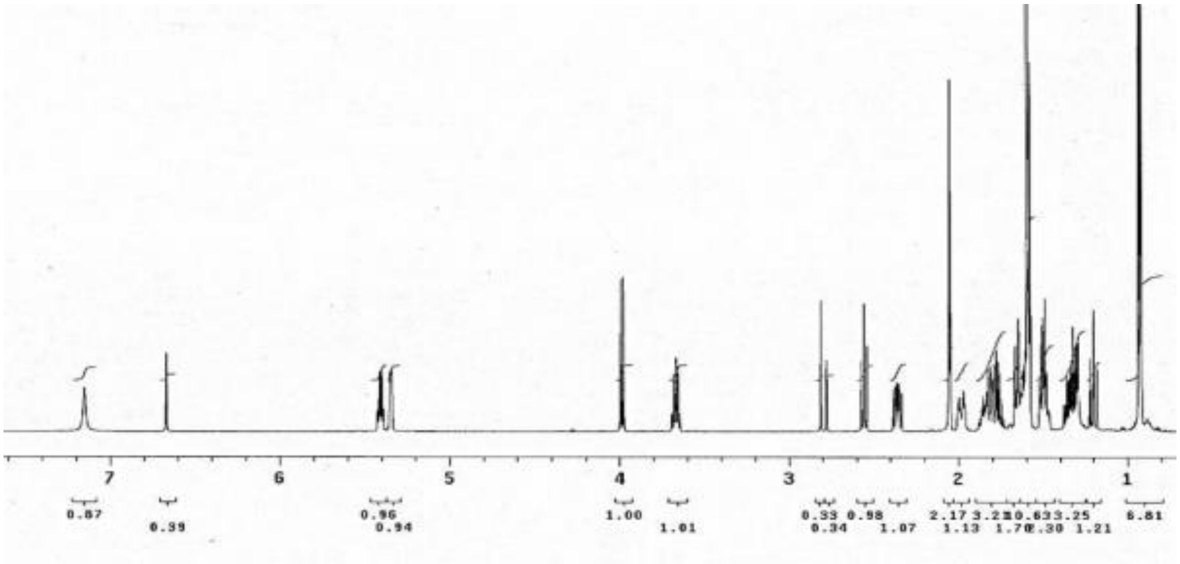

This work, synthetic sample (600 MHz)

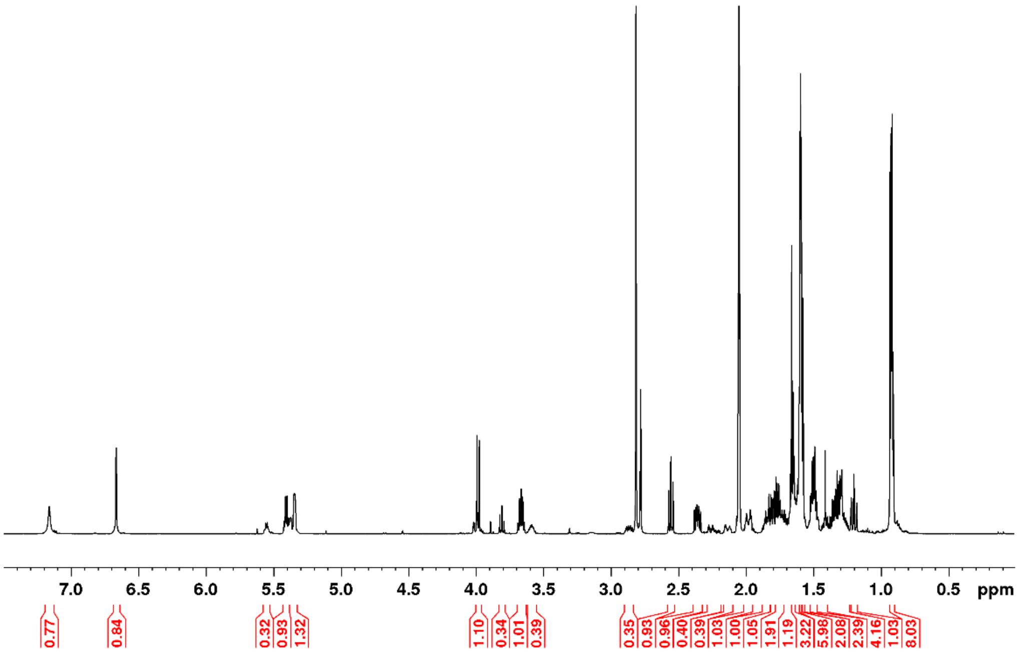

Figure 2.5: Comparison of ^{1}H-NMR data in acetone-d_6.

Table 2.3: Comparison of ^{13}C-NMR (using ONLY major peaks from synthetic work).

No.	Natural Sample	Synthetic Sample
1	178.8	178.9
2	49.7	49.7
3	97.5	97.5
4	40.9	41
5	30.9	30.9
6	33.4	33.4
7	120.9	120.9
8	133.7	133.8
9	33.0	33.0
10	38.8	38.8
11	82.1	82.1
12	135.4	135.4
13	122.9	122.9
14	13.0	13.1
15	30.8	30.8
16	50.8	50.8
17	47.3	47.3
18	25.6	25.6
19	22.9	22.9
20	23.1	23.2
21	23.9	23.9
22	11.2	11.3

Dai, J. *et al.*, authentic sample (150 MHz)

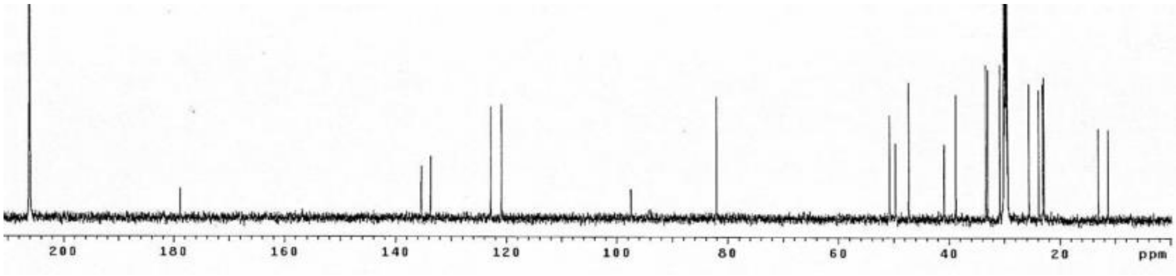

This work, synthetic sample (150 MHz)

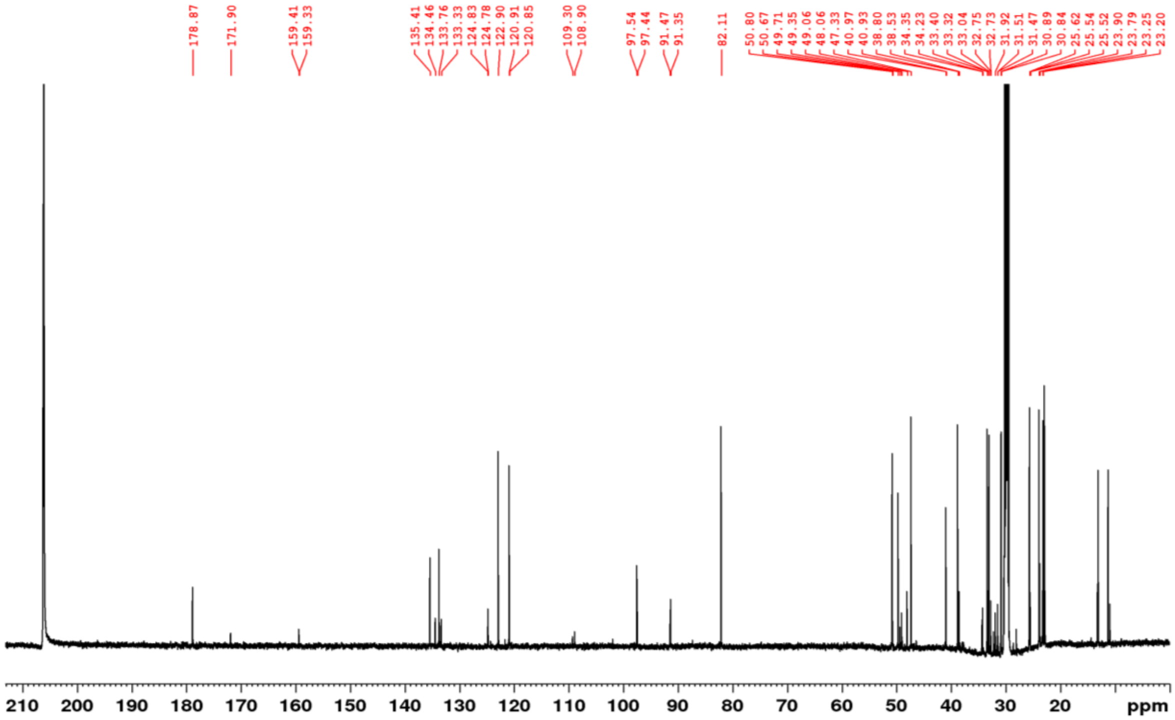

Figure 2.6: Comparison of ^{13}C-NMR data in acetone-d_6.

Appendix A

Relevant Spectra for Chapter 1

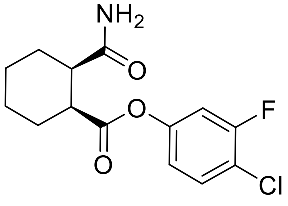
NH2
O
O
O
F
Cl

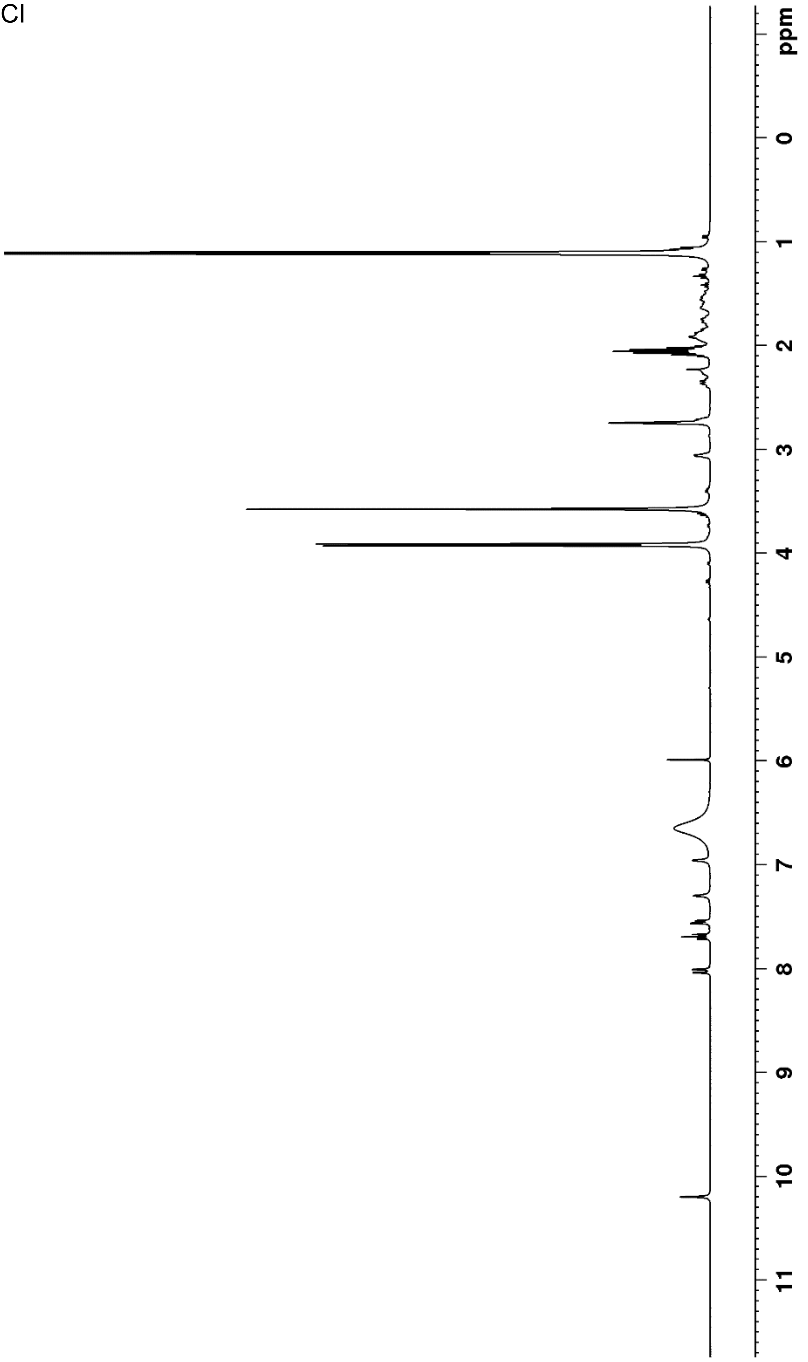
ppm
0
1
2
3
4
5
6
7
8
9
10
11

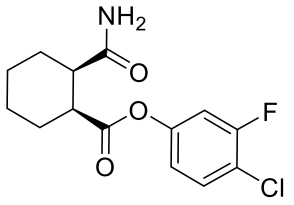
NH2
O
O
O
F
Cl

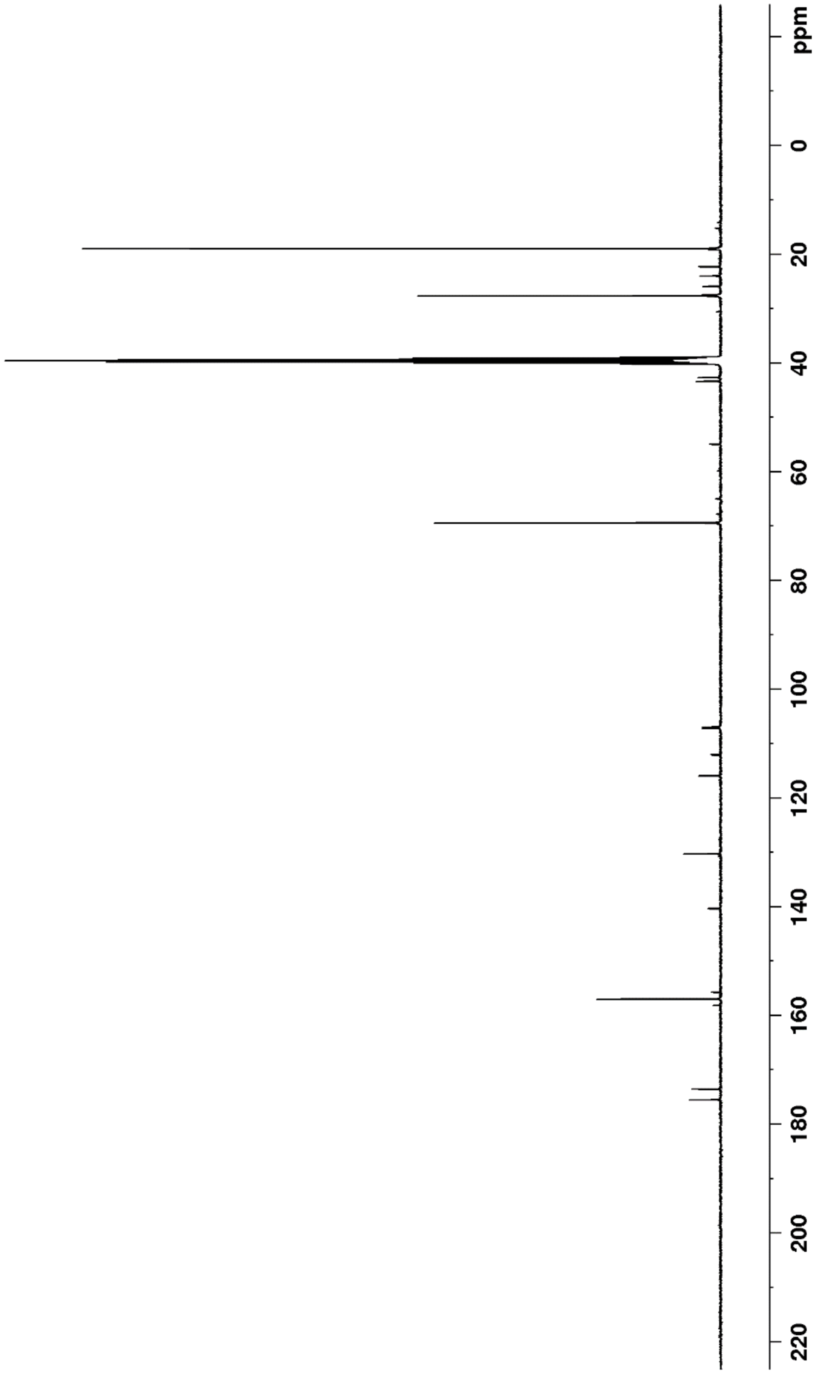
ppm
-20
0
20
40
60
80
100
120
140
160
180
200
220

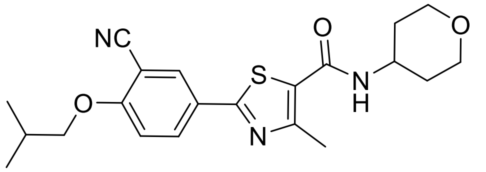
NC
O
S
N
O
N
H
O

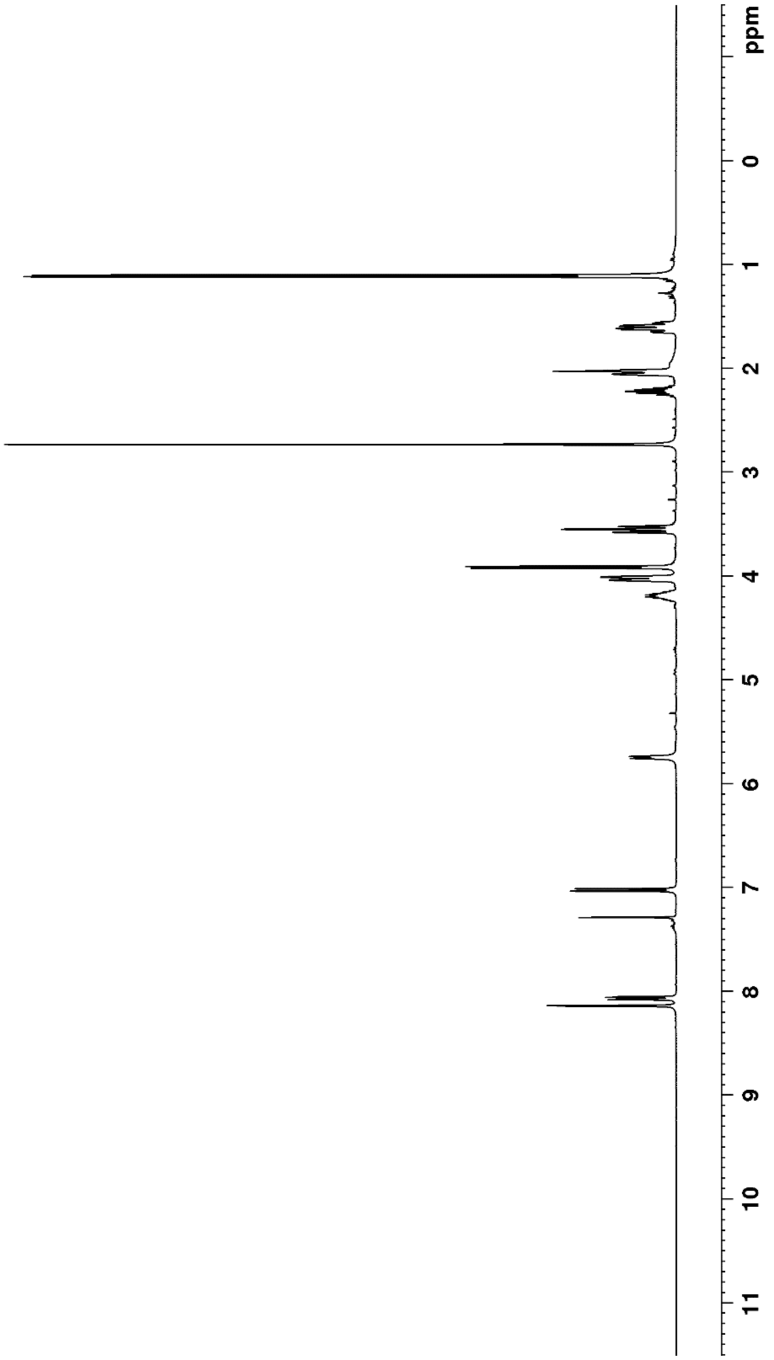
ppm
0
1
2
3
4
5
6
7
8
9
10
11

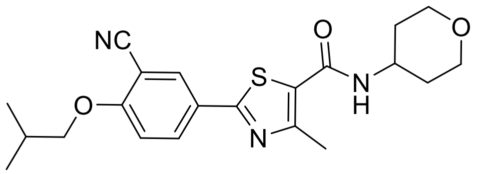
NC
O
S
N
O
N
H
O

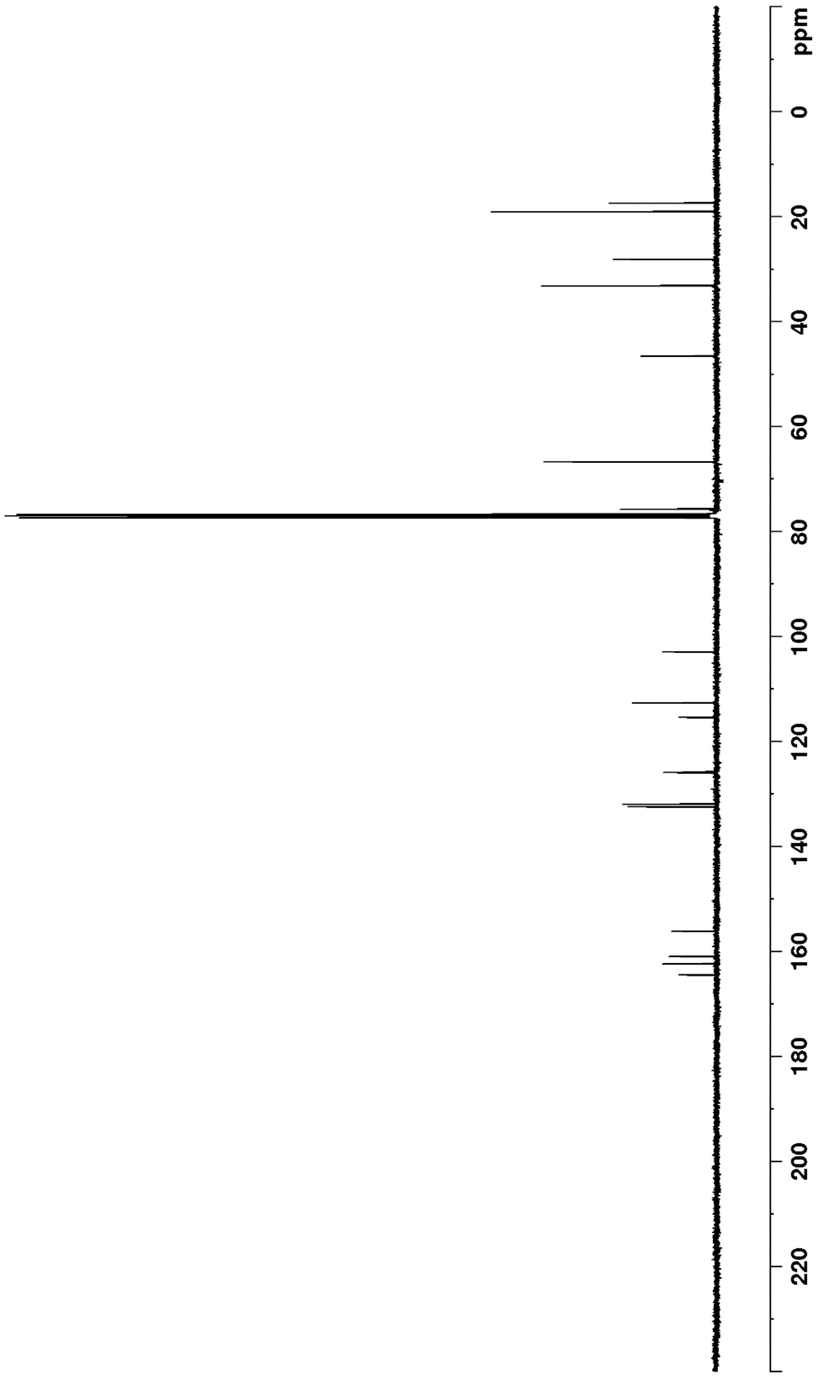
ppm
0
20
40
60
80
100
120
140
160
180
200
220

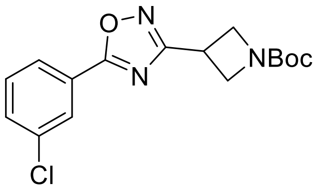
O
N
N
NBoc
Cl

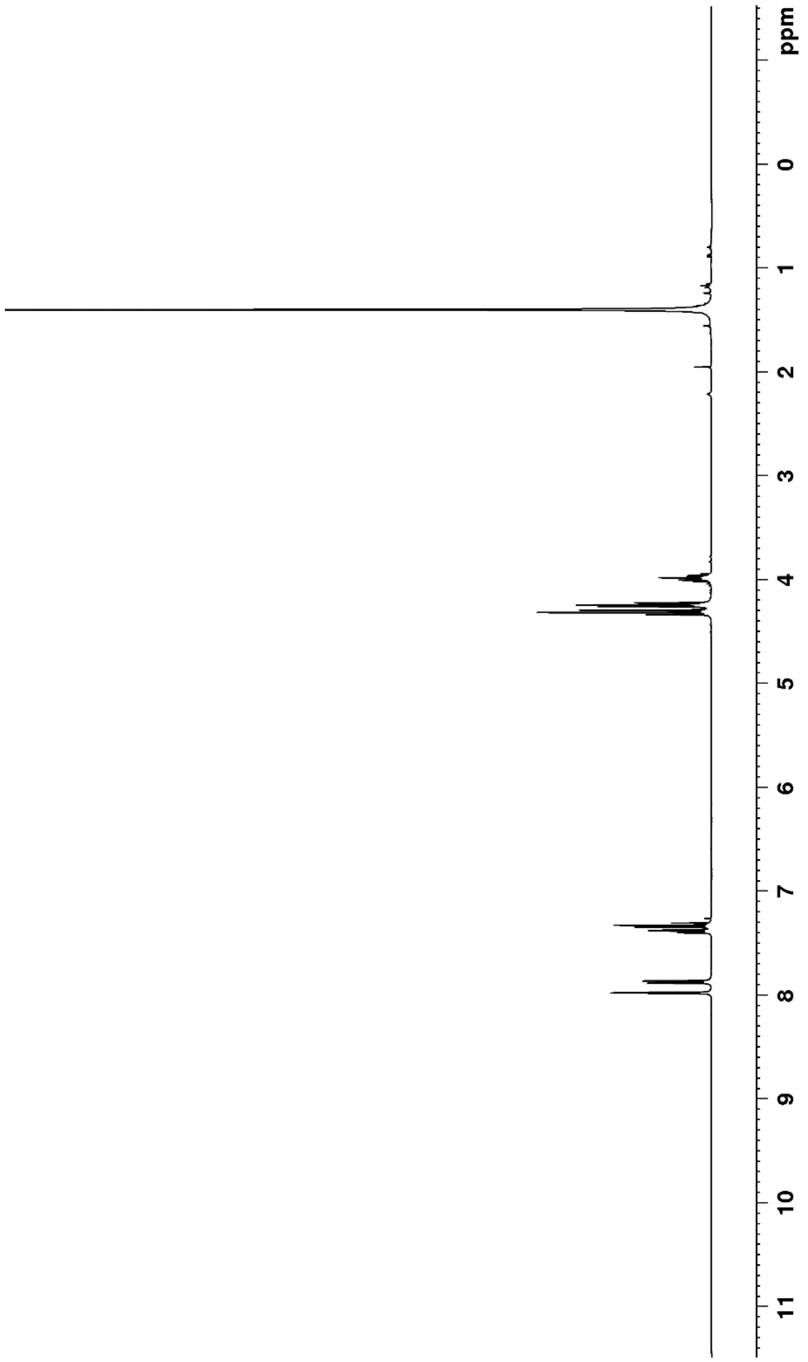
ppm
0
1
2
3
4
5
6
7
8
9
10
11

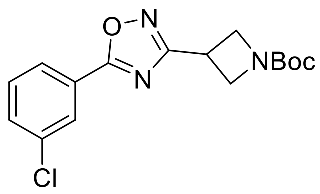
O
N
N
NBoc
Cl

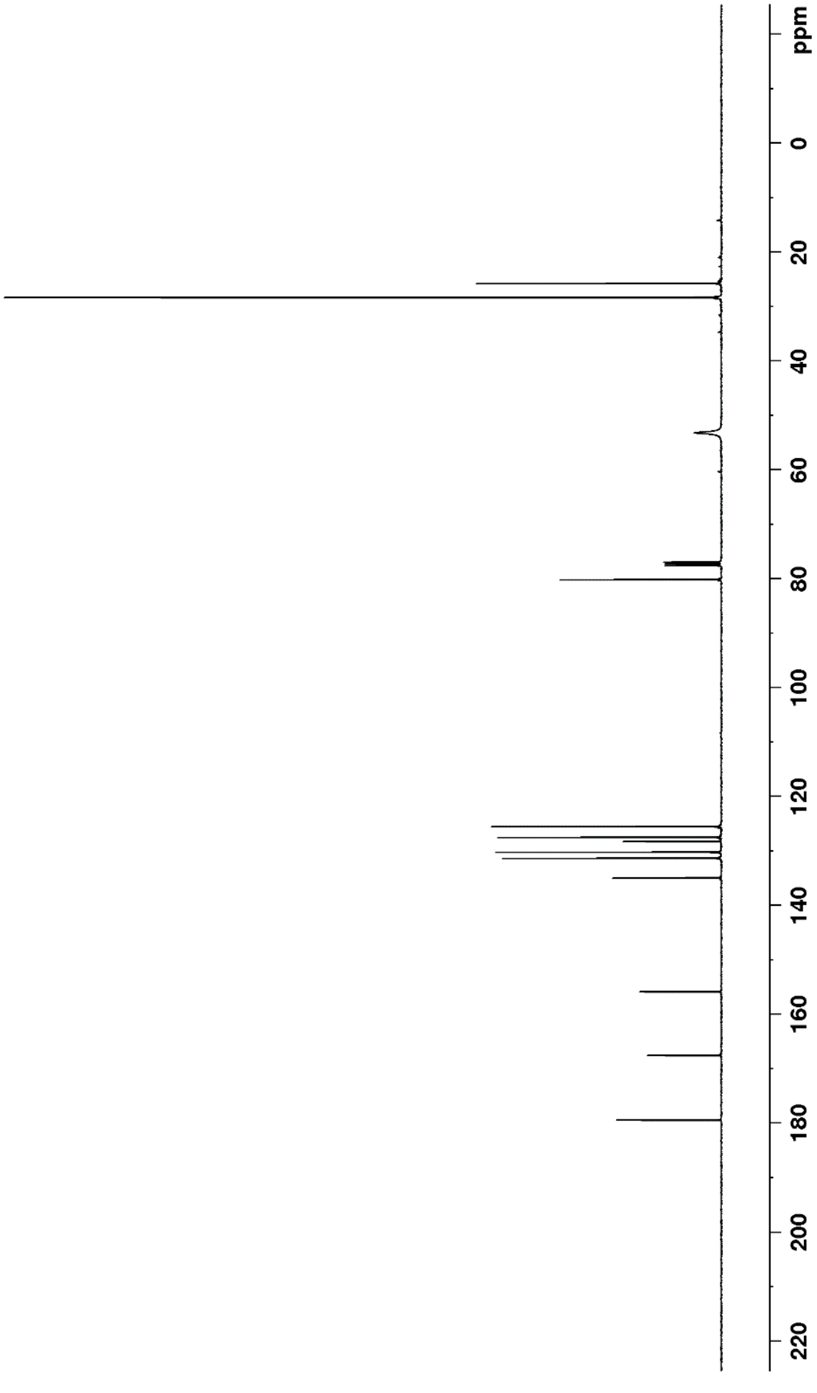
ppm
0
20
40
60
80
100
120
140
160
180
200
220

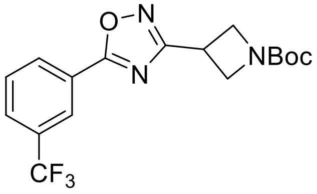

O
N
N
NBoc
CF3

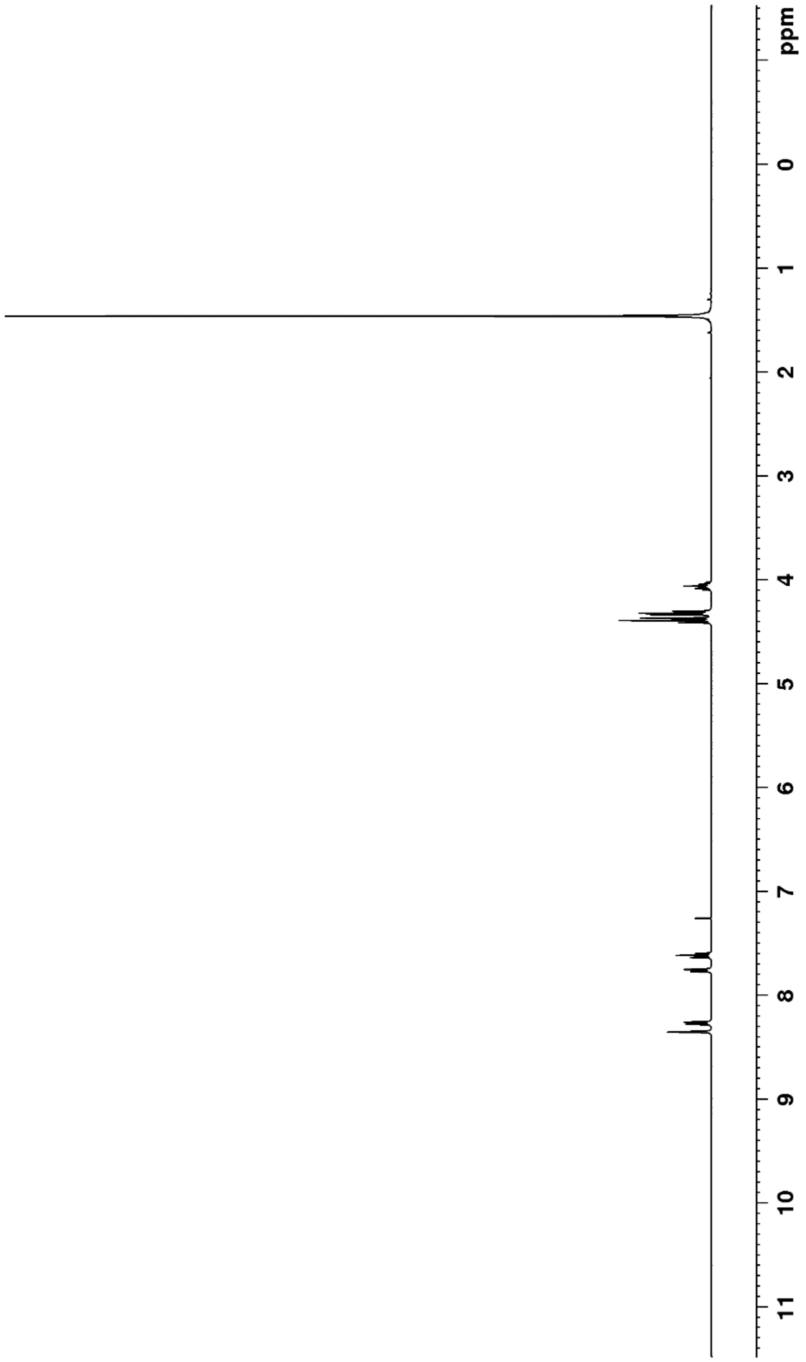

ppm
0
1
2
3
4
5
6
7
8
9
10
11

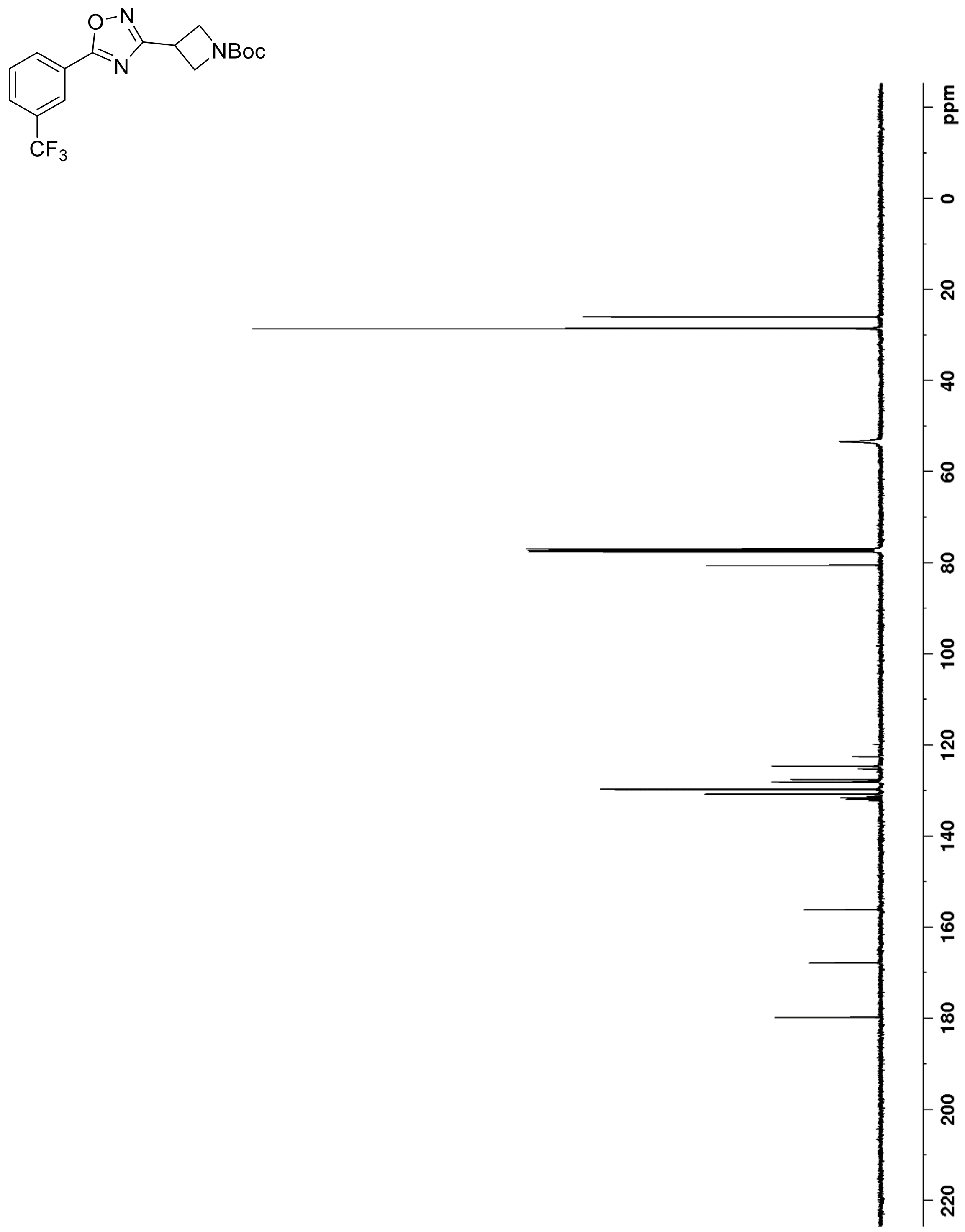
O
N
N
NBoc
CF3
ppm
-20
0
20
40
60
80
100
120
140
160
180
200
220

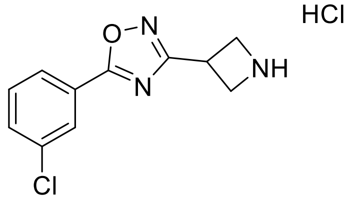
O
N
N
NH
HCl
Cl

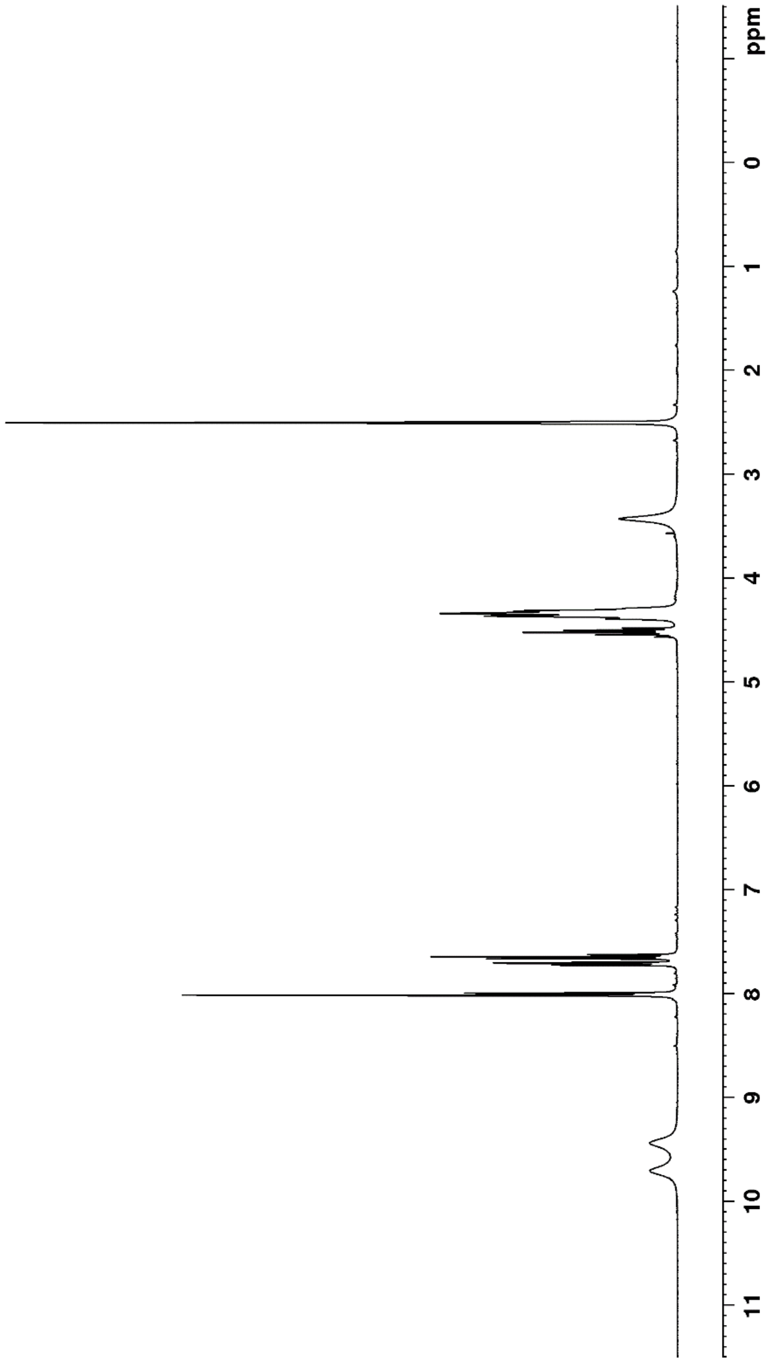
ppm
0
1
2
3
4
5
6
7
8
9
10
11

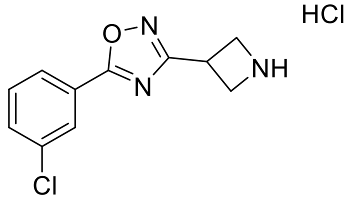
O
N
N
NH
HCl
Cl

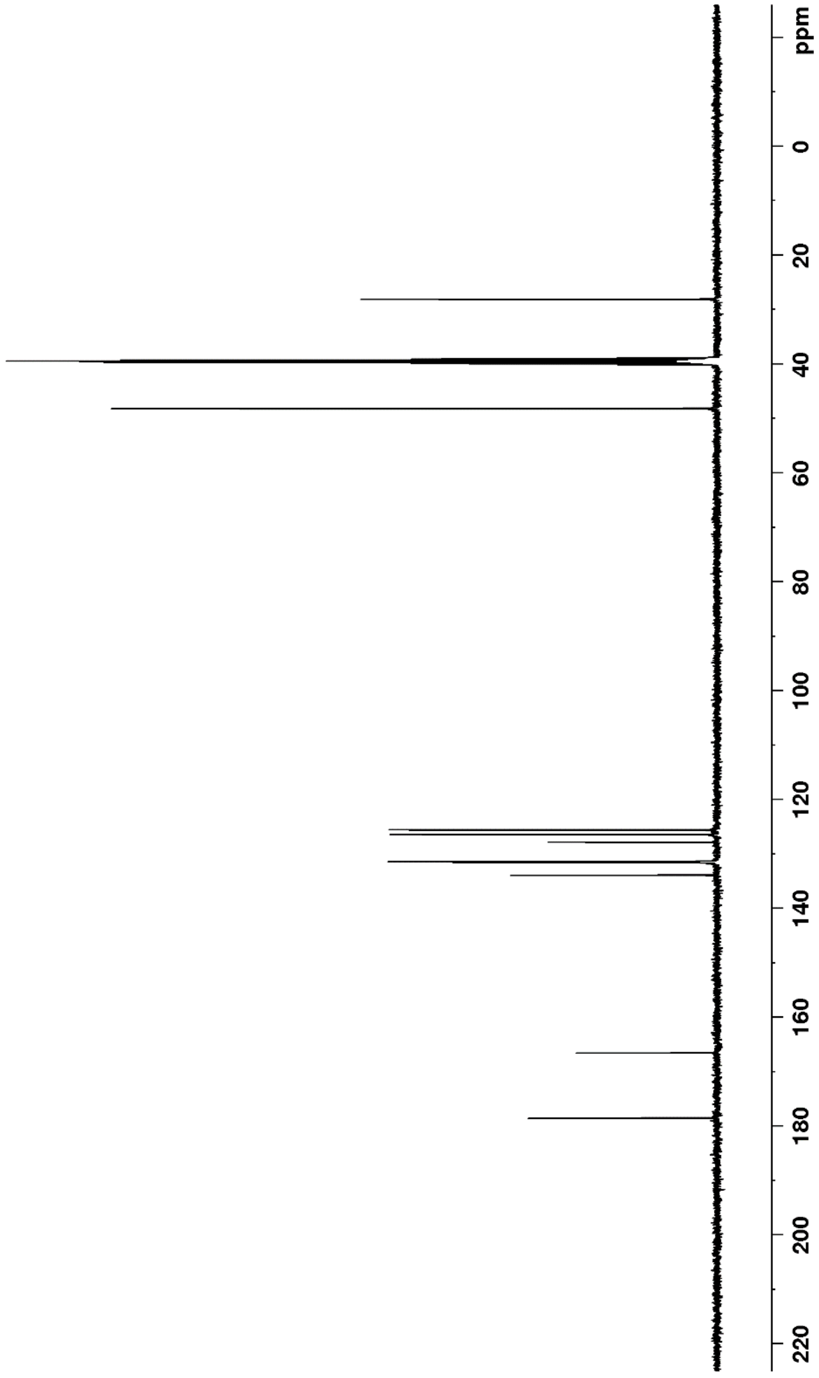
ppm
0
20
40
60
80
100
120
140
160
180
200
220

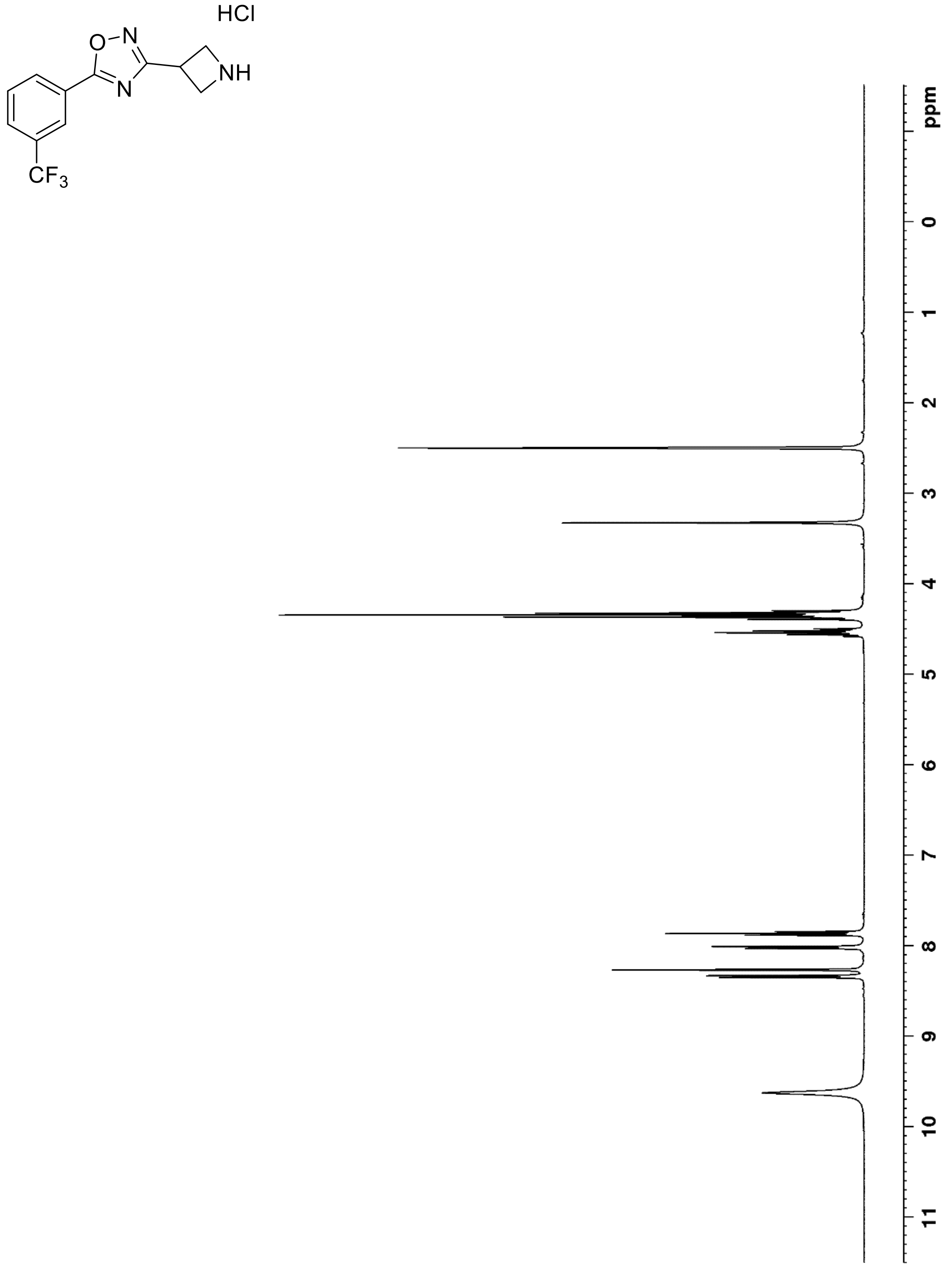
HCl
O
N
N
NH
CF_3
ppm
0
1
2
3
4
5
6
7
8
9
10
11

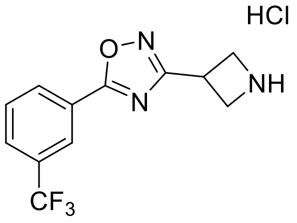
HCl
O
N
N
NH
CF3

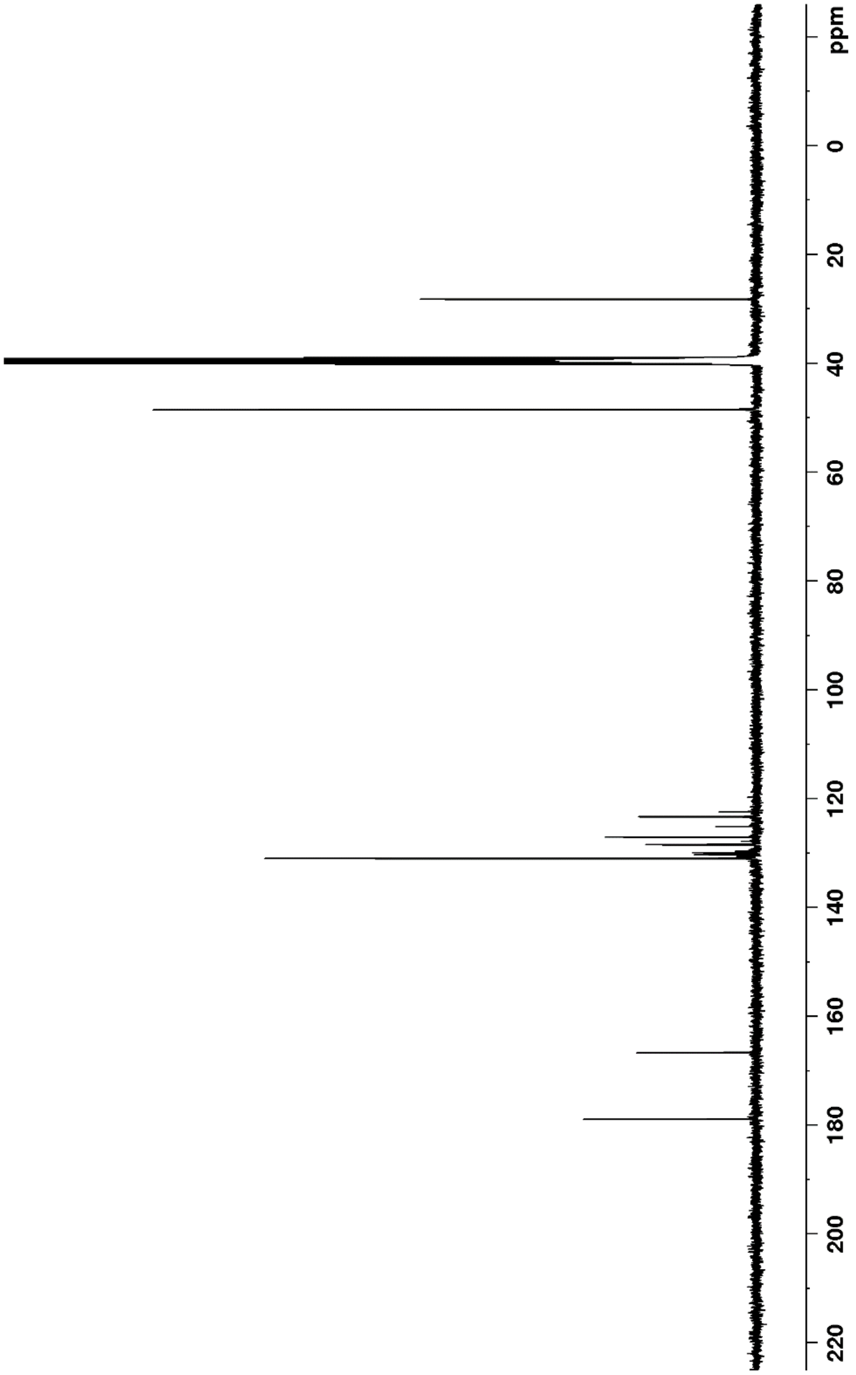
ppm
0
20
40
60
80
100
120
140
160
180
200
220

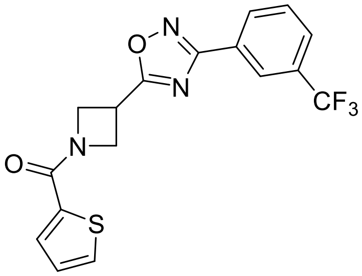
O
N
S
O
N
N
CF3

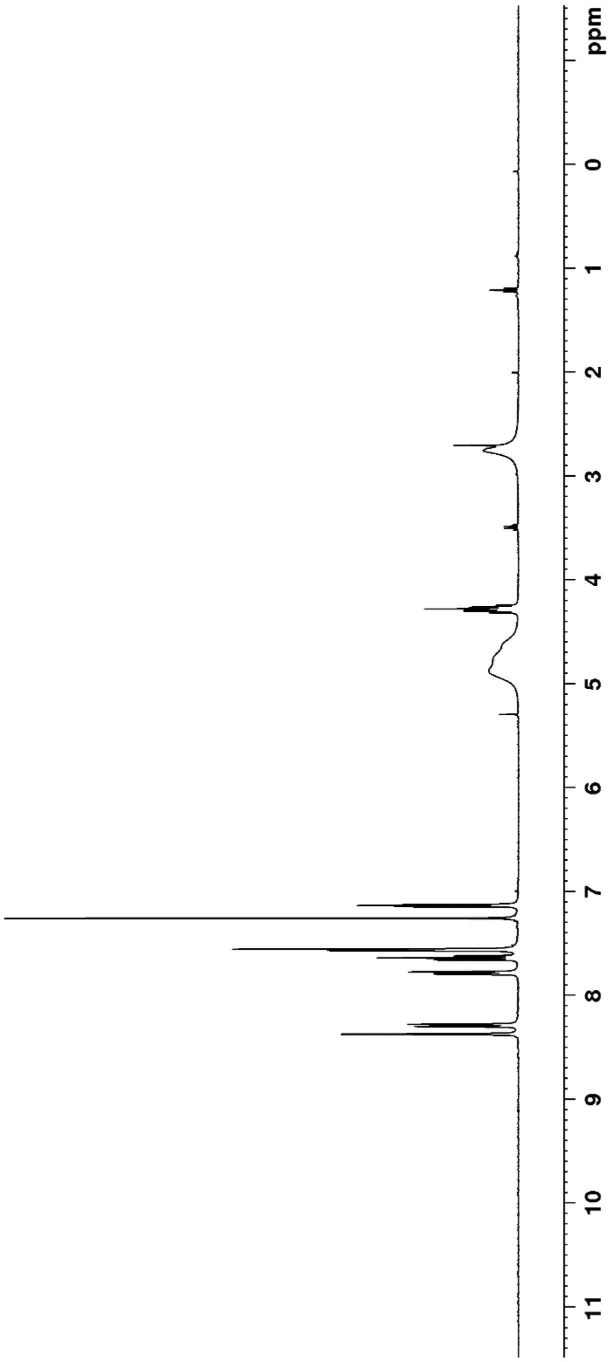
ppm
0
1
2
3
4
5
6
7
8
9
10
11

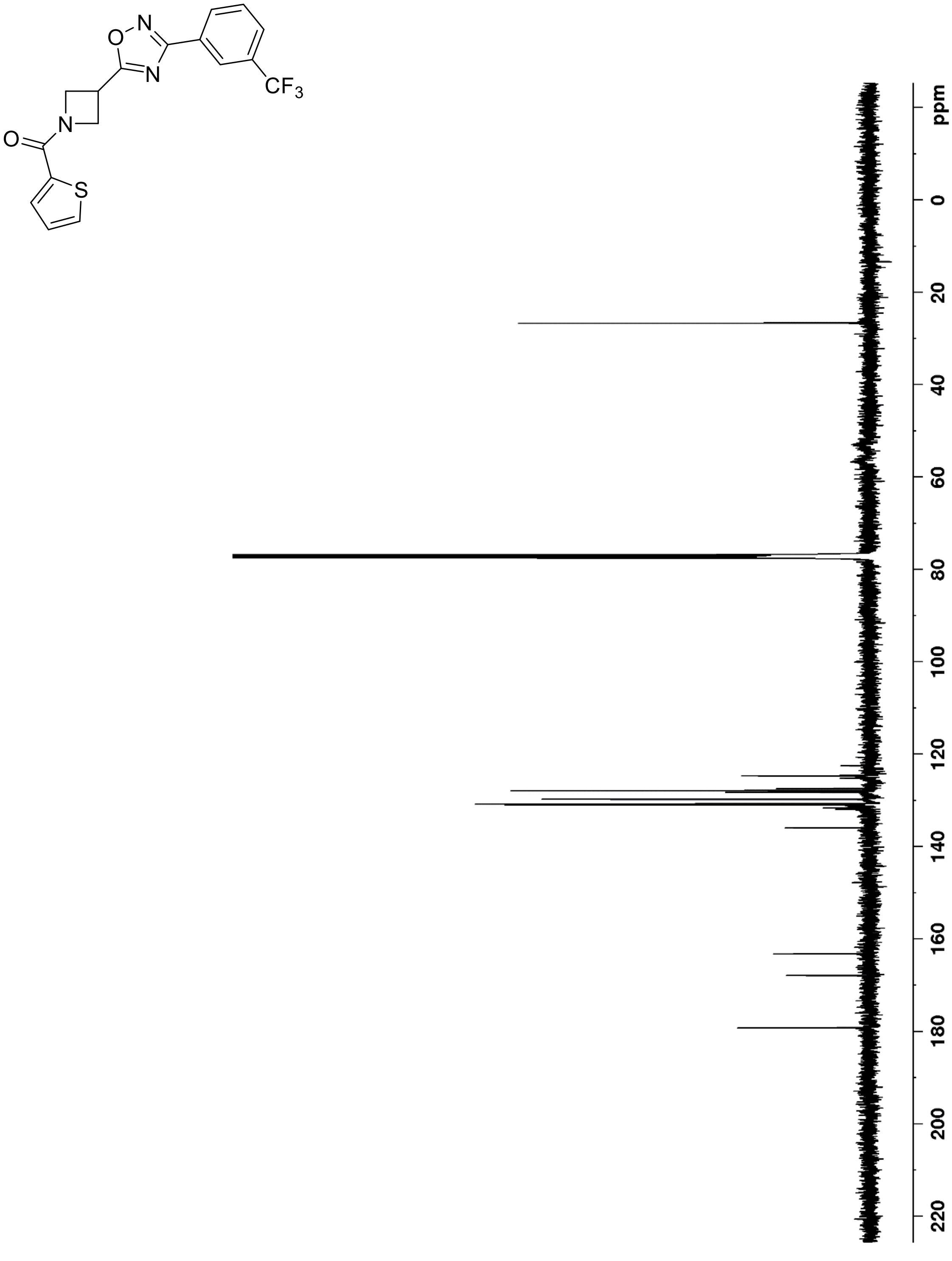
O
N
O
N
N
S
CF3
ppm
220
200
180
160
140
120
100
80
60
40
20
0

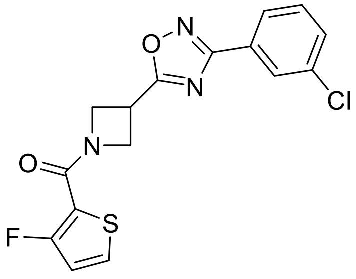
O
N
N
O
N
Cl
F
S

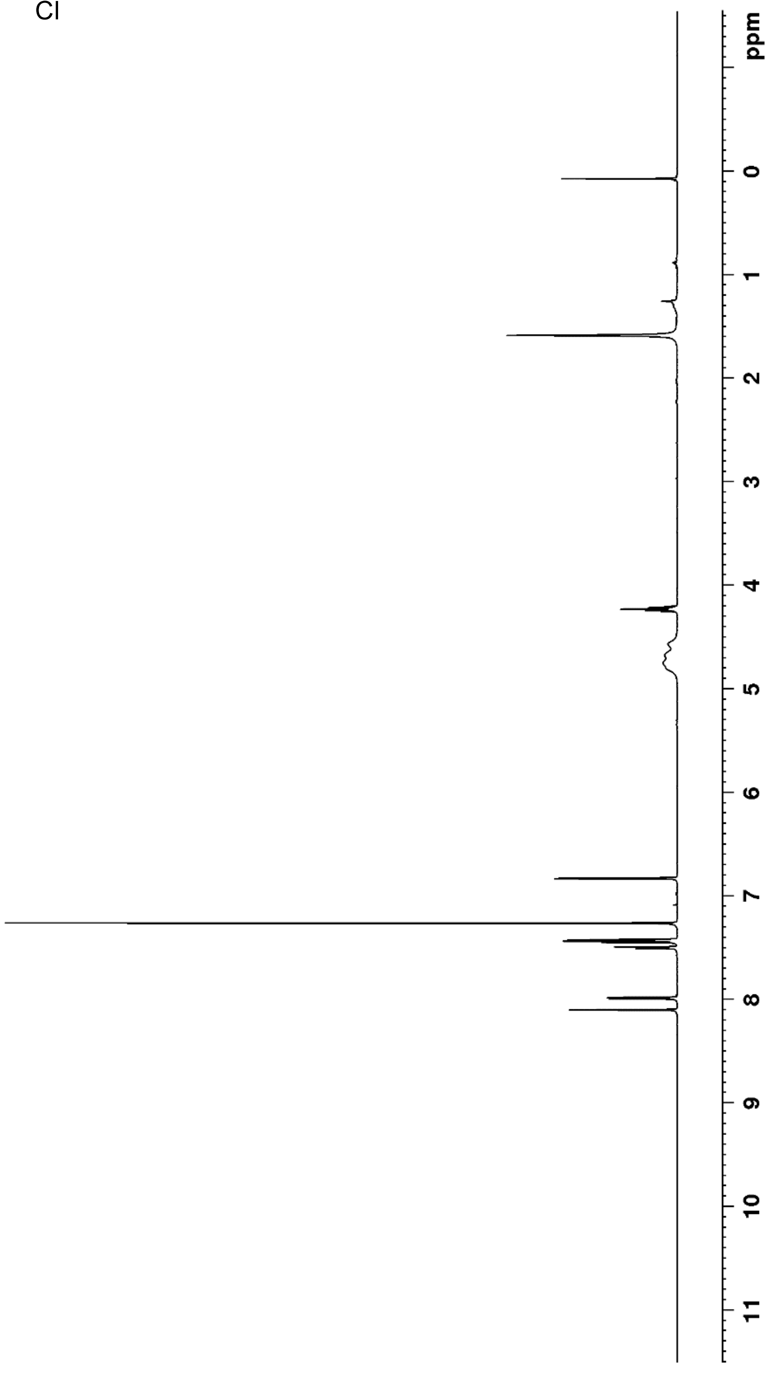
ppm
0
1
2
3
4
5
6
7
8
9
10
11

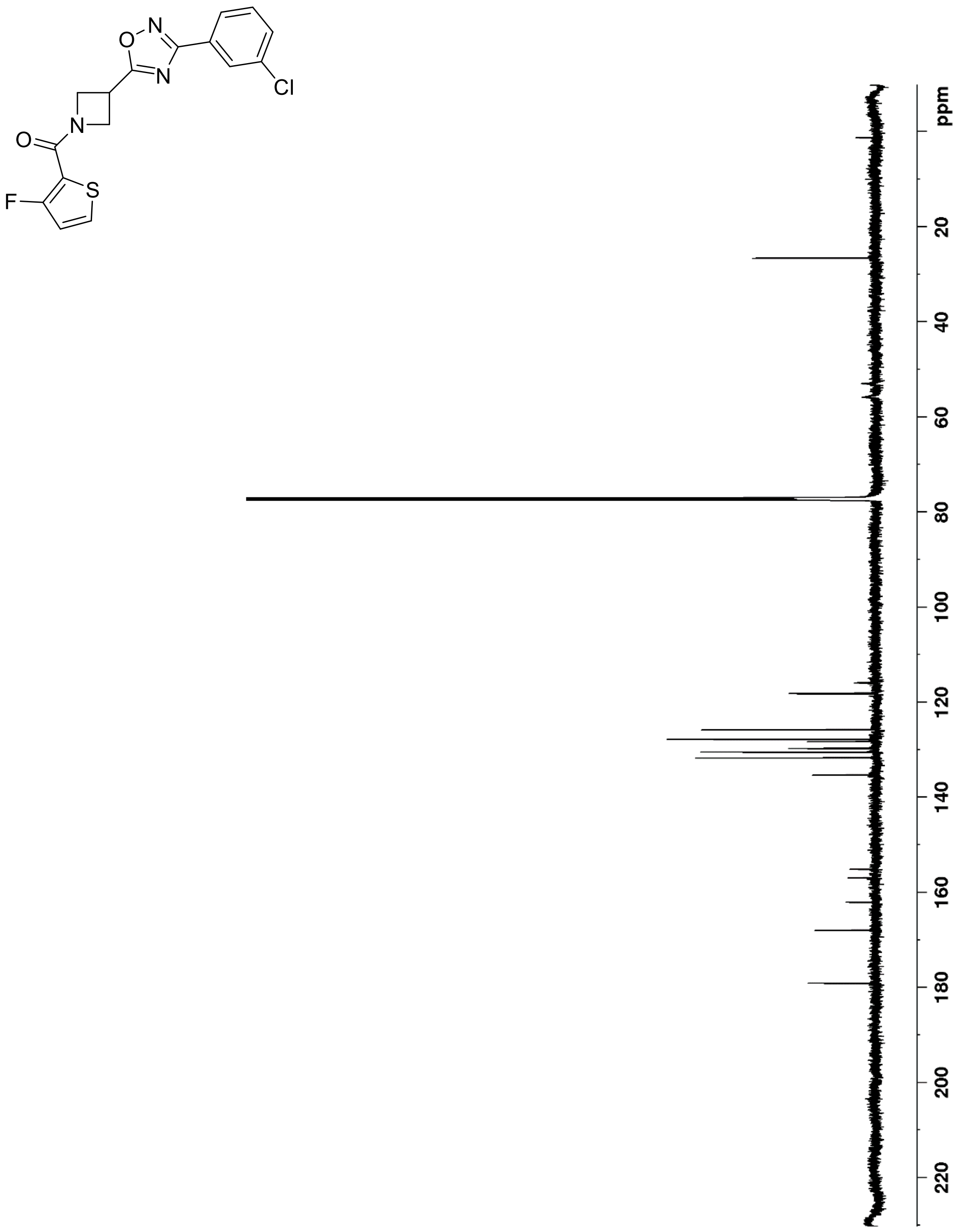
O
N
N
Cl
N
O
F
S
ppm
20
40
60
80
100
120
140
160
180
200
220

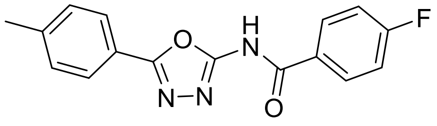

O
H
N
F
N
N
O

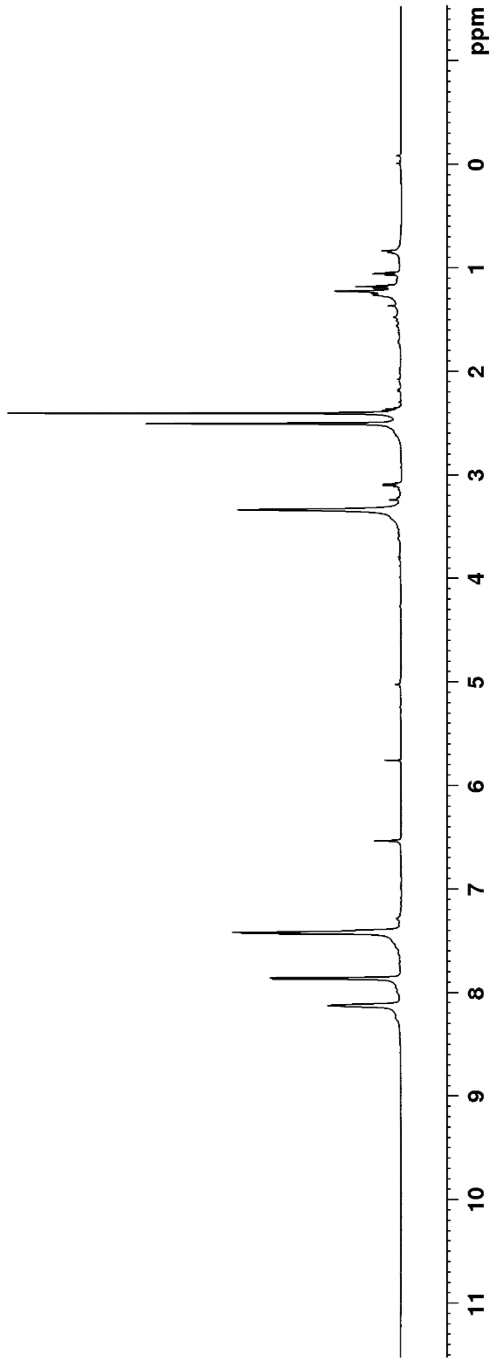

ppm
0
1
2
3
4
5
6
7
8
9
10
11

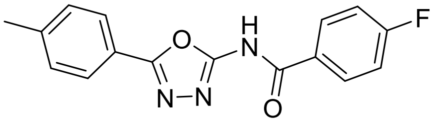

H
N
O
N–N
O
F

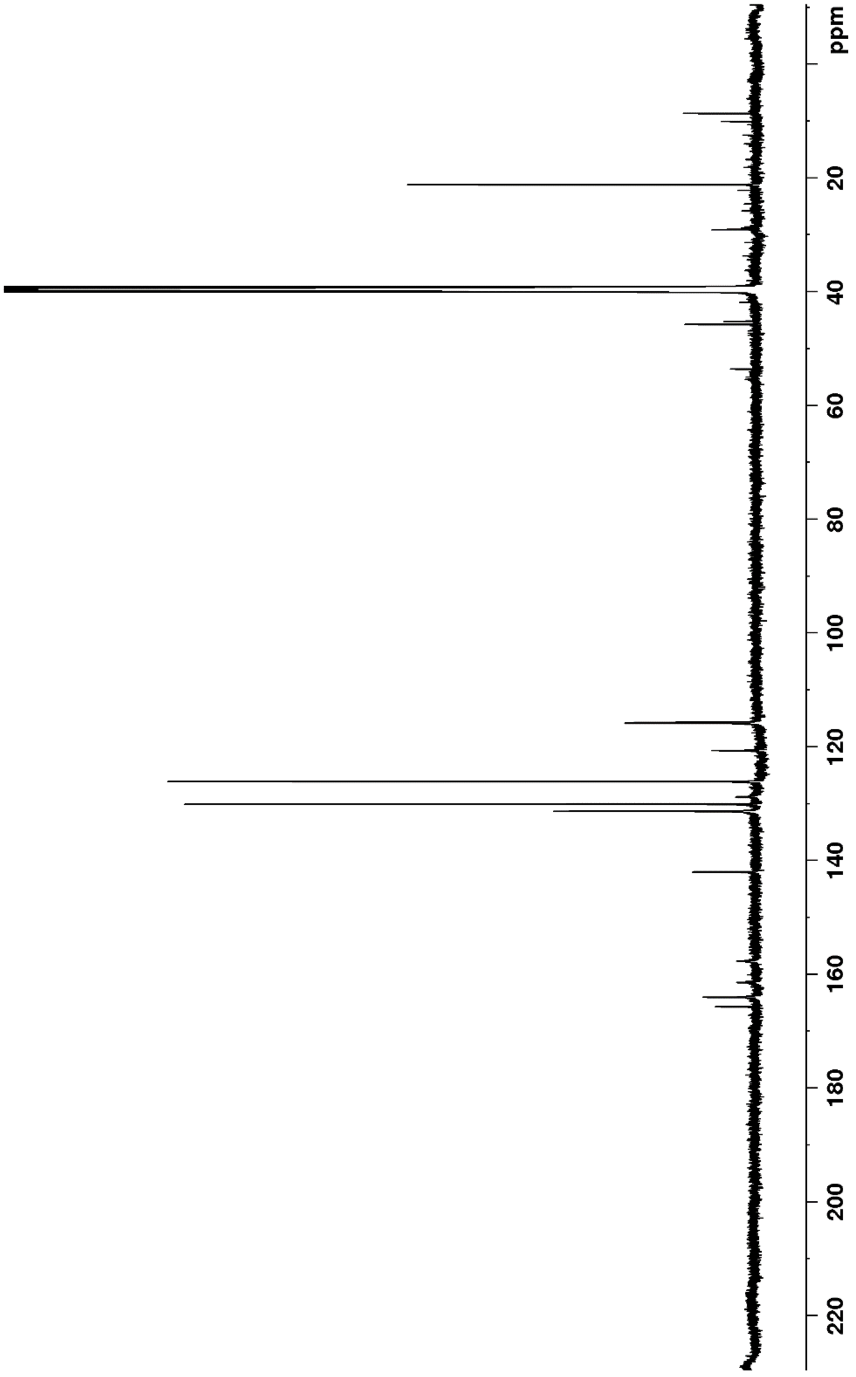

ppm
20
40
60
80
100
120
140
160
180
200
220

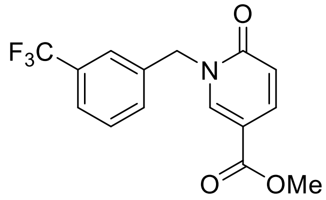
O
F3C
N
O
OMe

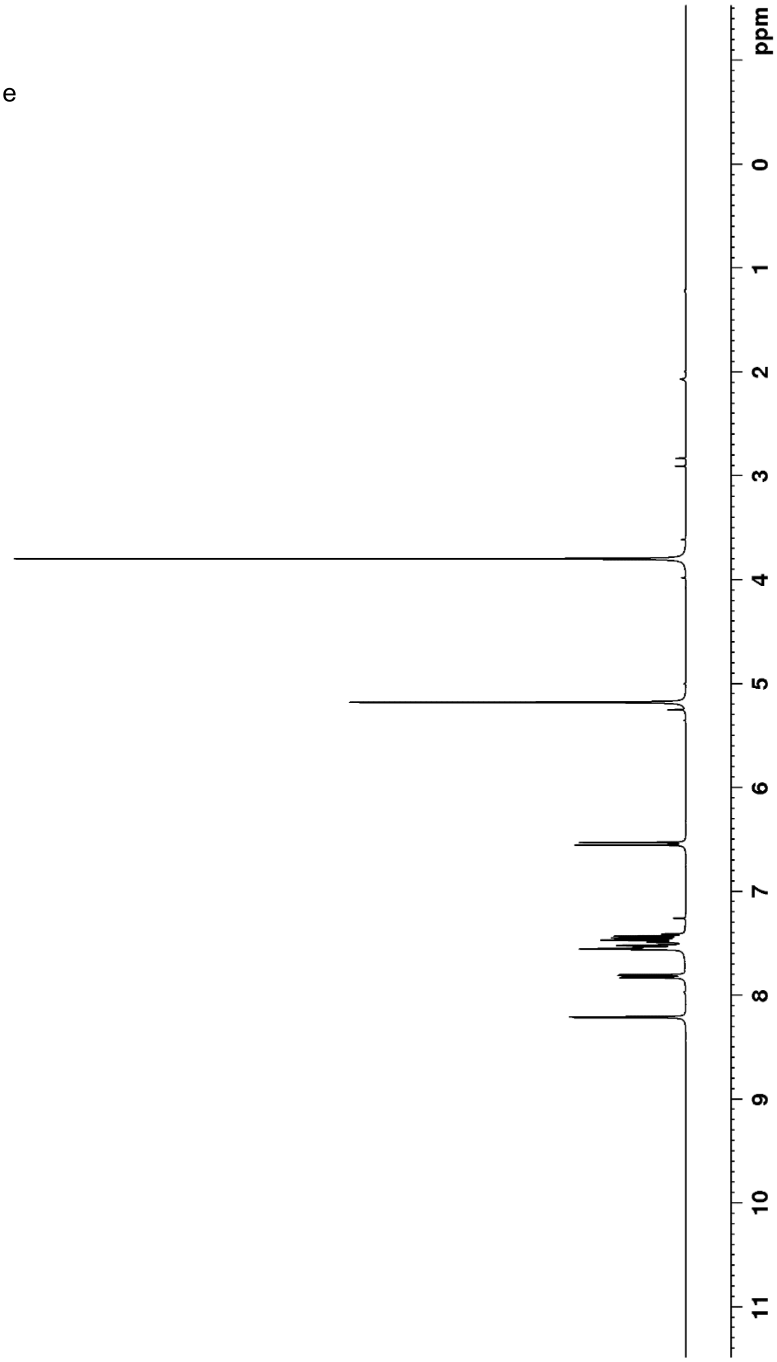
ppm
0
1
2
3
4
5
6
7
8
9
10
11

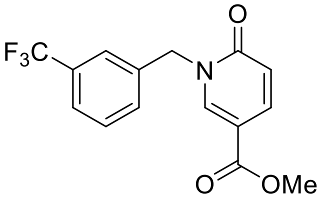
F3C
N
O
O
OMe

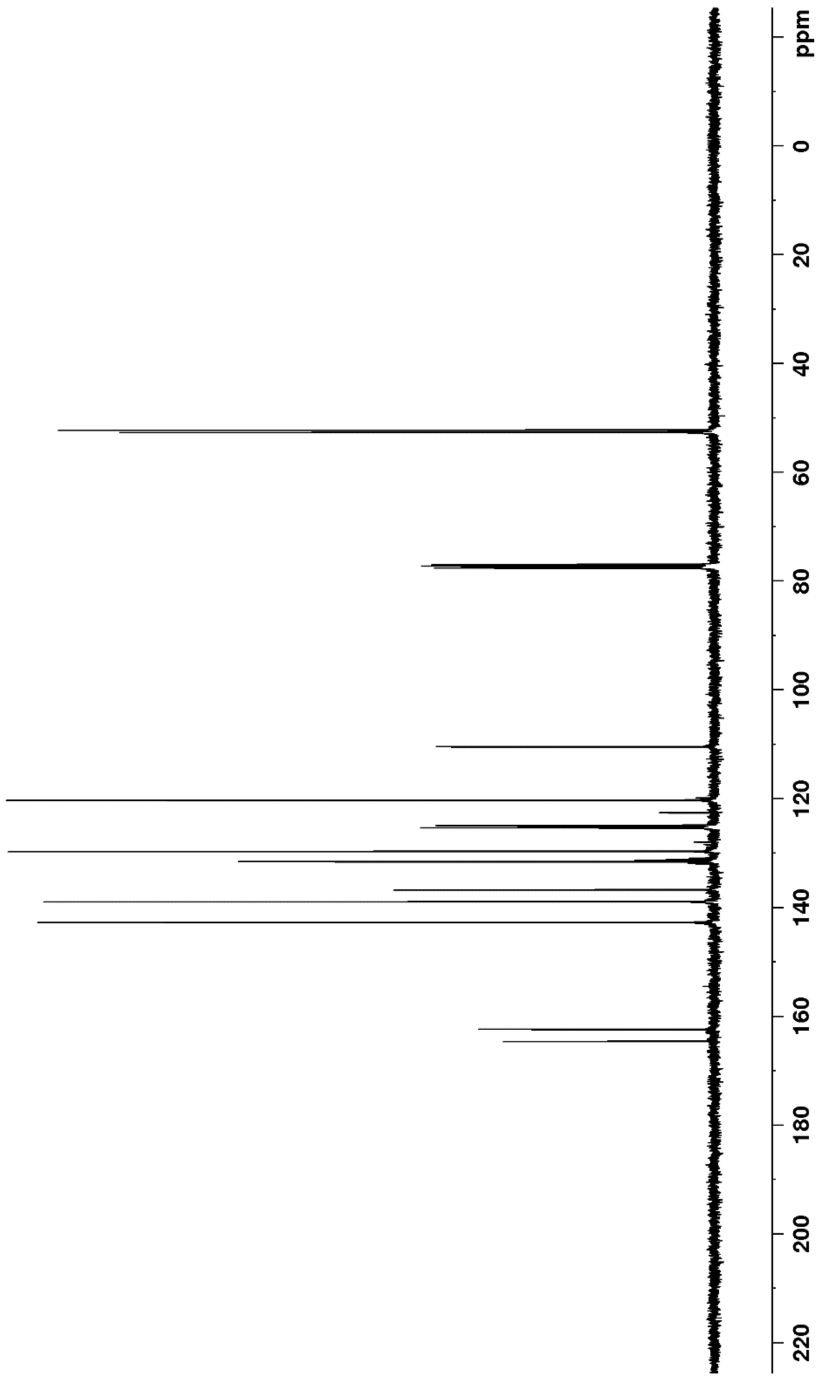
ppm
0
20
40
60
80
100
120
140
160
180
200
220

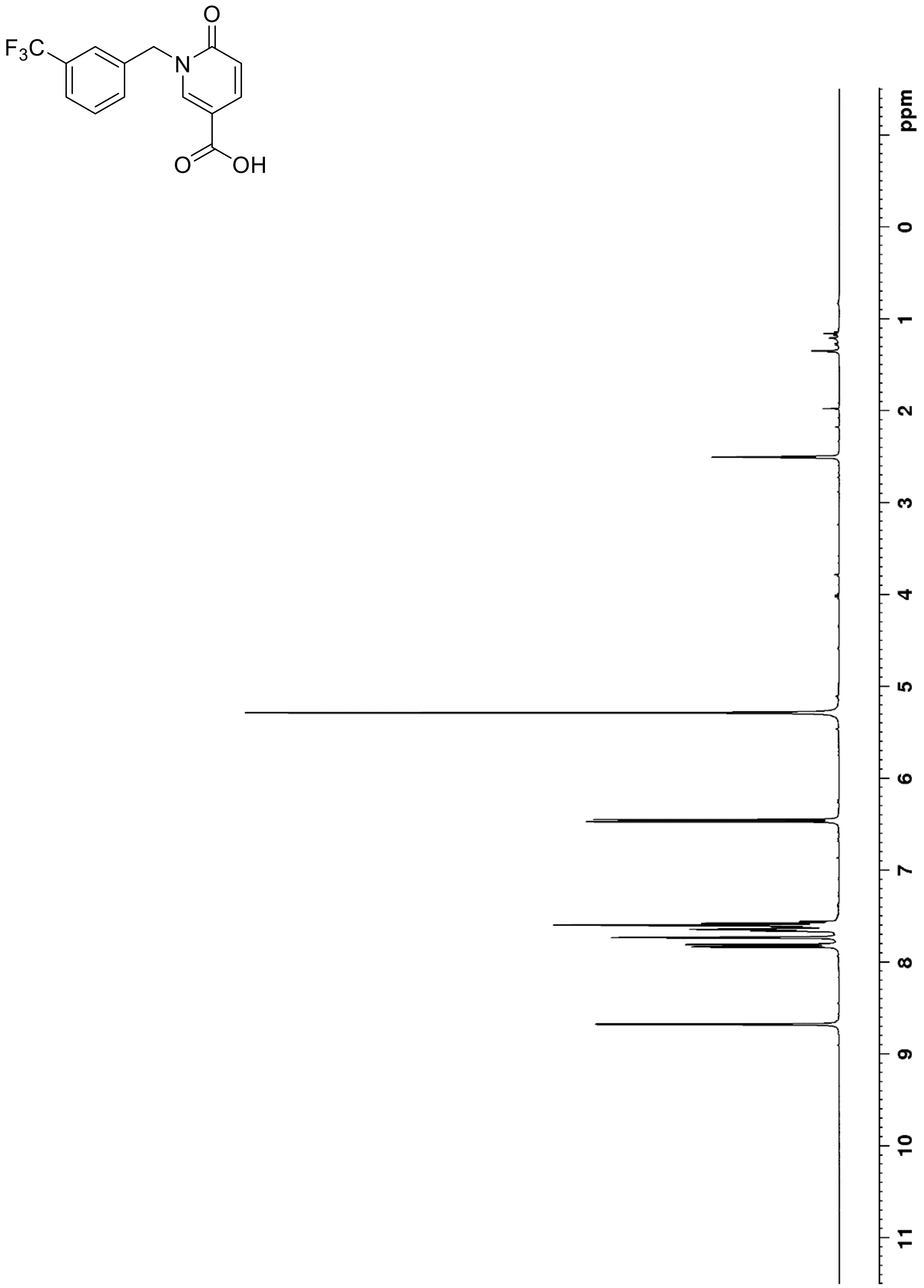
F3C
N
O
O
OH
ppm
0
1
2
3
4
5
6
7
8
9
10
11

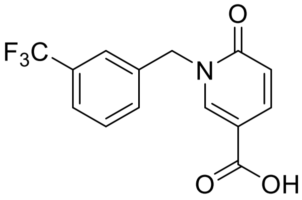

F3C
N
O
O
OH

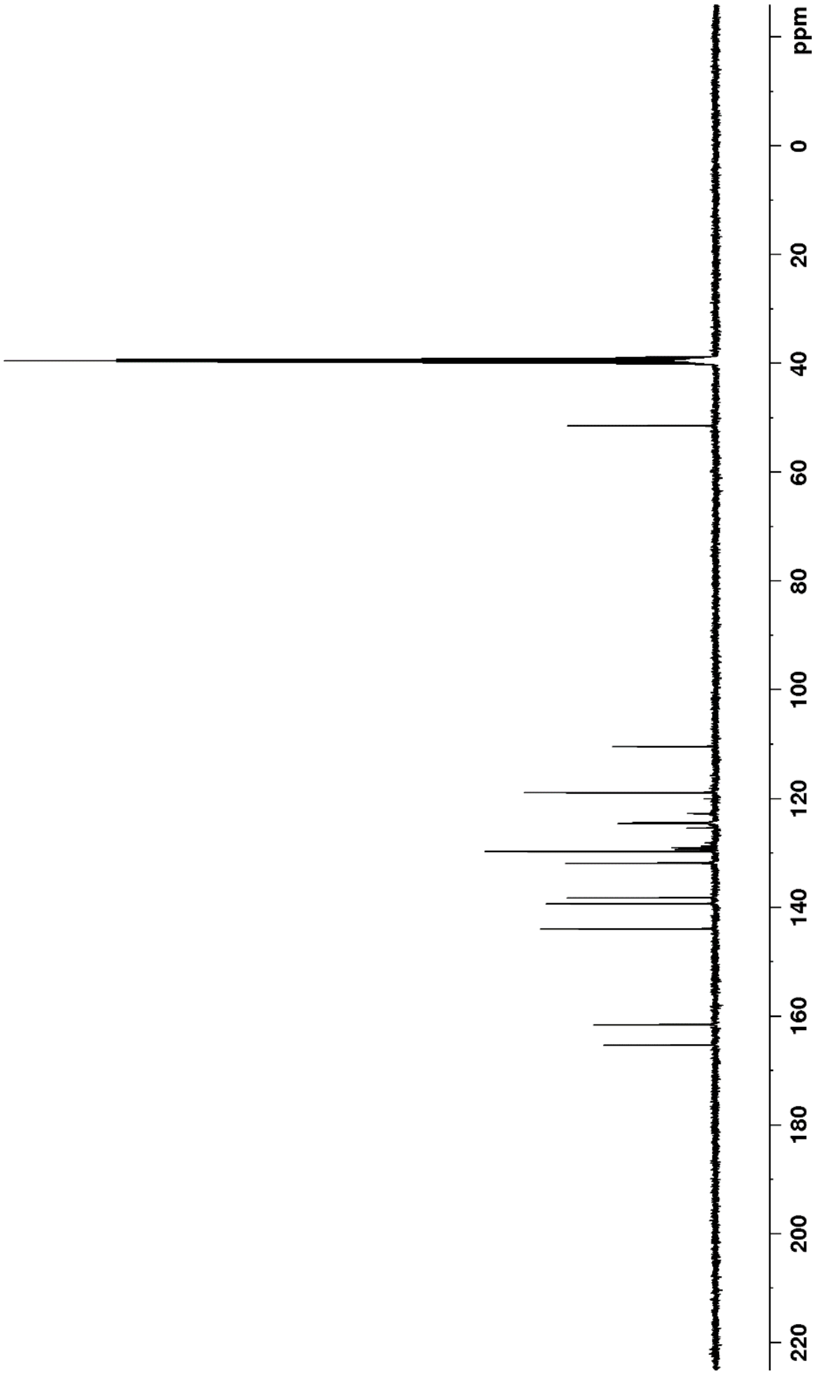

ppm
-20
0
20
40
60
80
100
120
140
160
180
200
220

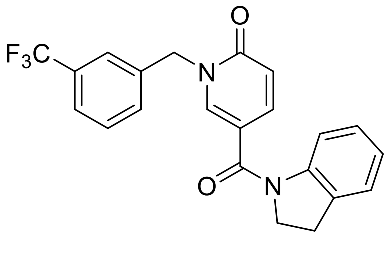
F3C
N
O
O
N

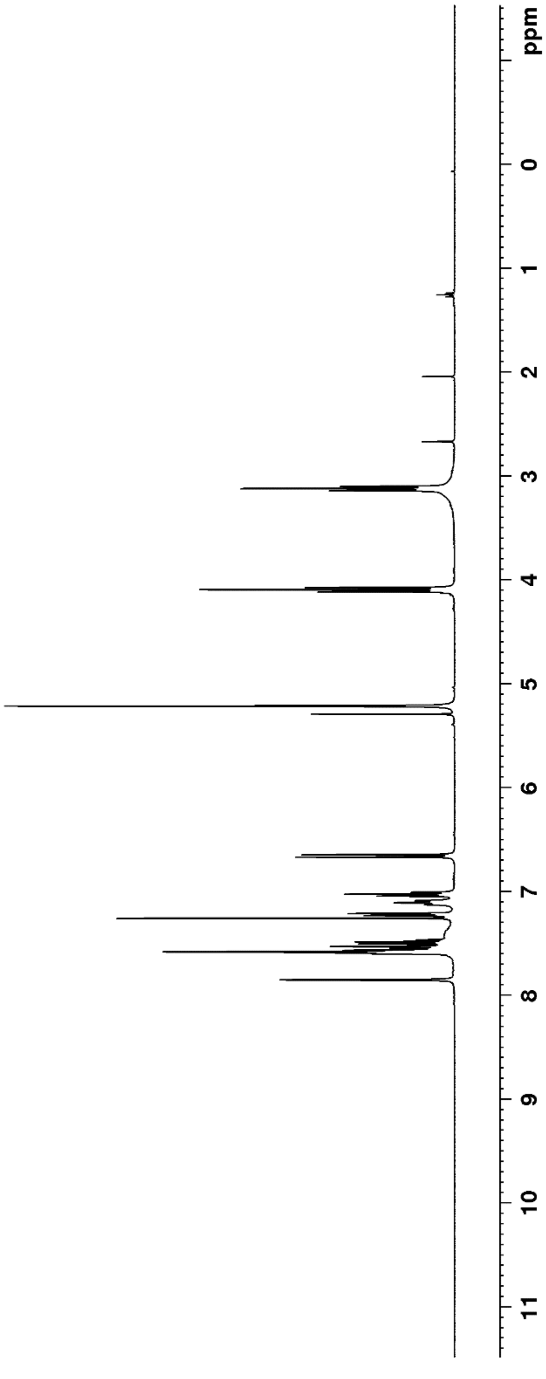
ppm
0
1
2
3
4
5
6
7
8
9
10
11

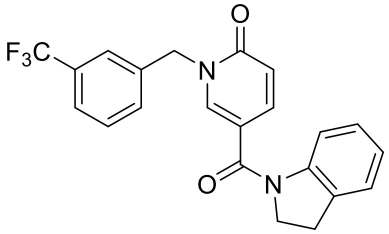
F3C
O
N
O
N

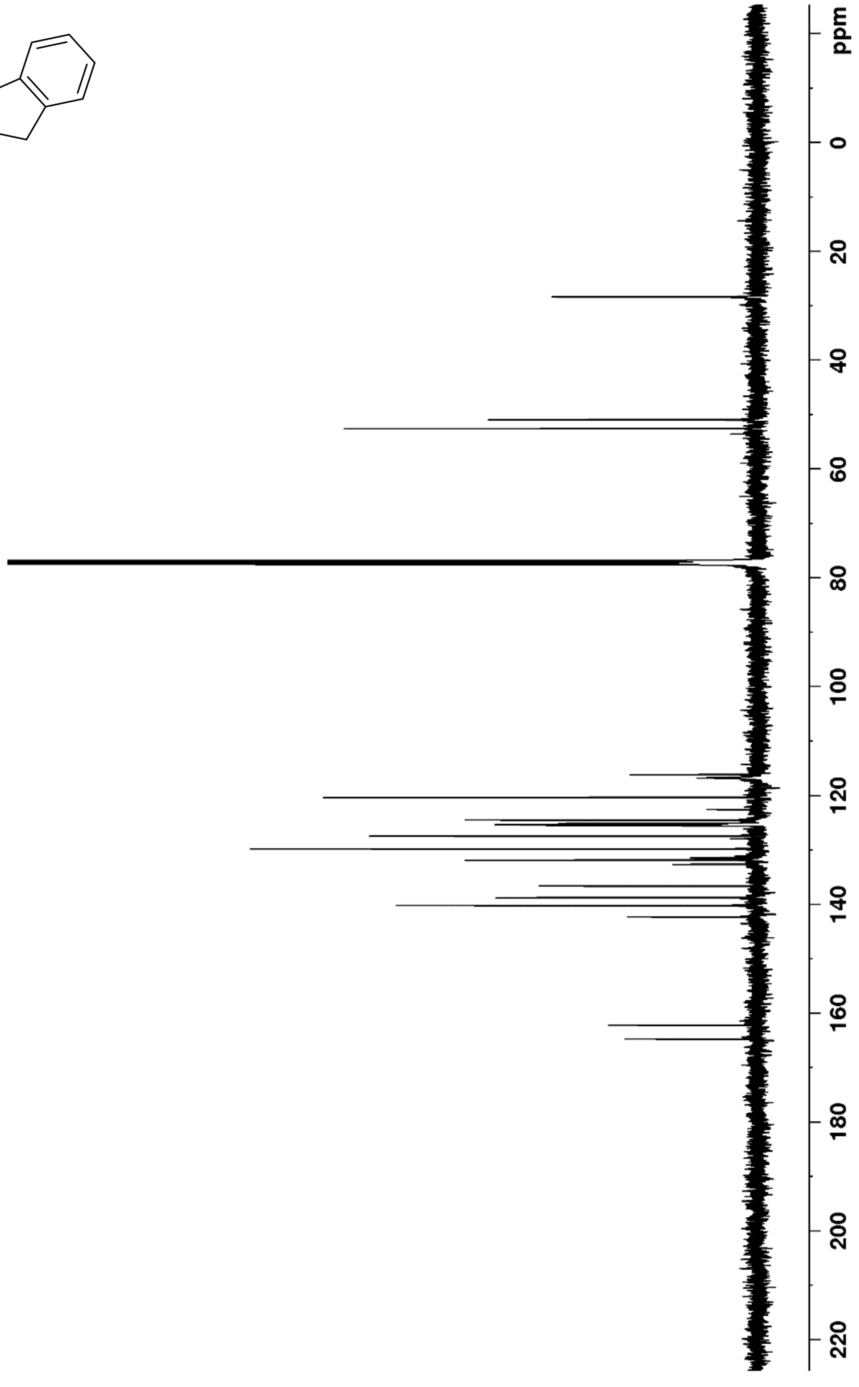
ppm
0
20
40
60
80
100
120
140
160
180
200
220

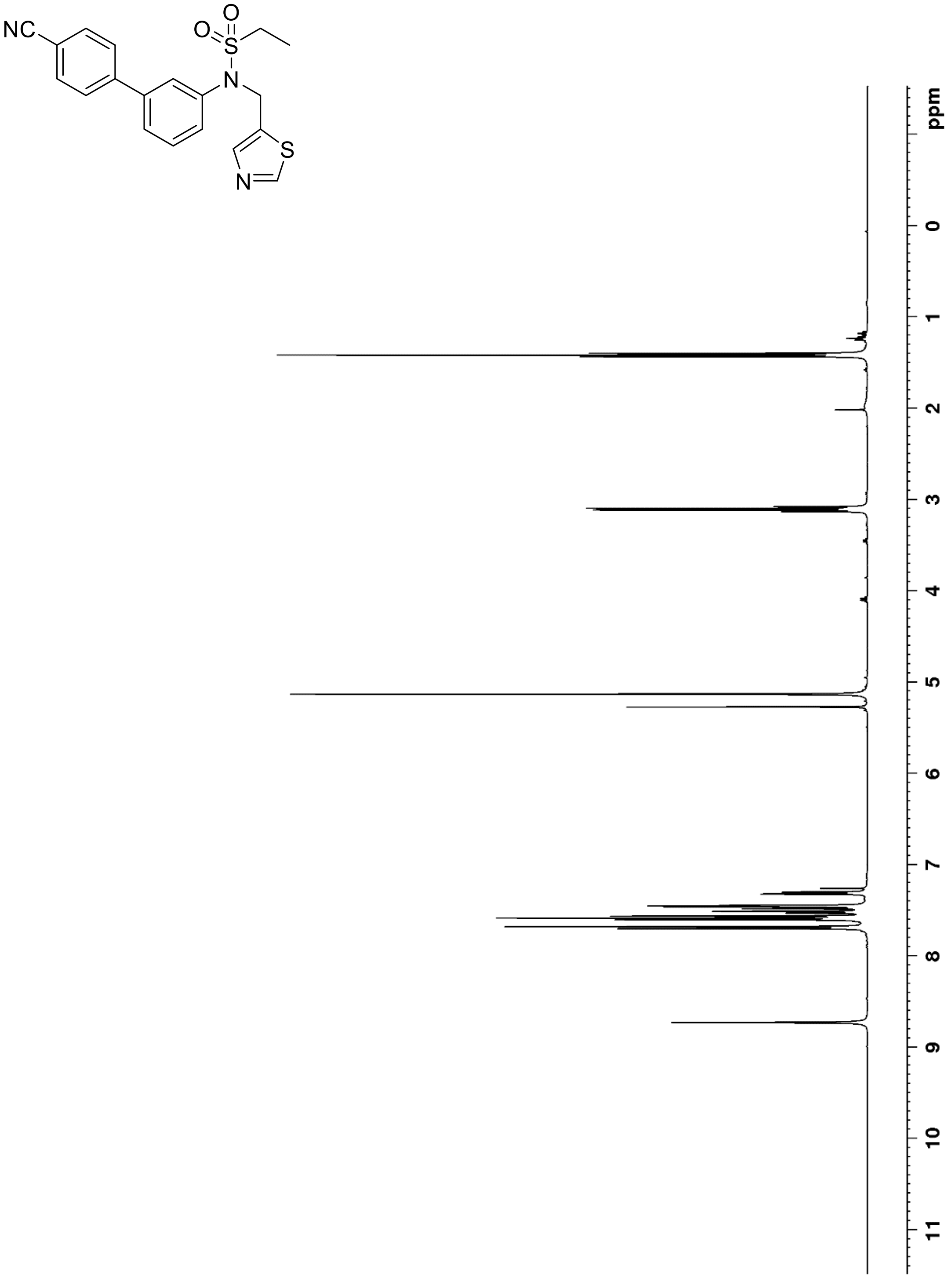
NC
O
O
S
N
S
N
ppm
0
1
2
3
4
5
6
7
8
9
10
11

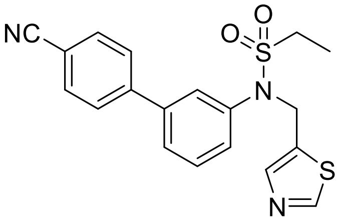

NC
O
O
S
N
S
N

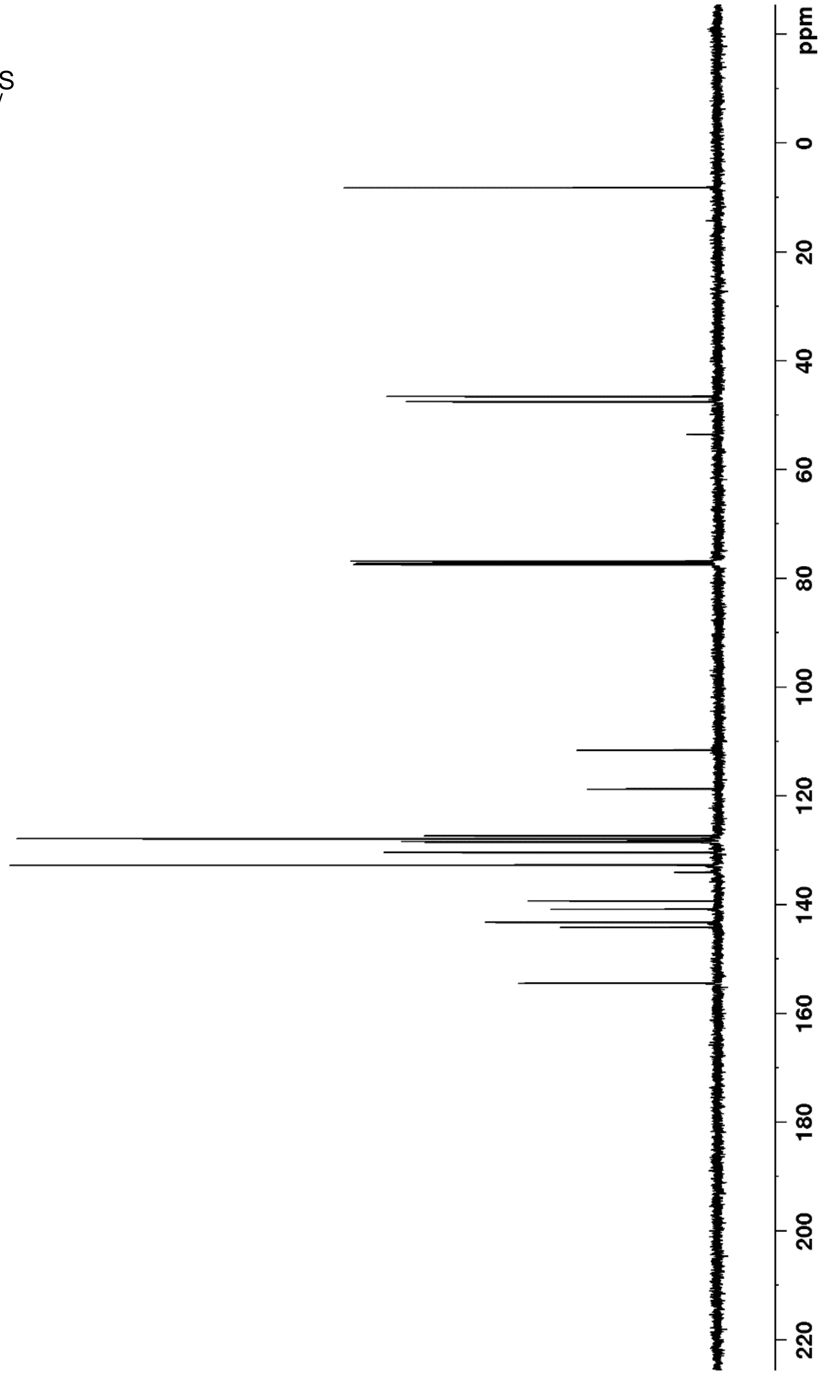

ppm
0
20
40
60
80
100
120
140
160
180
200
220

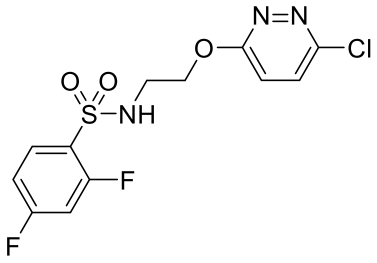
N=N
O
Cl
O
O
S
NH
F
F

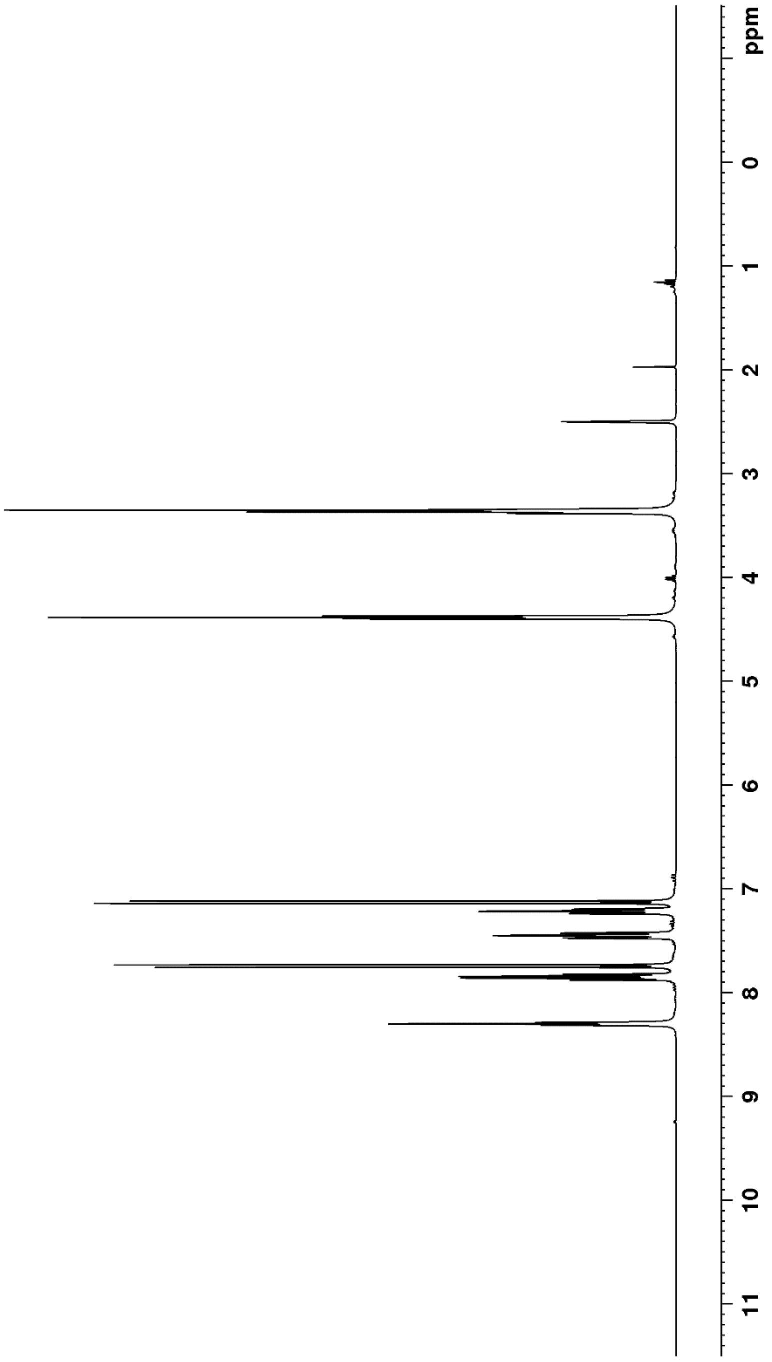
ppm
0
1
2
3
4
5
6
7
8
9
10
11

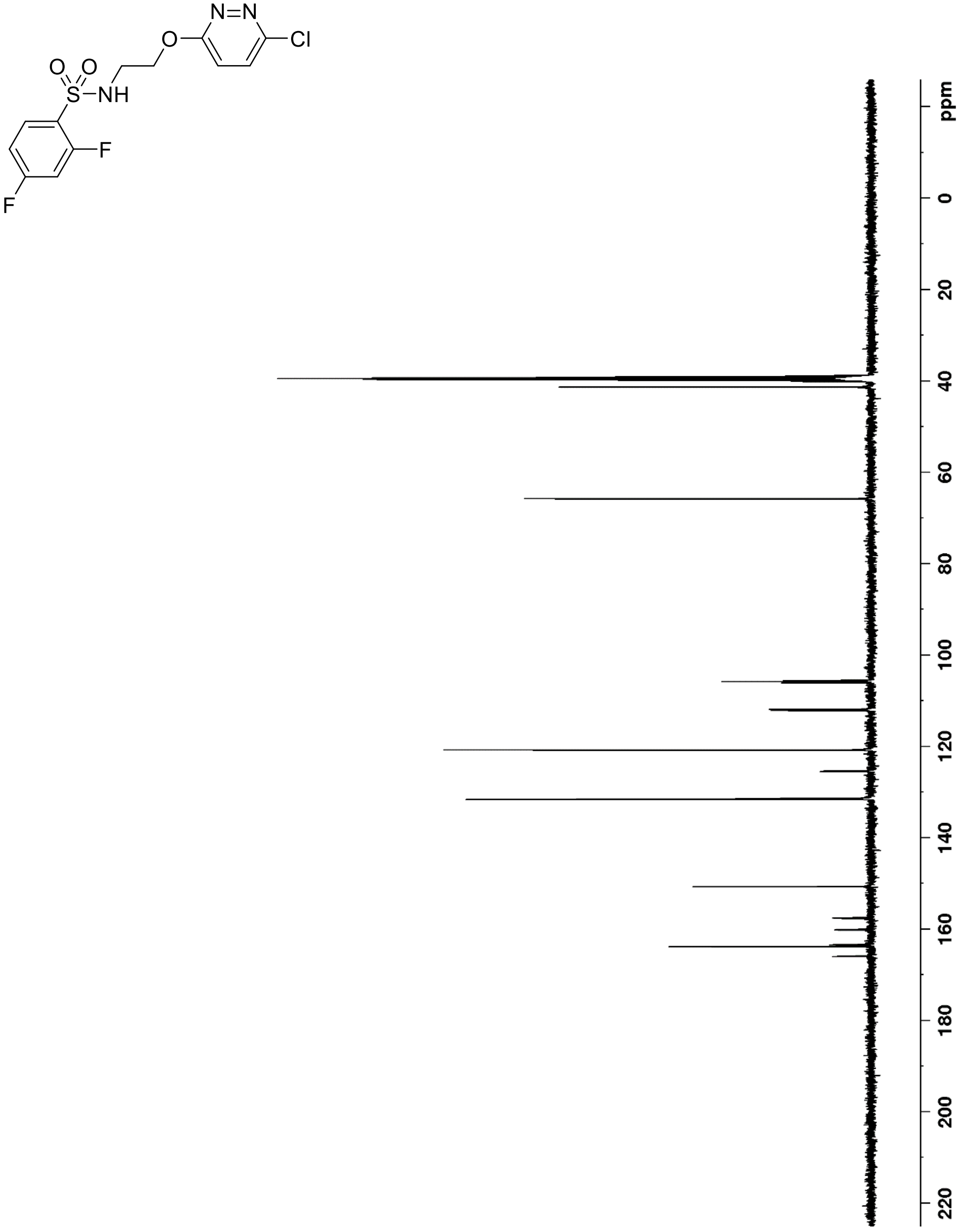
N=N
O
Cl
O
O
S
NH
F
F
ppm
-20
0
20
40
60
80
100
120
140
160
180
200
220

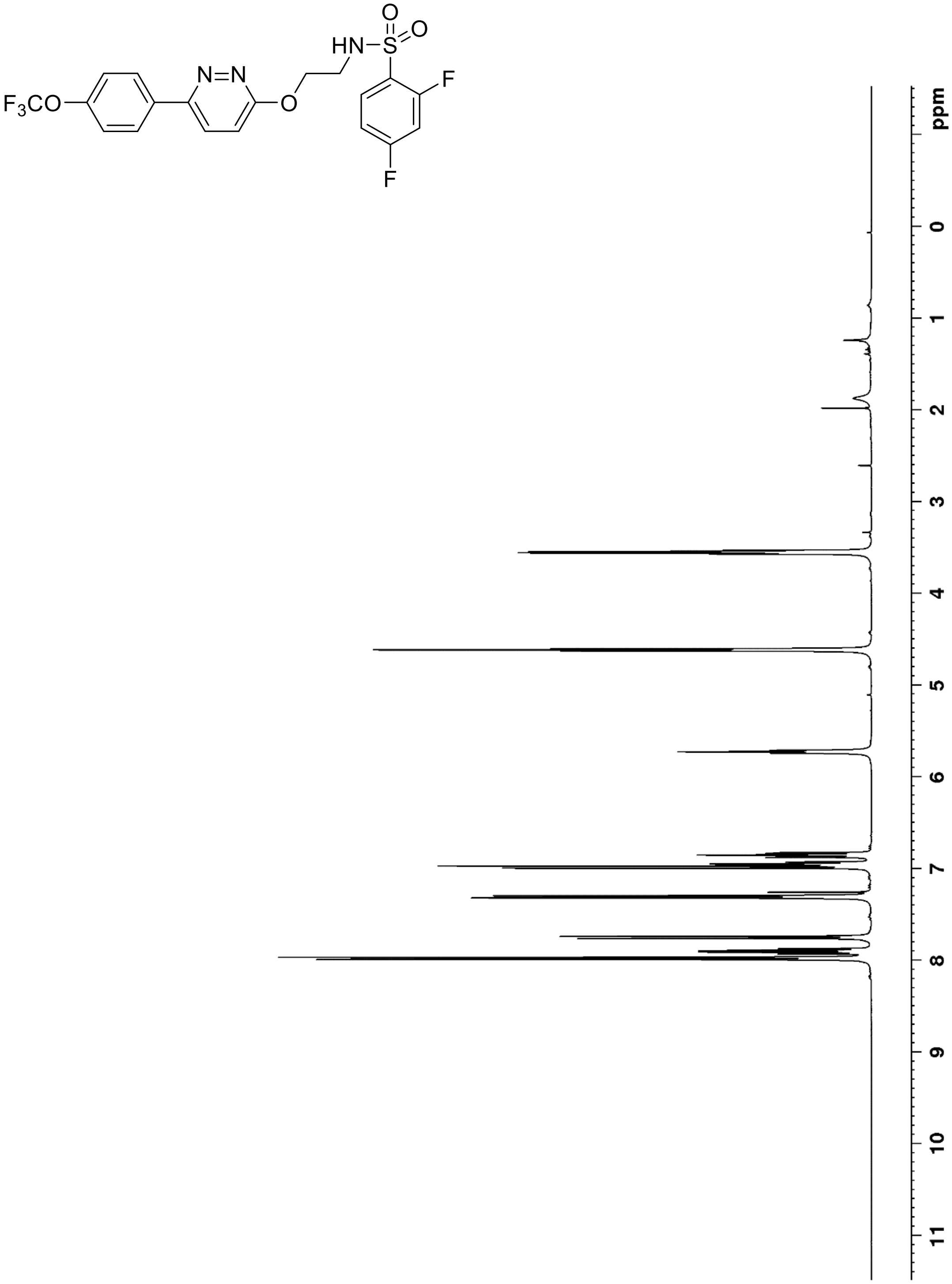
F$_3$CO
N=N
O
HN
S
O
O
F
F
ppm
0
1
2
3
4
5
6
7
8
9
10
11

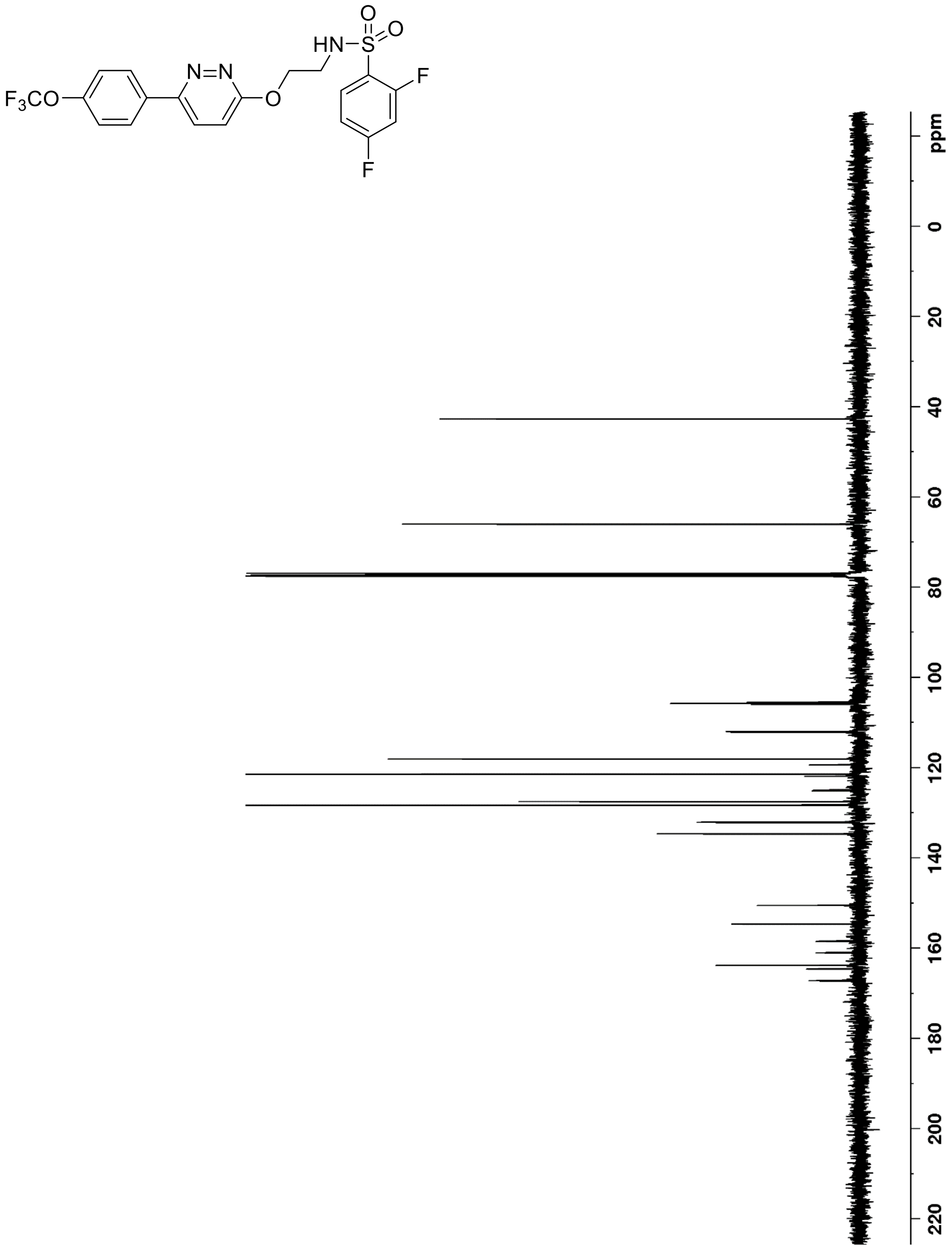
F3CO
N=N
O
HN
S
O
O
F
F
ppm
0
20
40
60
80
100
120
140
160
180
200
220

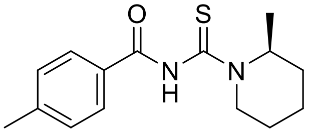
O
S
N
H
N

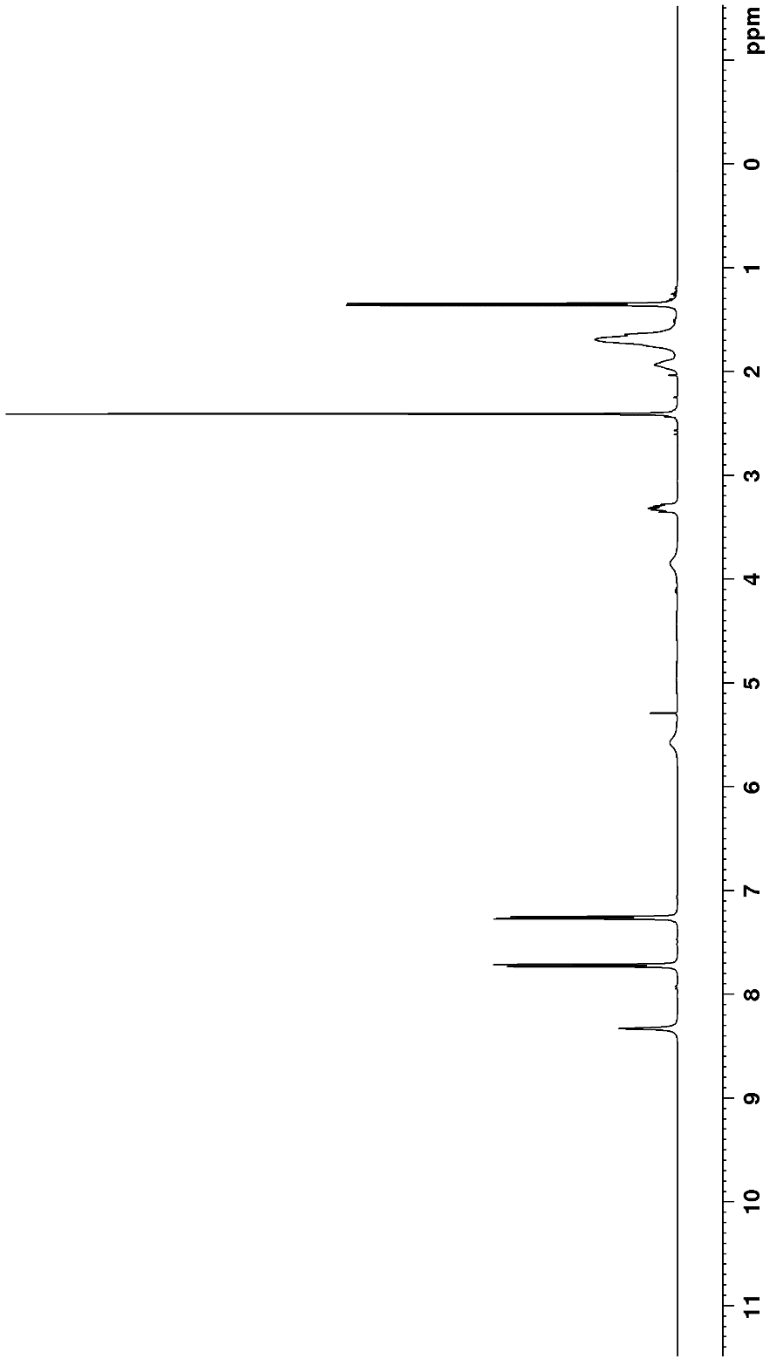
ppm
0
1
2
3
4
5
6
7
8
9
10
11

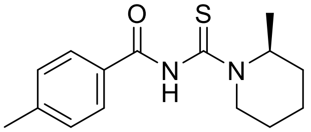
O
S
N
H
N

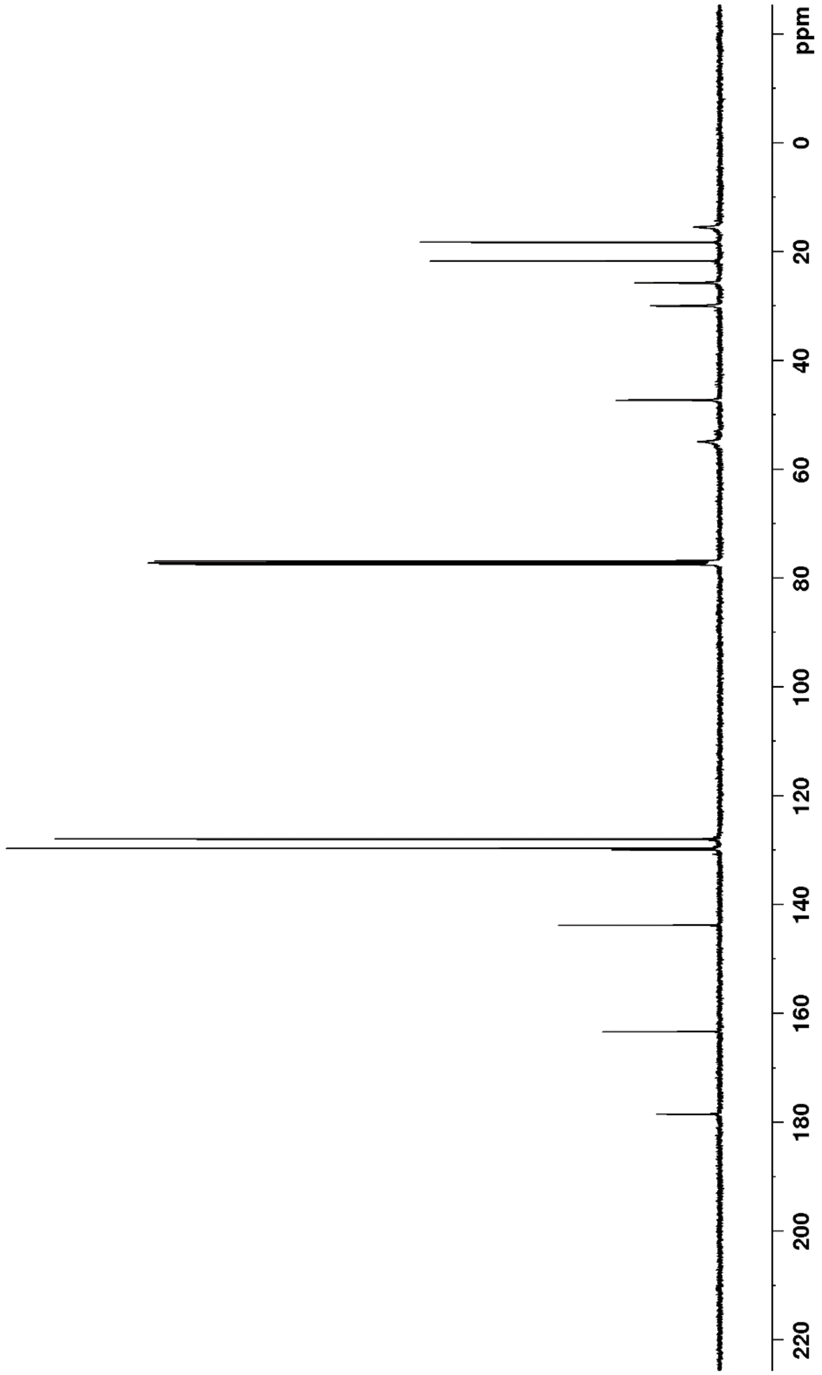
ppm
-20
0
20
40
60
80
100
120
140
160
180
200
220

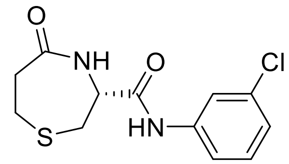
O
NH
O
Cl
S
HN

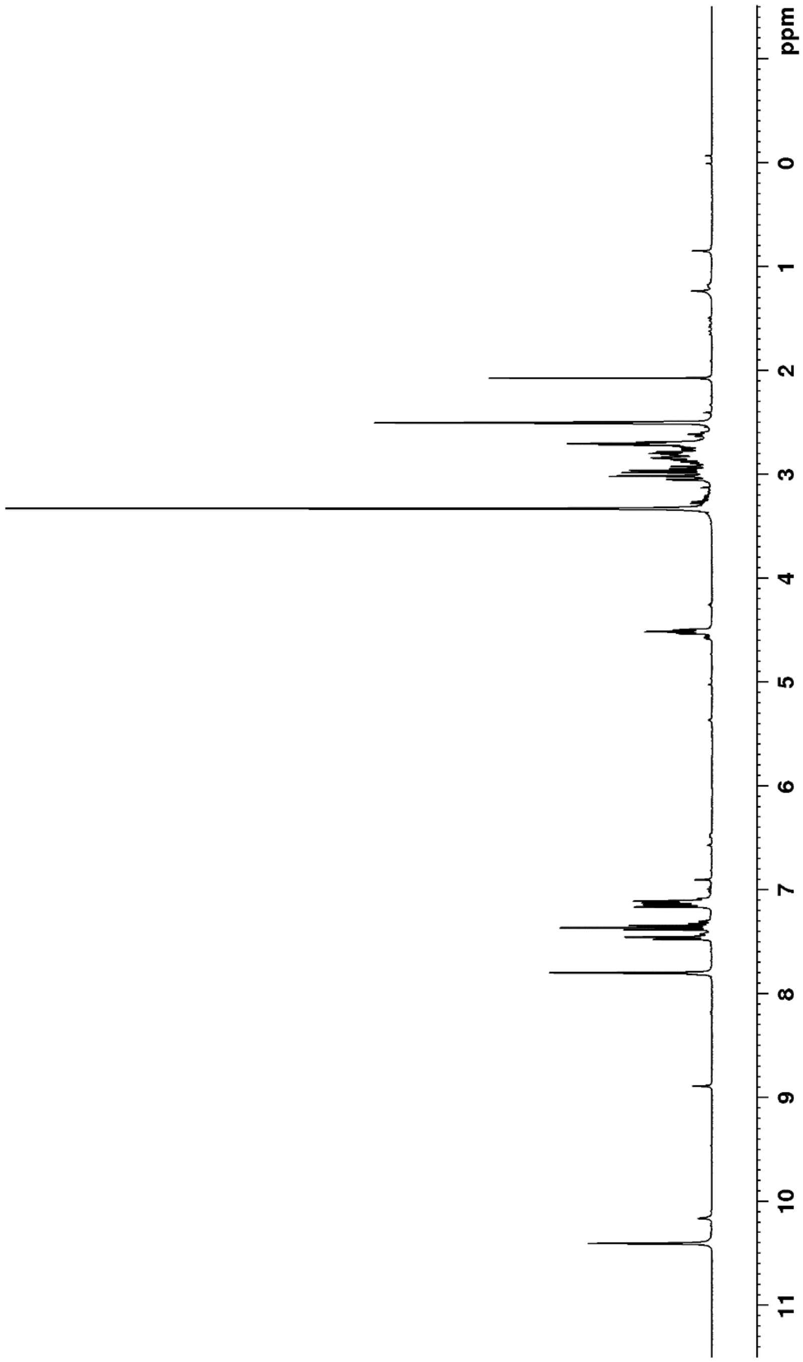
ppm
0
1
2
3
4
5
6
7
8
9
10
11

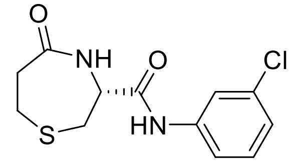
O
NH
O
Cl
HN
S

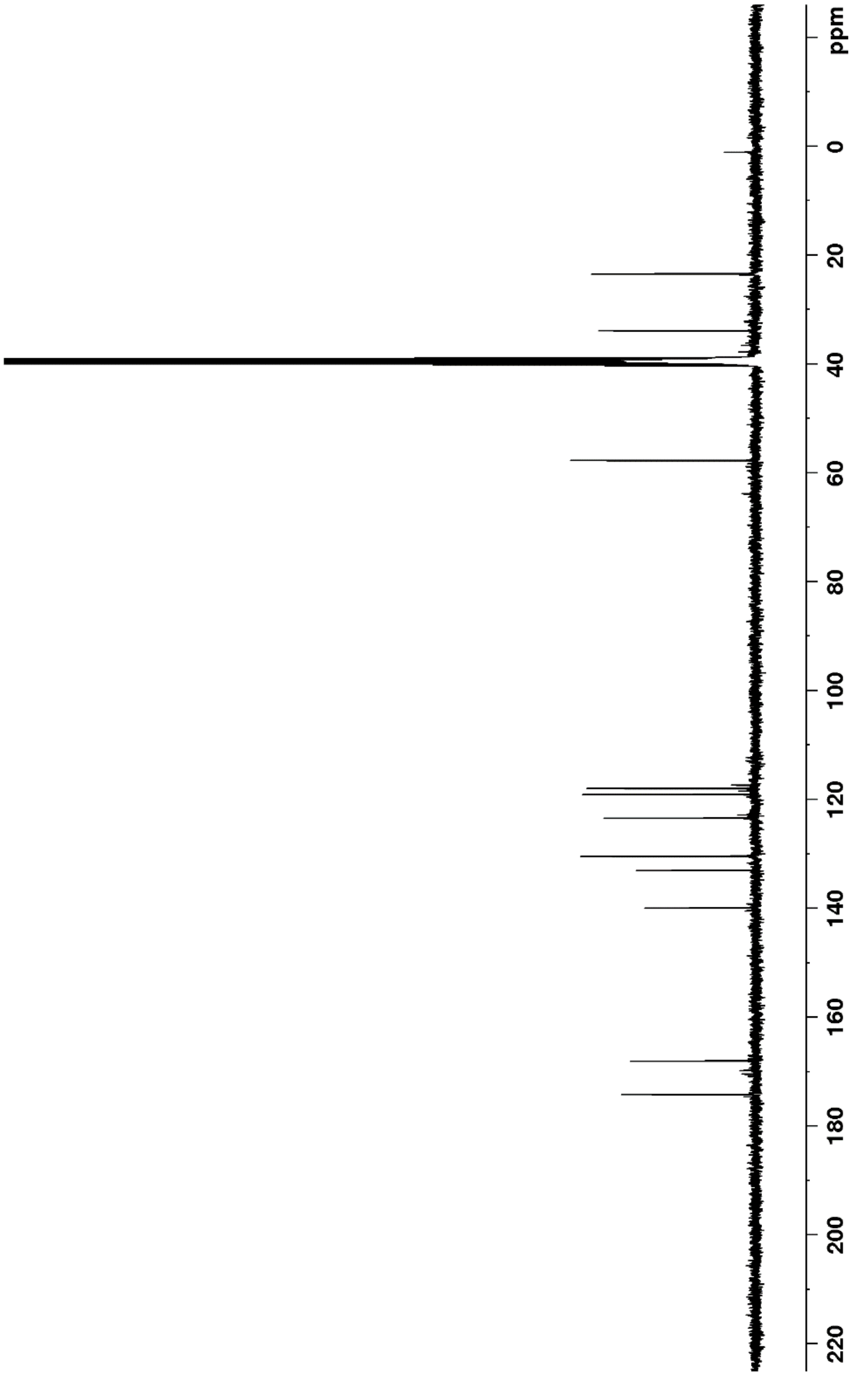
ppm
0
20
40
60
80
100
120
140
160
180
200
220

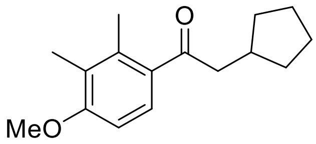
O
MeO

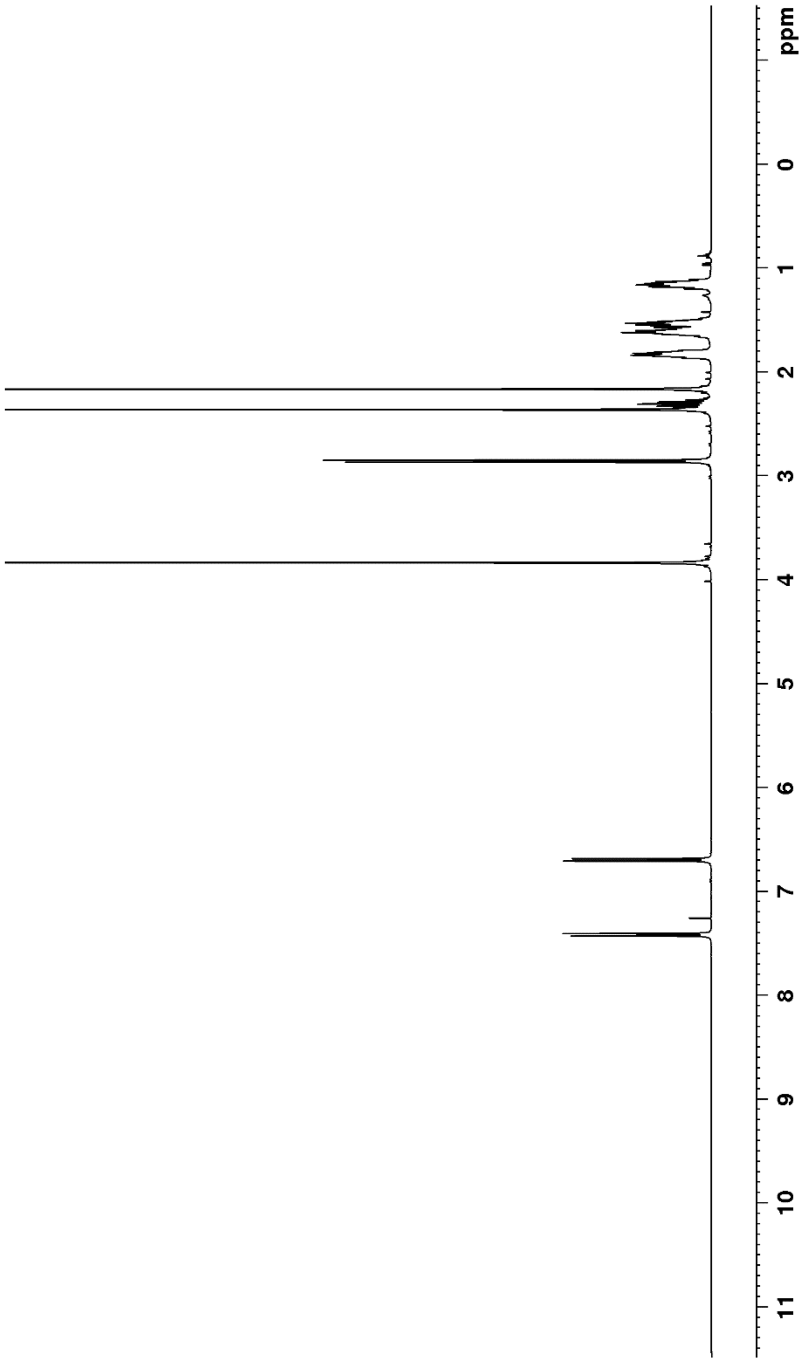
ppm
0
1
2
3
4
5
6
7
8
9
10
11

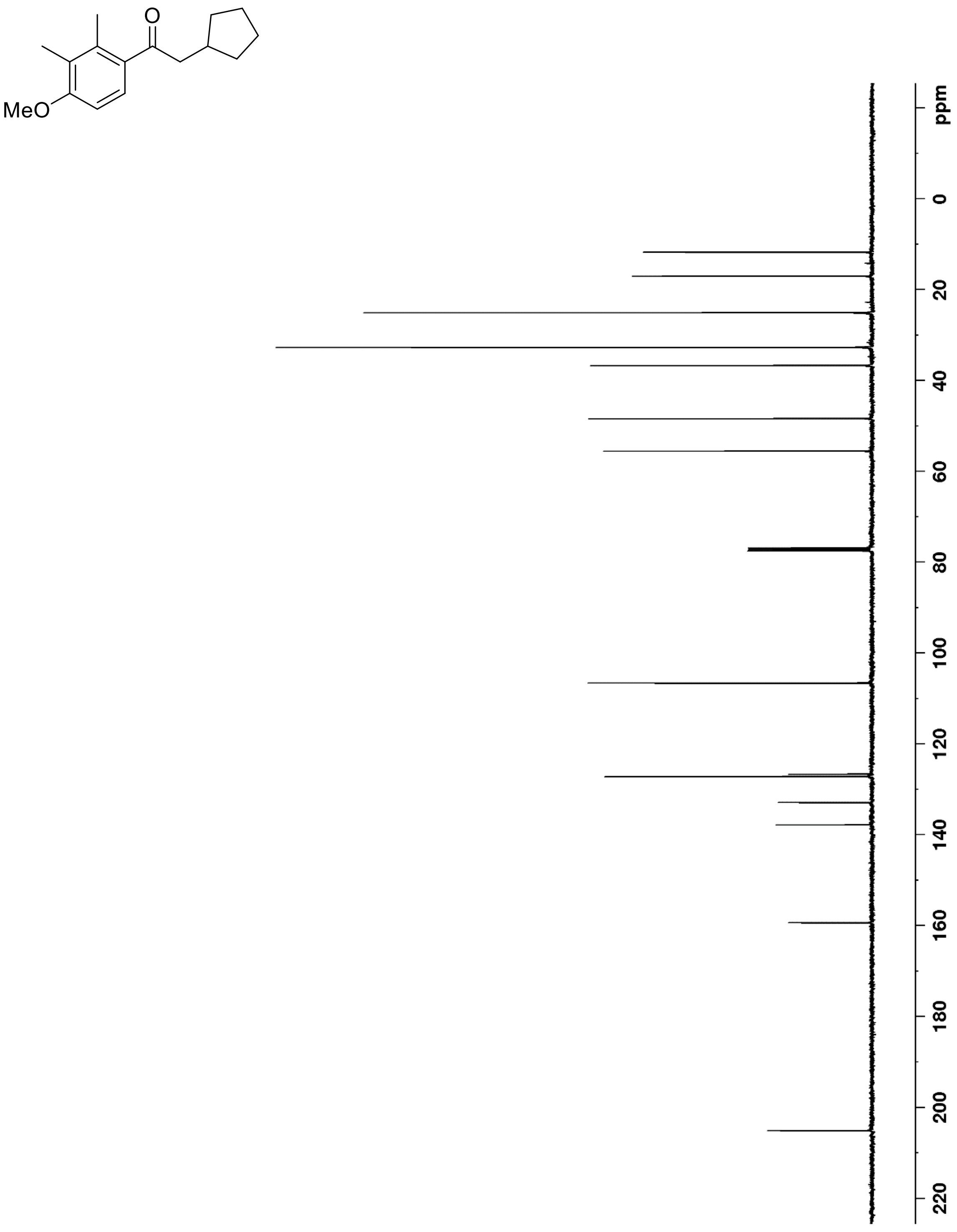
MeO
O
ppm
0
20
40
60
80
100
120
140
160
180
200
220

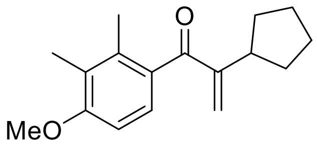
MeO
O

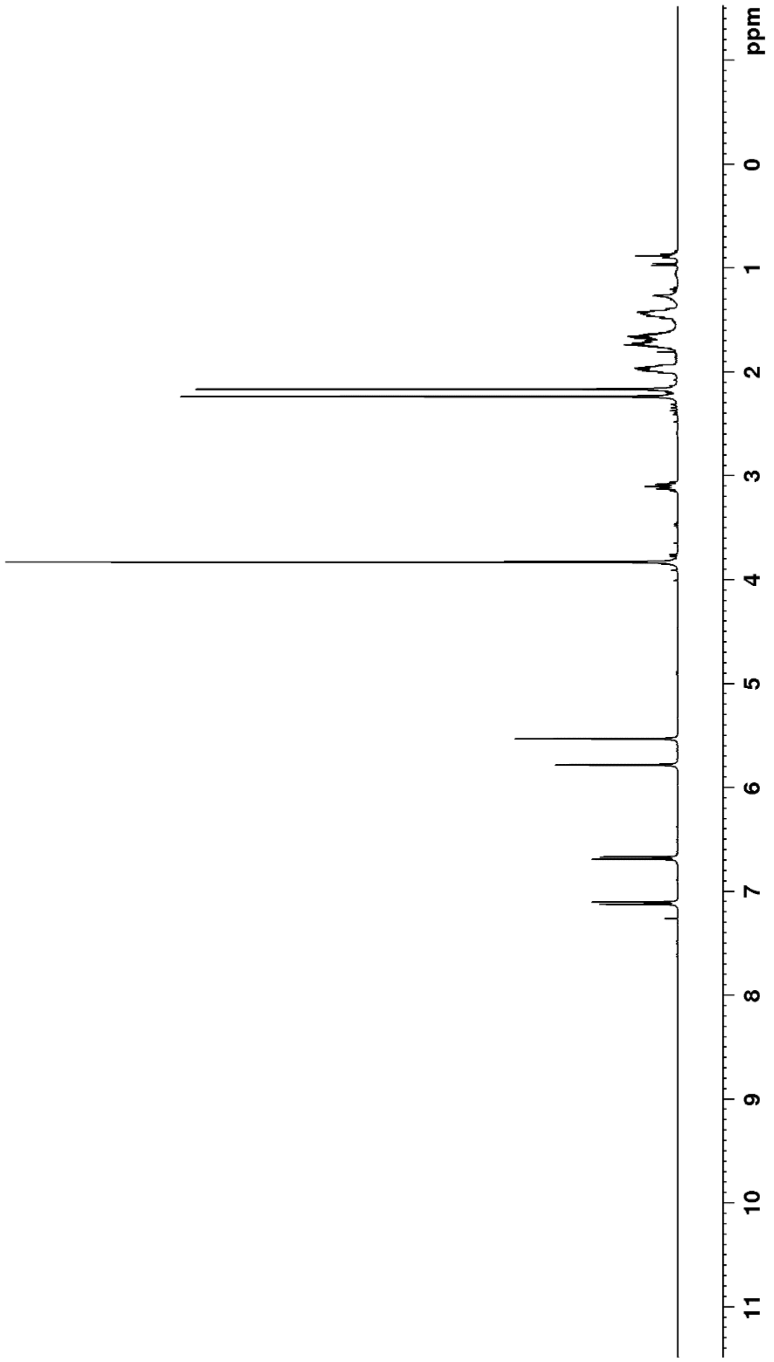
ppm
0
1
2
3
4
5
6
7
8
9
10
11

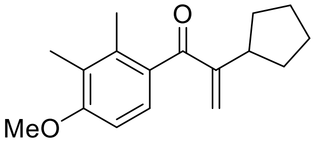

O
MeO

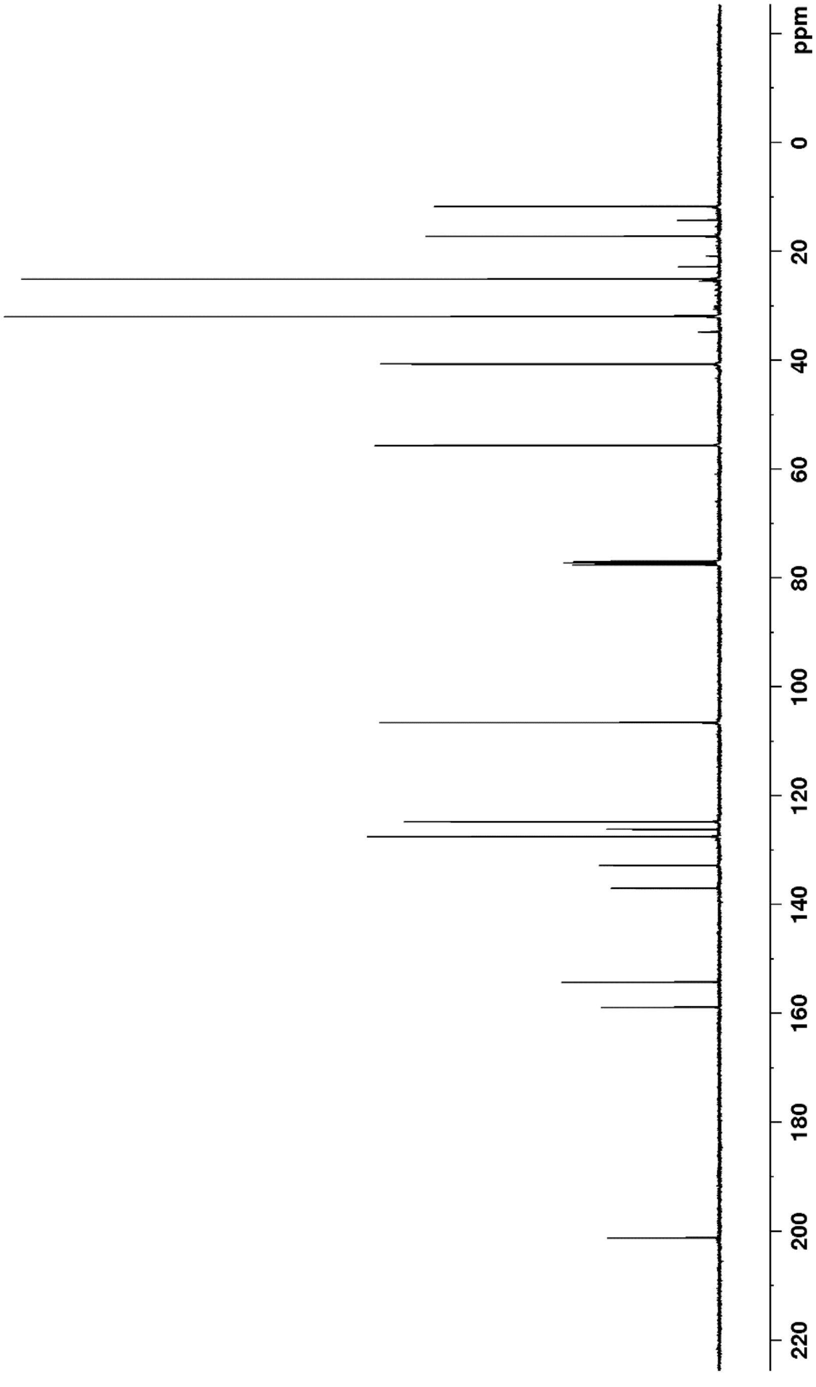

ppm
0
20
40
60
80
100
120
140
160
180
200
220

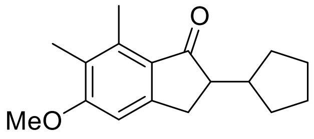
O
MeO

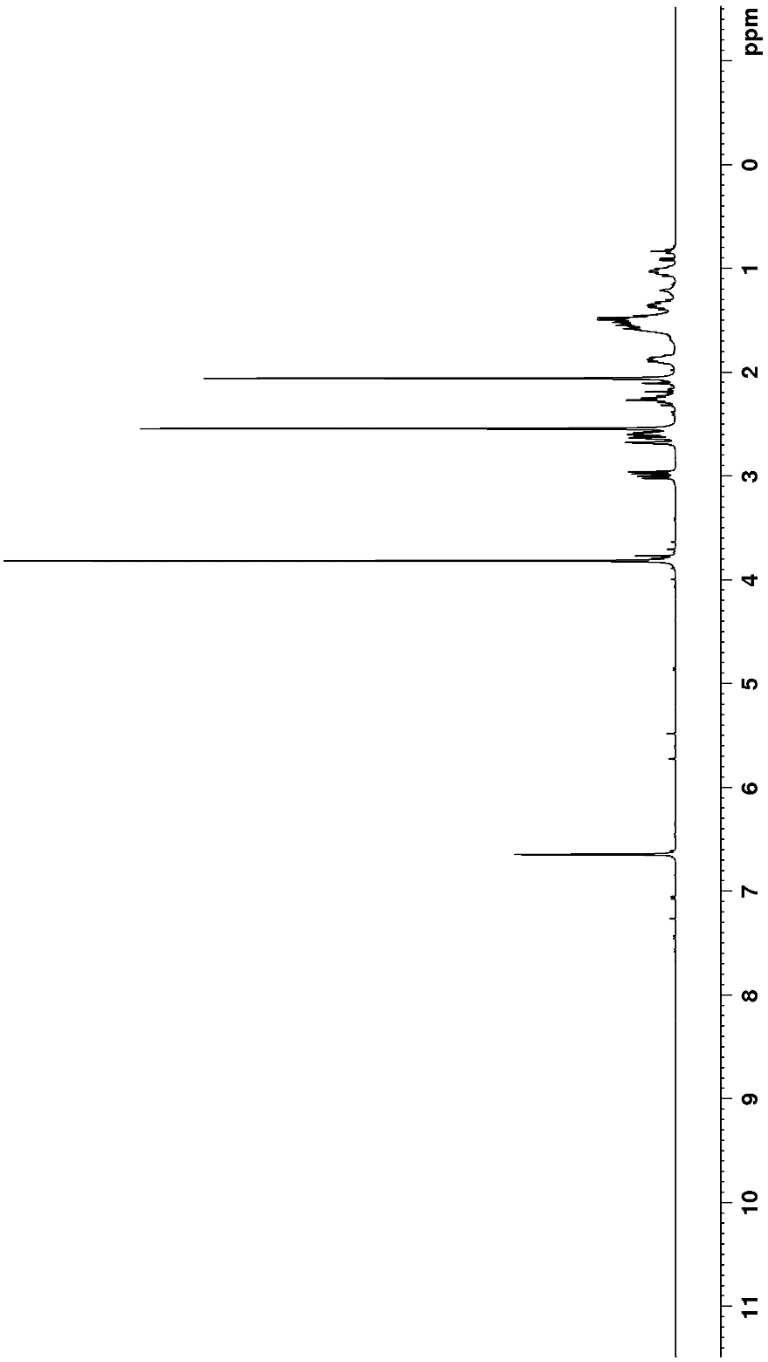
ppm
0
1
2
3
4
5
6
7
8
9
10
11

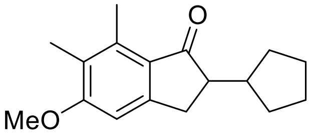
O
MeO

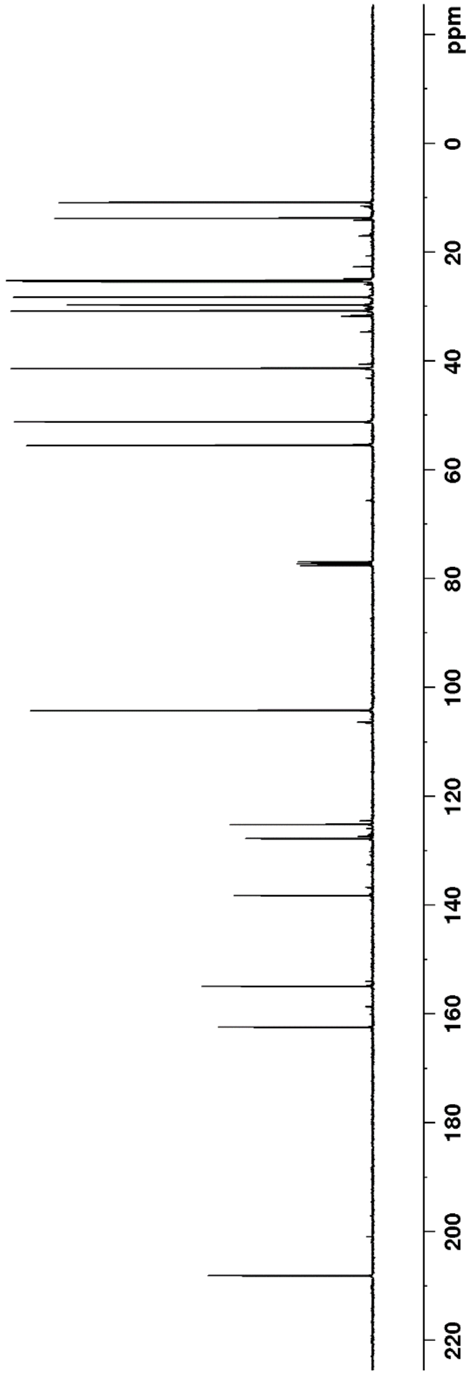
ppm
0
20
40
60
80
100
120
140
160
180
200
220

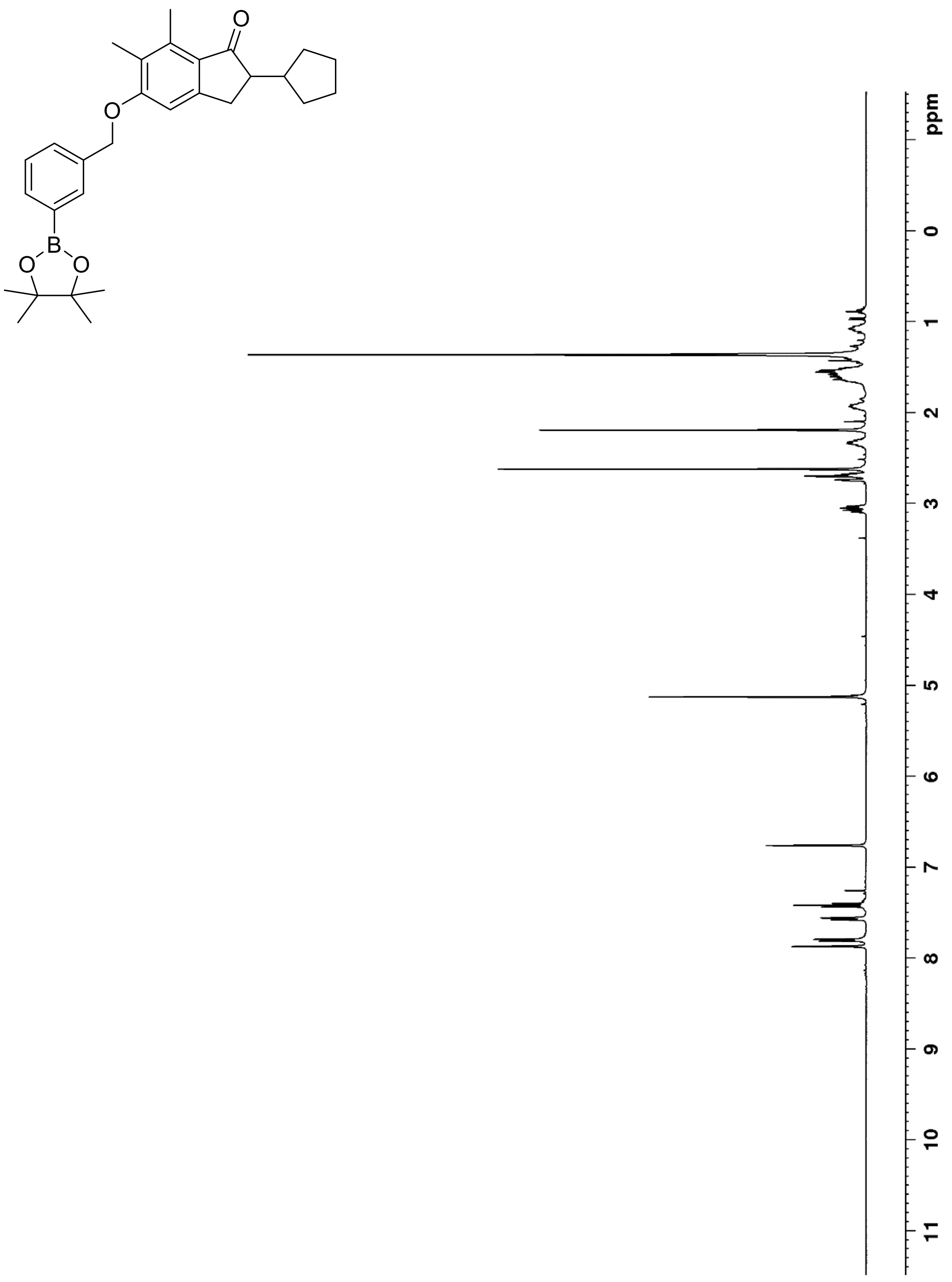
O
O
B
O
O
ppm
0
1
2
3
4
5
6
7
8
9
10
11

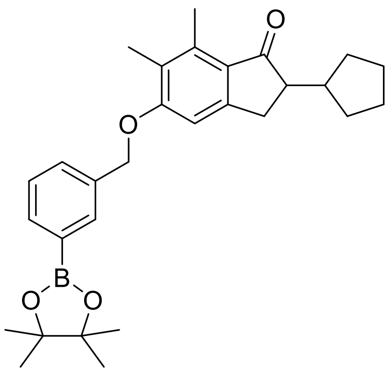
O
O
B
O
O

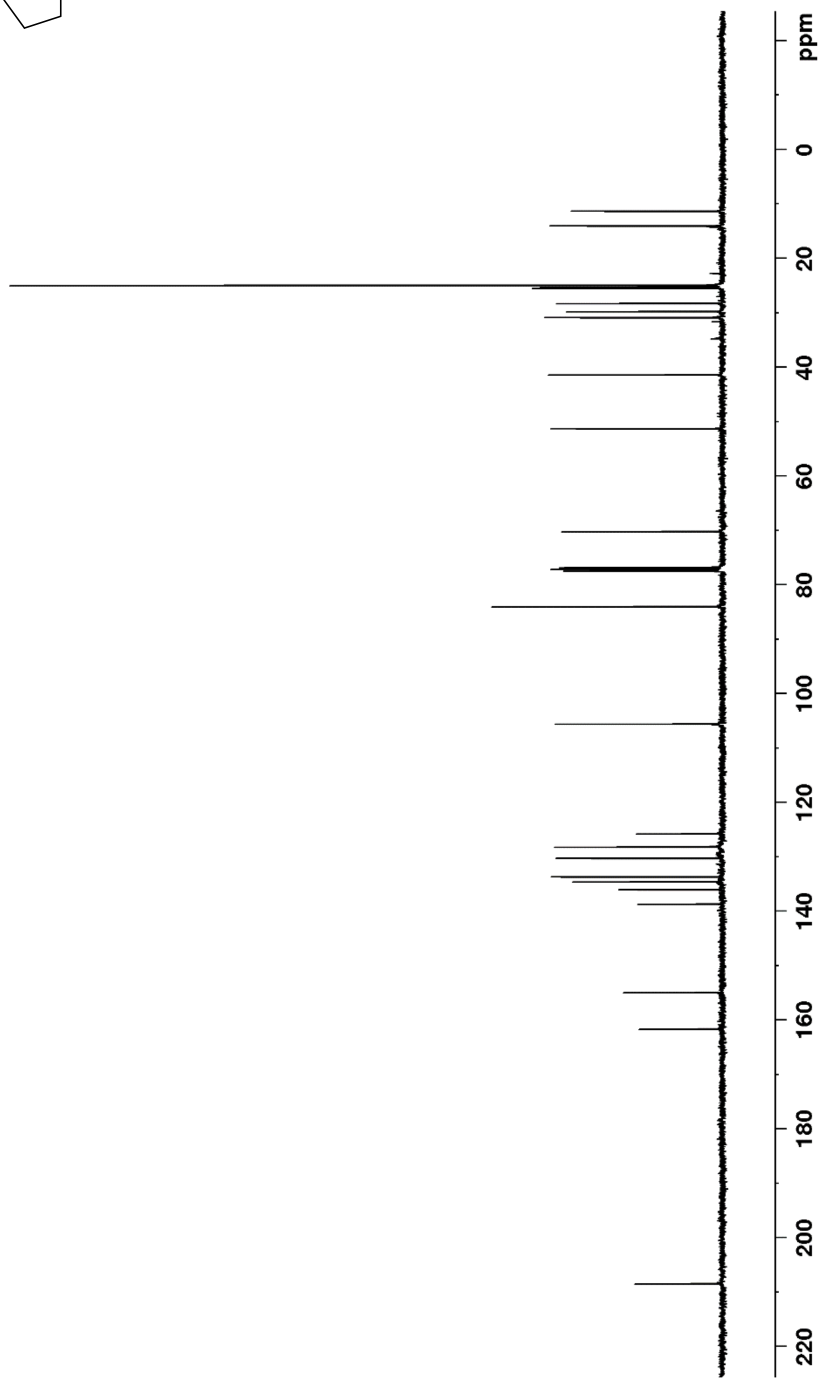
ppm
0
20
40
60
80
100
120
140
160
180
200
220

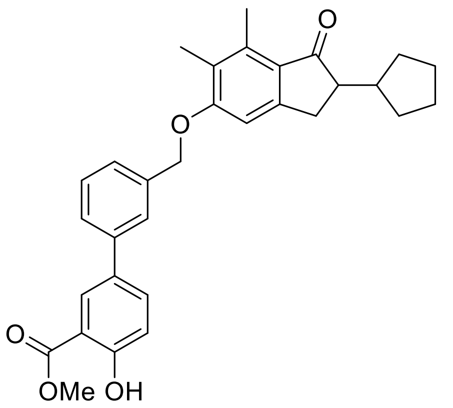
O
O
O
OMe OH

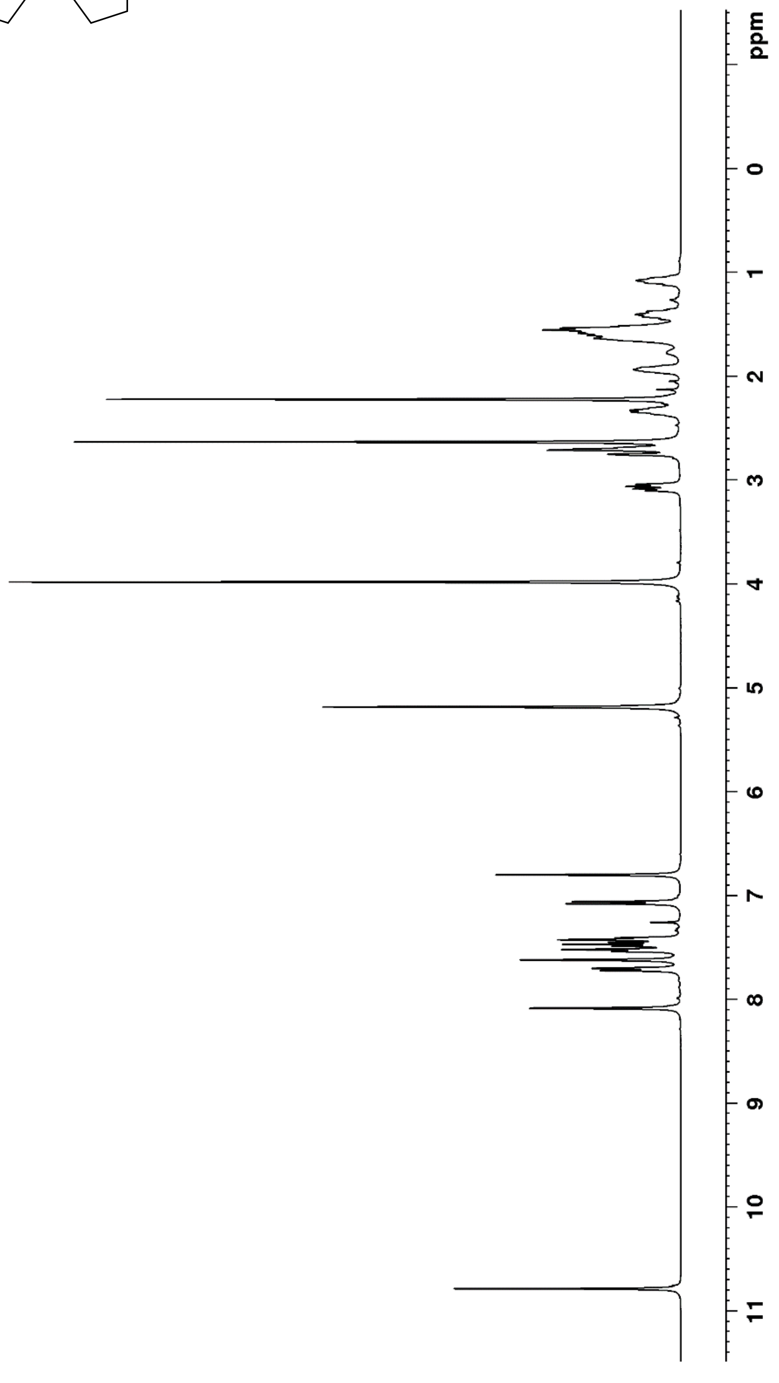
ppm
0
1
2
3
4
5
6
7
8
9
10
11

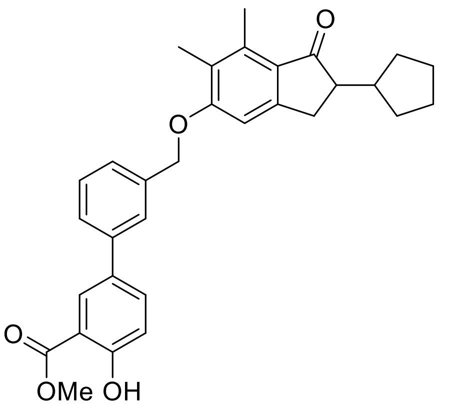
O
O
O
OMe OH

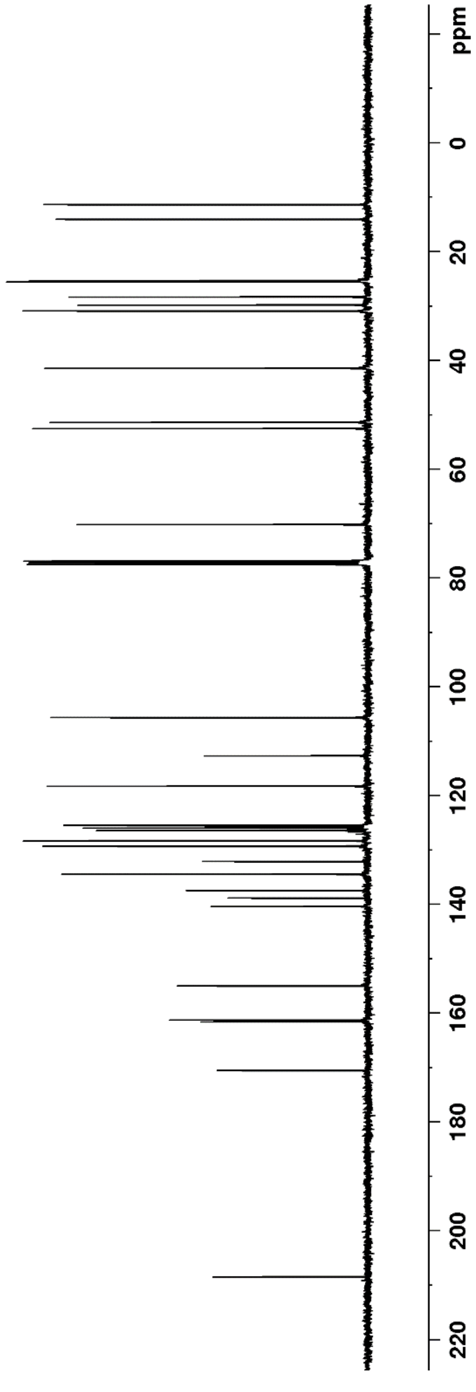
ppm
0
20
40
60
80
100
120
140
160
180
200
220

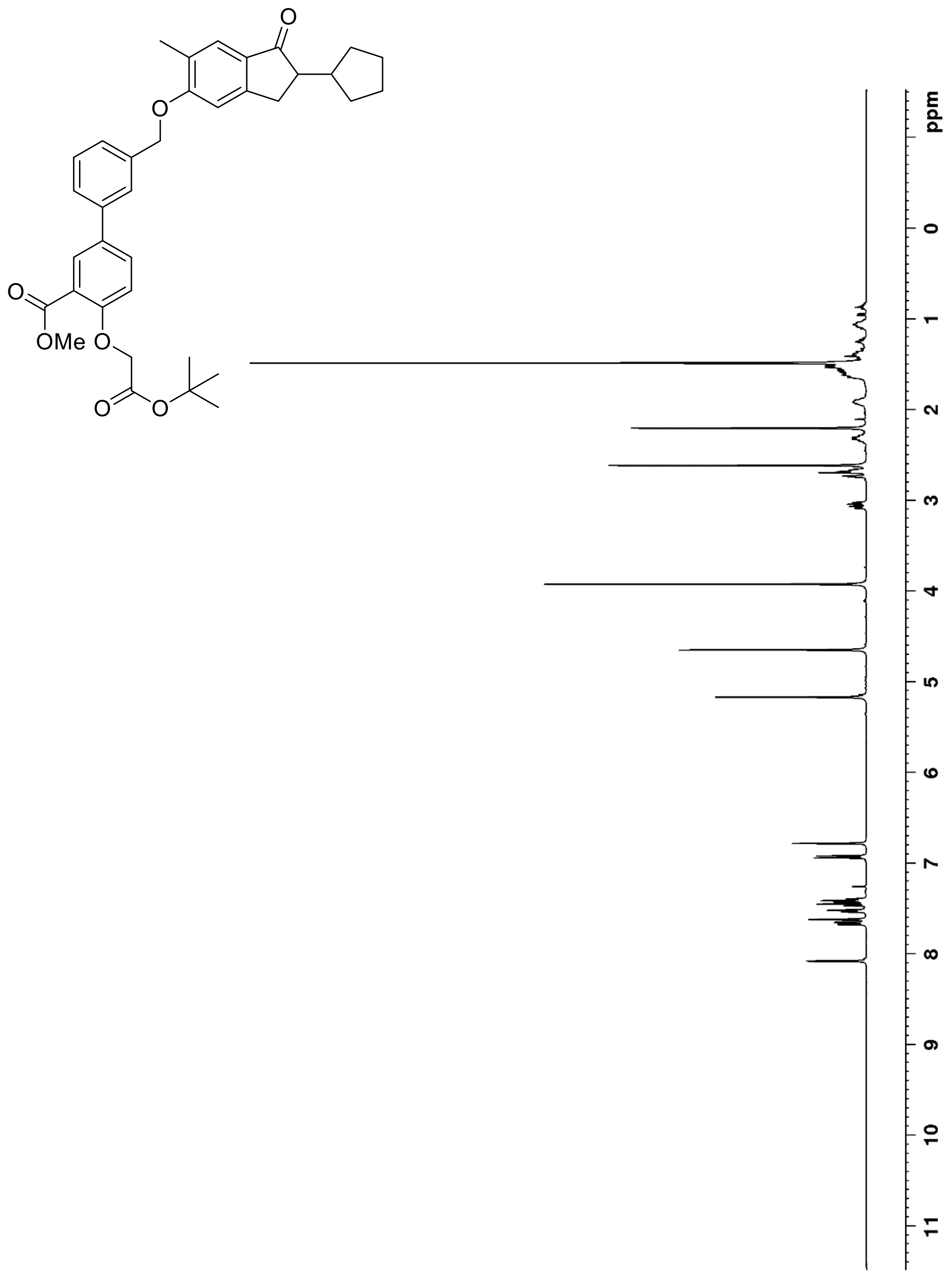
O
OMe
O
O
O
O
O
ppm
0
1
2
3
4
5
6
7
8
9
10
11

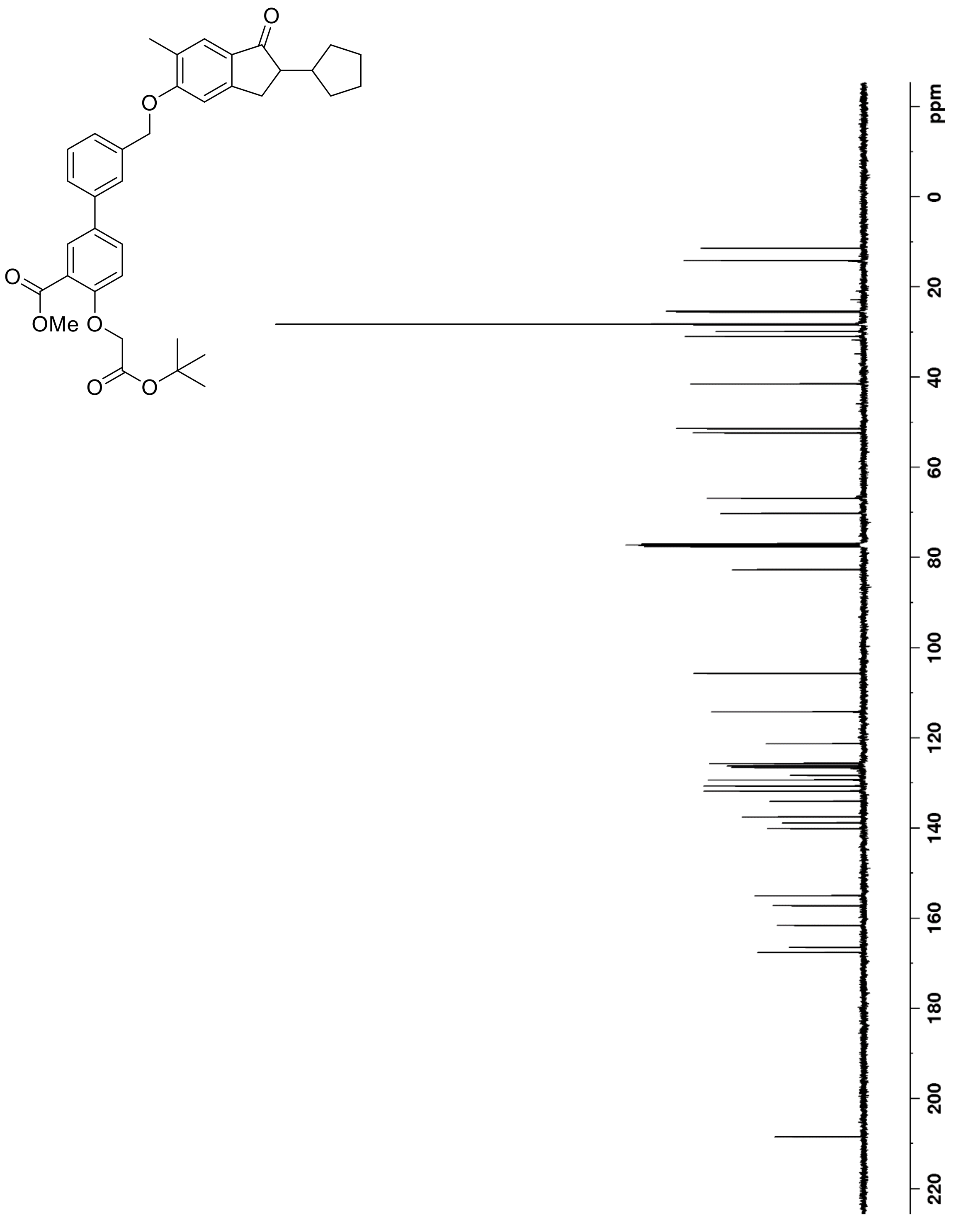
O
O
O
OMe
O
O
O
ppm
0
20
40
60
80
100
120
140
160
180
200
220

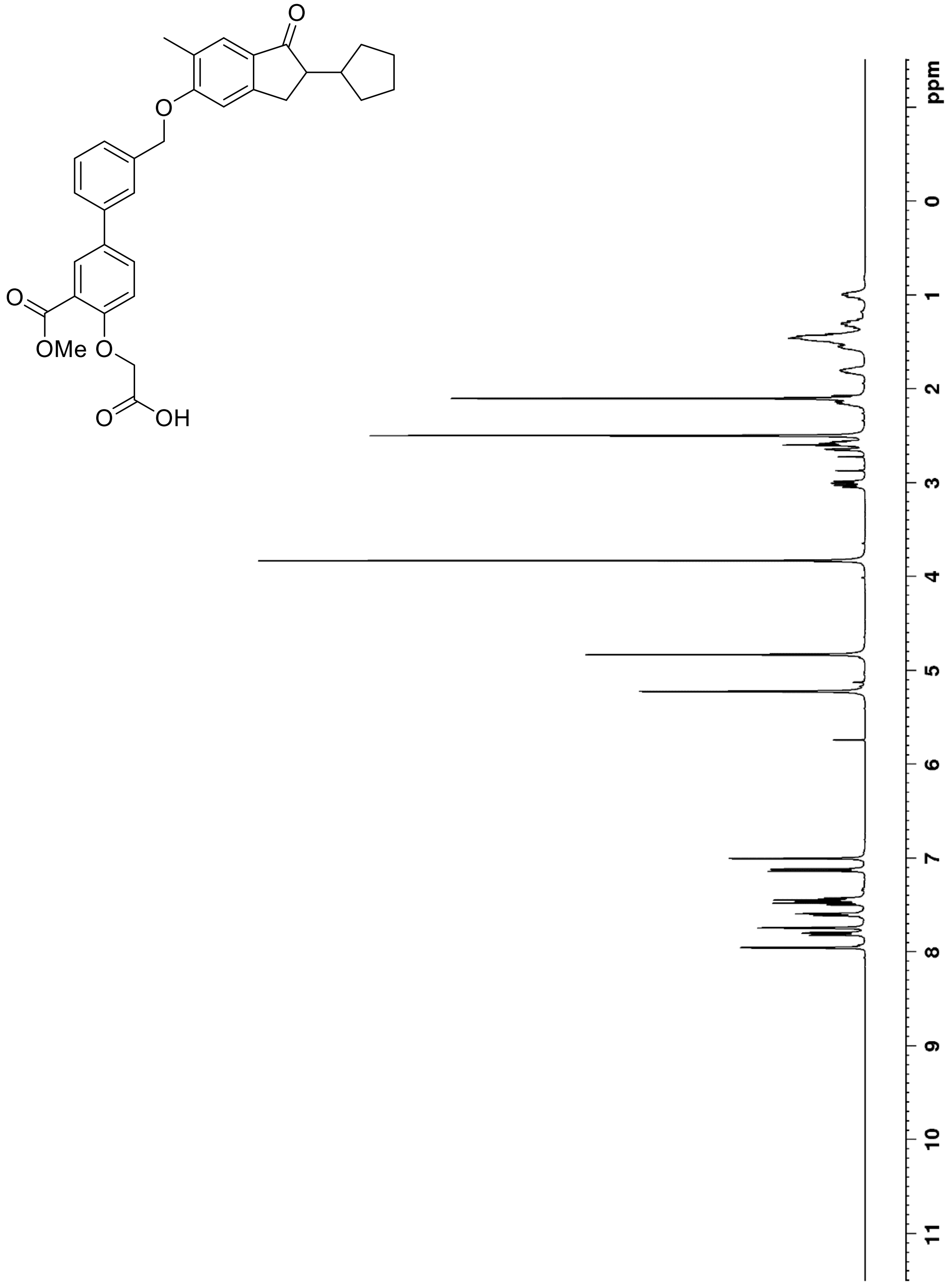
O
OMe
O
O
OH
O
O
ppm
0
1
2
3
4
5
6
7
8
9
10
11

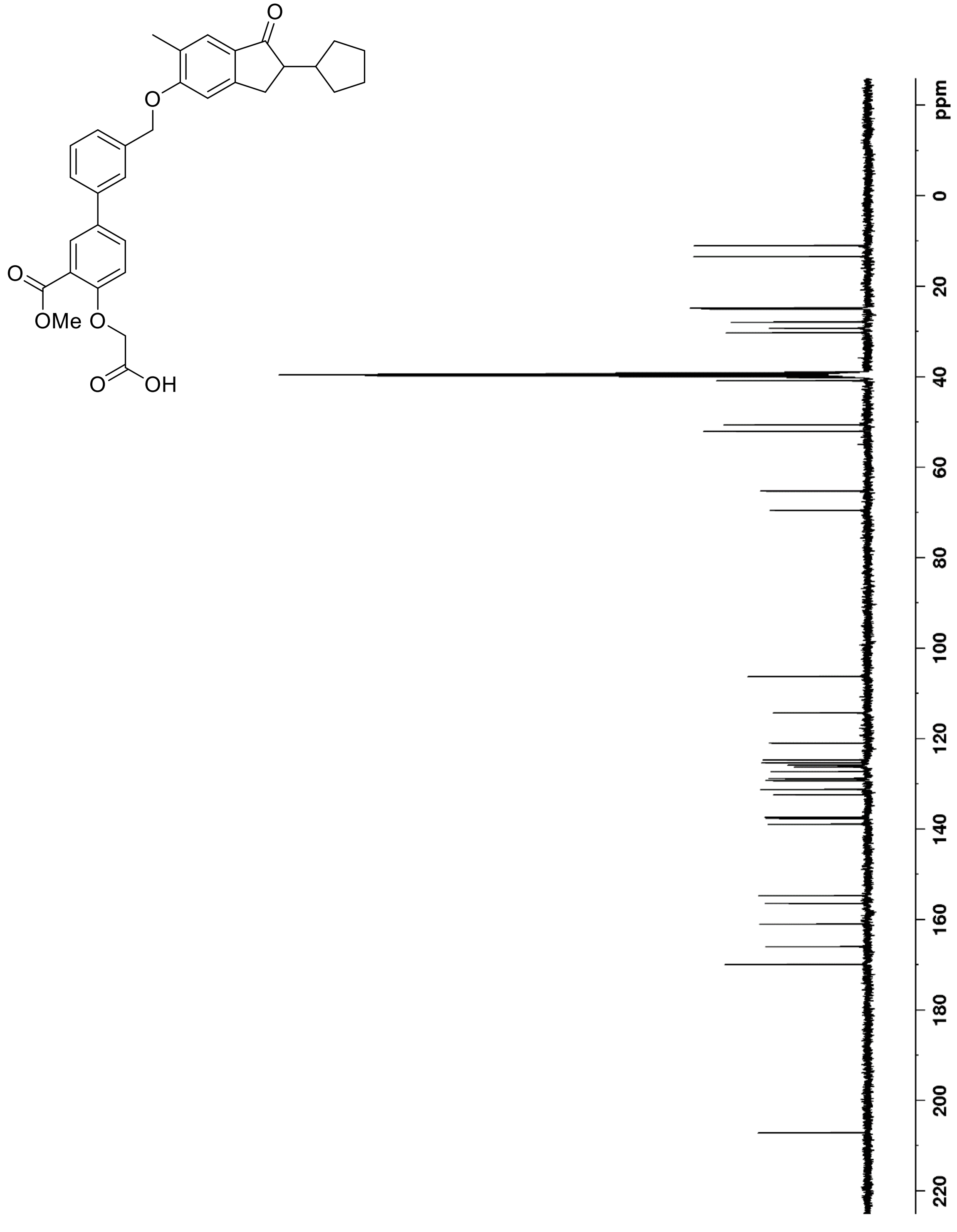
O
O
OMe
O
O
OH
O
ppm
0
20
40
60
80
100
120
140
160
180
200
220

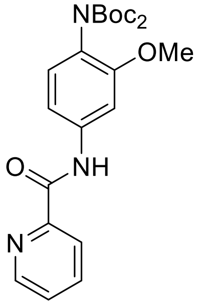
NBoc2
OMe
NH
O
N

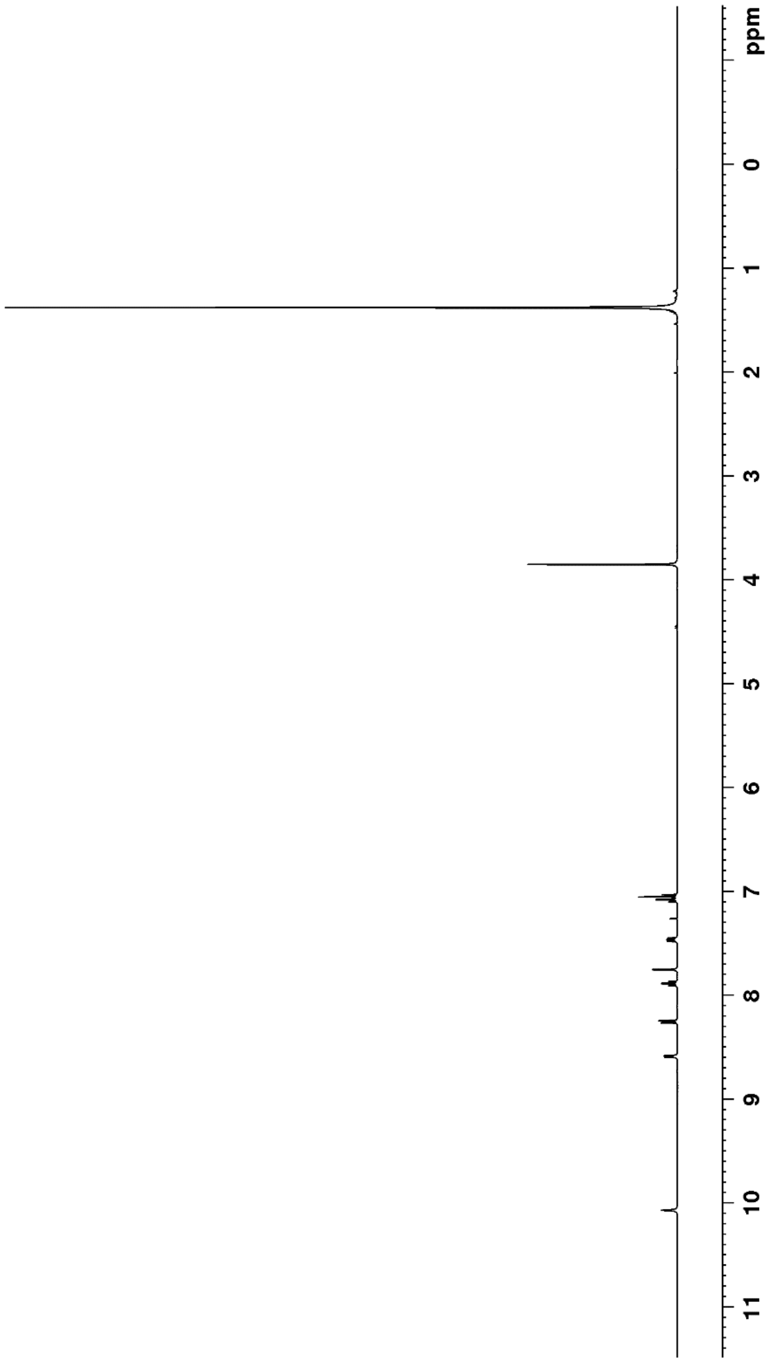
ppm
0
1
2
3
4
5
6
7
8
9
10
11

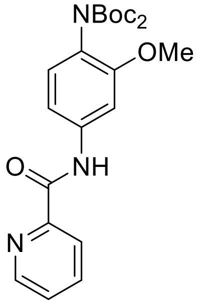
NBoc$_2$
OMe
O
NH
N

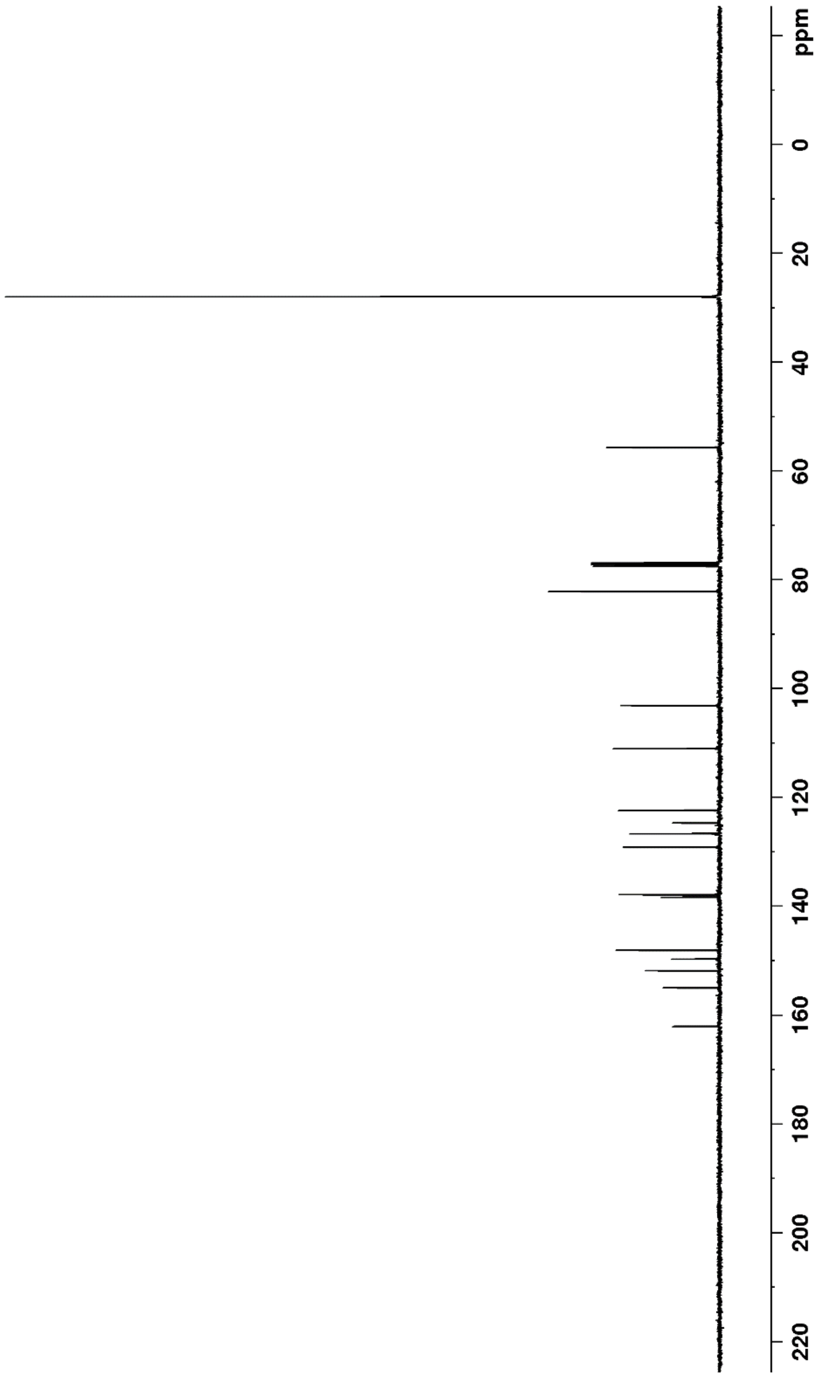
ppm
0
20
40
60
80
100
120
140
160
180
200
220

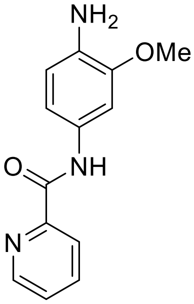
NH2
OMe
O
NH
N

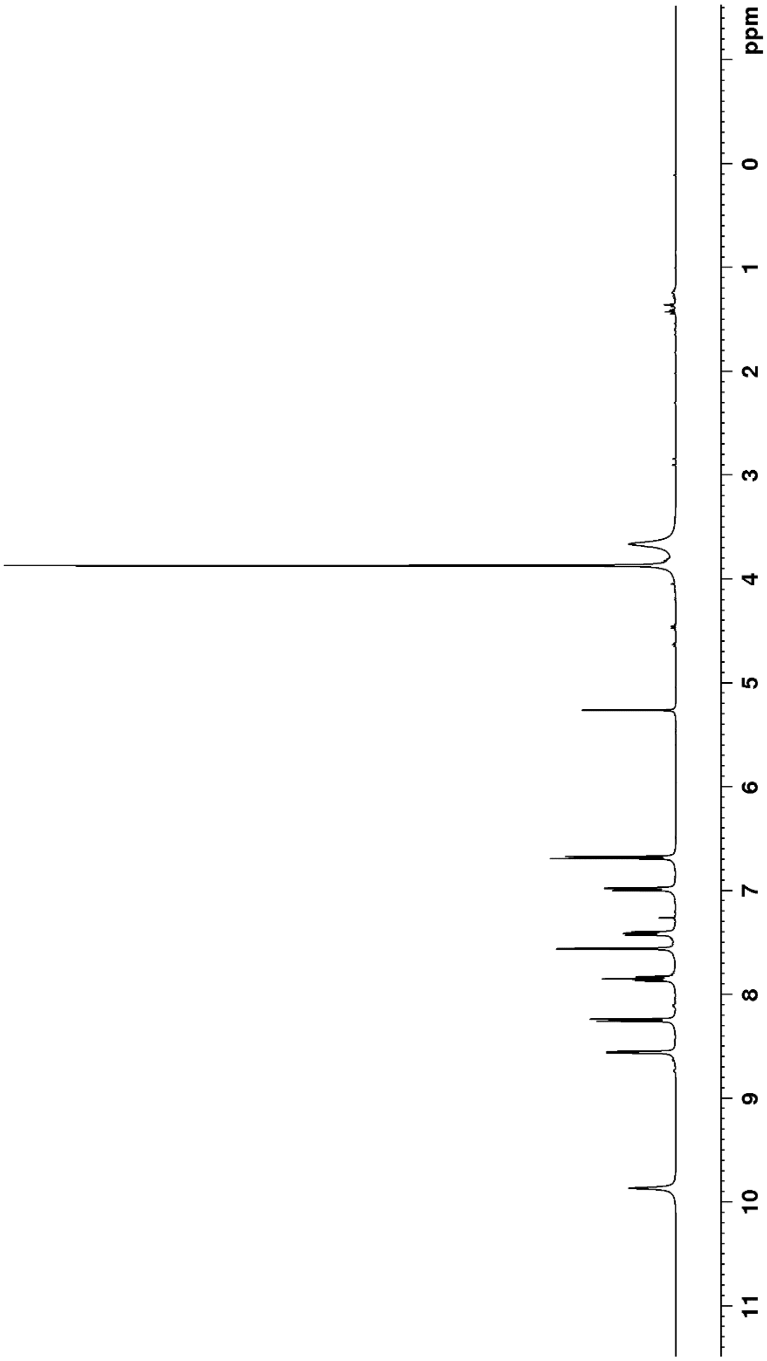
ppm
0
1
2
3
4
5
6
7
8
9
10
11

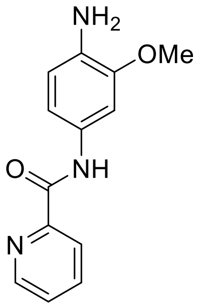
NH2
OMe
O
NH
N

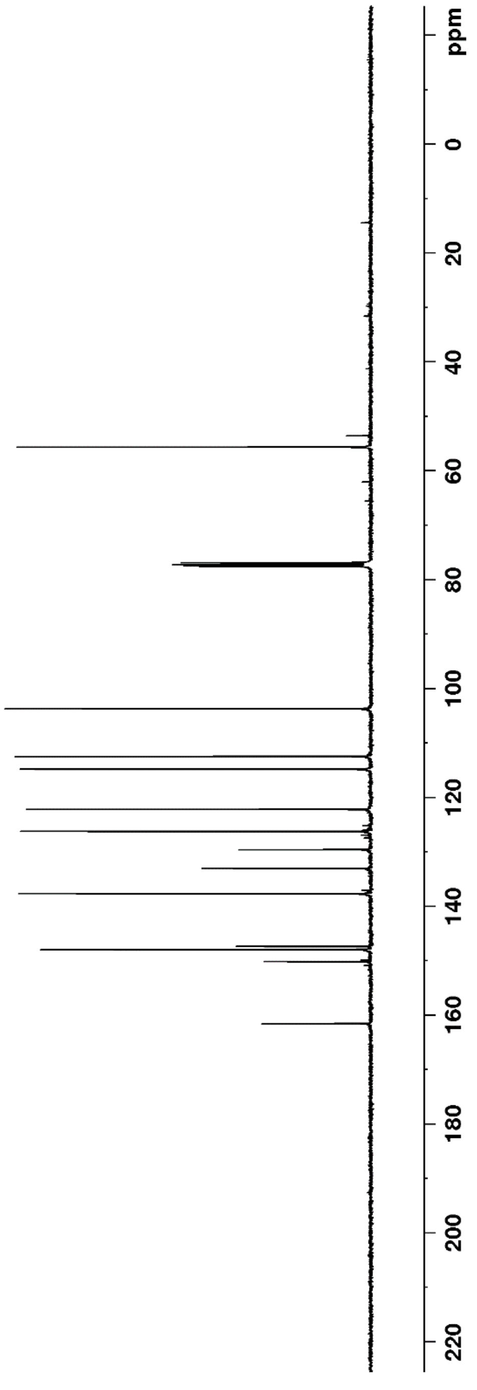
ppm
-20
0
20
40
60
80
100
120
140
160
180
200
220

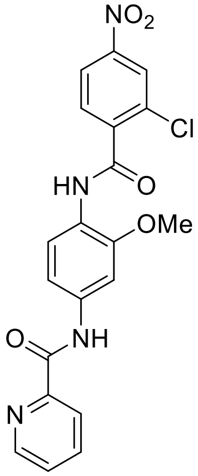
NO2
Cl
HN
O
OMe
O
NH
N

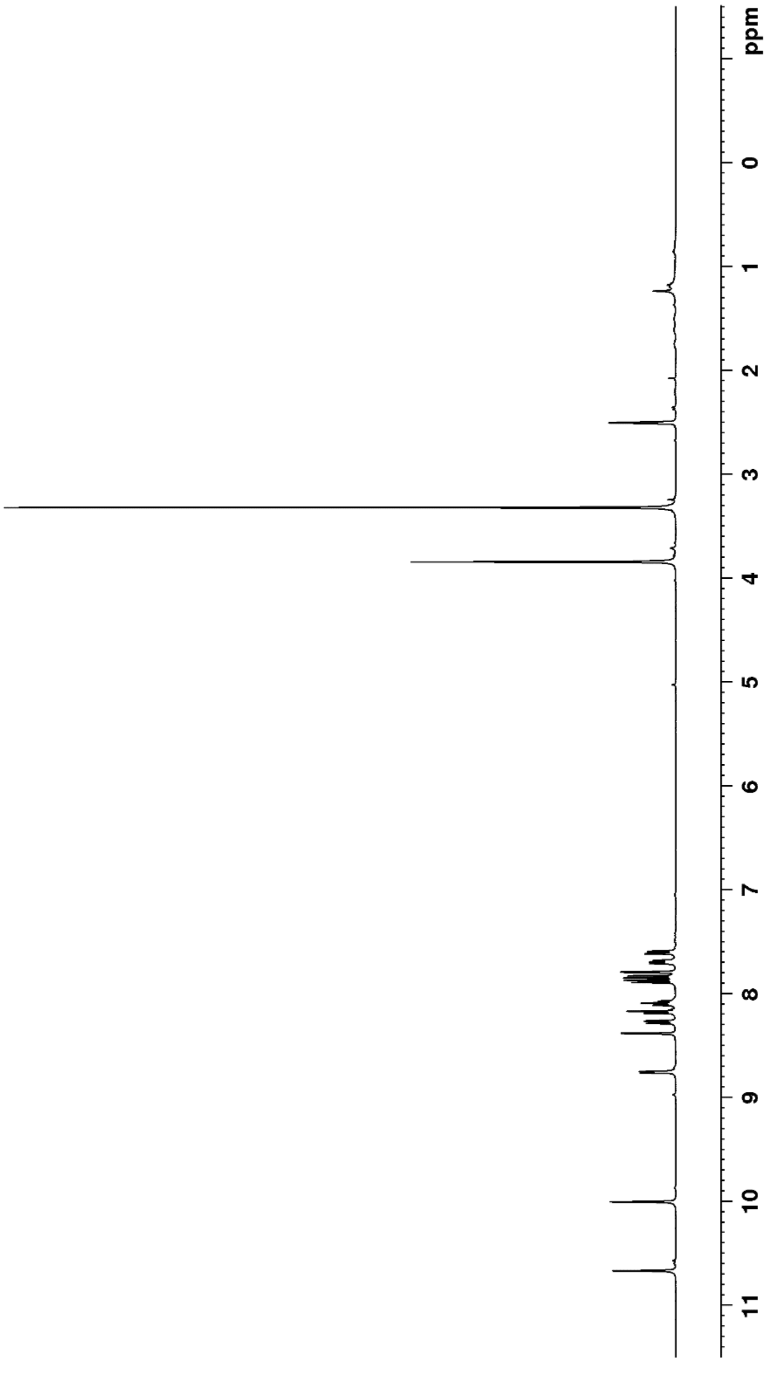
ppm
0
1
2
3
4
5
6
7
8
9
10
11

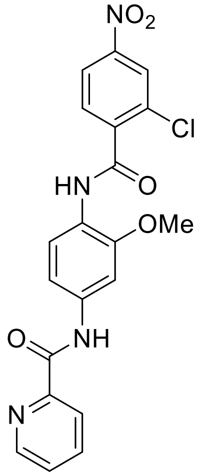
NO2
Cl
HN
O
OMe
O
NH
N

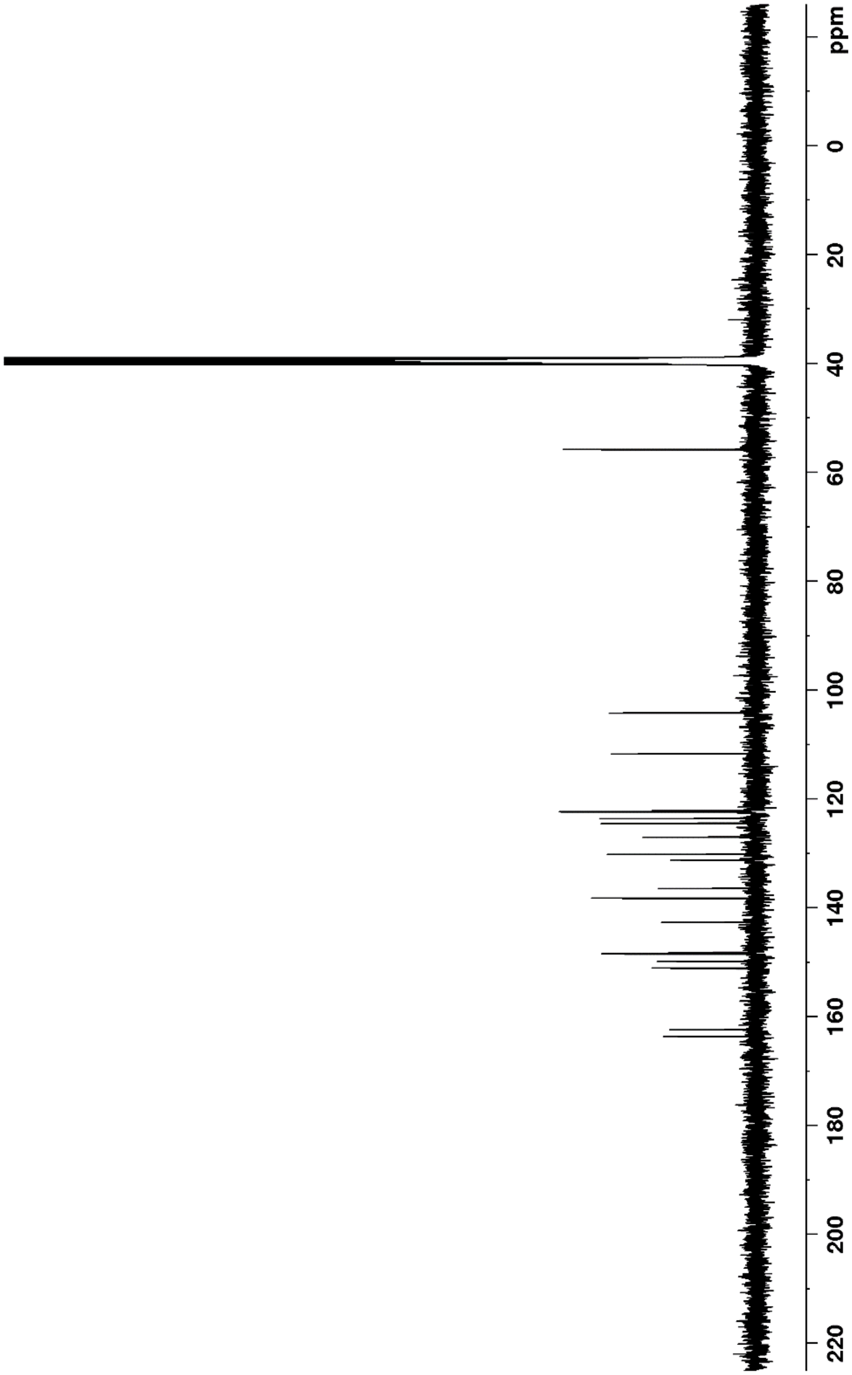
ppm
0
20
40
60
80
100
120
140
160
180
200
220

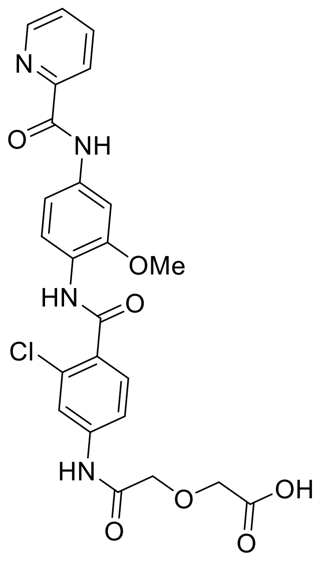

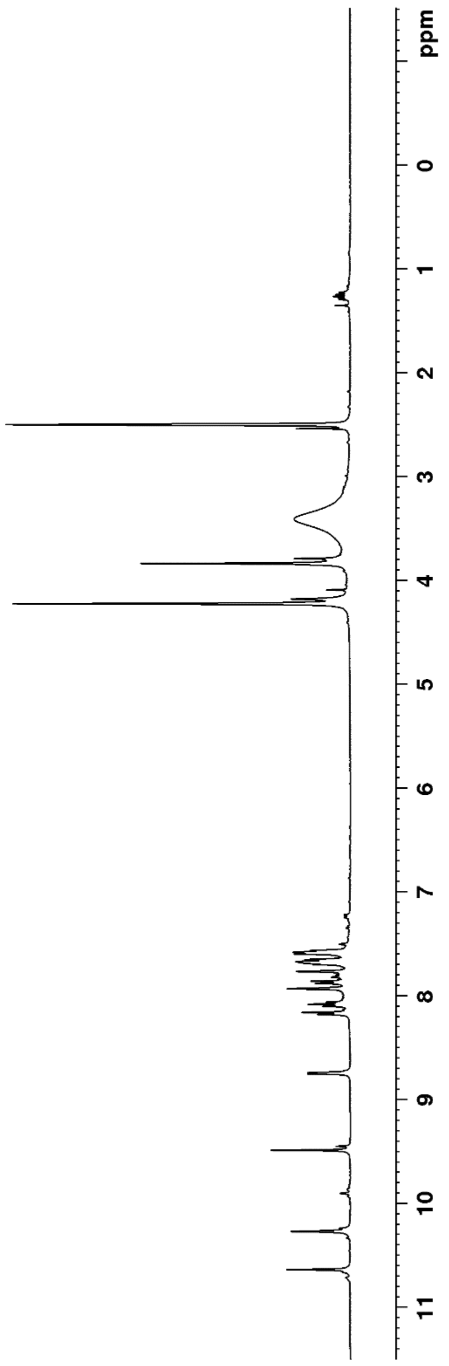
ppm
0
1
2
3
4
5
6
7
8
9
10
11

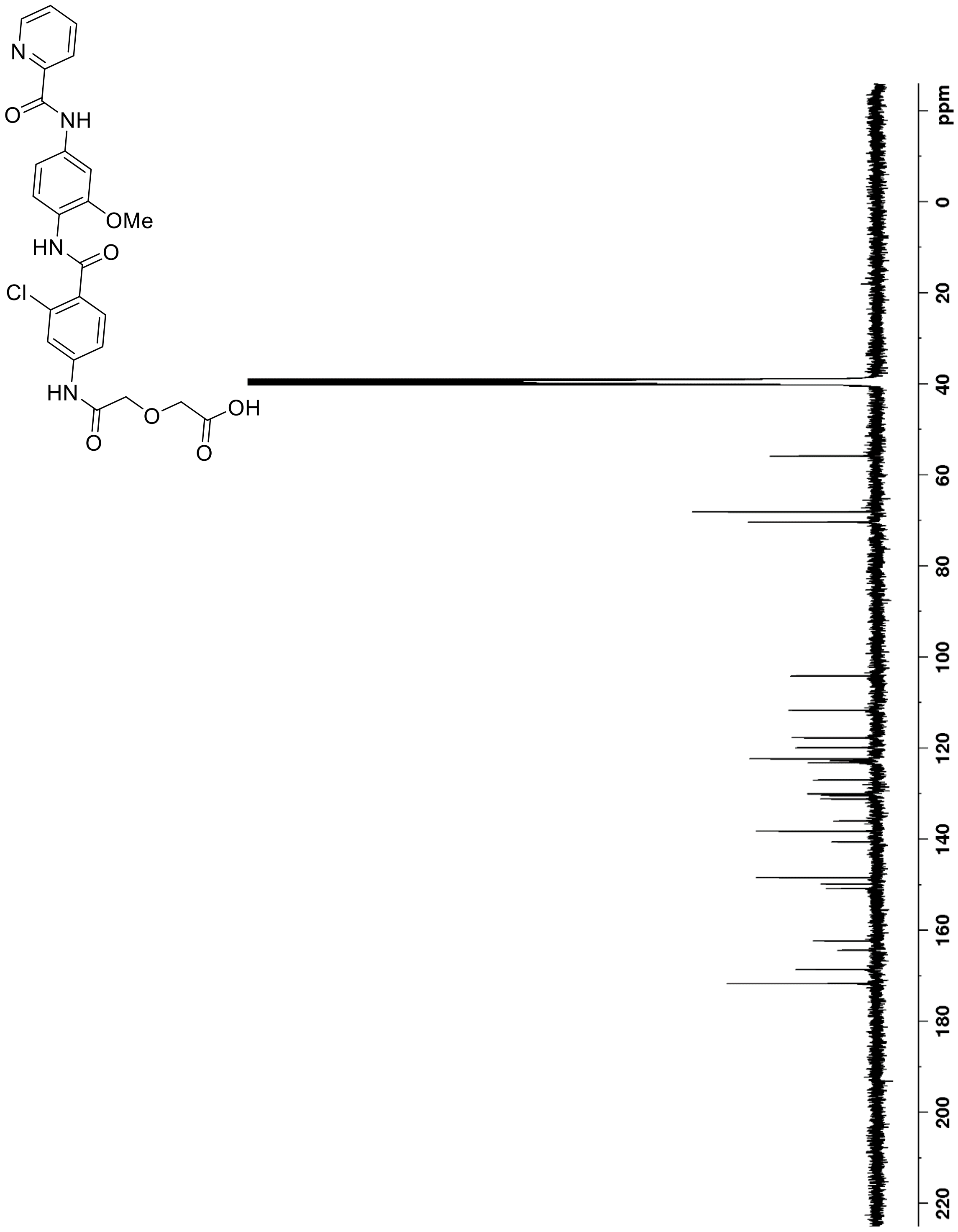
N
O
NH
OMe
HN
O
Cl
HN
O
O
OH
O
ppm
0
20
40
60
80
100
120
140
160
180
200
220

Appendix B

Relevant Spectra for Chapter 2

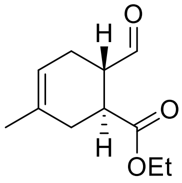
H
O
O
H
OEt

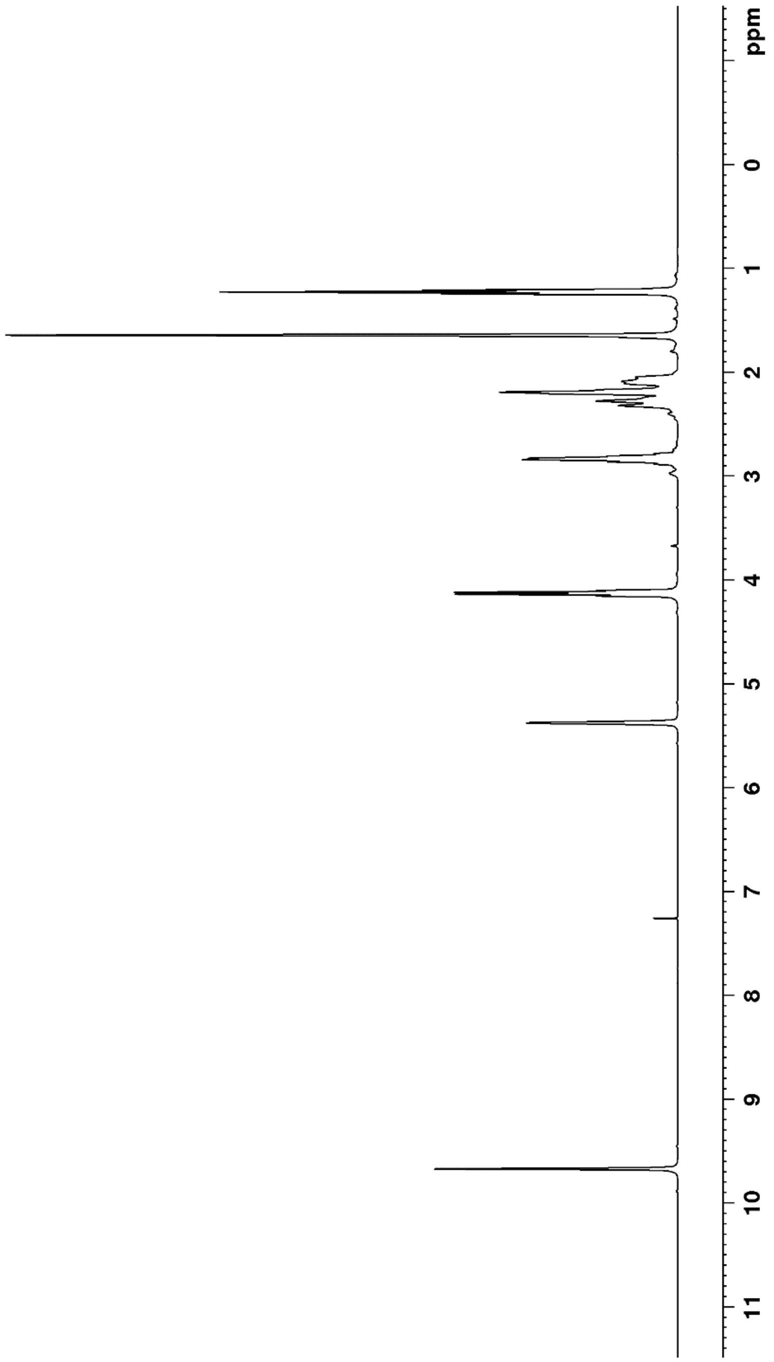
11
10
9
8
7
6
5
4
3
2
1
0
ppm

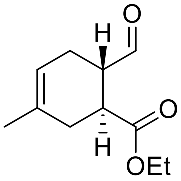
H
O
O
H
OEt

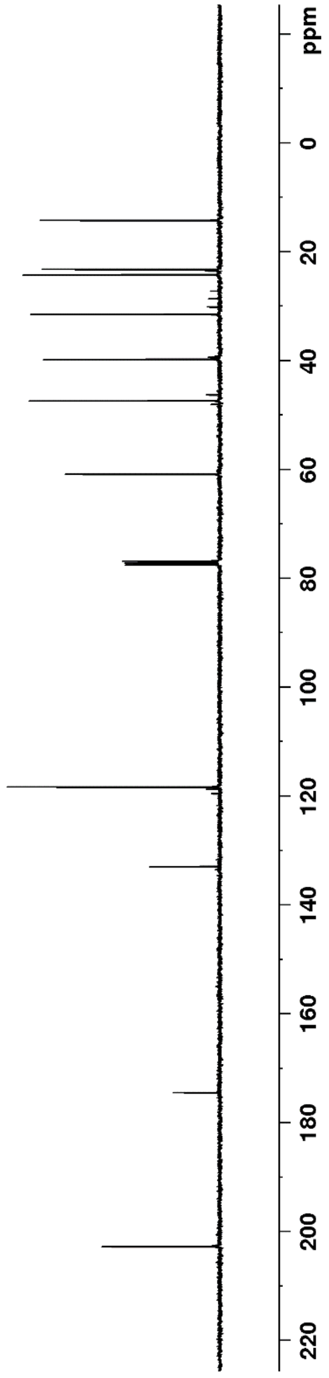
ppm
0
20
40
60
80
100
120
140
160
180
200
220

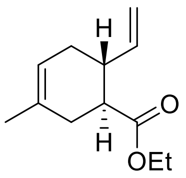
H
H
O
OEt

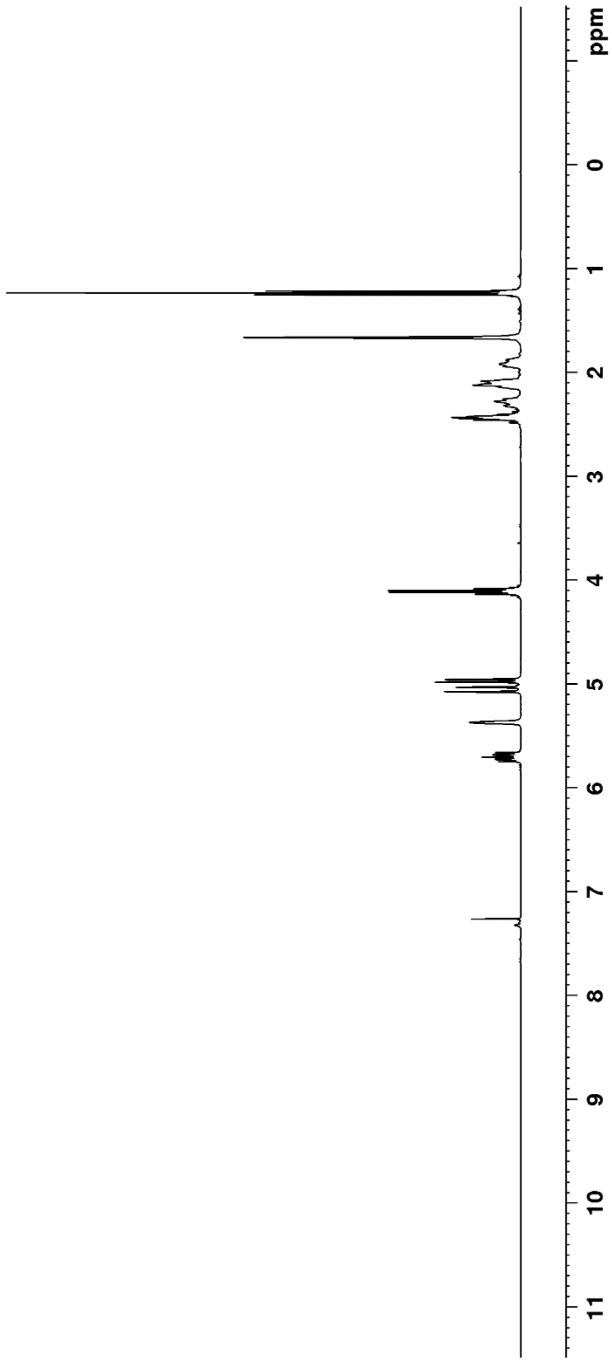
ppm
0
1
2
3
4
5
6
7
8
9
10
11

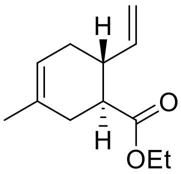
H
O
H
OEt

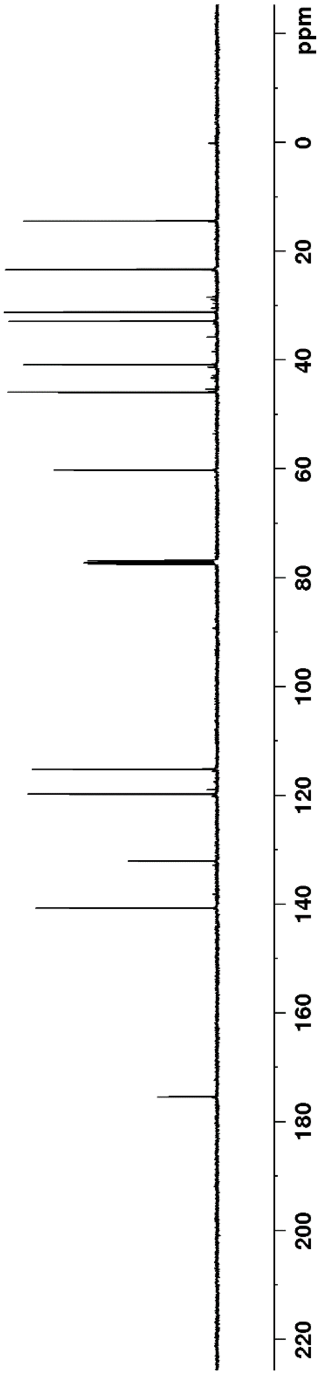
ppm
0
20
40
60
80
100
120
140
160
180
200
220

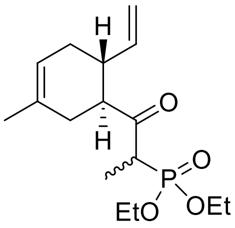
H
O
H
P
O
EtO
OEt

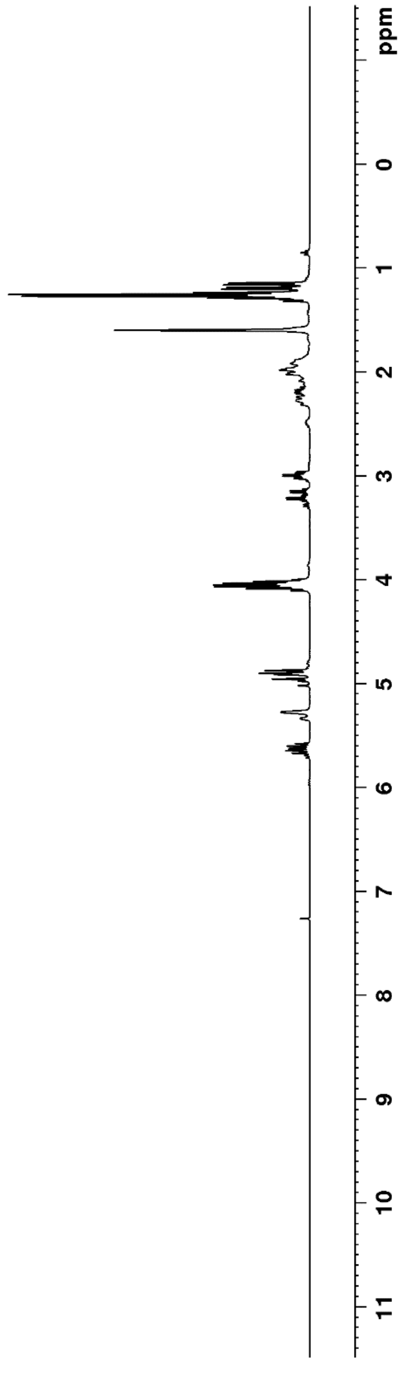
ppm
0
1
2
3
4
5
6
7
8
9
10
11

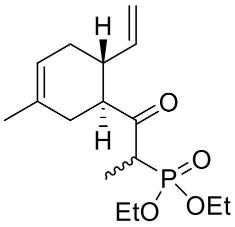
H
O
H
P
O
EtO
OEt

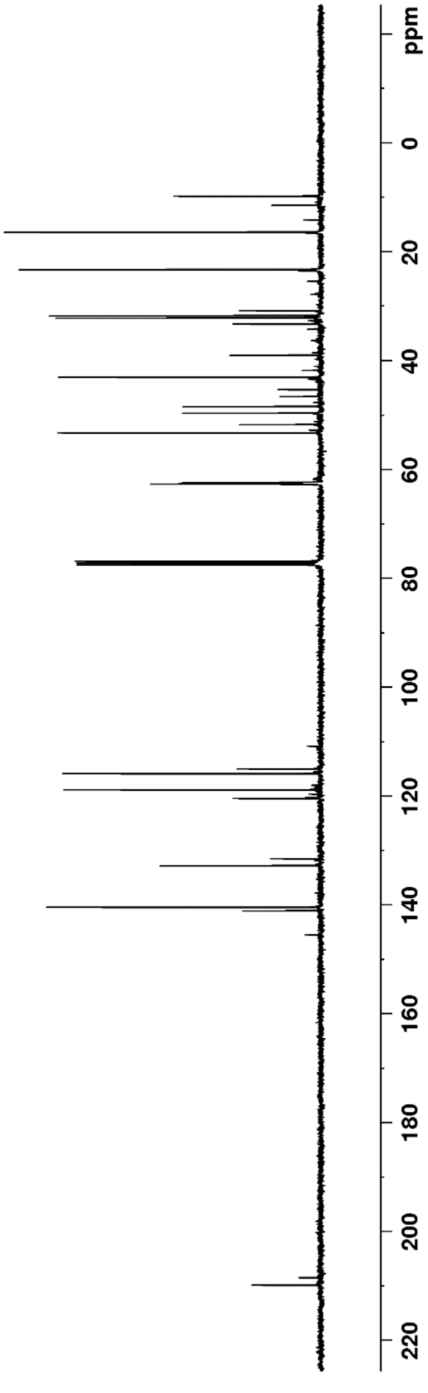
ppm
-20
0
20
40
60
80
100
120
140
160
180
200
220

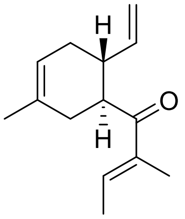
H
O
H

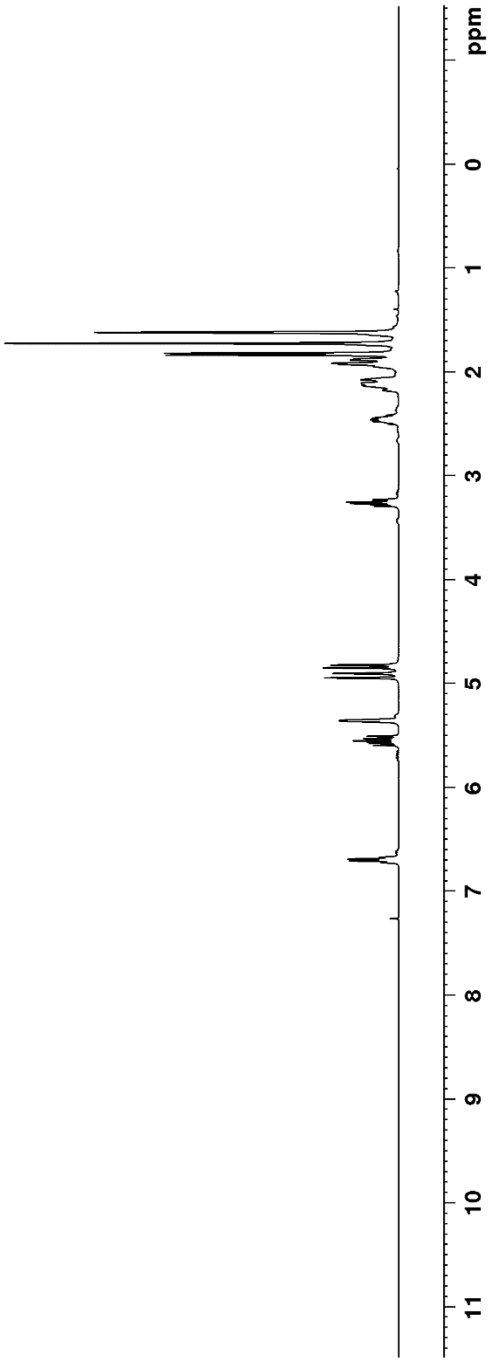
ppm
0
1
2
3
4
5
6
7
8
9
10
11

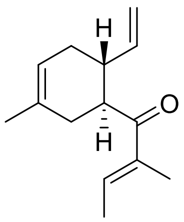
H
O
H

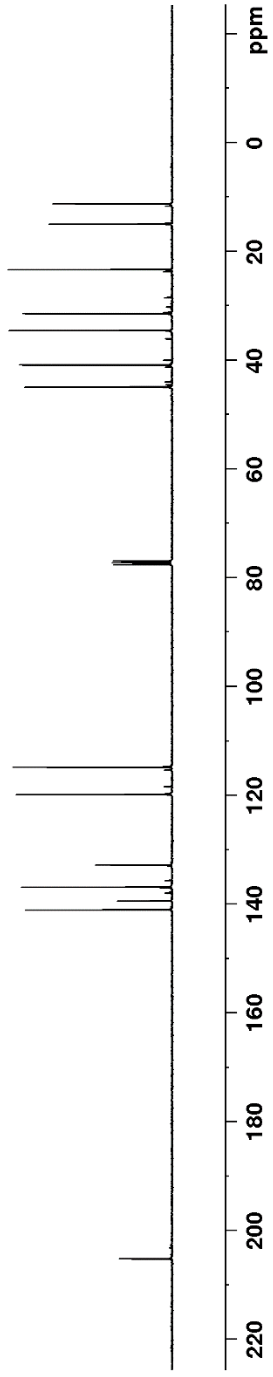
ppm
0
20
40
60
80
100
120
140
160
180
200
220

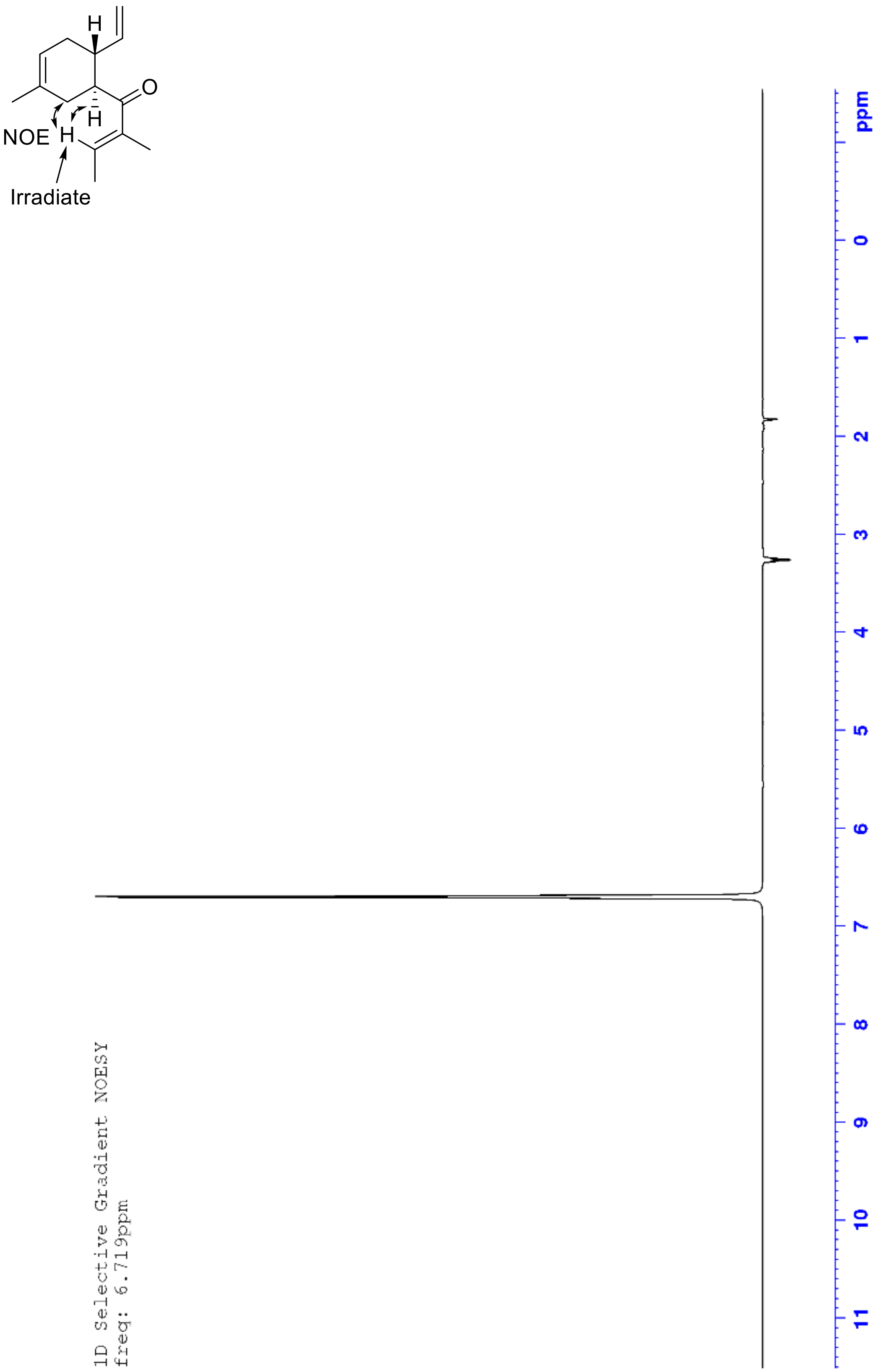
H
O
H
NOE
H
Irradiate
1D Selective Gradient NOESY
freq: 6.719ppm
ppm
0
1
2
3
4
5
6
7
8
9
10
11

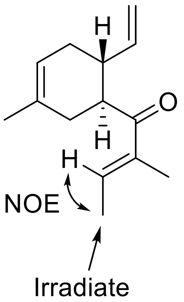
H
O
H
H
NOE
Irradiate

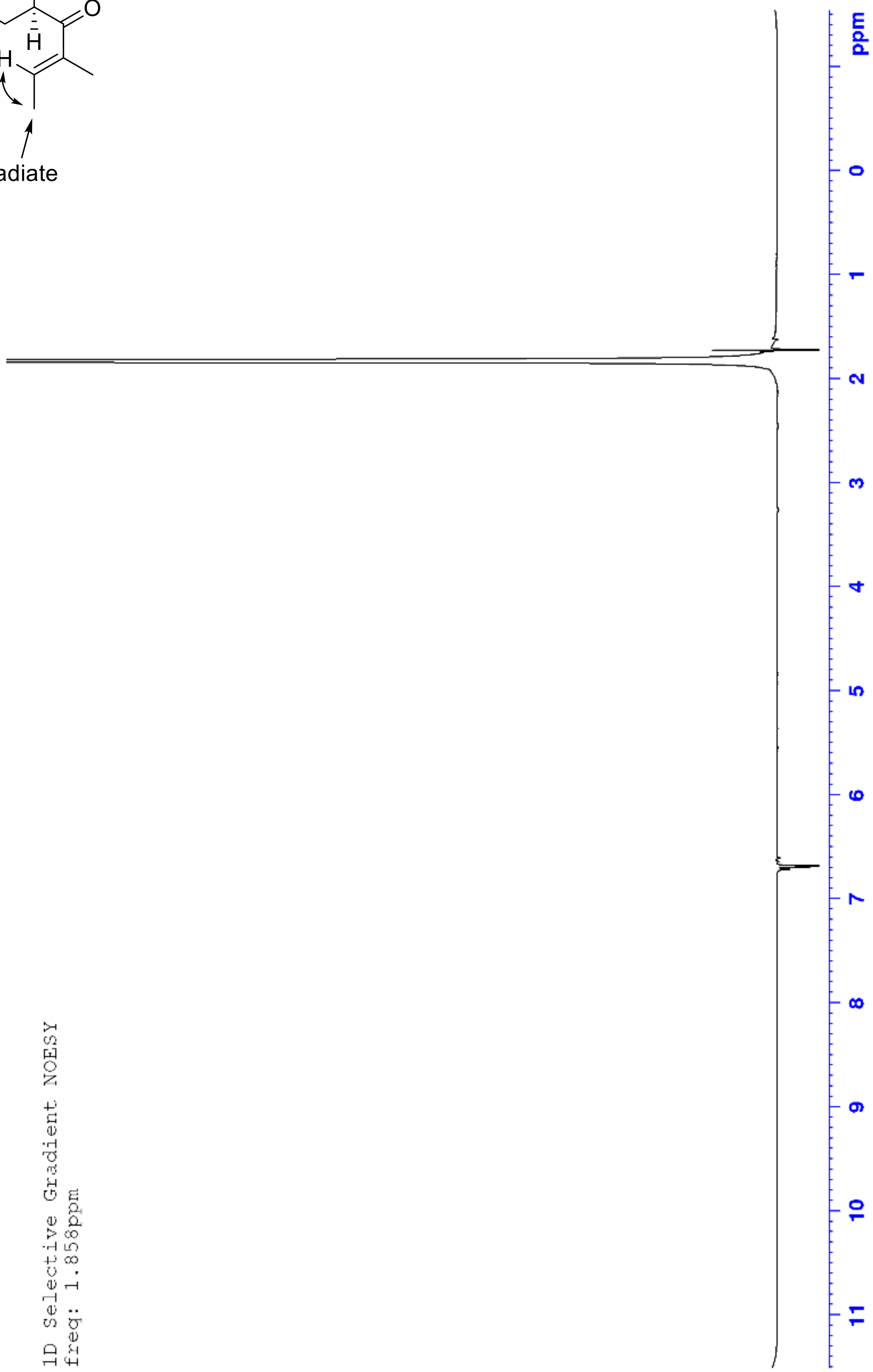
1D Selective Gradient NOESY
freq: 1.858ppm

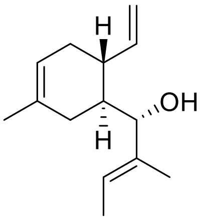
H
OH
H

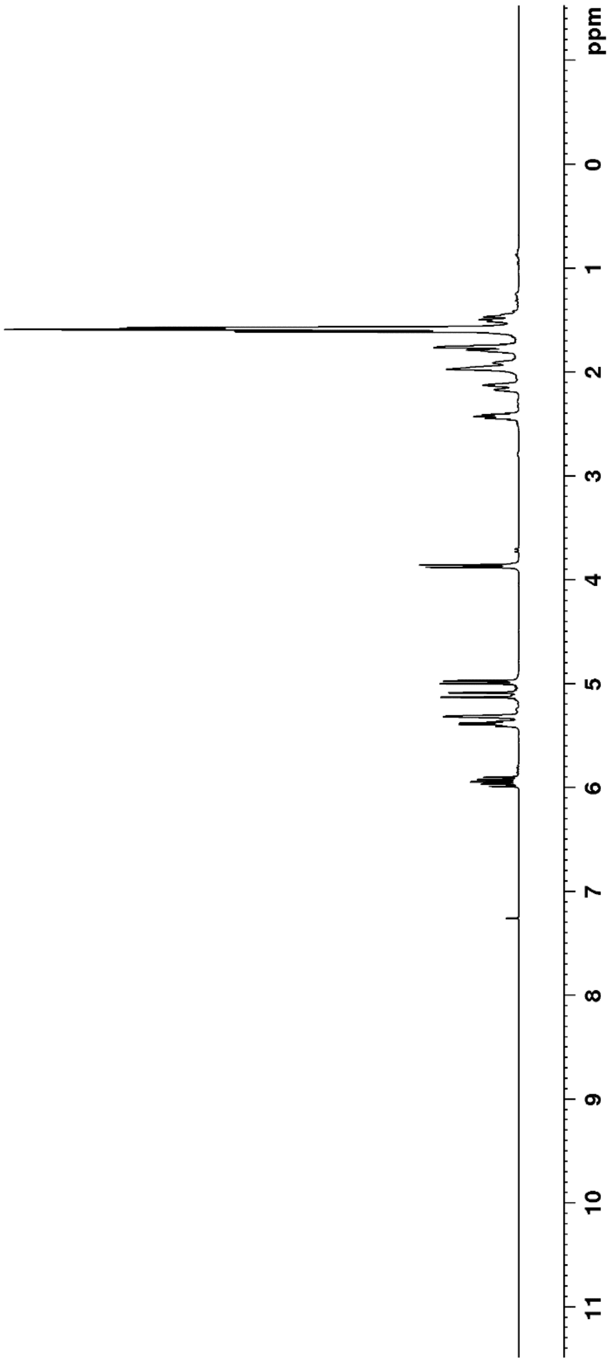
ppm
0
1
2
3
4
5
6
7
8
9
10
11

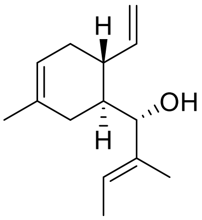
H
OH
H

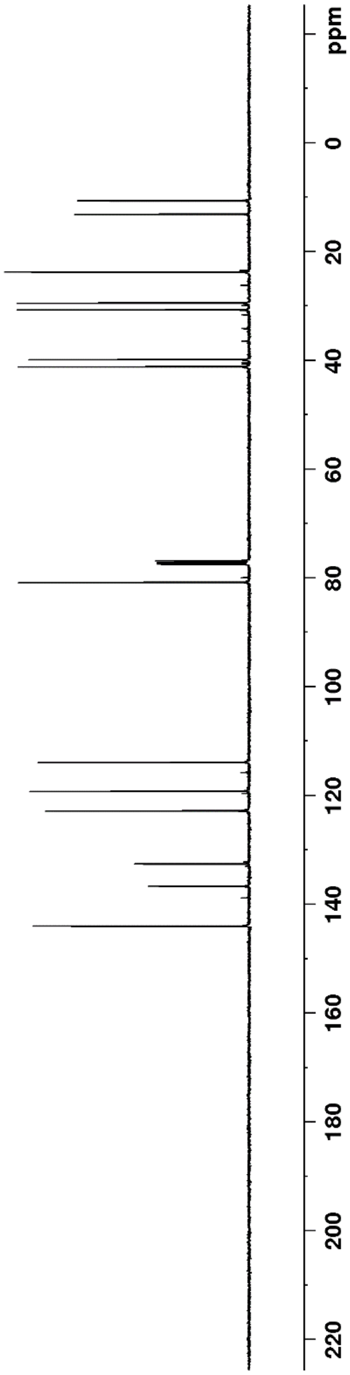
ppm
0
20
40
60
80
100
120
140
160
180
200
220

Mosher Ester Analysis

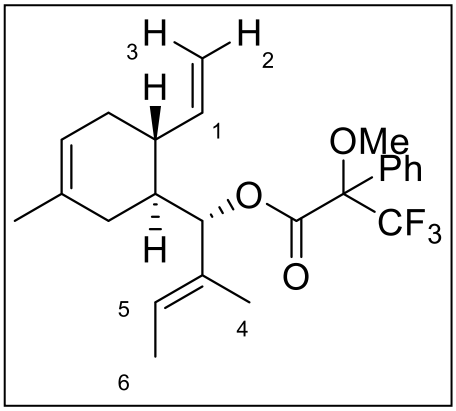

			$\Delta\delta^{SR}(=\delta_S-\delta_R)$	
	S	R	ppm	Hz (400 MHz)
5	5.3366	5.3016	0.03500	14.000
6	1.5599	1.5552	0.00465	1.86
4	1.6418	1.6516	-0.00985	-3.94
1	5.7457	5.8070	-0.06130	-24.52
2	4.8436	4.9411	-0.09753	-39.01
3	4.8776	4.9883	-0.11068	-44.27

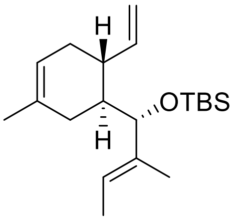
H
OTBS
H

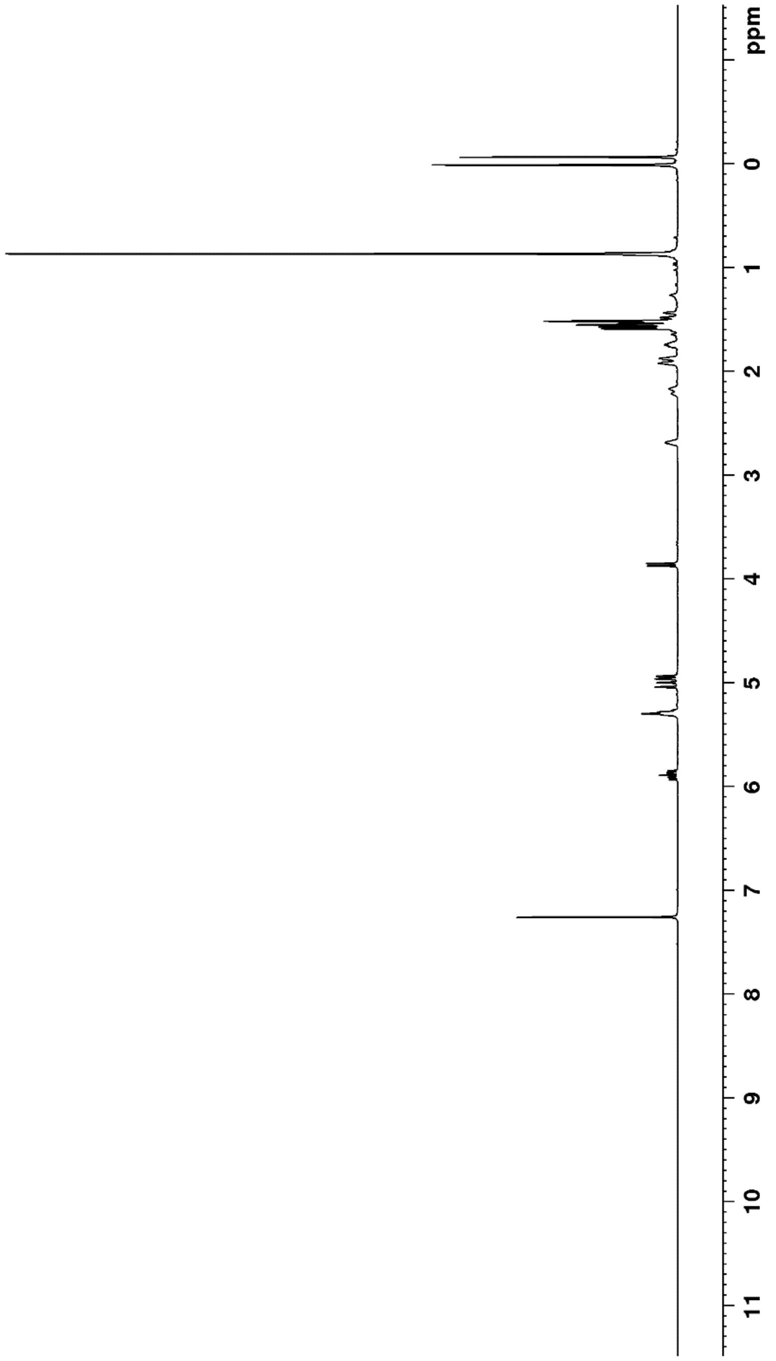
ppm
0
1
2
3
4
5
6
7
8
9
10
11

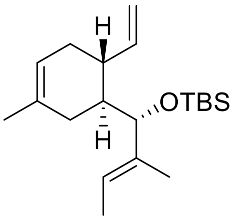
H
OTBS
H

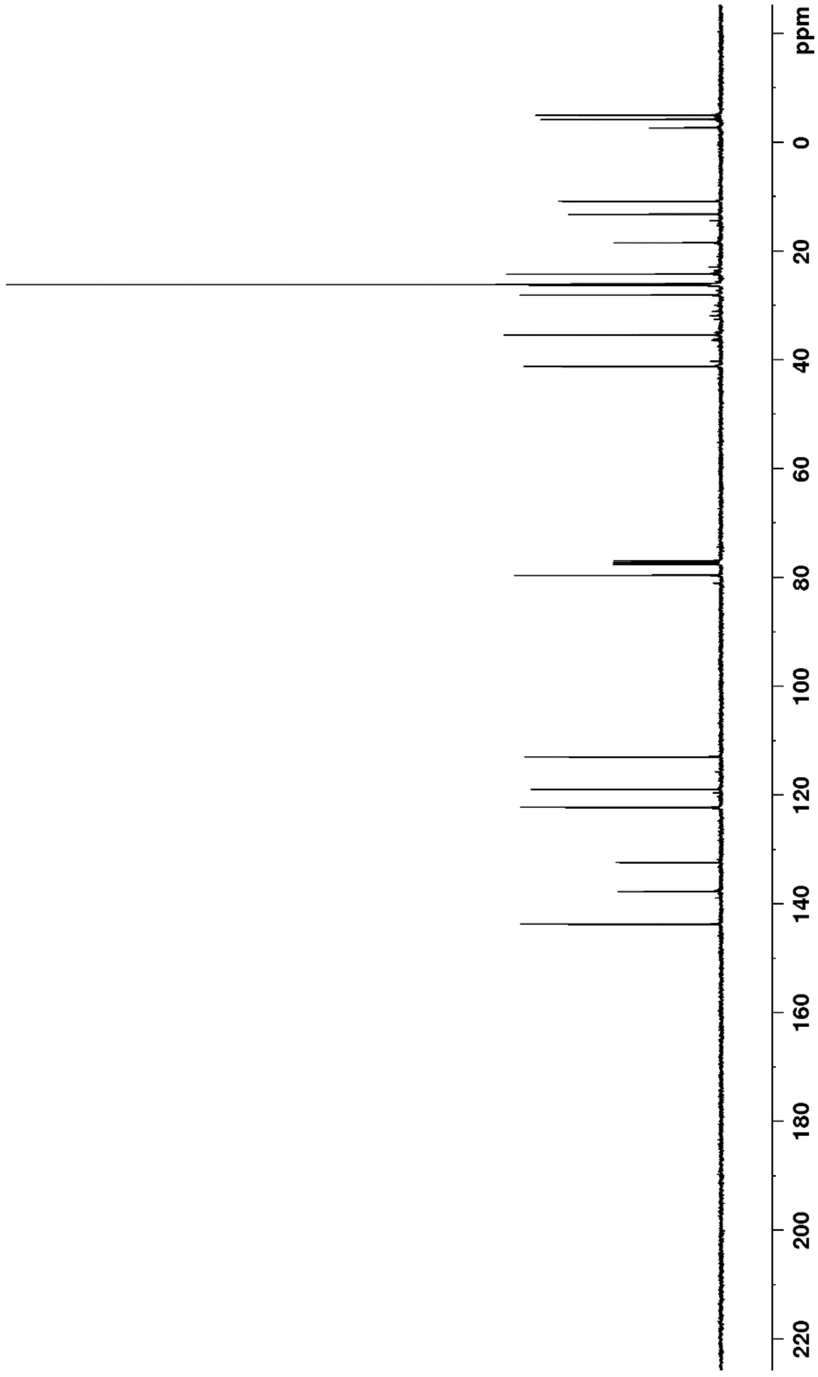
ppm
0
20
40
60
80
100
120
140
160
180
200
220

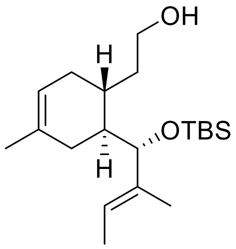
OH
H
OTBS
H

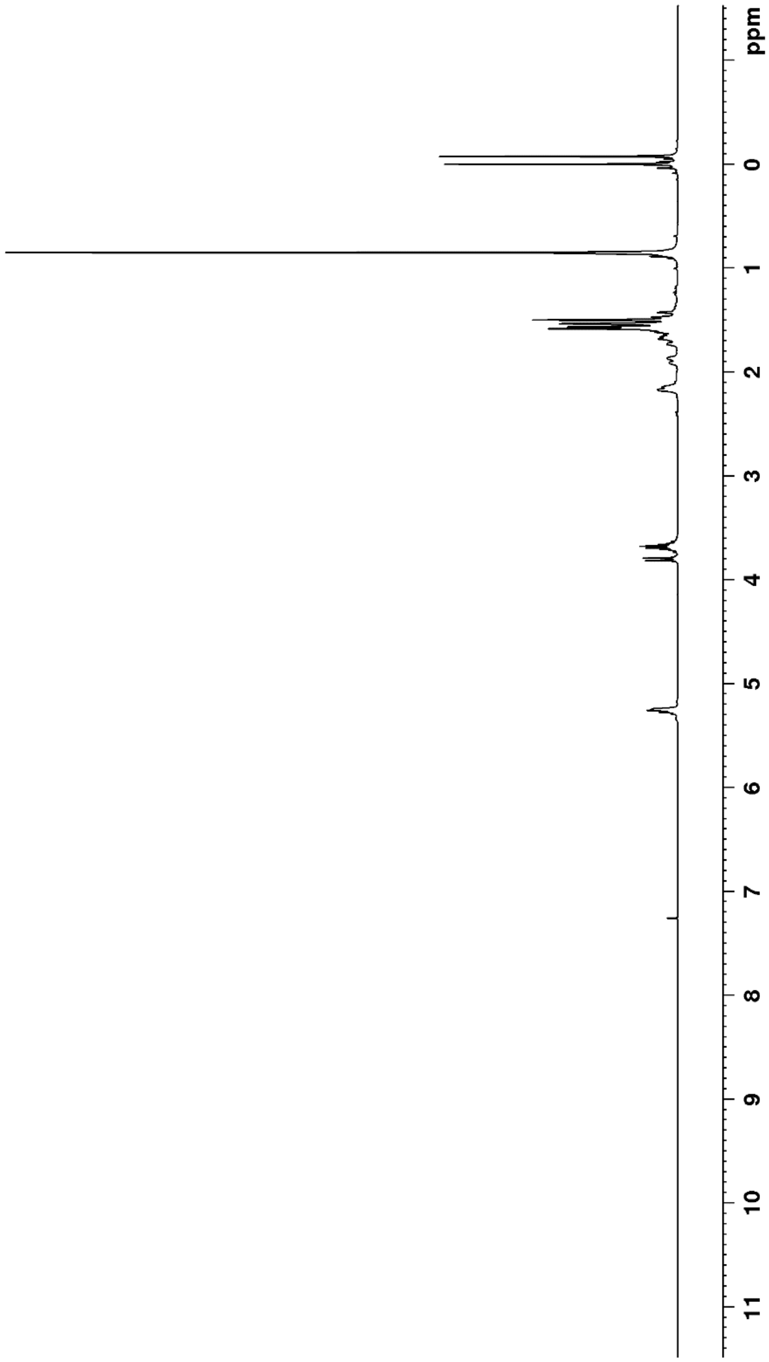
ppm
0
1
2
3
4
5
6
7
8
9
10
11

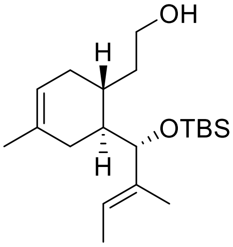
OH
H
OTBS
H

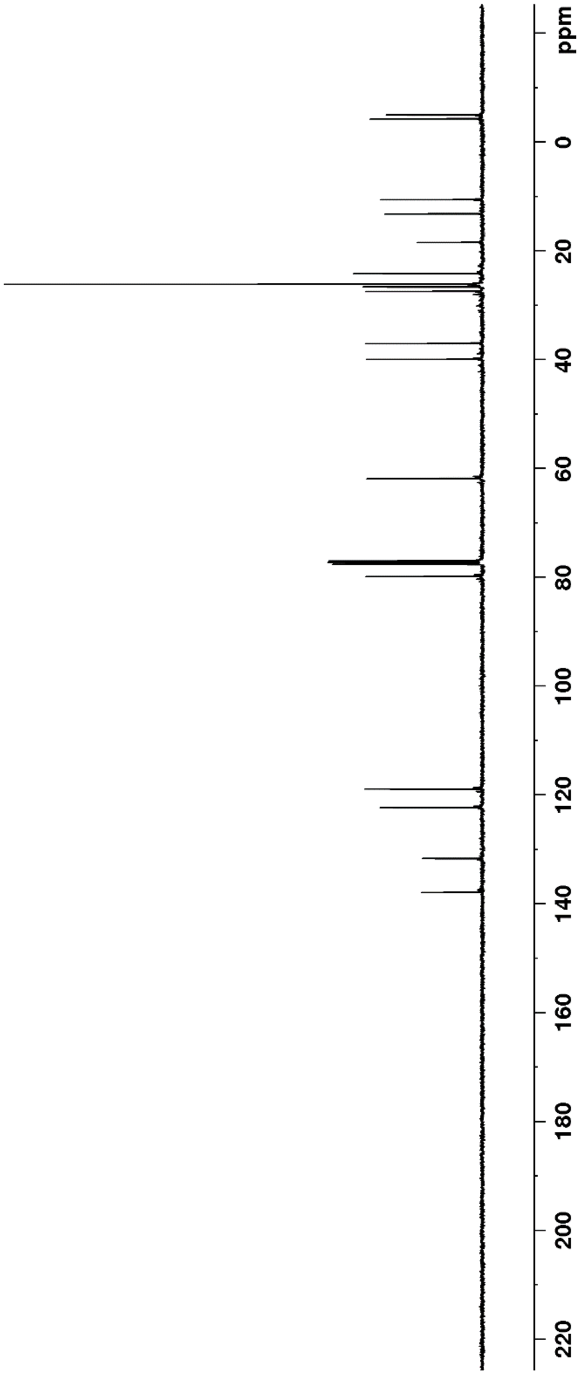
ppm
0
20
40
60
80
100
120
140
160
180
200
220

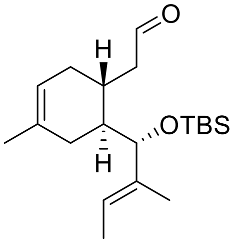
O
H
OTBS
H

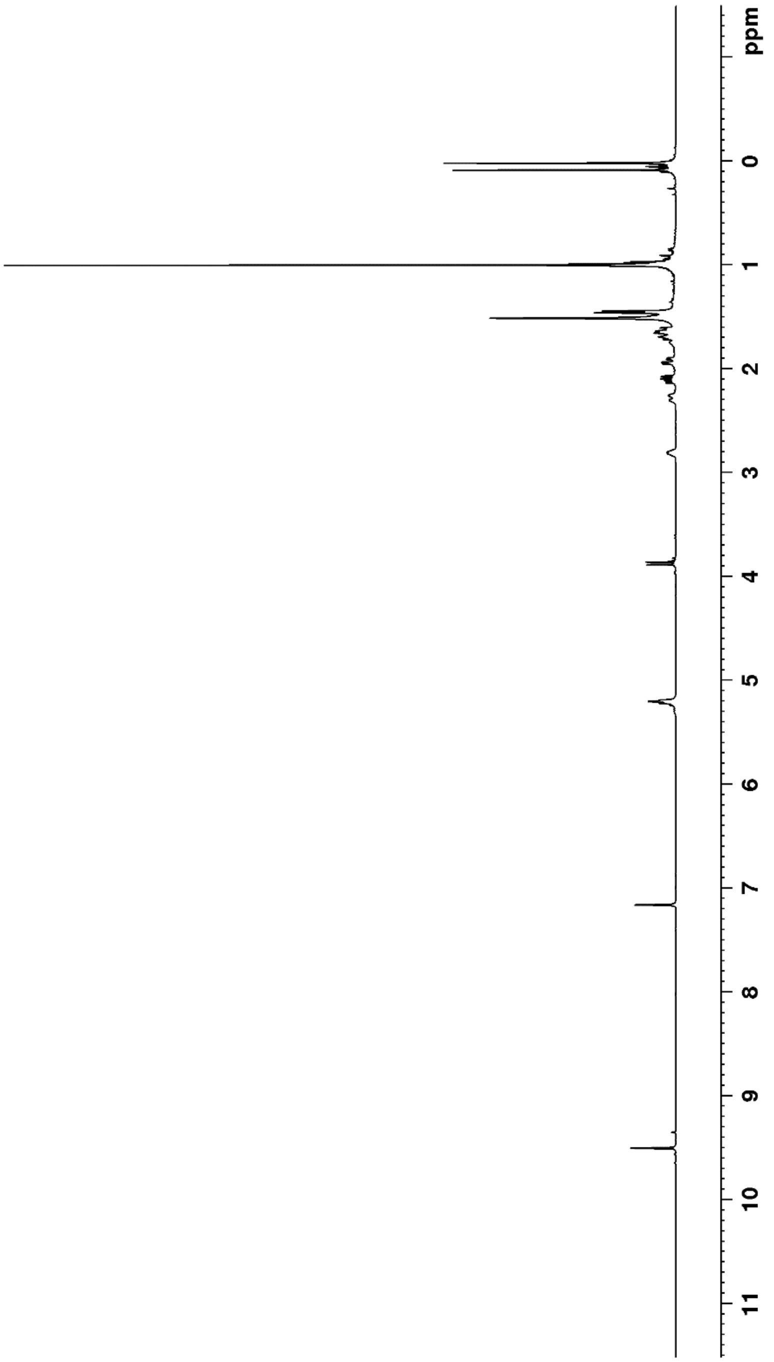
ppm
0
1
2
3
4
5
6
7
8
9
10
11

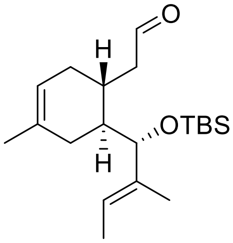
O
H
OTBS
H

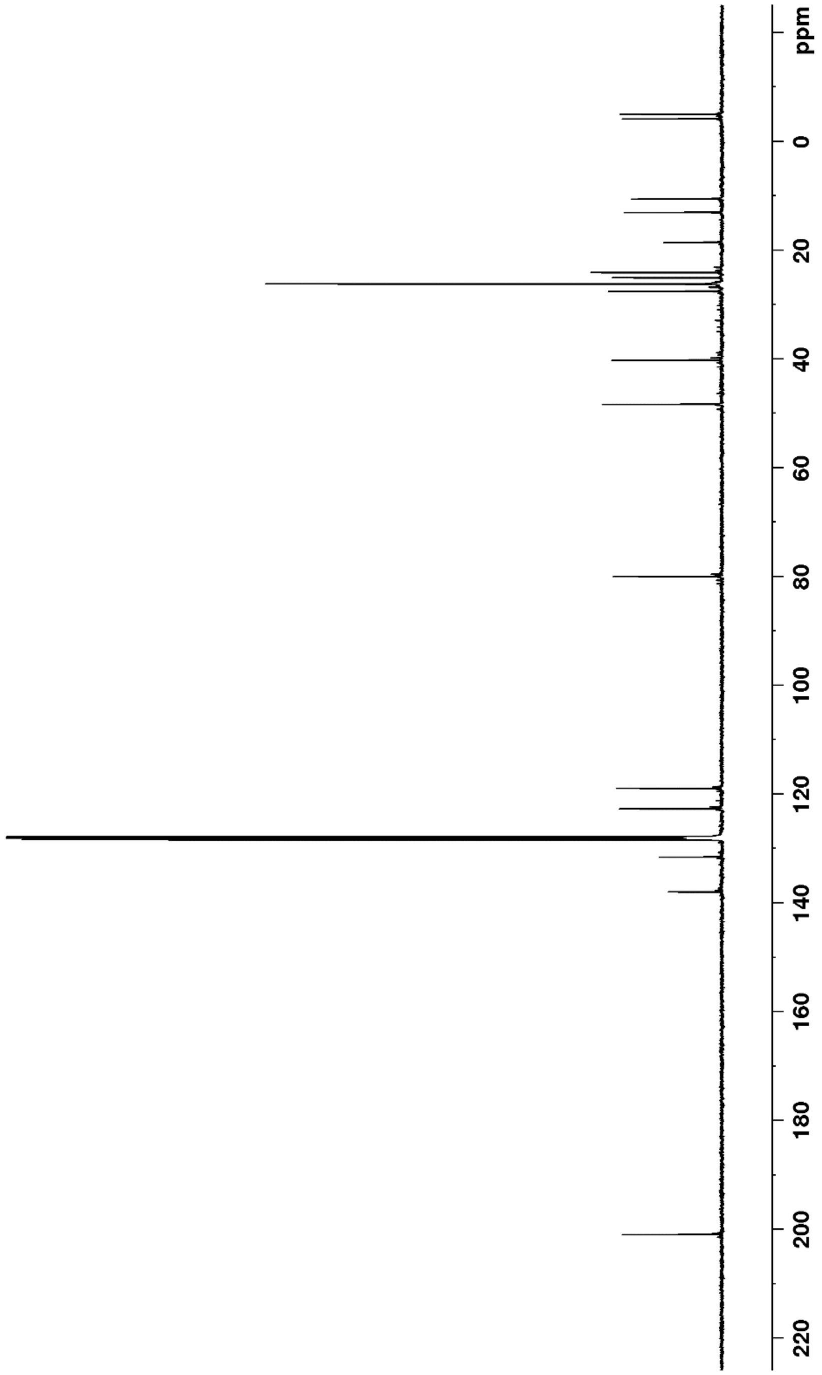
ppm
0
20
40
60
80
100
120
140
160
180
200
220

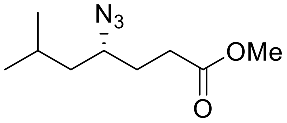
N3
OMe
O

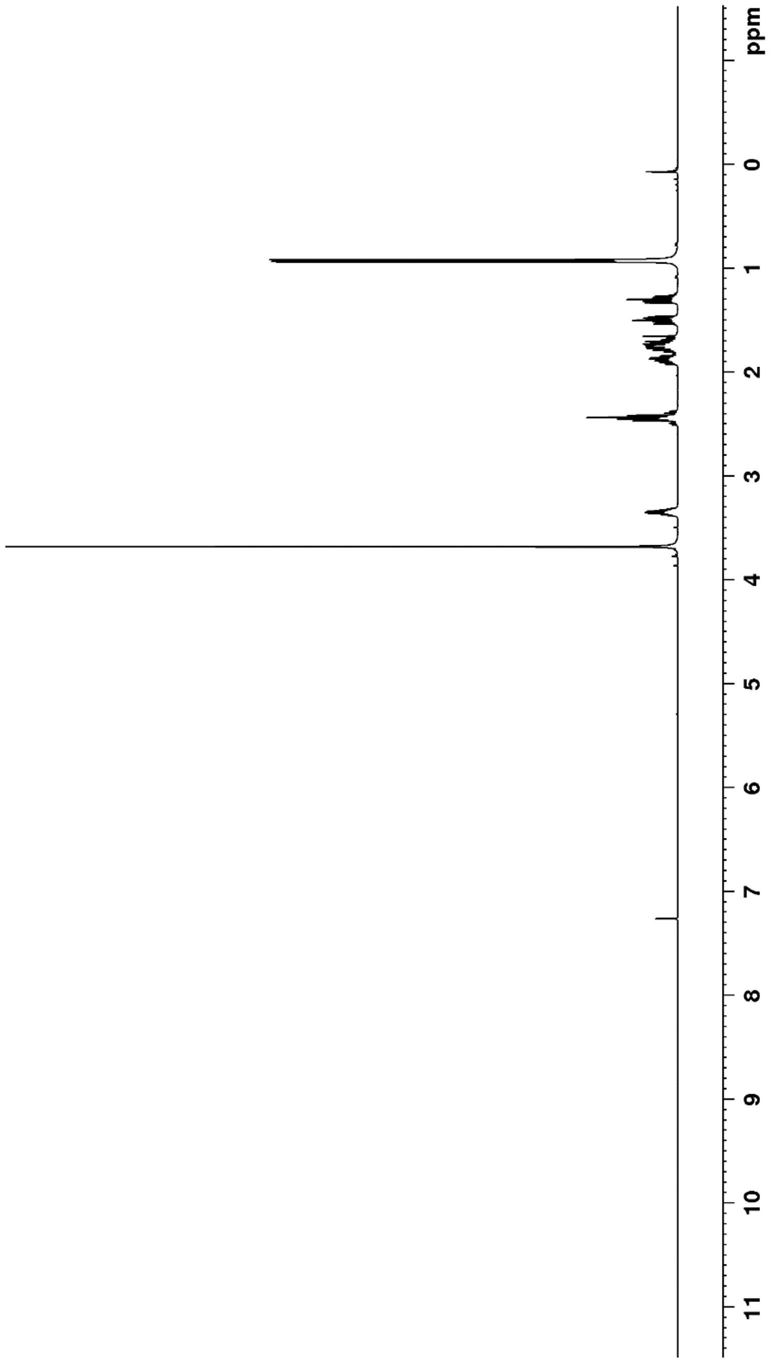
ppm
0
1
2
3
4
5
6
7
8
9
10
11

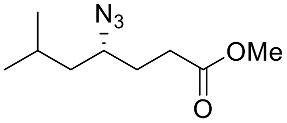
N3
OMe
O

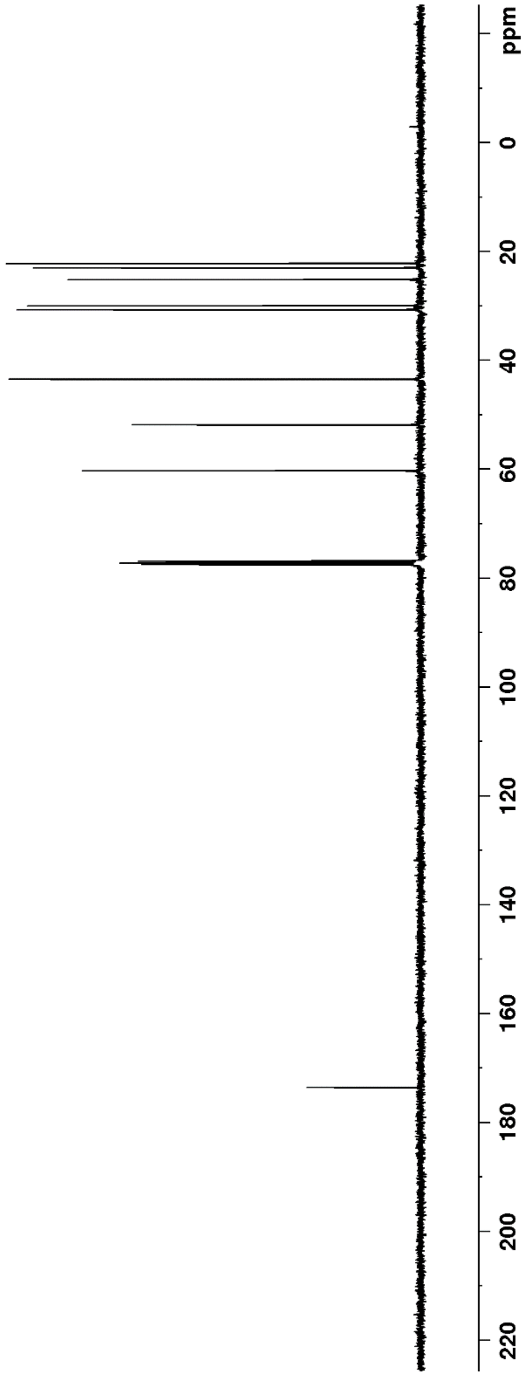
ppm
0
20
40
60
80
100
120
140
160
180
200
220

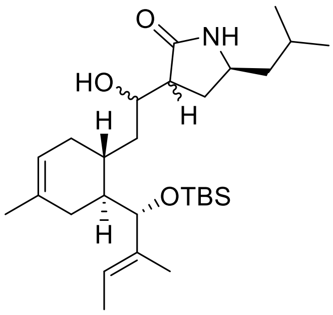
O
NH
HO
H
H
OTBS
H

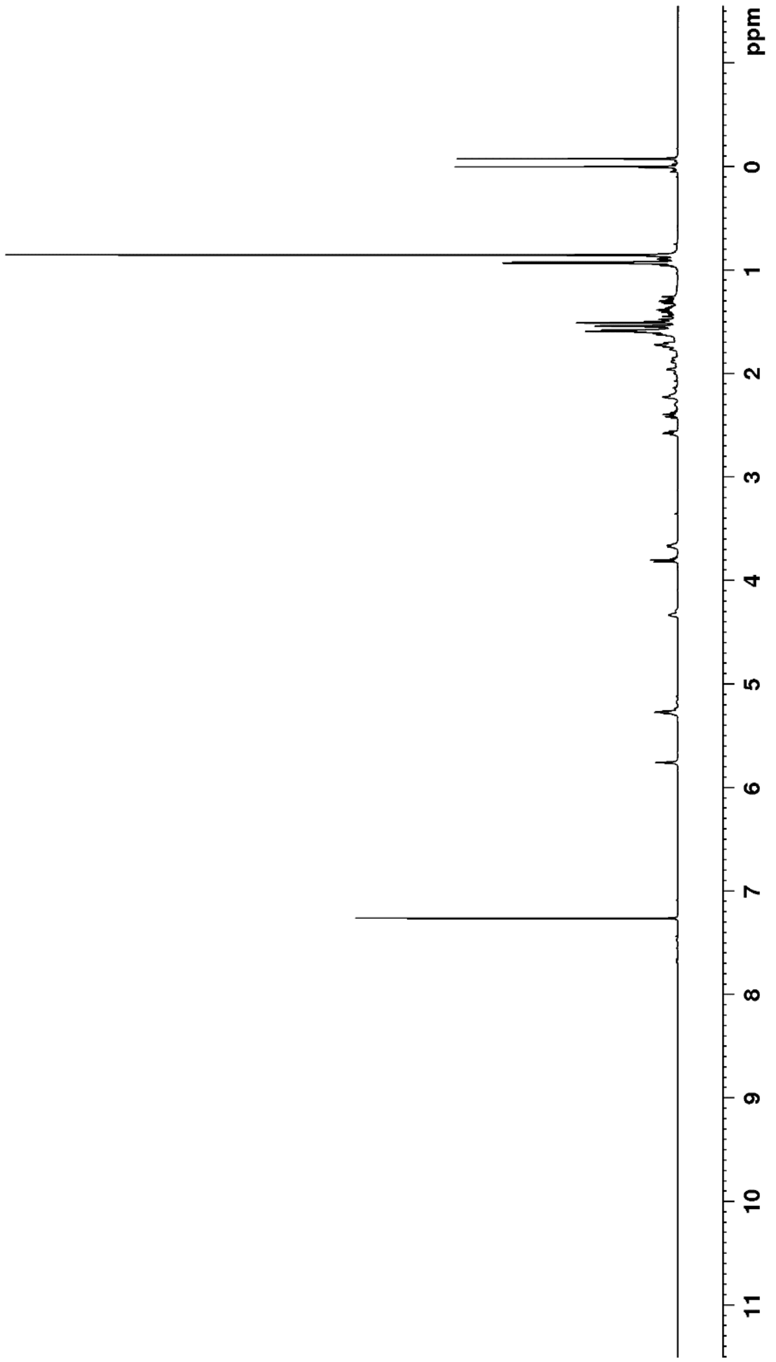
ppm
0
1
2
3
4
5
6
7
8
9
10
11

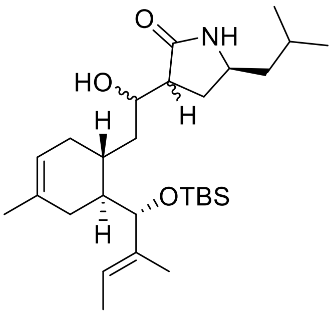
O
NH
HO
H
H
OTBS
H

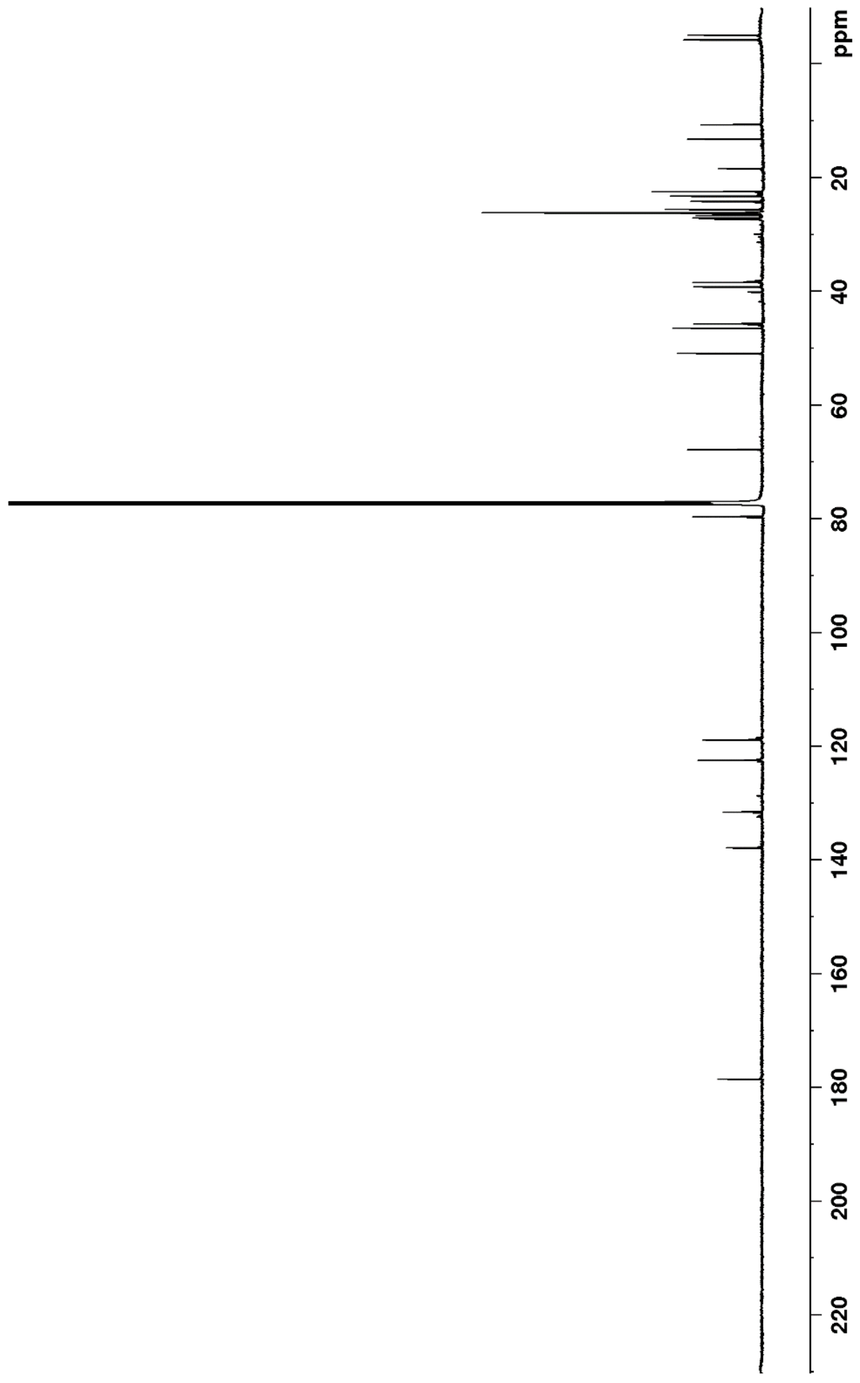
ppm
20
40
60
80
100
120
140
160
180
200
220

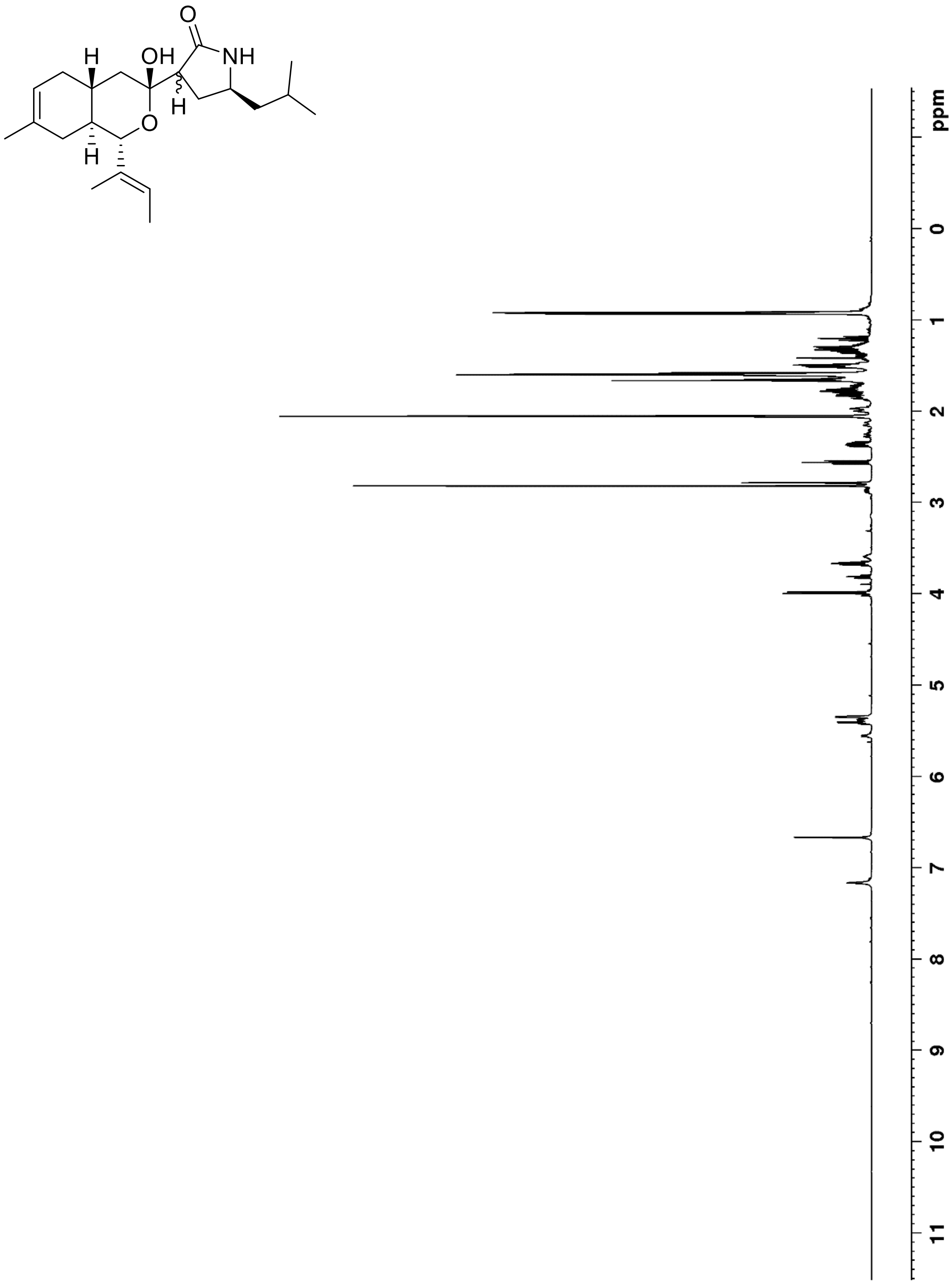
O
OH
NH
H
H
O
H
ppm
0
1
2
3
4
5
6
7
8
9
10
11

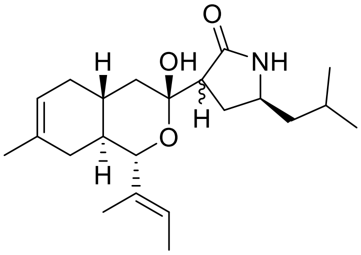
O
OH
NH
H
H
O
H

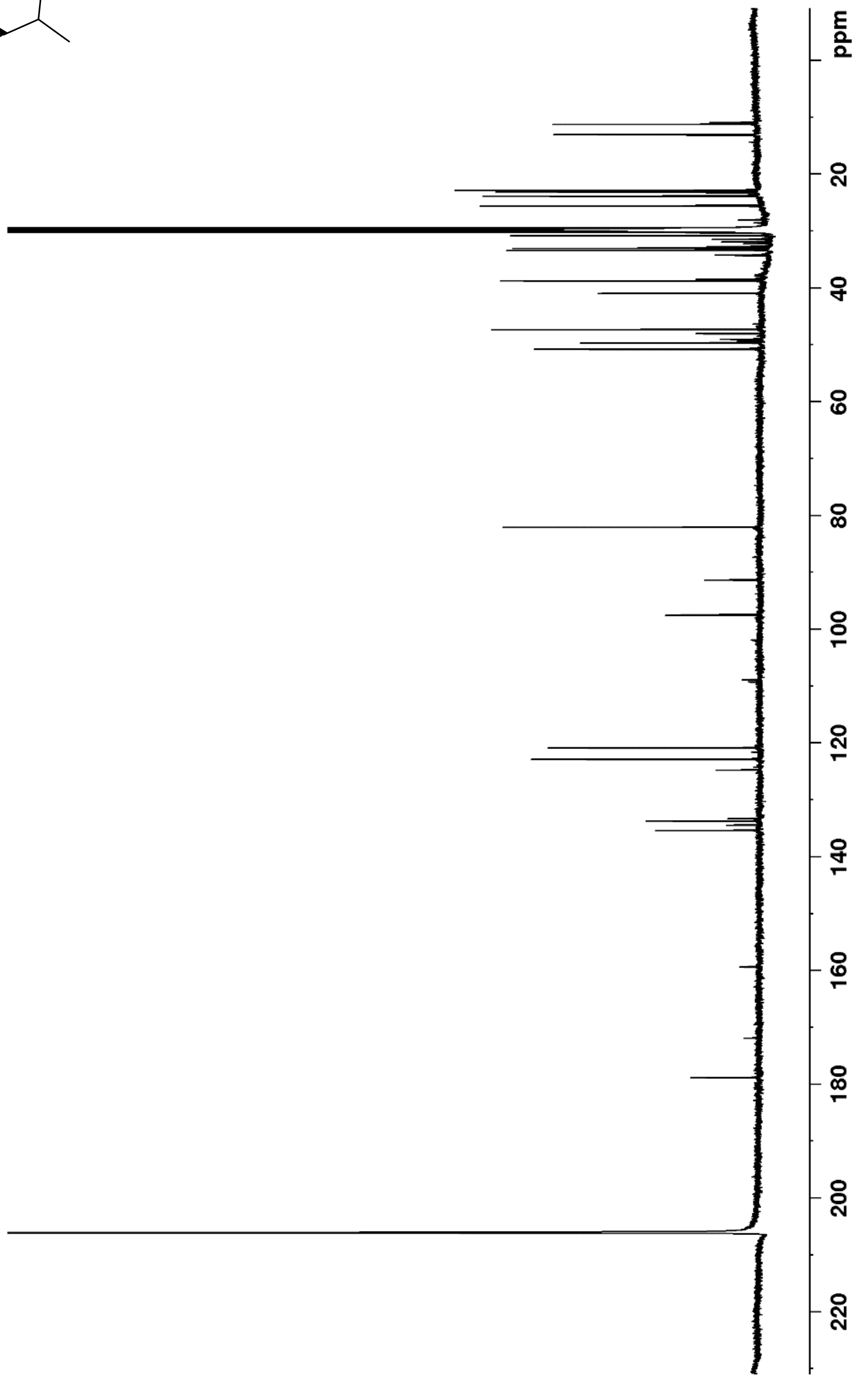
ppm
20
40
60
80
100
120
140
160
180
200
220

References

1.Kroeze, W.K.; Sheffler, D.G.; Rother, B.L. G-protein-coupled receptors at a glance. *J. Cell. Sci*. **2003**, 116, 4867-4869.

2.Vassilatis, D.K.; Hohmann, J.G.; Zeng, H.; Li, F.; Ranchalis, J.E.; Mortrud, M.T.; Brown, A.; Rodriguez, S.S.; Weller, J.R.; Wright, A.C.; Bergmann, J.E.; Gaitanaris, G.A. The G protein-coupled receptor repertoires of human and mouse. *PNAS*, **2003**, 100(8), 4903-4908.

3.Lv, X.; Liu, J.; Shi, Q.; Tan, Q.; Wu, D.; Skinner, J.J.; Walker, A.L.; Zhao, L.; Gu, X.; Chen, N.; Xue, L.; Si, P.; Zhang, L.; Wang, Z.; Katritch, V.; Liu, Z.; Stevens, R.C. *In vitro* expression and analysis of the 826 human G protein-coupled receptors. *Protein. Cell.* **2016**, 7(5), 325-337.

4.Fredriksson, R.; Lagerström, M.C.; Lundin, L.G.; Schiöth, H.B. The G-protein-coupled receptors in the human genome form five main families. Phylogenetic analysis, paralogon groups, and fingerprints. *Mol. Pharmacol.* **2003**, 63(6), 1256-1272.

5.Sriram, K.; Insel, P.A. GPCRs as targets for approved drugs: How many targets and how many drugs? *Mol. Pharmacol.* **2019**, mol.117.111062.

6.Hauser, A.S.; Attwood, M.M.; Rask-Anderson, M.; Schiöth, H.B.; Gloriam, D.E. Trends in GPCR drug discovery: new agents, targets and indications. *Nat. Rev. Drug Disc.* **2017**, 16, 829-842.

7.Saikia, S.; Bordoloi, M.; Sarmah, R. Establsihed and In-trial GPCR Families in Clinical Trials: A Review for Target Selection. *Curr. Drug Targets.* **2019**, 20(5), 522-539.

8.Premont, R.T.; Gainetdinov, R.R. Physiological Roles of G Protein-Coupled Receptor Kinases and Arrestins. *Annu. Rev. Physiol.* **2007**, 69, 511-534.

9.Rosenbaum, D.M.; Rasmussen, S.G.F.; Kobilka, B.K. The structure and function of G-protein-coupled receptors. *Nature,* **2009**, 459(7245), 356-363.

10.Julius, D.; Nathans, J. Signaling by Sensory Receptors. *Cold Spring Harb. Perspect. Biol.* **2012**, 4(1), a005991.

11.Tao, Y.X.; Yuan, Z.H.; Xie, J. G protein-coupled receptors as regulators of energy homeostasis. **2013**, 114, 1-43.

12.Walther, C.; Ferguson, S.S.G. Minireview: Role of Intracellular Scaffolding Proteins in the Regulation of Endocrine G Protein-Coupled Receptor Signaling. **2015**, 29(6), 814-830.

13.Lombardi, M.S.; Kavelaars, A.; Heijnen, C.J. Role and modulation of G protein-coupled receptor signaling in inflammatory processes. *Crit. Rev. Immunol.* **2002**, 22(2), 141-163.

14.a. Møller, T.C.; Moreno-Delgado, M.; Pin, J-P.; Kniazeff, J. Class C G protein-coupled receptors: reviving old couples with new partners. *Biophys. Rep.* **2017**, 3(4-6), 57-63.

b. PDB ID: 6N52. del Torrent, C.L.; Pérez-Benito, L.; Tresadern, G. Computational Drug Design Applied to the study of Metabotropic Glutamate Receptors. *Molecules*. **2019**, 24 (6), 1098.

15. Niswender, C.M.; Conn, P.J. Metabotropic Glutamate Receptors: Physiology, Pharmacology, and Disease. *Annu. Rev. Pharmacol. Toxicol.* **2010**, 50, 295-322.
16. Levitz, J.; Habrian, C.; Bharill, S.; Fu, Z.; Vafabakhsh, R.; Isacoff, E.Y. Mechanism of Assembly and Cooperativity of Homomeric and Heteromeric Metabotropic Glutamate Receptors. *Neuron*. **2016**, 92, 143-159.
17. Willard, S.S.; Koochekpour, S. Glutamate, Glutamate Receptors, and Downstream Signaling Pathways. *Int. J. Biol. Sci.* **2013**, 9(9), 948-959.
18. Jaffe, D.B.; Brown, T.H. Metabotropic glutamate receptor activation induces calcium waves within hippocampal dendrites. *J. Neurophysiol.* **1994**, 72(1), 471-474.
19. Liu, K.; Southall, N.; Titus, S.A.; Inglese, J.; Eskay, R.L.; Shinn, P.; Austin, C.P.; Heilig, M.A.; Zheng, W. A Multiplex Calcium Assay for Identification of GPCR Agonists and Antagonists. *Assay Drug Dev. Technol.* **2010**, 8(3), 367-379.
20. Jiang, M.; Bajpayee, N.S. Molecular Mechanisms of Go Signaling. *Neurosignals.* **2009**, 17(1), 23-41.
21. Tuteja, N. Signaling through G protein coupled receptors. *Plant. Signal. Behav.* **2009**, 4(10), 942-947.
22. Syrovatkina, V.; Alegre, K.O.; Dey, R.; Huang, X-Y. Regulation, Signaling, and Physiological Functions of G-proteins. *J. Mol. Biol.* **2016**, 428(19), 3850-3868.
23. Schultz, S.H.; North, S.W.; Shields, C.G. Schizophrenia: a review. *Am. Fam. Physician.* **2007**, 75(12), 1821-1829.
24. Chong, H.Y.; Teoh, S.L.; Wu, D.B-C.; Kotirum, S.; Chiou, C-F.; Chaiyakunapruk, N. Global economic burden of schizophrenia: a systematic review. *Neuropsychiatr. Dis. Treat.* **2016**, 12, 357-373.
25. Patel, K.R.; Cherian, J.; Gohil, K.; Atkinson, D. Schizophrenia: Overview and Treatment Options. *PT.* **2014**, 39(9), 638-645.
26. Higashi, K.; Medic, G.; Littlewood, K.J.; Diez, T.; Granström, O.; De Hert, M. Medication adherence in schizophrenia: factors influencing adherence and consequences of nonadherence, a systematic literature review. *Ther. Adv. Psychopharmacol*. **2013**, 3(4), 200-218.
27. Haddad, P.M.; Brain, C.; Scott, J. Nonadherence with antipsychotic medication in schizophrenia: challenges and management strategies. *Patient Relat. Outcome Meas.* **2014**, 5, 43-62.
28. Remington, G.; Foussias, G.; Fervaha, G.; Agid, O.; Takeuchi, H.; Lee, J.; Hahn, M. Treating Negative Symptoms in Schizophrenia: an Update. *Curr. Treat. Options Psychiatry.* **2016**, 3, 133-150.
29. Goff, D.C.; Hill, M.; Barch, D. The treatment of cognitive impairment in schizophrenia. *Pharmacol. Biochem. Behav.* **2011**, 99(2), 245-253.

30. Bowie, C.R.; Harvey, P.D. Cognitive deficits and functional outcome in schizophrenia. *Neuropsychiatr. Dis. Treat.* **2006**, 2(4), 531-536.
31. Henriksen, M.G.; Nordgaard, J.; Jannson, L.B. Genetics of Schizophrenia: Overview of Methods, Findings and Limitations. *Front. Hum. Neurosci.* **2017**, 11, 322.
32. Jaaro-Peled, H.; Ayhan, Y.; Pletnikov, M.V.; Sawa, A. Review of Pathological Hallmarks of Schizophrenia: Comparison of Genetic Models with Patients and Nongenetic Models. *Schizophr. Bull.* **2010**, 36(2), 301-313.
33. Javitt, D.C.; Zukin, S.R. Recent advances in the phencyclidine model of schizophrenia. *Am. J. Psychiatry.* **1991**, 148(10), 1301-1308.
34. Domino, E.F.; Luby, E.D. Phencyclidine/Schizophrenia: One View Toward the Past, The Other to the Future. *Schizophr. Bull.* **2012**, 38(5), 914-919.
35. Steeds, H.; Carhart-Harris, R.L.; Stone, J.M. Drug models of schizophrenia. *Ther. Adv. Psychopharmacol.* **2015**, 5(1), 43-58.
36. Murray, J.B. Phencyclidine (PCP): a dangerous drug, but useful in schizophrenia research. *J. Psychol.* **2002**, 136(3), 319-327.
37. Bertron, J.L.; Seto, M.; Lindsley, C.W. DARK Classics in Chemical Neuroscience: Phencyclidine (PCP). *ACS Chem. Neurosci.* **2018**, 9(10), 2459-2474.
38. Ramsey, A.J. NR1 knockdown mice as a representative model of the glutamate hypothesis of schizophrenia. *Prog. Brain. Res.* **2009**, 179, 51-58.
39. Mohn, A.R.; Gainetdinov, R.R.; Garon, M.G.; Koller, B.H. Mice with Reduced NMDA Receptor Expression Display Behaviors Related to Schizophrenia. *Cell.* **1999**, 98, 427-436.
40. Yasuda, K.; Hayashi, Y.; Yoshida, T.; Kashiwagi, M.; Nakagawa, N.; Michikawa, T.; Tanaka, M.; Ando, R.; Huang, A.; Hosoya, T.; McHugh, T.K.; Kuwahara, M.; Itohara, S. Schizophrenia-like phenotypes in mice with NMDA receptor ablation in intralaminar thalamic nucleus cells and gene therapy-based reversal in adults. *Trans. Psychiatry.* **2017**, 7(2), e1047.
41. Gupta, K.; Hardingham, G.E.; Chandran, S. NMDA receptor-dependent glutamate excitotoxicity in human embryonic stem cell-derived neurons. *Neurosci. Lett.* **2013**, 543, 95-100.
42. Portera-Cailliau, C.; Price, D.L.; Martin, L.J. Non-NMDA and NMDA receptor-mediated excitotoxic neuronal deaths in adult brain are morphologically distinct: Further evidence for an apoptosis-necrosis continuum. *J. Comp. Neurol.* **1998**, 378, 88-104.
43. Rothman, S.M.; Olney, J.W. Excitotoxicity and the NMDA receptor. *Trends Neurosci.* **1986**, 10(7), 299-302.
44. Bridges, T.M.; Lindsley, C.W. G-protein-coupled receptors: from classical modes of modulation to allosteric mechanisms. *ACS Chem. Biol.* **2008**, 3, 530-542.
45. Lindsley, C.W. The Akt/PKB family of protein kinases: a review of small molecule inhibitors and progress towards target validation: a 2009 update. *Curr. Top. Med. Chem.* **2010**, 10, 458-477.

46. Grover, A.K. Use of Allosteric Targets in the Discovery of Safer Drugs. *Med. Princ. Pract.* **2013**, 22(5), 418-426.
47. Amaro, R.E. Toward Understanding “the Ways” of Allosteric Drugs. *ACS Cen. Sci.* **2017**, 3(9), 925-926.
48. Nussinov, R.; Tsai, C-J. Allostery in Disease and in Drug Discovery. *Cell*. **2013**, 153 (2), 293-305.
49. Freedman, N.J.; Lefkowitz, R.J. Desensitization of G protein-coupled receptors. *Recent Prog. Horm. Res.* **1996**, 51, 319-351.
50. Kelly, E.; Bailey, C.P.; Henderson, G. Agonist-selective mechanisms of GPCR desensitization. *Br. J. Pharmacol.* **2008**, 153, S379-S388.
51. Gainetdinov, R.R.; Premont, R.T.; Bohn, L.M.; Lefkowitz, R.J.; Caron, M.G. Desensitization of G Protein-Coupled Receptors and Neuronal Functions. *Annu. Rev. Neurosci.* **2004**, 27, 107-144.
52. Holtmann, M.H.; Roettger, B.F.; Pinon, D.I.; Miller, L.J. Role of Receptor Phosphorylation in Desensitization and Internalization of the Secretin Receptor. *J. Biol. Chem.* **1996**, 271, 23566-23571.
53. Allouche, S.; Noble, F.; Marie, N. Opioid receptor desensitization: mechanisms and its link to tolerance. *Front. Pharmacol*. **2014**, 5, 280.
54. Porter-Stransky, K.A.; Weinshenker, D. Arresting the Development of Addiction: The Role of β-Arrestin 2 in Drug Abuse. *J. Pharmacol. Exp. Ther.* **2017**, 361(3), 341-348.
55. Bohn, L.M.; Gainetdinov, R.R.; Caron, M.G. G protein-coupled receptor kinase/β-arrestin systems and drugs of abuse. *Neuromolecular Med.* **2004**, 5(1), 41-50.
56. Wang, L.; Martin, B.; Brenneman, R.; Luttrell, L.M.; Maudsley, S. Allosteric Modulators of G Portein-Coupled Receptors: Future Therapeutics for Complex Physiological Disorders. *J. Pharmacol. Exp. Ther.* **2009**, 331, 340-348.
57. Korcynska, M.; Clark, M.J.; Valant, C.; Xu, J.; M, E.V.; Albold, S.; Weiss, D.R.; Torosyan, H.; Huang, W.; Kruse, A.C.; Lyda, B.R.; May, L.T.; Baltos, J.; Sexton, P.M.; Kobilka, B.K.; Christopolous, A.; Shoichet, B.K.; Sunahara, R.K. Structure-based discovery of selective positive allosteric modulators of antagonists for the M_2 muscarinic acetylchloline receptor. *PNAS*. **2018**, 115(10), E2419-E2428.
58. Patel, M.M.; Patel, B.M. Crossing the Blood-Brain Barrier: Recent Advances in Drug Delivery to the Brain. *CNS Drugs.* **2017**, 31(2), 109-133.
59. Trinh, P.N.H.; May, L.T.; Leach, K.; Gregory, K.J. Biased agonism and allosteric modulation of metabotropic glutamate receptor 5. *Clin. Sci.* **2018**, 132 (21), 2323-2338.
60. López-Muñoz, F.; Alamo, C.; García- García, P. The discovery of chlordiazepoxide and the clinical introduction of benzodiazepines: half a century of anxiolytic drugs. *J. Anxiety Disord.* **2011**, 25(4), 554-562.

61. Griffin III, C.E.; Kaye, A.M.; Bueno, F.R.; Kaye, A.D. Benzodiazepine Pharmacology and Central Nervous System-Mediated Effects. *Ochsner J.* **2013**, 13 (2), 214-223.
62. Möhler, H.; Fritschy, J.M.; Rudolph, U. A New Benzodiazepine Pharmacology. *J. Pharmacol. Exp. Ther.* **2002**, 300(1), 2-8.
63. Cruzado, J.M.; Moreno, P.; Torregrosa, J.V.; Taco, O.; Mast, R.; Gómez-Vaquero, C.; Polo, C.; Revuelta, I.; Francos, J.; Torras, J.; García-Barras, A.; Bestard, O.; Grinyó. A Randomized Study Comparing Parathyroidectomy with Cinacalcet for Treating Hypercalcemia in Kidney Allograft Recipients with Hyperparathyroidism. *J. Am. Soc. Nephrol.* **2016**, 27(8), 2487-2494.
64. Veljkovic, N.; Vucicevic, J.; Tassini, S.; Glisic, S.; Veljkovic, V.; Radi, M. Preclicinal discovery and development of maraviroc for the treatment of HIV. *Expert Opin. Drug. Discov.* **2015**, 10(6), 671-684.
65. Dorr, P.; Westby, M.; Dobbs, S.; Griffin, P.; Irvine, B.; Macartney, M.; Mori, J.; Rickett, G.; Smith-Burchnell, C.; Napier, C.; Webster, R.; Armour, D.; Price, D.; Stammen, B.; Wood, A.; Perros, M. Maraviroc (UK-427,857), a Potent, Orally Bioavailable, and Selective Small-Molecule Inhibitor of Chemokine Receptor CCR5 with Broad-Spectrum Anti-Human Immunodificiency Virus Type 1 Activity. *Antimicrob. Agents Chemother.* **2005**, 49(11), 4721-4732.
66. Lindsley, C.W.; Emmitte, K.A.; Hopkins, C.R.; Bridges, T.M.; Gregory, K.J.; Niswender, C.M.; Conn, P.J. Practical Strategies and Concepts in GPCR Allosteric Modulator Discovery: Recent Advances with Metabotropic Glutamate Receptors. *Chem. Rev.* **2016**, 116(11), 6707-6741.
67. Melancon, B.J.; Hopkins, C.R.; Wood, M.R.; Emmitte, K.A.; Niswender, C.M.; Chrisopoulos, A.; Conn, P.J.; Lindsley, C.W. Allosteric Modulation of Seven Transmembrane Spanning Receptors: Theory, Practice and Opportunities for Central Nervous System Drug Discovery. *J. Med. Chem.* **2012**, 55, 1445-1464.
68. Wang, Q.; Zheng, M.; Huang, Z.; Liu, X.; Zhou, H.; Chen, Y.; Shi, T.; Zhang, J. Toward understanding the molecular basis for chemical allosteric modulator design. *J. Mol. Graph. Model.* **2012**, 38, 324-333.
69. White, J.H.; Wise, A.; Main, M.J.; Green, A.; Fraser, N.J.; Disney, G.H.; Barnes, A.A.; Emson, P.; Foord, S.M.; Marshall, F.H. Heterodimerization is required for the formation of a functional GABA(B) receptor. *Nature*. **1998**, 396(6712), 679-682.
70. Cui, M.; Jiang, P.; Maillet, E.; Max, M.; Margolskee, R.F.; Osman, R. The heterodimeric sweet taste receptor has multiple potential ligand binding sites. *Curr. Pharm. Des.* **2006**, 12(35), 4591-4600.
71. Li, X.; Staszewski, L.; Xu, H.; Durick, K.; Zoller, M.; Adler, E. Human receptors for sweet and umami taste. *PNAS*. **2002**, 99(7), 4692-4696.

72. Ohishi, H.; Sigemoto, R.; Nakanishi, S.; Mizuno, N. Distribution of the messenger RNA for a metabotropic glutamate receptor, mGluR2, in the central nervous system of the rat. *Nueroscience*. **1993**, 53, 1009-1018.
73. Ohishi, H.; Shigemoto, R.; Nakanishi, S.; Mizuno, N. Distribution of the mRNAs for L-2-amino-4-phosphonobutyrate-sensitive metabotropic glutamate receptors, mGluR4 and mGluR7, in the brain. *J. Comp. Neurol.* **1995**, 360, 555-570.
74. Neki, A.; Ohishi, H.; Kaneko, T.; Shigemoto, R.; Nakanishi, S.; Mizuno, N. Pre- and postsynaptic localization of a metabotropic gluatamate receptor, mGluR2, in the rat brain: an immunohistochemical study with a monoclonal antibody. *Neurosci. Lett.* **1996**, 202, 197-200.
75. Bradley, S.R.; Standaert, D.G.; Rhodes, K.J.; Rees, H.D.; Testa, C.M.; Levey, A.I.; Conn, P.J. Immunohistochemical localization of subtype 4a metabotropic glutamate receptors in the rate and mouse basal ganglia. *J. Comp. Neurol.* **1999**, 407, 33-46.
76. Doumazane, E.; Scholler, P.; Zwier, J.M.; Trinquet, E.; Rondard, P.; Pin, J.P. A new approach to analyze cell surface protein complexes reveals specific heterodimeric metabotropic glutamate receptors. *FASEB.* **2011**, 25, 66-77.
77. Ferraguti, F.; Shigemoto, R. Metabotropic glutamate receptors. *Cell Tissue Res.* **2006**, 326, 483-504.
78. Kammermeier, P.J. Functional and Pharmacological Characteristics of Metabotropic Glutamate Receptors 2/4 Heterodimers. *Mol. Pharmacol.* **2012**, 82, 438-447.
79. Stachowicz, K.; Klak, K.; Klodzinska, A.; Chojnacka-Wojcik, E.; Pilc, A. Anxiolytic-like effects of PHCCC, an allosteric modulator of mGluR4 receptors, in rats. *Eur. J. Pharmacol*. **2004**, 498(1-3), 153-156
80. Sławińska, A.; Wierońska, J.M.; Stachowicz, K.; Pałucha-Poniewiera, A.; Uberti, M.A.; Bacolod, M.A.; Doller, D.; Pilc, A. Anxiolytic- but not antidepressant-like activity of LU AF21934, a novel, selective positive allosteric modulator of the mGlu$_4$ receptor. *Neuropharmacology.* **2013**, 66, 225-235.
81. Wieronska, J. M.; Stachowicz, K.; Palucha-Poniewiera, A.; Acher, F.; Branski, P.; Pilc, A. Metabotropic glutamate receptor 4 novel agonist LSP1−2111 with anxiolytic, but not antidepressant-like activity, mediated by serotonergic and GABAergic systems. *Neuropharmacology.* **2010**, 59, 627−634.
82. Kalinichev, M.; Le Poul, E.; Boléa, C.; Girard, F.; Campo, B., Fonsi; M., Royer-Urios, I.; Browne, S.E.; Uslaner, J.M.; Davis, M.J.; Raber, J.; Duvoisin, R.; Bate, S.T.; Reynolds, I.J.; Poli, S.; Celanire, S. Characterization of the Novel Positive Allosteric Modulator of the Metabotropic Glutamate Receptor 4 ADX88178 in Rodent Models of Neuropsychiatric Disorders. *J. Pharmacol. Exp. Ther.* **2014**, 350, 495-505.
83. Linden, A.M.; Shannon, H.; Baez, M.; Yu, J.L.; Koester, A.; Schoepp, D.D. Anxiolytic-like activity of the mGLU2/3 receptor agonist LY354740 in the

elevated plus maze test is disrupted in metabotropic glutamate receptor 2 and 3 knock-out mice. *Psychopharmacology.* **2005**, 179(1), 284-291.

84. Galici, R.; Jones, C.K.; Hemstapat, K.; Nong, Y.; Ecehmendia, N.G.; Williams, L.C.; de Paulis, T.; Conn, P.J. Biphenyl-indanone A, a positive allosteric modulator of the metabotropic glutamate receptor subtype 2, has antipsychotic- and anxiolytic-like effects in mice. *J. Pharmacol. Exp. Ther.* **2006,** 318(1), 173-185.
85. Galici, R.; Echemendia, N.G.; Rodriguez, A.L.; Conn, P.J. A Selective Allosteric Potentiator of Metabotropic Glutamate (mGlu) 2 Receptors Has Effects Similar to an Orhtosteric mGlu$_{2/3}$ Receptor Agonist in Mouse Models Predictive of Antipsychotic Activity. *J. Pharmacol. Exp. Ther.* **2005**, 315(3), 1181-1187.
86. Yin, S.; Noetzel, M.J.; Johnson, K.A.; Zamorano, R.; Jalan-Sakrikar, N.; Gregory, K.J.; Conn, P.J.; Niswender, C.M. Selective Actions of Novel Allosteric Modulators Reveal Functional Heteromers of Metabotropic Glutamate Receptors in the CNS. *J. Neurosci.* **2014**, 34(1), 79-94.
87. Reynolds, J.N.; Wickens, J.R. Dopamine-dependent plasticity of corticostriatal synapses. *Neural Netw.* **2002**, 15(4-6), 507-521.
88. Ding, J.; Peterson, J.D.; Surmeier, D.J. Corticostriatal and Thalamostriatal Synapses Have Distinctive Properties. *J. Neurosci.***2008**, 28(25), 6483-6492.
89. Calbresi, P.; Picconi, B.; Tozzi, A.; Di Filippo, M. Dopamine-mediated regulation of corticostriatal synaptic plasticity. *Trends Neurosci.* **2007**, 30(5), 211-219.
90. Fisher, S.D.; Robertson, P.B.; Black, M.J.; Redgrave, P.; Sagar, M.A.; Abraham, W.C.; Reynolds, J.N.J. Reinforcement determines the timing dependence of corticostriatal synaptic plasticity in vivo. *Nat. Comm.* **2017**, 334(8), 1-13.
91. Shepherd, G.M.G. Corticostriatal connectivity and its role in disease. *Nat. Rev. Neurosci.* **2013**, 14(4), 278-291.
92. Rovira, X.; Malhaire, F.; Scholler, P.; Rodrigo, J.; Gonzalez-Bulnes, P.; Pin, J-P.; Giraldo, J.; Goudet, C. Overlapping binding sites drive allosteric agonism and positive cooperativity in type 4 metabotropic glutamate receptors. *FASEB*. **2015**, 29(1), 116-130.
93. Niswender, C.M.; Johnson, K.A.; Luo, Q.; Ayala, J.E.; Kim, C.; Conn, P.J.; Weaver, C.D. A novel assay of G$_{i/o}$ protein-linked receptor coupling to potassium channels provides new insights into the pharmacology of the group III metabotropic glutamate receptors. *Mol. Pharmacol*. **2008**, 73(4), 1213-1224.
94. Williams, R.; Johnson, K.A.; Gentry, P.R.; Niswender, C.M.; Weaver, C.D.; Conn, P.J.; Lindsley, C.W.; Hopinks, C.R. Synthesis and SAR of a Novel Positive Allosteric Modulator (PAM) of the Metabotropic Glutamate Receptor 4 (mGluR 4). **2009**, 19(17), 4967-4970.
95. Rovira, X.; Harrak, Y.; Trapero, A.; González-Bulnes, P.; Malhaire, F.; Pin, J-P.; Goudet, C.; Giraldo, J.; Llebaria, A. Exploring the Active Conformation

of Cyclohexane Carboxylate Positive Allosteric Modulators of the Type 4 Metabotropic Glutamate Receptor. *Chem. Med. Chem.* **2004**, 9, 2685-2698.

96. Niswender, C.M.; Johnson, K.A.; Weaver, C.D.; Jones, C.K.; Xiang, Z.; Luo, Q.; Rodriguez, A.L.; Marlo, J.E.; de Paulis, T.; Thompson, A.D.; Days, E.L.; Nalywajko, T.; Austin, C.A.; Williams, M.B.; Ayala, J.E.; Williams, R.; Lindsley, C.W.; Conn, P.J. Discovery, Characterization, and Antiparkinsonian Effect of Novel Positive Allosteric Modulators of Metabotropic Glutamate Receptor 4. *Mol. Pharmacol.* **2008**, 74(5), 1345-1358.
97. Bennouar, K-E.; Uberti, M.A.; Melon, C.; Bacolod, M.D.; Jimenez, H.N.; Cajina, M.; Goff, L.K.; Koller, D.; Gubellini, P. Synergy between L-DOPA and a novel positive allosteric modulator of metabotropic glutamate receptor 4: Implications for Parkinson's disease treatment and dyskinesia. *Neuropharmacology*. **2013**, 66, 158-169.
98. Lavey, B.J.; Kozlowski, J.A.; Zhou, G.; Tong, L.; Yu, W.; Wong, M.K.C.; Shankar, B.B.; Shih, N-Y.; Siddiqui, M.A.; Rosner, K.E.; Dai, C.; Popovici-Muller, J.; Girijavallabhan, V.M.; Li, D.; Rizvi, R.; Chen, L.; Yang, D-Y.; Feltz, R.; Kim, S-H. Hydantoin derivatives for the treatment of inflammatory disorders. World Patent 2007084451, July 26, 2007.
99. Niu, P.; Kang, J.; Tian, X.; Song, L.; Liu, H.; Wu, J.; Yu, W.; Chang, J. Synthesis of 2-Amino-1,3,4-oxdiazoles and 2-Amino-1,3,4-thiadiazoles via Sequential Condensation and I_2-Mediated Oxidative C-O/C-S Bond Formation. *J. Org. Chem.* **2015**, 80 (2), 1018-1024.
100. Tang, J.; Liu, F.; Nagy, E.; Miller, L.; Kirby, K.A.; Wilson, D.J.; Wu, B.; Sarafianos, S.G.; Parniak, M.A.; Wang, Z. 3-Hydroxypyrimidine-2,4-diones as Selective Active Site Inhibitors of HIV Reverse Transcriptase-Associated RNase H: Design, Synthesis, and Biochemical Evaluations. *J. Med. Chem*. **2016**, 59 (6), 2648-2659.
101. Kikuo, Y.; Takezaki, T.; Ohuchi, R.; Ohuyabu, H.; Tanimoto, Y.; Toshimi, S.; Yamaguchi, T.; Akihiro, I.; Norio, H.; Tsutomu, I. Hydrazinopyridazine compound, process for production thereof, and use thereof as medicament. US4,599,333, July 8, 1986.
102. Blondeau, P.; Gauthier, R.; Berse, C.; Gravel, D. Synthesis of Some Stable 7-Halo-1,4-thiazepines. Potential Substituted Penam Precursors. *Can. J. Chem.* **1971**, 49 (23), 3866-3876.
103. Berque-Bestel, I.; Lezoulc'h, F.; Jockers, R. Bivalent Ligands as Specific Pharamacological Tools for G Protein-Coupled Receptor Dimers. *Curr. Drug Discov. Technol.* **2008**, 5(4), 312-318.
104. Glass, M.; Govindpani, K.; Furkert, D.P.; Hurst, D.P.; Reggio, P.H.; Flanagan, J.U. One for the Price of Two…Are Bivalent Ligands Targeting Cannabinoid Receptor Dimers Capable of Simultaneously Binding to both Receptors. *Trends Pharmacol. Sci.* **2016**, 37(5), 353-363.
105. Erez, M.; Takemori, A.E.; Portoghese, P.S. Narcotic Antagonistic Potency of Bivalent Ligands Which Contain β-Naltrexamine. Evidence for Bridging between Proximal Recognition Sites. *J. Med. Chem*. **1982**, 25, 847-849.

106. Busnelli, M.; Kleinau, G.; Muttenthaler, M.; Stoev, S.; Manning, M.; Bibic, L.; Howell, L.A.; McCormick, P.J.; Di Lascio, S.; Braida, D.; Sala, M.; Rovati, G.E.; Bellini, T.; Chini, B. Design and Characterization of Superpotent Bivalent Ligands Targeting Oxytocin Receptor Dimers via a Channel-Like Structure. *J. Med. Chem.* **2016**, 59(15), 7152-7166.
107. Tanaka, T.; Nomura, W.; Narumi, T.; Masuda, A.; Tamamura, H. Bivalent Ligands of CXCR4 with Rigid Linkers for Elucidation of the Dimerization State in Cells. *J. Am. Chem. Soc.* **2010**, 132(45), 15899-15901.
108. Matera, C.; Pucci, L.; Fiorentini, C.; Fucile, S.; Missale, C.; Grazioso, G.; Clementi, F.; Zoli, M.; De Amici, M.; Gotti, C.; Dallanoce, C. *Eur. J. Med. Chem*. **2015**, 101, 367-383.
109. Matera, C.; Flammini, L.; Quadri, M.; Vivo, V.; Ballabeni, V.; Holzgrabe, U.; Mohr, K.; De Amici, M.; Barocelli, E.; Bertoni, S.; Dallanoce, C. Bis(ammonio)alkane-type agonists of muscarinic acetylcholine receptors: Synthesis, *in vitro* functional characterization, and *in vivo* evaluation of their analgesic activity. *Eur. J. Med. Chem.* **2014**, 75, 222-232.
110. Akgün, E.; Javed, M.I.; Lunzer, M.M.; Smeester, B.A.; Beitz, A.J.; Portoghese, P.S. Ligands that interact with putative MOR-mGluR5 heteromer in mice with inflammatory pain produce potent antinociception. *Proc. Natl. Acad. Sci. USA.* **2013**, 110(28), 11595-11599.
111. Portoghese, P.S.; Roninsisvalle, G.; Larson, D.L.; Yim, C.B.; Sayre, L.M.; Takemori, A.E. Opioid agonist and antagonist bivalent ligands as receptor probes. *Life Sci.* **1982**, 31(12-13), 1283-1286.
112. Russo, O.; Berthouze, M.; Giner, M.; Soulier, J-L.; Rivail, L.; Sicsic, S.; Lezoulc'h, F.; Jockers, R.; Berque-Bestel, I. Synthesis of Specific Bivalent Probes That Functionally Interact with 5-HT$_4$ Receptor Dimers. *J. Med. Chem.* **2007**, 50(18), 4482-4492.
113. Soulier, J-L.; Russo, O.; Giner, M; Rivail, L.; Berthouze, M.; Ongeri, S.; Maigret, B.; Fischmeister, R.; Lezoualc'h, F.; Sicsic, S.; Berque-Bestel, I. Design and Synthesis of Spceific Probes for Human 5-HT$_4$ Receptor Dimerization Studies. **2005**, 48(20), 6220-6228.
114. Xu, L.; Josan, J.S.; Vagner, J.; Caplan, M.R.; Hruby, V.J.; Mash, E.A.; Lynch, R.M.; Morse, D.L.; Gillies, R.J. Heterobivalent ligands target cell-surface receptor combinations in vivo. *Proc. Natl. Acad. Sci. USA.* **2012**, 109(52), 21295-21300.
115. Lensing, C.J.; Freeman, K.T.; Schnell, S.M.; Adank, D.N.; Speth, R.C.; Haskell-Luevano, C. An *in vitro* and *in vivo* investigation of bivalent ligands that display preferential binding and functional activity for different melanocortin receptor homodimers. *J. Med. Chem.* **2016**, 59(7), 3112-3128.
116. Akgün, E.; Javed, M.I.; Lunzer, M.M.; Powers, M.D.; Sham, Y.Y.; Watanabe, Y.; Portoghese, P.S. Inhibition of Inflammatory and Neuropathic Pain by Targeting a Mu Opioid Receptor/Chemokine Receptor5 Heteromer (MOR-CCR$_5$). **2015**, 58(21), 8647, 8657.
117. Daniels, D.J.; Lenard, N.R.; Etienne, C.L.; Law, P-Y.; Roerig, S.C.; Portoghese, P.S. Opioid-induced tolerance and dependence in mice is

modulated by the distance between pharmacophores in a bivalent ligand series. *Proc. Natl. Acad. Sci. USA.* **2005**, 102(52), 19208-19213.

118. Smeester, B.A.; Lunzer, M.M.; Akgün, E.; Beitz, A.J.; Portoghese, P.S. Targeting putative mu opioid/metabotropic glutamate receptor-5 heteromers produces potent antinociception in a chronic murine bone cancer model. *Eur. J. Pharmacol.* **2014**, 743, 48-52.
119. Vauquelin, G.; Charlton, S.J. Exploring avidity: understanding the potential gains in functional affinity and target residence time of bivalent and heterobivalent ligands. *Br. J. Pharmacol.* **2013**, 168(8), 1771,1785.
120. Olson, K.M.; Keresztes, A.; Tashiro, J.K.; Daconta, L.V.; Hruby, V.J.; Streicher, J.M. Synthesis and Evaluation of a Novel Bivalent Selective Antagonist for the Mu-Delta Opioid Receptor Heterodimer that Reduces Morphine Withdrawal in Mice. *J. Med. Chem*. **2018**, 61, 6075-6086.
121. Delgado, D.M.; Møller, T.C.; Ster, J.; Giraldo, J.; Maurel, D.; Rovira, X.; Scholler, P.; Zwier, J.M.; Perroy, J.; Durroux, T.; Trinquet, E.; Prezeau, L.; Rondard, P.; Pin, J-P. Pharmacological evidence for a metabotropic glutamate receptor heterodimer in neuronal cells. *eLife*. **2017**, 6, e25233.
122. Bonnefous, C.; Vernier, J-M.; Hutchinson, J.H.; Gardner, M.F.; Cramer, M.; James, J.K.; Rowe, B.A.; Daggett, L.P.; Schaffhauser, H.; Kamenecka, T.M. Biphenyl-indanones: Allosteric potentiators of the metabotropic glutamate subtype 2 receptor. *Bioorg. Med. Chem. Lett.* **2005**, 15, 4354-4358.
123. Urizar, E.; Yano, H.; Kolster, R.; Galés, C.; Lambert, N.; Javitch, J.A. CODA-RET reveals functional selectivity as a result of GPCR heteromerization. *Nat. Chem. Bio.* **2011**, 7, 624-630.
124. Miner, J.; Hoffhines, A. The Discovery of Aspirin's Antithrombotic Effects. *Tex. Heart Inst. J.* **2007**, 34 (2), 179-186
125. Lévesque, H.; Lafont, O. Aspirin throughout the ages: a historical review. *Rev. Med. Interne.* **2000**, 21, 8s-17s.
126. Miller, E.L. The penicillins: a review and update. *J. Midwifery Womens Health.* **2002**, 47 (6), 426-434.
127. Wall, M. Camptothecin and taxol: Discovery to clinic. *Med. Res. Rev.* **1999**, 18 (5), 299-314.
128. Endo, A. A historical perspective on the discovery of statins. *Proc. Jpn. Acad. Ser. B. Phys. Biol. Sci.* **2010**, 86 (5), 484-493.
129. Newman, D.J.; Cragg, G.M. Natural Products as Sources of New Drugs over the 30 Years from 1981-2010. *J. Nat. Prod.* **2012**, 75 (3), 311-335.
130. Harvey, A.L.; Edrada-Ebel, R.; Quinn, R.J. The re-emergence of natural products for drug discovery in the genomics era. *Nat. Rev. Drug Disc.* **2015**, 14, 111-129.
131. Cragg, G.M.; Schepartz, S.A.; Suffness, M.; Grever, M.R. The taxol supply crisis. New NCI policies for handling the large-scale production of novel natural product anticancer and anti-HIV agents. *J. Nat. Prod.* **1993**, 56 (10), 1657-1668.
132. Ho, T.T.; Tran, Q.T.; Chai, C.L. The polypharmacology of natural products. *Future Med. Chem.* **2018**, 10 (11), 1361-1368.

133.Zeng, Z-P.; Jiang, J-G. Analysis of the adverse reactions induced by natural product-derived drugs. *Br. J. Pharmacol.* **2010**, 159 (7), 1374-1391.
134.Bailey, D.; Dresser, G.K. Natural products and adverse drug interactions. *CMAJ*. **2004**, 170 (10), 1531-1532.
135.Bhattaram, V.A.; Graefe, U.; Kohlert, C.; Veit, M.; Derendorf, H. Pharmacokinetics and bioavailability of herbal mediincal products. *Phytomedicine*. **2002**, 9, 1-33.
136.Ojima, I.; Chakravarty, S.; Inoue, T.; Lin, S.; He, L.; Horwitz, S.B.; Kuduk, S.D.; Danishefsky, S.J. *Proc. Natl. Acad. Sci.* **1999**, 96 (8), 4256-4261.
137.Rodrigues, T.; Reker, D.; Schneider, P.; Schneider, G. Counting on natural products for drug design. *Nat. Chem.* **2016**, 8, 531-541.
138.Broach, J.R.; Thorner, J. High-throughput screening for drug discovery. **1996**, 384, 14-16.
139.Major, J.S. Minireview: Challenges of High Throughput Screening Against Cell Surface Receptors. *J. Recept. Signal Transduct. Res.* **1995**, 15 (1-4), 595-607.
140.Macarron, R.; Banks, M.N.; Bojanic, D.; Burns, D.J.; Cirovic, D.A>; Garyantes, T.; Green, D.V.S.; Hertzberg, R.P.; Janzen, W.P.; Paslay, J.W.; Schopfer, U.; Sittampalam, G.S. Impact of high-throughput screening in biomedical research. *Nat. Rev. Drug Discov.* **2011**, 10, 188-195.
141.Bleicher, K.H.; Böhm, H-J.; Müller, K.; Alanine, A.I. Hit and lead generation: beyond high-throughput screening. *Nat. Review. Drug. Discov.* **2003**, 2, 369-378.
142.Panza, F.; Lozupone, M.; Solfrizzi, V.; Sardone, R.; Piccininni, C.; Dibello, V.; Stallone, R.; Giannelli, G.; Bellomo, A.; Daniele, A.; Seripa, D.; Logroscino, G.; Imbimbo, B.P. BACE inhibitors in clinical development for the treatment of Alzheimer's disease. *Expert Rev. Neurother.* **2018**, 18 (11), 847-857.
143.Mullard, A. BACE inhibitor bust in Alzheimer trial. *Nat. Rev. Drug Discov.* **2017**, 16, 155.
144.Lahiri, D.K.; Maloney, B.; Long, J.M.; Greig, N.H. Lessons from a BACE1 inhibitor trial: Off-site but not off base. *Alzheimers Diment.* **2014**, 10 (5), S411-S419.
145.Bender, A.; Bojanic, D.; Davies, J.W>; Crisman, T.J.; Mikahilov, D.; Scheiber, J.; Jenkins, J.L.; Deng, Z.; Hill, W.A.G.; Popov, M.; Jacoby, E.; Glick, M. Which aspects of HTS are empirically correlated with downstream success? *Curr. Opin. Drug Discov. Devel.* **2008**, 11(3), 327-337.
146.Henrich, C.J.; Beutler, J.A. Matching the Power of High Throughput Screening to the Chemical Diversity of Natural Products. *Nat. Prod. Rep.* **2013**, 30 (10), 1284-1298.
147.Coria-Téllez, A.V.; Montalvo-Gónzalez, E.; Yahia, E.M.; Obledo-Vázquez, E.N. *Annona muricata*: A comprehensive review on its traditional medicinal uses, phytochemicals, pharmacological activities, mechanisms of activity and toxicity. *Arab. J. Chem.* **2018**, 11 (5), 662-691.
148.Moghadamtousi, S.Z.; Fadaeinasab, M.; Nikzad, S.; Mohan, G.; Ali, H.M.; Kadir, H.A. *Annona muricata* (Annonaceae: A Review of Its Traditional

Uses, Isolated Acetogenins and Biological Activites. *Int. J. Mol. Sci.* **2015**, 16 (7) 15625-15658.

149. Gajalakshmi, S.; Vijayalakshmi, S.; Devi Rajeswari, V. Phytochemical and pharmacological properties of *Annona muricata*: A review. *Int. J. Pharm. Pharm. Sci.* **2012**, 4 (2), 3-6.
150. Liu, Y.H.; Hu, X.P.; Li, W.; Cao, X.Y.; Yang, H.R.; Lin, S.T.; Xu, C.B.; Liu, S.X.; Li, C.F. Antimicrobial and antitumor activity and diversity of endophytic fungi from traditional Chinese medical plant *Cephalotaxus hainanensis* Li. *Genet. Mol. Res.* **2016**, 15 (2), 1-11.
151. Zhang, D.; Ge, H.; Xie, D.; Chen, R.; Zou, J-H.; Tao, X.; Dai, J. Periconiasins A-C, New Cytotoxic Cytochalasans with an Unprecedented 9/6/5 Tricyclic Ring System from Endophytic Fungus *Periconia* sp. *Org. Lett.* **2013**, 15 (7), 1674-1677.
152. Zhang, D.; Tao, X.; Liu, J.; Chen, R.; Zhang, M.; Li, L.; Fang, X.; Yu, L-Y.; Dai, J. Periconiasin G, a new cytochalasan with unprecedented 7/6/5 tricyclic ring system from the endophytic fungus *Periconia* sp. *Tet. Lett.* **2016**, 7 (17), 796-799.
153. Zhang, D.; Tao, X.; Chen, R.; Liu, J.; Li, L.; Fang, X.; Yu, L.; Dai, J. Pericoannosin A, a Polyketic Synthase-Nonribosomal Peptide Synthetase Hybrid Metabolite with New Carbon Skeleton from the Endophytic Fungus *Periconia* sp. *Org. Lett.* **2015**, 17 (17), 4304-4307.
154. Tian, C.; Lei, X.; Wang, Y.; Dong, Z.; Liu, G.; Tang, Y. Total Syntheses of Periconiasins A-E. *Angew. Chem. Int. Ed.* **2016**, 55 (24), 6992-6996.
155. Lücke, D.; Linne, Y.; Hempel, K.; Kalesse, M. Total Synthesis of Pericoannosin A. *Org. Lett.* **2018**, 20 (15), 4475-4477.
156. Kulkarnia, S.J.; Pedduri, Y.; Chittiboyina, A.G.; Avery, M.A. Asymmetric Total Synthesis of the Caspase-1 Inhibitor (-)-Berkeleyamide A. *J. Org. Chem.* **2010**, 75 (9), 3113-3116.
157. Hayashi, Y.; Samanta, S.; Gotoch, H.; Ishikawa, H. Asymmetric Diels-Alder Reactions of α,β-Unsaturated Aldehydes Catalyzed by a Diarylprolinol Silyl Ether Salt in the Presence of Water. *Angew. Chem. Int. Ed.* **2008**, 47 (35), 6634-6637.
158. Graham, S.L.; Scholz, T.H. A new mode of reactivity of N-methoxy-N-methylamides with strongly basic reagents. *Tet. Lett.* **1990**, 31 (44), 6269-6272.
159. Hiaro, A.; Itsuno, S.; Nakahama, S.; Yamazaki. Asymmetric reduction of aromatic ketones with chiral alkoxy-amineborane complexes. *J. Chem. Soc. Chem. Commun.* **1981**, 7, 315-317.
160. Corey, E.J.; Bakshi, R.K.; Shibata, S. Highly enantioselective borane reduction of ketones catalyzed by chiral oxazaborolidines. Mechanism and synthetic implications. *J. Am. Chem. Soc.* **1987**, 109 (18), 5551-5553.
161. Corey, E.J.; Bakshi, R.K.; Shibata, S.; Chen, C.P.; Signh, V.K. A stable and easily prepared catalyst for the enantioselective reduction of ketones. Application to multistep syntheses. **1987**, 109 (25), 7925-7926.

162. Chérest, M.; Felkin, H.; Prudent, N. Torsional strain involving partial bonds. The stereochemistry of the lithium aluminum hydride reduction of some simple open-chain ketones. *Tet. Lett.* **1968**, 9 (18), 2199-2204.
163. Anh, N.T.;, Eisenstein, O. (1977) Nouv J Chim 1: 61-70
164. Anh, N.T.; Eisenstein, O.; Lefour, J.M.; Tran Huu Dau, M.E. Orbital factors and asymmetric induction. *J. Am. Chem. Soc.* **1973**, 95 (18), 6146-6147.
165. Potter, G.T.; Jayson, G.C.; Miller, G.J.; Gardiner, J.M. An Updated Synthesis of the Diazo-Transfer Reagent Imidazole-1-sulfonyl Azide Hydrogen Sulfate. *J. Org. Chem*. **2016**, 81, 3443-3446.
166. Brown, H.C.; Chen, J.C. Hydroboration. 57. Hydroboration with 9-Borabicyclo[3.3.1]nonane of Alkenes Containing Representative Functional Groups. *J. Org. Chem.* **1981**, 46, 3978-3988.
167. Sullivan, D.F.; Woodbury, R.P.; Rathke, M.W. The Self-Condensation Reaction of Lithium Ester Enolates. Isolation of a Ketene Intermediate. *J. Org. Chem.* **1977**, 42 (11), 2038-2039.
168. Seebach, D.; Amstutz, R.; Laube, T.; Schweizer, W.B.; Dunitz, J.D. Structures of Three Lithium Ester Enolates by X-ray Diffraction: Derivation of Reaction Path for Cleavage into Ketene and Alcoholate. *J. Am. Chem. Soc.* **1985**, 107, 5403-5409.
169. Loubinoux, B.; Sinnes, J-L.; O'Sullivan, A.C. Synthesis of Substructures of Soraphen A: Formation of the Enoalte of Benzyl Propionate. *J. Chem. Soc. Perkin Trans.* **1995**, 521-525.
170. Taylor, L.T. Supercritical Fluid Chromatography. *Anal. Chem.* **2010**, 82 (12), 4925-4935.
171. Taylor, L.T. Supercritical fluid chromatography for the 21st century. *J. Supercrit. Fluid.* **2009**, 47 (3), 566-573.
172. Sperry, J.; Harris, E.B.J.; Brimble, M.A. Total Synthesis and Absolute Configuration of (-)-Berkeleyamide A. *Org. Lett.* **2010**, 12 (3), 420-423.
173. Hoye, T.R.; Jeffrey, C.S.; Shao, F. Mosher ester analysis for the determination of absolute configurations of stereogenic (chiral) carbinol carbons. *Nat. Protoc.* **2007**, 2, 2451-2458.